



AALBORG UNIVERSITY  
STUDENT REPORT

# Frost formation in air to air counterflow heat exchangers... and how to prevent it?

In collaboration with Airmaster A/S

Dzhanan Metin Osman  
Diana State  
Nils Kristian Kure Rasmussen

MASTER THESIS  
January 2019





**AALBORG UNIVERSITET**  
STUDENTERRAPPORT

**Study Board of Civil Engineering**

Thomas Manns Vej 23  
DK - 9220 Aalborg Øst  
Tlf. 99 40 93 09  
www.en.ses.aau.dk

**Title:** Frost formation in air to air heat exchangers... and how to prevent it?

**Study programme:** Master of Science (MSc) in Technology in Building Energy Design

**Project:** Master's Thesis

**Project period:** September 2018 - January 2019

**Supervisors:**

Rasmus Lund Jensen  
Michal Pomianowski

**External research partner:**

Erik Bjoern

Dzhanan Metin Osman

Diana State

**Nils Rasmussen**

Nils Kristian Kure Rasmussen

**Number of pages:** 154

**Synopsis:**

This report is the product of a master's thesis project, completed by a group of Building Energy Design students from Aalborg University.

With the increasing requirements for energy efficiency, the minimum requirements for heat recovery have become stricter. However, with high heat recovery efficiency, the problem of frost formation in heat exchangers emerges.

This report focuses on analyzing under which climatic conditions frost appears. Based on that, different frost prevention strategies are compared in terms of impact on energy consumption and indoor environment.

The frost formation process with different indoor humidity levels is also investigated.

Finally, the risk of frost for different geographical locations is evaluated.

*By signing this document, each member of the group confirms that everyone has participated in the project work and that everyone collectively binds the content of the report. The content of the report is freely available, but publication (with source) may only be in agreement with the authors.*



# Acknowledgements

Firstly, we would like to thank our supervisors, Michal Pomianowski and Rasmus Lund Jensen, for their guidance, support and valuable feedback in the course of writing this thesis.

Secondly, we would like to thank Erik Bjoern and the team at Airmaster for providing the experimental set-up, interest in working with us and continuous collaboration throughout the project.

We would also like to express our gratitude to Hicham Johra and Kim Trangbæk Joensson. Their guidance, patience and help during the calibration process and the experimental part of the project was very valuable and highly appreciated.

Our thanks also goes to Ivan Nikolaisson for his continuous help with the Sensirion sensors.

Finally, we would like to thank our families and close ones for their support, motivation and endless patience with us during this semester.



# Abstract

This report examines how the preheating, bypass and imbalance frost prevention methods impact the energy consumption and indoor environmental quality and aims to identify the most optimal one. Moreover, analysis on the influence of certain outdoor and indoor conditions on frost formation are also provided.

To accomplish this goal, the dynamic simulation software, BSim, has been used to find out the critical outdoor and corresponding indoor conditions for frost formation. The analysed geographical locations for outdoor climate are Southern Scandinavia, Central Europe, Southern Germany and Austria, and Scotland. As for indoor climate, building usage types for classrooms and offices are considered. The findings are that an indoor relative humidity range of 20-40 % with 22 °C extraction temperature corresponds to outdoor temperatures causing frost.

To determine the energy consumption of the frost prevention strategies, the frost limit temperature for the above mentioned indoor conditions has been identified by conducting experimental tests on a counterflow plate heat exchanger. Climatic chambers have been used to maintain the defined operation conditions. The outcome is that frost appears on the exhaust port at 0 °C exhaust temperature. The calculations revealed that there is no difference in the energy required to maintain the temperature above this limit among the investigated frost prevention methods.

In terms of impact on indoor environmental quality, indoor air quality and thermal comfort have been criteria for assessment. For the analysed climatic conditions, the indoor air quality is not compromised with any of the methods. However, imbalance would jeopardize the thermal climate due to risk of draught because of the higher infiltration.

Finally, it has been observed that indoor relative humidity affects the area where frost starts forming on the exhaust port and that with low humidity levels, where the dew point is below 0 °C, frost forms without any condensation.



# Abbreviations

---

<b>Symbol</b>	<b>Description</b>
<i>AAU</i>	Aalborg University
<i>AHU</i>	Air-handling unit
<i>BSim</i>	Building simulation software
<i>RH</i>	Relative humidity

---



# Nomenclature

Symbol	Description
$C_h$	Heat capacity rate on the warm side [ $\frac{W}{K}$ ]
$C_c$	Heat capacity rate on the cold side [ $\frac{W}{K}$ ]
$C_{ph}$	Specific heat capacity for the warm side [ $\frac{J \cdot kg}{K}$ ]
$C_{pc}$	Specific heat capacity for the cold side [ $\frac{J \cdot kg}{K}$ ]
$h_{out}$	Outdoor air enthalpy [ $\frac{kJ}{kg}$ ]
$h_{sup}$	Supply air enthalpy [ $\frac{kJ}{kg}$ ]
$h_{sup'}$	Supply air enthalpy with imbalance [ $\frac{kJ}{kg}$ ]
$h_{ext}$	Extraction air enthalpy [ $\frac{kJ}{kg}$ ]
$h_{exh}$	Exhaust air enthalpy [ $\frac{kJ}{kg}$ ]
$h_{exh'}$	Freezing limit air enthalpy [ $\frac{kJ}{kg}$ ]
$h_{mix}$	Enthalpy of combined bypass and cold airstream [ $\frac{kJ}{kg}$ ]
$m_h$	Mass flow rate on the warm side [ $\frac{kg}{s}$ ]
$m_{nominal}$	Mass flow rate on the nominal side (equal to the warm side) [ $\frac{kg}{s}$ ]
$m_c$	Mass flow rate on the cold side [ $\frac{kg}{s}$ ]
$m_{c,im}$	Cold side mass flow with imbalance [ $\frac{kg}{s}$ ]
$m_{bypass}$	Mass flow of bypassed air [ $\frac{kg}{s}$ ]
$m_{inf}$	Mass flow rate of infiltration air [ $\frac{kg}{s}$ ]
$P$	Atmospheric pressure [Pa]
$P_s$	Saturation pressure [Pa]
$Q_{max}$	Maximum heat flow [W]
$Q_{max\ possible}$	Maximum possible heat flow based on freezing point temperature [W]
$Q_{sup\ fan\ (nominal\ flow)}$	Fan power with nominal flow [W]

Symbol	Description
$Q_{sup\ fan\ (imbalanced\ flow)}$	Fan power with imbalanced flow [W]
$RH_{out}$	Outdoor air relative humidity [-]
$RH_{sup}$	supply air relative humidity [-]
$RH_{sup'}$	supply air relative humidity with imbalance [-]
$RH_{ext}$	Extraction air relative humidity [-]
$RH_{exh}$	Exhaust air relative humidity [-]
$t_{out}$	Outdoor air temperature [ $^{\circ}C$ ]
$t_{sup}$	Supply air temperature [ $^{\circ}C$ ]
$t_{sup'}$	Supply temperature with imbalance [ $^{\circ}C$ ]
$t_{ext}$	Extraction air temperature [ $^{\circ}C$ ]
$t_{exh}$	Exhaust air temperature [ $^{\circ}C$ ]
$t_{exh'}$	Freezing limit temperature [ $^{\circ}C$ ]
$t_{mix}$	Temperature of combined bypass and cold airstream [ $^{\circ}C$ ]
$x_{out}$	Outdoor air absolute humidity [ $\frac{kg}{kg}$ ]
$x_{sup}$	Supply air absolute humidity [ $\frac{kg}{kg}$ ]
$x_{sup'}$	Supply air absolute humidity with imbalance [ $\frac{kg}{kg}$ ]
$x_{ext}$	Extraction air absolute humidity [ $\frac{kg}{kg}$ ]
$x_{exh}$	Exhaust air absolute humidity [ $\frac{kg}{kg}$ ]
$x_{exh'}$	Freezing limit absolute humidity [ $\frac{kg}{kg}$ ]
$\eta_{t,im}$	Temperature efficiency with imbalance [-]
$\eta_{fan}$	Fan efficiency [-]
$\Delta P_{sup\ fan\ (nominal\ flow)}$	Pressure drop on the supply fan with nominal airflow [Pa]
$\rho$	Density of air [ $\frac{kg}{m^3}$ ]
$\varphi$	Relative humidity [-]

# Contents

<b>List of Tables</b>	<b>xv</b>
<b>List of Figures</b>	<b>xvi</b>
<b>1 Introduction</b>	<b>1</b>
1.1 Problem statement . . . . .	2
1.2 Methodology . . . . .	2
1.3 Delimitation . . . . .	2
1.4 Structure of the thesis . . . . .	2
<b>2 Defrost and frost prevention methods</b>	<b>4</b>
<b>3 Heat exchanger specifications</b>	<b>6</b>
<b>4 Test conditions</b>	<b>7</b>
4.1 Validation test conditions . . . . .	7
4.2 Experimental test conditions . . . . .	7
<b>5 Experimental setup and measurements</b>	<b>13</b>
5.1 Experimental setup . . . . .	13
5.2 Measurements . . . . .	16
5.3 Test procedure . . . . .	19
<b>6 Performance data verification</b>	<b>21</b>
<b>7 Frost formation limits</b>	<b>25</b>
7.1 Test procedures . . . . .	25
7.2 Risk of frost for the chosen geographical locations . . . . .	26
7.3 Test conditions and results . . . . .	28
7.3.1 Test conditions . . . . .	28
7.3.2 Results . . . . .	29
7.4 Airmaster’s frost prevention control strategy . . . . .	33
<b>8 Calculation validation</b>	<b>36</b>
<b>9 Impact of frost prevention methods</b>	<b>42</b>
9.1 Imbalance test . . . . .	42
9.2 Impact on energy consumption . . . . .	44
9.3 Impact on indoor environmental quality . . . . .	46
<b>10 Comparison of dynamic with static efficiency</b>	<b>47</b>
<b>11 Challenges and problems during the measurements</b>	<b>51</b>
11.1 Cooling system . . . . .	51
11.2 Other challenges . . . . .	54
<b>12 Conclusion</b>	<b>57</b>

<b>13 Future work</b>	<b>59</b>
<b>Bibliography</b>	<b>60</b>
<b>A Defrost methods</b>	<b>63</b>
<b>B Test conditions</b>	<b>64</b>
B.1 Experimental test conditions . . . . .	64
<b>C Test set-up</b>	<b>76</b>
C.1 Sensor calibration and measurement uncertainty . . . . .	77
C.2 Infiltration rate of the experimental facility . . . . .	92
C.3 Leakage test for the heat exchangers and heat recovery unit . . . . .	92
<b>D Performance data verification</b>	<b>94</b>
<b>E Frost formation limits</b>	<b>105</b>
E.1 Experimental analysis . . . . .	105
E.1.1 Risk of frost for the chosen geographical locations . . . . .	118
<b>F Impact of defrost methods</b>	<b>121</b>
F.1 Defrost methods . . . . .	121
<b>G Comparison of dynamic with static efficiency</b>	<b>123</b>
<b>H Calculations</b>	<b>125</b>
H.1 Input data . . . . .	125
H.2 Imbalance method . . . . .	127
H.3 Bypass method . . . . .	131
H.4 Air preheating method . . . . .	132
H.5 Step-by-step walk through the excel spreadsheet . . . . .	132

# List of Tables

3.1	Heat exchanger specifications . . . . .	6
4.1	Test conditions for performance data verification according to DS/EN 308:1997 [6] . . . . .	7
4.2	Outdoor ambient temperature range for the representative locations . . . . .	11
4.3	Relative humidity range for the extracted air . . . . .	12
5.1	Sensirion sensor for relative humidity and temperature details [30] . . . . .	17
5.2	UltraLink details [20] . . . . .	18
5.3	Measurement uncertainties [5] . . . . .	20
5.4	Allowed deviations for arithmetic mean values and individual measurements [5] . . . . .	20
6.1	Mean and individual measurement deviations for the dry test (infiltration dampers closed)	21
6.2	Mean and individual measurement deviations for the wet test (infiltration dampers closed)	21
6.3	Input and output conditions for one measurement point with wet conditions . . . . .	24
7.1	Frost formation test conditions . . . . .	28
13.1	Heat exchanger specifications for fututre work . . . . .	59
C.1	Calibration polynomials for the thermocouples . . . . .	83
C.2	Difference between reference thermometer and each Sensirion sensor . . . . .	87
C.3	Difference between IC-meter and each Sensirion sensor for relative humidity . . . . .	91
C.4	Absolute humidity calculation for IC-meter and each sensor . . . . .	92
C.5	Leakage test results for the heat exchangers and heat recovery unit . . . . .	93
D.1	The properties of a standard volume . . . . .	94
D.2	Mean and individual measurement deviations for the dry test (infiltration dampers open)	95
D.3	Mean and individual measurement deviations for the wet test (infiltration dampers open)	95
D.4	Mean and individual measurement deviations for the wet test (balanced airflows) . . . . .	101
F.1	Fan voltage input steps and imbalance ratio for each step . . . . .	121

# List of Figures

2.1	Comparison of heat recovery and additional energy consumption for air treatment in an air-handling unit with counter-flow heat exchanger under a) preheating b) 50 % bypass c) Variable bypass ratio required for frost-free plate surface [1] . . . . .	5
3.1	Klingenburg - GS 25/250 and GS-K 25/250 . . . . .	6
4.1	Initial number of locations . . . . .	8
4.2	Final number of locations . . . . .	8
4.3	Cumulative number of hours based on outdoor ambient temperature only for the representative locations . . . . .	9
4.4	Cumulative number of hours based on outdoor ambient absolute humidity only for the representative locations . . . . .	10
4.5	Yearly percentage of hours below 0 °C (left) and yearly percentage of hours below 0.0026 kg/kg absolute humidity (30-35 % indoors relative humidity) (right) . . . . .	11
5.1	Experimental setup . . . . .	14
5.2	3D drawing for AHU with airflow path . . . . .	15
5.3	AHU working principle . . . . .	16
5.4	Thermocouple grid placed on the heat exchanger . . . . .	17
5.5	Lindab Ultralink extraction airflow direction - warm room . . . . .	18
5.6	Lindab Ultralink supply airflow direction - cold room . . . . .	18
5.7	Pressure tap on the side . . . . .	19
5.8	Pressure tap on the extraction side . . . . .	19
6.1	Temperature efficiency comparison for the dry test (infiltration dampers closed) . . . . .	22
6.2	Temperature efficiency comparison for the wet test (infiltration dampers closed) . . . . .	22
6.3	Exhaust temperature comparison for the dry test (infiltration dampers closed) . . . . .	23
6.4	Exhaust temperature comparison for the wet test (infiltration dampers closed) . . . . .	23
6.5	Air treatment on the warm and cold side measured vs. Klingenburg . . . . .	24
7.1	Indoor relative humidity - outdoor temperature relation for Gothenburg - classroom . . . . .	26
7.2	Indoor relative humidity - outdoor temperature relation for Gothenburg - office . . . . .	27
7.3	Percentage of critical indoor relative humidity ranges from the total number of yearly working hours with 22 °C as indoor temperature . . . . .	27
7.4	Frost formation test conditions presented on an Ix-diagram - mean temperatures . . . . .	29
7.5	Frost formation test conditions presented on an Ix-diagram - mean temperatures for outdoor, supply and extraction; minimum local temperature for exhaust . . . . .	30
7.6	Temperature gradient on exhaust port for all test conditions . . . . .	31
7.7	Frost formation location with different conditions . . . . .	32

7.8	Temperature gradient on all ports - Condition 2 . . . . .	33
7.9	Airmaster's temperature sensor on exhaust port (marked with a red circle) . . . . .	34
7.10	Airmaster's temperature sensor location in relation to the thermocouple readings . . . . .	34
8.1	Heat exchanger data from imbalance test . . . . .	36
8.2	Temperature Increase from balance to imbalanced flow . . . . .	37
8.3	Flow on cold and hot side from balance imbalanced flow . . . . .	37
8.4	Supply and extraction flow with closed to open bypass . . . . .	38
8.5	Supply and extraction temperature with closed and open bypass . . . . .	38
8.6	Bypass measurement . . . . .	39
8.7	Preheater on/off measurement . . . . .	40
8.8	Air temperatures from when the preheater is switched on until it is switched off . . . . .	40
9.1	Imbalance between supply and exaction airflows - infiltration damper realistically open and fully open . . . . .	42
9.2	Relationship between voltage and ratio supply / extraction . . . . .	43
9.3	Temperature efficiency and imbalance ratio - infiltration damper realistically open and fully open . . . . .	44
9.4	Imbalance ratio correlation with outdoor temperature / indoor relative humidity - Gothenburg (classroom) . . . . .	45
10.1	Dynamic yearly temperature efficiency for Gothenburg - classroom . . . . .	48
10.2	Dynamic yearly temperature efficiency for Gothenburg - office . . . . .	48
10.3	Percentage of operation conditions from the period with heat recovery working (exhaust temperature extracted from Klingenburg) . . . . .	49
10.4	Percentage of operation conditions from the period with heat recovery working (exhaust temperature decreased with 2 °C) for wet/frost - Gothenburg . . . . .	49
10.5	Percentage of operation conditions from the period with heat recovery working (exhaust temperature decreased with 2 °C) for wet/frost - Groningen . . . . .	49
10.6	Percentage of operation conditions from the period with heat recovery working (exhaust temperature decreased with 2 °C) for wet/frost - Innsbruck . . . . .	50
11.1	Airmaster cooling system out of order . . . . .	51
11.2	Component overview for cooling and heating of the room . . . . .	52
11.3	Cooling system from AAU inside the cold room . . . . .	53
11.4	Updated Airmaster cooling system with defrost function . . . . .	53
11.5	Cooling system from AAU out of order . . . . .	54
11.6	Flow oscillating because off close ducts . . . . .	55
11.7	Duct fallen down . . . . .	55
12.1	Evaluation of frost formation risk in the investigated geographical locations . . . . .	58
A.1	Voltmeter and watt meter to measure power consumption . . . . .	63
B.1	Cumulative number of hours based on outdoor ambient temperature for all the initially selected locations . . . . .	64
B.2	Cumulative number of hours based on outdoor ambient absolute humidity for all the initially selected locations . . . . .	64
B.3	Full year outdoor ambient temperature variations for the representative locations . . . . .	65

B.4	Cumulative number of hours based on outdoor ambient temperature for all the final locations	65
B.5	Cumulative number of hours based on outdoor ambient absolute humidity for all the final locations . . . . .	66
B.6	Outdoor temperature variations for the working hours during the whole year for all the final locations . . . . .	66
B.7	Relative humidity in a classroom during January, February, November, December for the chosen representative locations for working hours . . . . .	67
B.8	Relative humidity in an office during January, February, November, December for the chosen representative locations for working hours . . . . .	67
B.9	Cumulative number of working hours based on outdoor ambient temperature for Southern Scandinavia (representative location Gothenburg) . . . . .	68
B.10	Cumulative number of working hours based on outdoor ambient temperature for England and Central Europe (representative location Groningen) . . . . .	68
B.11	Cumulative number of working hours based on outdoor ambient temperature for Southern Germany and Austria (representative location Innsbruck) . . . . .	69
B.12	Cumulative number of working hours based on outdoor ambient temperature for Scotland (representative location Leuchars) . . . . .	69
B.13	Cumulative number of working hours based on outdoor ambient absolute humidity for Southern Scandinavia (representative location Gothenburg) . . . . .	70
B.14	Cumulative number of working hours based on outdoor ambient absolute humidity for England and Central Europe (representative location Groningen) . . . . .	70
B.15	Cumulative number of working hours based on outdoor ambient absolute humidity for Southern Germany and Austria (representative location Innsbruck) . . . . .	71
B.16	Cumulative number of working hours based on outdoor ambient absolute humidity for Scotland (representative location Leuchars) . . . . .	71
C.1	"Figure 4 Temperature measuring plane" from DS308:1997 - page 12 . . . . .	76
C.2	Installation of thermocouples on the grid . . . . .	77
C.3	Thermocouple schematic . . . . .	77
C.4	Calibration set-up . . . . .	78
C.5	Thermocouple calibration curve . . . . .	79
C.6	Error due to calibration curve for all thermocouples . . . . .	82
C.7	Photos from the calibration process . . . . .	85
C.8	Differential pressure transducer calibration curve . . . . .	86
C.9	Error due to calibration curve . . . . .	86
C.10	Sensirion temperature comparison with reference thermometer at 25 °C . . . . .	88
C.11	Sensirion temperature comparison with reference thermometer at 15 °C . . . . .	88
C.12	Sensirion temperature comparison with reference thermometer at 0 °C . . . . .	89
C.13	Sensirion temperature comparison with reference thermometer at -15 °C . . . . .	89
C.14	Placement of Sensirion, reference thermometer and IC-meter . . . . .	90
C.15	Sensirion temperature comparison with reference thermometer and IC-meter . . . . .	90
C.16	Sensirion relative humidity comparison with IC-meter . . . . .	91
D.1	Temperature efficiency comparison for the dry test (infiltration dampers open) . . . . .	95
D.2	Temperature efficiency comparison for the wet test (infiltration dampers open) . . . . .	96
D.3	Exhaust temperature comparison for the dry test (infiltration dampers open) . . . . .	96
D.4	Exhaust temperature comparison for the wet test (infiltration dampers open) . . . . .	97

D.5	Mean air temperatures and extraction relative humidity during the dry test (infiltration dampers closed) . . . . .	97
D.6	Mass flow during the dry test (infiltration dampers closed) . . . . .	98
D.7	Mean air temperatures and extraction relative humidity during the wet test (infiltration dampers closed) . . . . .	98
D.8	Mass flow during the wet test (infiltration dampers closed) . . . . .	99
D.9	Mean air temperatures and extraction relative humidity during the dry test (infiltration dampers open) . . . . .	99
D.10	Mass flow during the dry test (infiltration dampers open) . . . . .	100
D.11	Mean air temperatures and extraction relative humidity during the wet test (infiltration dampers open) . . . . .	100
D.12	Mass flow during the wet test (infiltration dampers open) . . . . .	101
D.13	Temperature efficiency comparison for the wet test (balanced mass flow) . . . . .	102
D.14	Exhaust temperature comparison for the wet test (balanced mass flow) . . . . .	102
D.15	Mean air temperatures and extraction relative humidity during the wet test (balanced mass flow) . . . . .	103
D.16	Mass flow during the wet test (balanced mass flow) . . . . .	103
D.17	Exhaust temperature comparison for the balanced wet test with uncertainties . . . . .	104
E.1	Frost formation - condition 1 . . . . .	105
E.2	Mean air temperature and extraction relative humidity - condition 1 . . . . .	106
E.3	Mass flow - condition 1 . . . . .	106
E.4	Temperature gradient across outdoor and exhaust port (balanced massflows) - condition 1 . . . . .	107
E.5	Temperature gradient across outdoor and exhaust port (imbalanced massflows) - condition 1 . . . . .	107
E.6	Temperature readings from all sensors on exhaust port - condition 2 . . . . .	108
E.7	Small droplets of condensation at second 1000 - condition 2 . . . . .	108
E.8	Bigger droplets of condensation at second 3000 - condition 2 . . . . .	109
E.9	Condensation at second 6000 - condition 2 . . . . .	109
E.10	Frost formation at second 12000 - condition 2 . . . . .	110
E.11	Mean air temperature and extraction relative humidity - condition 2 . . . . .	110
E.12	Mass flow - condition 2 . . . . .	111
E.13	Temperature gradient across outdoor and exhaust port - condition 2 . . . . .	111
E.14	Mean air temperature and extraction relative humidity - condition 3 . . . . .	112
E.15	Mass flow - condition 3 . . . . .	112
E.16	Frost formation - condition 3 . . . . .	113
E.17	Temperature gradient across outdoor and exhaust port - condition 3 . . . . .	114
E.18	Mean air temperature and extraction relative humidity - condition 4 . . . . .	115
E.19	Mass flow - condition 4 . . . . .	115
E.20	Frost formation - condition 4 . . . . .	116
E.21	Temperature gradient across outdoor and exhaust port - condition 4 . . . . .	117
E.22	Indoor relative humidity - outdoor temperature relation for Groningen - classroom . . . . .	118
E.23	Indoor relative humidity - outdoor temperature relation for Groningen - office . . . . .	118
E.24	Indoor relative humidity - outdoor temperature relation for Innsbruck - classroom . . . . .	119
E.25	Indoor relative humidity - outdoor temperature relation for Innsbruck - office . . . . .	119
E.26	Indoor relative humidity - outdoor temperature relation for Leuchars - classroom . . . . .	120
E.27	Indoor relative humidity - outdoor temperature relation for Leuchars - office . . . . .	120
F.1	Mean air temperature - infiltration damper realistically opening . . . . .	122

---

F.2	Mean air temperature -infiltration damper fully open . . . . .	122
G.1	Distribution of heat exchanger operation conditions during the year for Gothenburg - classroom . . . . .	123
G.2	Distribution of heat exchanger operation conditions during the year for Gothenburg - office	123
G.3	Distribution of heat exchanger operation conditions during the year for Groningen - classroom	123
G.4	Distribution of heat exchanger operation conditions during the year for Groningen - office	123
G.5	Distribution of heat exchanger operation conditions during the year for Innsbruck - classroom	124
G.6	Distribution of heat exchanger operation conditions during the year for Innsbruck - office .	124
G.7	Distribution of heat exchanger operation conditions during the year for Leuchars - classroom and office . . . . .	124
H.1	Calculation parameters illustrated . . . . .	126

# 1 | Introduction

Legal requirements regarding energy efficiency and rational exploitation of the energy resources [1] are getting stricter in countries with cold climates due to high space heating consumption [25] and rising environmental awareness. For space heating in cold climates is consumed between 40-60 % from the total energy [25] and 30-60 % from the total space heating consumption is due to heating up the incoming fresh air [16]. For that reason, the minimum demand for heat recovery in ventilation units has been increased from 67 % to 73 % from January 2018 by Ecodesign and in the respective EU countries [9].

Although there is a big energy saving potential in ventilation units with high heat recovery, in cold climates it can lead to frost formation on the plate surface of the warm side. During winter, when the plate surface temperature falls below freezing point, there is a risk of condensation and frost formation. Consequently, when the highest heat recovery efficiency is needed, it cannot be provided. Frosting leads to reduction of the heat recovery efficiency, increase in pressure drop in the return airflow channels, higher electricity consumption for the fans, and draught in the space due to low supply air temperature. In case of severe frosting, there is also a risk of damage of the heat exchanger. [23] [32]

Even though the topic has raised concerns for the past 35 years, the published papers related to frost formation in heat exchangers are limited. Frost formation has been detected by many researchers but only few have investigated frost prevention or defrost methods. Due to that, literature states that the problem of frost is still unresolved and even the most commonly used defrost methods face challenges in cold climates. [23]

This report focuses on frost prevention methods for air-to-air counterflow plate heat exchangers. Such recuperators precondition the outdoor supply air by using the energy from the return airstream. Heat is transferred from the return to the supply air. In counterflow heat exchangers, the supply and return airstreams flow along each other, separated by aluminium/ plastic plates. The heat exchanger is hermetically sealed, and therefore, the two flows are unmixed. They are very popular in the Northern countries because of their reliability, long service-life due to no moving parts, operation with unmixed fluids and high heat recovery efficiency [32].

The purpose of the report is to define the most energy efficient and indoor environmental-friendly frost prevention method/methods based on literature review, calculations, experiments and simulations. This will be achieved by finding the outdoor temperature below which frost would occur (so-called "frost limits"). Based on that, the energy consumption and indoor air quality impact of the different methods is investigated. Additionally, the influence of different indoor conditions on frost formation and temperature distribution across the ports is analysed. For that purpose, a counterflow plate heat exchanger will be tested under a range of outdoor ambient conditions corresponding to winter conditions for countries in cold climatic zones and indoor air conditions, matching different building usage types, namely schools and offices. Furthermore, the required minimum heat recovery efficiency will be compared to the efficiency in freezing conditions.

## 1.1 Problem statement

The main questions of this thesis are: What is the most energy efficient and indoor environmental-friendly frost prevention method? How does the indoor climate impact frost formation? Moreover, is the minimum heat recovery efficiency representative for all outdoor temperature conditions?

To answer these questions, the following sub-questions should be investigated.

- What are the most commonly used frost prevention and defrost methods?
- What is the frost limit and frost formation process under certain outdoor ambient and indoor return air conditions?
- Which method is the most energy efficient for frost prevention?
- How do they impact the indoor environmental quality?
- What is the static vs. dynamic temperature efficiency?

## 1.2 Methodology

As this report aims to give answers to questions which have gained interest in the last decades by the research community but are still unresolved, the logical way to start the investigation is by reviewing the existing literature on the topic. That includes mainly research articles and technical/academical books.

The next step is conducting experimental tests under predefined boundary conditions. The indoor temperature and relative humidity conditions are defined based on dynamic simulations, using BSim.

Lastly, the collected data is interpreted analytically and numerically.

## 1.3 Delimitation

Since the main topic in this research is frost formation on plate heat exchangers, it will only focus on outdoor conditions representative for cold climates, though not for arctic. As for indoor air, conditions regarding residential buildings will not be considered. Moreover, the position of the investigated heat exchanger is horizontal, not vertical. Finally, even though the experimental set-up includes a variety of mechanical and electrical systems, it is not the purpose of this report to examine their technical characteristics.

## 1.4 Structure of the thesis

The thesis starts with a literature review on the most commonly used defrost and frost prevention methods, followed by a description of the boundary conditions for the experimental tests. It also provides a description of the test set-up including on-site photos. To validate the test set-up, the provided heat recovery efficiencies from the manufacturer's software are compared with the efficiencies obtained from experiments under the same temperature and relative humidity conditions. Once the set-up is validated, the next part provides analysis on the results from the conducted tests regarding

frost limits under defined outdoor and indoor conditions. Based on these limits, the impact of the different frost prevention methods on energy consumption is calculated. Additionally, their influence on the indoor air quality is also looked into.

Finally, the static heat recovery efficiency is investigated regarding real-life operation conditions and is compared with the dynamic efficiency.

## 2 | Defrost and frost prevention methods

In this chapter, the most commonly used and investigated frost prevention and defrost methods are first shortly described and then a literature review is provided.

Frost formation is a problem in the "cold zone" of a heat exchanger, characterized by the area with the highest risk of frost formation, where the return air is in contact with the coldest plate surface. [1]

### **Preheating outdoor supply air**

With this frost prevention method, the ambient air is preheated by a heater before it enters the heat exchanger. The cold outdoor air is preheated to the threshold temperature, defined as the minimum supply air temperature at which the plate temperature in the "cold zone" of the heat exchanger will be kept above 0 °C, thus avoiding freezing. [2]

### **Bypass**

Bypass is used as a frost prevention technique, where all or part of the outdoor air is bypassed around the heat exchanger. The amount of bypassed air can be controlled by ambient threshold temperature values, exhaust air temperature or pressure increase over the heat exchanger. [23]

### **Imbalance by reducing outdoor airflow rate**

The imbalance method is used to remove frost. The outdoor airflow rate is reduced, while the exhaust airflow rate is kept unchanged. The temperature of the exhaust air leaving the heat exchanger is kept above dew point to avoid any condensation and consequently frost formation. [23]

### **Supply fan shut-off**

The supply fan shut-off is a defrost method, where the outdoor airflow rate is stopped, while the exhaust is kept unchanged. There is no heat recovery during the defrost cycles. It runs at set time intervals for a fixed time when the outdoor temperature is below the threshold temperature limit. This operation schedule provides the possibility to maintain acceptable indoor air quality. [10]

### **Recirculating room air**

With this defrost method, the outdoor air is stopped, and room air is recirculated through the heat exchanger at set time intervals for a fixed time when the outdoor temperature is below the threshold temperature limit. [10]

### **Literature review**

Jedlikowski et al. [1] have compared the heat recovery and additional energy consumption under the air preheating method with the bypass method with 50 % bypass and with variable bypass ratio, as seen in figure 2.1. Case a) is air preheating with an electric heater and a heating coil, case b) is with a 50 % bypass of the supply air, an electric heater and a heating coil, and case c) is with the required bypass ratio to keep frost-free plate surface and a heating coil. In the cases with air preheater (case a and b), the supply air temperature is preheated to the threshold temperature. The bottom column charts show the energy consumption and heat recovery for each case mentioned above. The total energy consumption for heating up the air from -20 to 20 °C with 1 m<sup>3</sup>/s airflow is 48 kW, which

is divided among an electric heater, heat recovery and a heating coil. Based on that, Jedlikowski's conclusion is that preheating fresh air provides highest heat recovery, while solely bypassing without preheating leads to highest additional energy consumption.

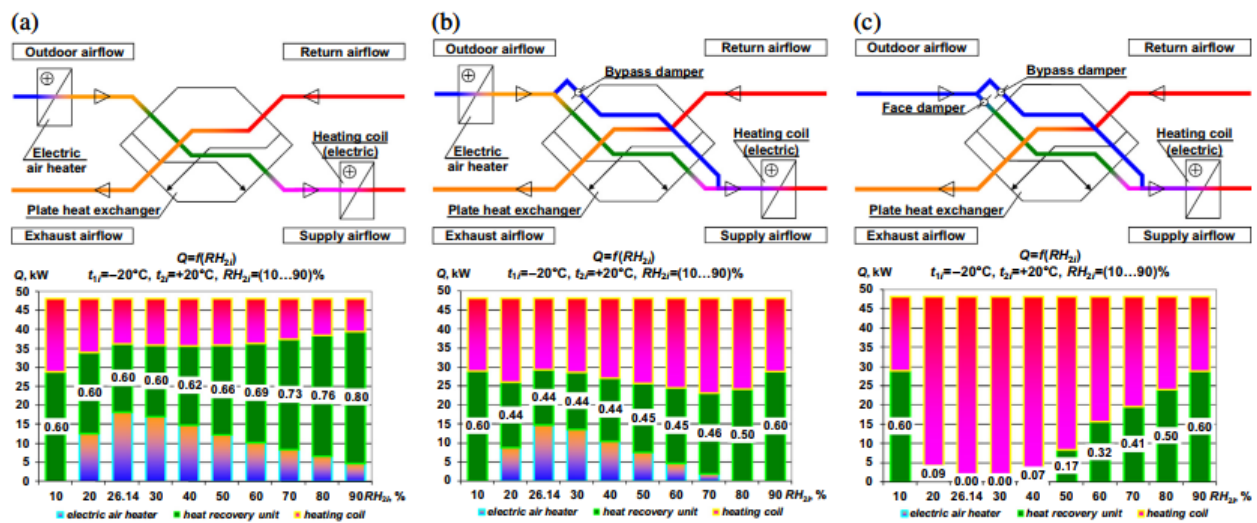


**Figure 2.1:** Comparison of heat recovery and additional energy consumption for air treatment in an air-handling unit with counter-flow heat exchanger under a) preheating b) 50 % bypass c) Variable bypass ratio required for frost-free plate surface [1]

According to Nasr et al. [23] and Phillips et al. [10], the disadvantages with the imbalance and supply fan shut-off techniques are that they cannot be used for longer periods since they create infiltration and can also compromise the indoor air quality and thermal comfort. To maintain the desired average ventilation rate, the decreased ventilation rate during the defrost cycles must be compensated by increasing the airflow rate, which in turn will decrease the heat recovery efficiency.

Moreover, the supply fan shut-off method would face challenges with buildings fulfilling the airtightness requirements of the building regulations. Due to low infiltration as a consequence of the stricter rules, the volume flow of the extracted air can become too low and the operation of the unit can stop.

Phillips et al. [10] describes the room air recirculation technique as the most efficient defrost strategy in extremely cold (arctic) climates with heating degree-days of above 7500. In such climates, it maintains the highest heat recovery compared to supply fan shut-off and other methods. The highest number of heating degree-days in Europe is 5524 (Finland, 2017) [12], thus the European climate is described as a milder one, compared to the arctic climate. In milder climates, the method of recirculating room air has the same seasonal performance as the supply fan shut-off method.

Further, with recirculation of room air, the desired average ventilation rate is maintained in the same way as with the imbalance and supply fan shut-off methods. Moreover, depending on the length of the defrost cycles, the indoor air quality can also be compromised. [10]

In conclusion, based on the above literature review, preheating outdoor air is found to be the most energy efficient frost prevention method, imbalance by reducing outdoor airflow rate is suitable for defrost and recirculation of room air is applicable for defrost in cases with more severe frost formation.

Since Airmaster has the preheating outdoor air, bypass and imbalance by reducing outdoor airflow rate methods in their ventilation units, the operation and efficiency of these will be experimentally tested.

### 3 | Heat exchanger specifications

Table 3.1 shows the specifications of the heat exchanger which will be tested.

Manufacturer	Klingenburg
Heat exchanger type	GS 25/250 (Aluminium)
Plate spacing	2.0 mm
Plate thickness	0.08 mm
Thermal conductivity	235 W/mK
Number of plates	119

**Table 3.1:** Heat exchanger specifications

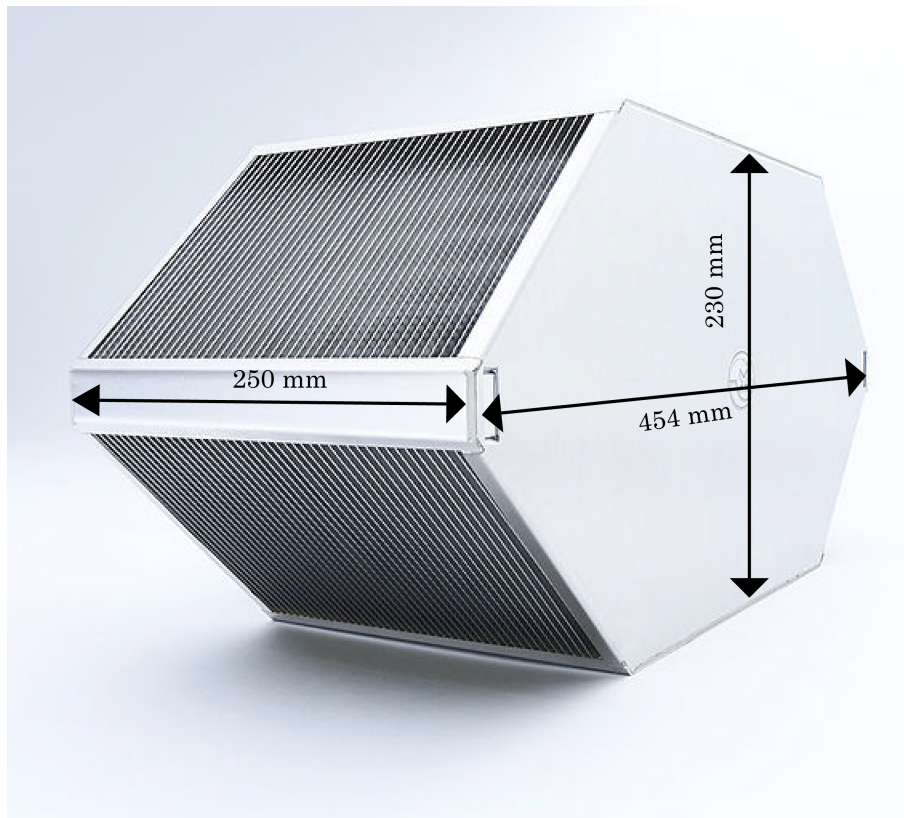


**Figure 3.1:** Klingenburg - GS 25/250 and GS-K 25/250

## 4 | Test conditions

In this chapter, information regarding the test conditions used for validating the heat recovery efficiency provided by the manufacturer and for the experiments can be found.

### 4.1 Validation test conditions

The test conditions used for verifying the performance data provided by the manufacturer are based on DS/EN 308:1997 [6]. The verification will be achieved by comparing the dry and wet heat recovery efficiency from the validation experiment with the efficiency provided by the manufacturer under the same conditions. Its purpose is to ensure that the set-up for the experiments is reliable.

Table 4.1 shows the test conditions used for verification of the performance data of the heat exchangers.

	Dry	Wet
<b>Indoor exhaust air</b>		
Temperature	25 °C	25 °C
Wet-bulb temperature	< 14 °C	18 °C
<b>Outdoor supply air</b>		
Temperature	5 °C	5 °C

**Table 4.1:** Test conditions for performance data verification according to DS/EN 308:1997 [6]

### 4.2 Experimental test conditions

#### Outdoor

Outdoor weather data from the coldest months for a number of locations, chosen based on the regions where Airmaster's products are sold, will be used to find the outdoor temperature range for the experiments. Using cumulative degree-day graphs, the severity of the frost problem will be evaluated for the different regions. These graphs also show the number of hours when a certain temperature occurs during a year.

Figure 4.1 shows the initial number of locations for which weather data is found and analysed. Hourly meteorological data in IWEC data set (1982-1999) has been downloaded from EnergyPlus [11]. The parameters which are interesting for this type of experiment are the outdoor ambient temperature and absolute humidity. Outdoor temperature is essential for frost formation in heat exchangers and absolute humidity is important for the humidity levels indoors, which also impacts freezing on the warm side of the heat exchanger [1].



Figure 4.1: Initial number of locations

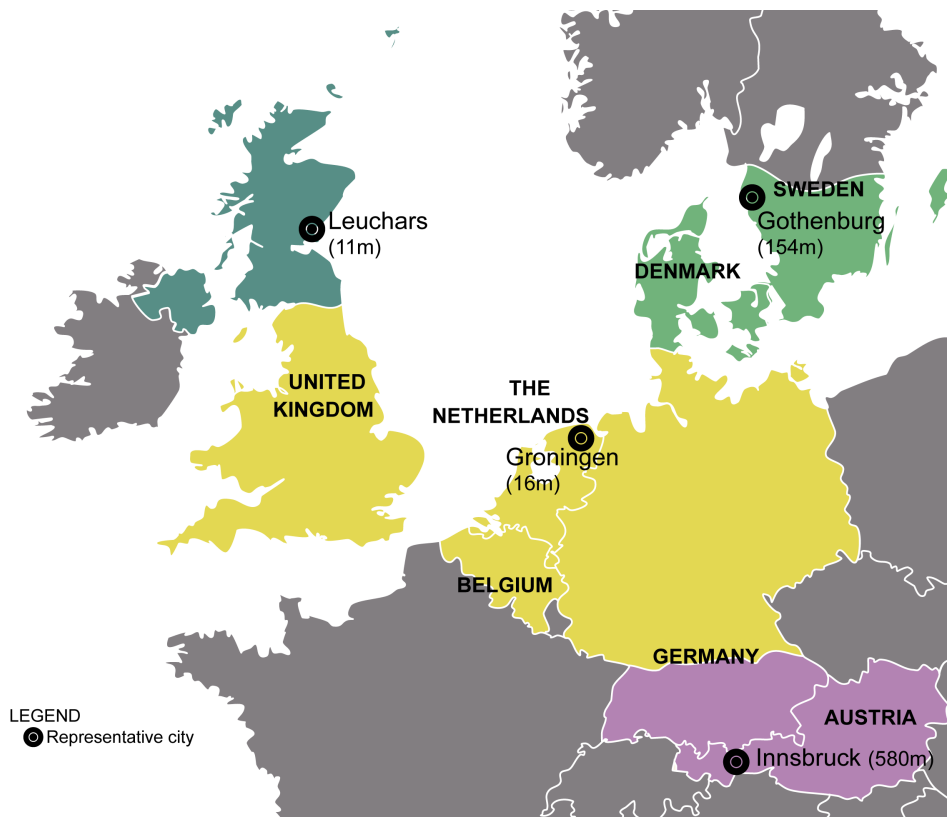
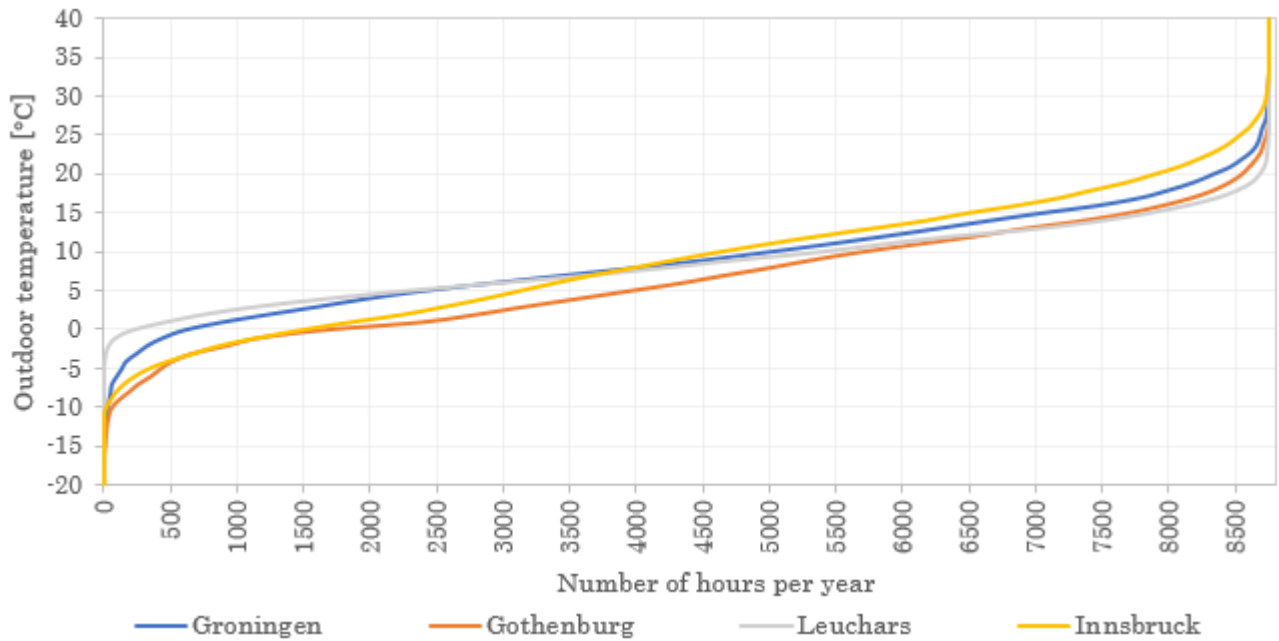
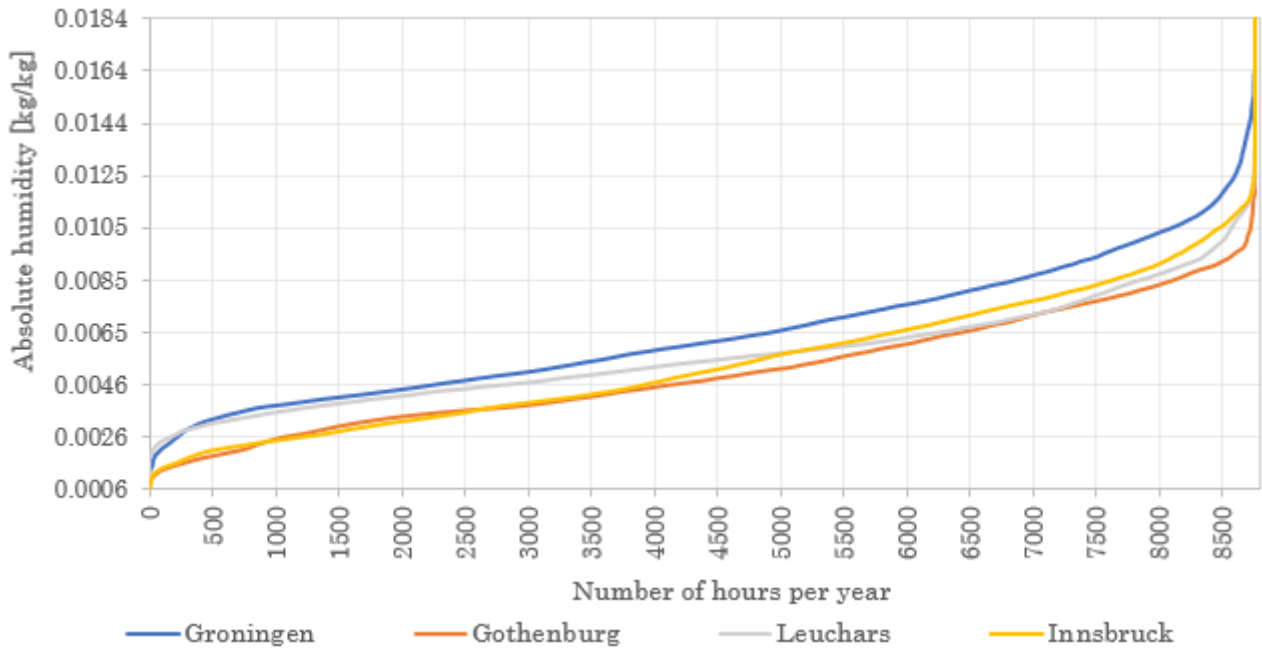


Figure 4.2: Final number of locations

After plotting outdoor temperature and absolute humidity in cumulative graphs for all the locations - figure 4.1 (shown in figure B.1 and B.2, in appendix), there have been distinguished four climatic regions each represented by one location, as seen in figure 4.2. The outdoor temperature and absolute humidity levels for some regions, for instance England, West Germany and Netherlands, have been very similar and therefore, they could be grouped in one region. Some locations having similar conditions have been excluded, as long as there is one remaining to represent the whole region. Figures 4.3 and 4.4 show the cumulative outdoor temperature and absolute humidity for the locations chosen as representative for the respective climatic zones. The graphs including all the final locations can be seen in figures B.4 and B.2, in appendix.



**Figure 4.3:** Cumulative number of hours based on outdoor ambient temperature only for the representative locations



**Figure 4.4:** Cumulative number of hours based on outdoor ambient absolute humidity only for the representative locations

To find out whether the four formed regions in figure 4.2 remain the same if only yearly working hours are considered, further analysis are made. Figure 4.5 shows the yearly percentage of hours below  $0^{\circ}\text{C}$  and below  $0.0026\text{ kg/kg}$  of outdoor absolute humidity for the representative locations for all and only working hours. The reason for looking into values below  $0^{\circ}\text{C}$  is because freezing happens with negative temperatures. When it comes to outdoor absolute humidity,  $0.0026\text{ kg/kg}$  results in 30-35 % indoor relative humidity (for office and classroom) based on the BSim simulation with regards to the coldest months (January, February, November, December). This range is chosen since it is the lowest common relative humidity range for all the representative locations, seen in figure 4.3, and because the lower the relative humidity is indoors, the higher the risk of frost is [1].

As one can see, the regions remain divided in the same way considering only working hours as well. Detailed cumulative graphs with only working hours for each region can be seen in appendix B.

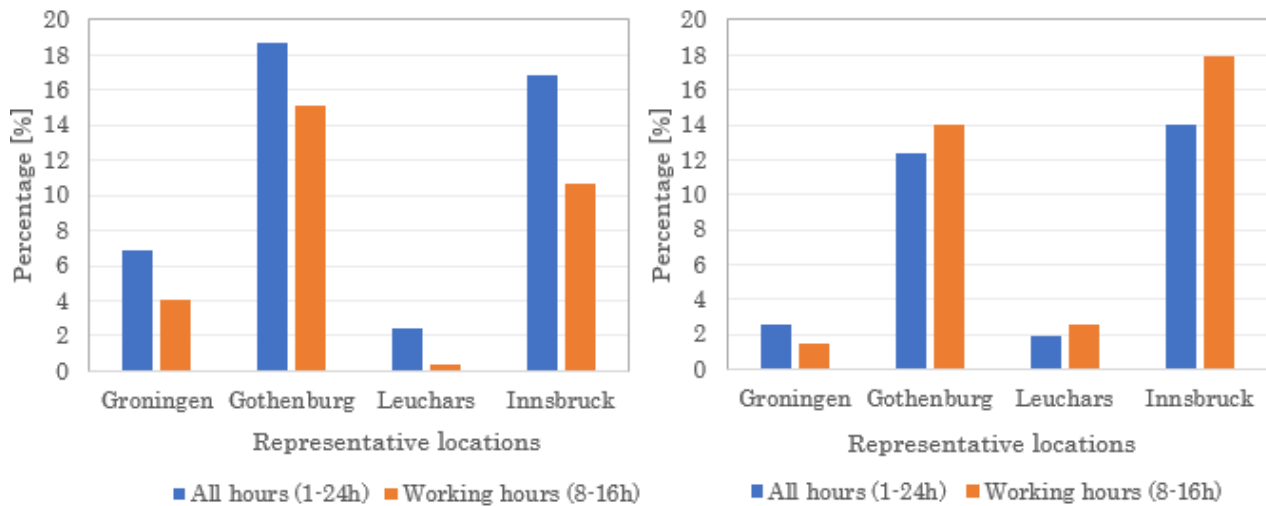


**Figure 4.5:** Yearly percentage of hours below 0 °C (left) and yearly percentage of hours below 0.0026 kg/kg absolute humidity (30-35 % indoors relative humidity) (right)

The outdoor temperature range for the experimental tests for the four locations is shown in table 4.2. It is based on the minimum ambient temperature during the working hours. The upper limit is kept at 5 °C, even though the ambient temperature rises above that. The outdoor temperature variations for the working hours during the year can be seen in figure B.6, in appendix.

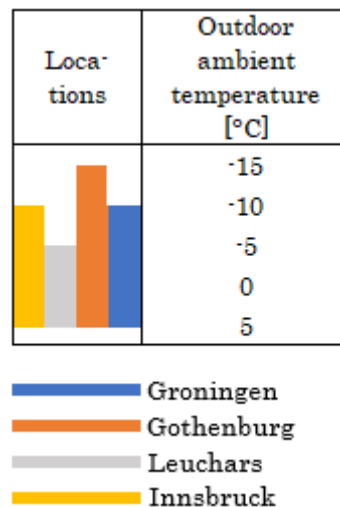


**Table 4.2:** Outdoor ambient temperature range for the representative locations

## Indoor

Regarding indoor conditions, temperature and relative humidity of the extracted air are important. Since these parameters will differ depending on the building usage type, this report focuses on two scenarios - a classroom and an office. The chosen building usage types are directly connected to the building types where Airmaster's products get installed.

To get information regarding the properties of the extracted air, BSim is used. The two scenarios are simulated, where the temperature of the extracted air is kept at around 22 °C and the relative humidity range is found by running simulations with the weather files for the representative locations for the coldest months of the year (January, February, November and December). It has been observed that

the difference in outdoor absolute humidity results in difference in the indoor relative humidity levels. Table 4.3 shows relative humidity range for the extracted air at 22 °C. The graphs with extracted air relative humidity within the working hours for the chosen locations can be seen in figures B.7 and B.8, in appendix.

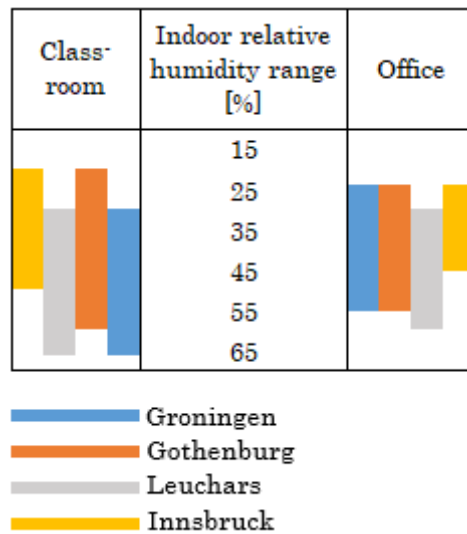


**Table 4.3:** Relative humidity range for the extracted air

The BSim model has been modelled with 24 pupils and one teacher for the classroom, corresponding to the average number of pupils in a class in the Danish schools [19] and four people in the office. The ventilation rate in the two rooms is designed and controlled based on CO<sub>2</sub> with maximum limit of 1000 ppm [33]. The input for the BSim models can be seen in appendix B.1, BSim input.

# 5 | Experimental setup and measurements

This section presents the experimental setup developed to test the performance of a counter-flow plate heat exchangers under frosting conditions, that is part of a decentralized mechanical ventilation unit.

## 5.1 Experimental setup

A schematic plan view of the experimental setup is shown in figure 5.1. The setup is designed to achieve outdoor temperatures corresponding to winter conditions and typical indoor conditions. It consists of an insulated shipping container divided into two environmental chambers: a warm chamber where the temperature and humidity is controlled by a duct electric heater and a humidifier and a cold chamber where the temperature is controlled by a cooling unit.

### Heating system

To achieve indoor conditions of a typical classroom or office, the temperature for the extracted air should be maintained at 22 °C, as described in section 4.2. For that reason, a circular electric duct heater is used to maintain the air temperature at the desired set point [36]. The heater, that is installed in the warm chamber is connected to a fan, that has the purpose to circulate the air in the room so that stratification does not occur. Moreover, in terms of control, the fan also helps to better control the temperature, as the sensor is measuring a uniform temperature of the well mixed chamber. In figure 5.1, the placement of the fan (no. 4) and the duct with the electric heater (no. 5) is shown. Both are placed at the ceiling level and the duct has a 90-degree bend towards the floor, so that the flow does not influence the extraction.

### Humidification system

The humidification system consists of a domestic water pump (no. 1), a water heater (no. 2) and the Vapac Minivap Humidifier (no. 3), as shown in figure 5.1. The pump provides water to the small water heater. After the water gets heated it is pumped to the humidifier, where it gets heated further until it boils. The steam is released into the ventilation duct after the circular electric duct heater (no. 5) [35]. The desired relative humidity that should be maintained stable is in the range 25 - 65 %, as described in section 4.2.

### Cooling system

The cooling unit consists of an evaporator placed in the cold chamber. The compressor and condenser are placed outside - on the roof of the container. The evaporator is connected to a duct system (no. 4) that provides cold air to the room, without influencing directly the air that is being supplied to the warm room. In addition, a circular electric duct heater is installed (no. 5) to defrost the evaporator and to maintain the ambient temperature in case higher set points are desired. The cooling unit is shown in figure 5.1.

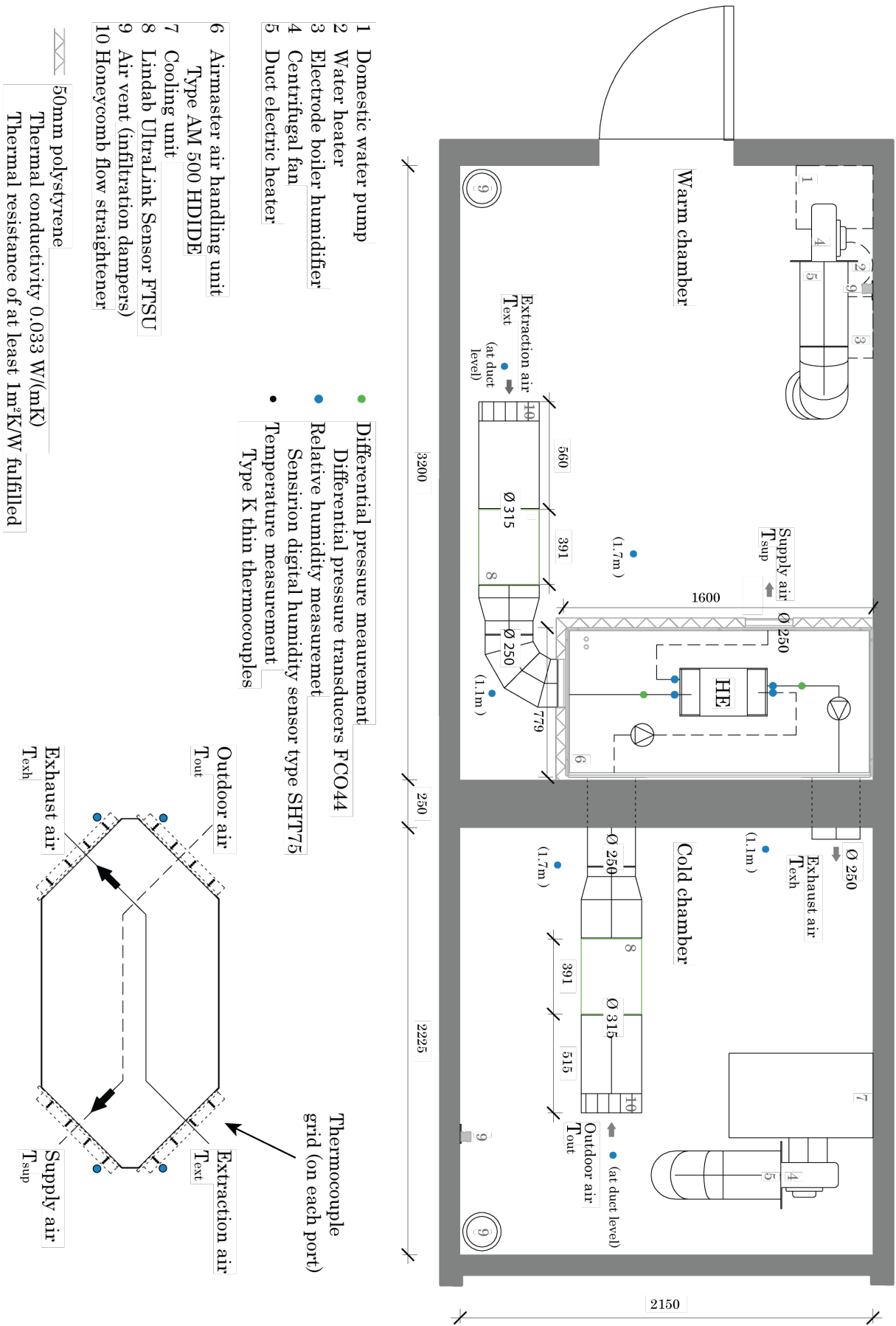


Figure 5.1: Experimental setup

## Control system

The control system is developed by Airmaster for all three systems. The humidification and heating system from the warm room can be controlled together. The parameters that can be adjusted are: temperature, relative humidity and fan speed. For the cooling unit from the cold room, the temperature and fan speed can be adjusted. Moreover, the decentralized ventilation unit has a developed control system that allows the adjustment of the following parameters:

- Airflow (by modifying the fan speed)
- Temperature supplied to the room (by activating comfort heater)
- Bypass damper

The entire experimental setup is accommodated to test the frost limits of the heat exchanger and the defrost methods described in section 2.

## Decentralized ventilation unit

The decentralized ventilation unit is placed in the warm chamber and it is tightly connected to the cold chamber through ducts. The operation principle of the unit is as following: air at outdoor conditions ( $t_{out}$ ) moves by suction in the ventilation unit passing through the heat exchanger and then is provided to the room ( $t_{sup}$ ), while the warm extraction air ( $t_{ext}$ ) moves by suction in the ventilation unit passing through the heat exchanger and then is exhausted ( $t_{exh}$ ) on the cold side, as shown in the 3D drawing in figure 5.2 and in the principle drawing of the ventilation unit in figure 5.3.

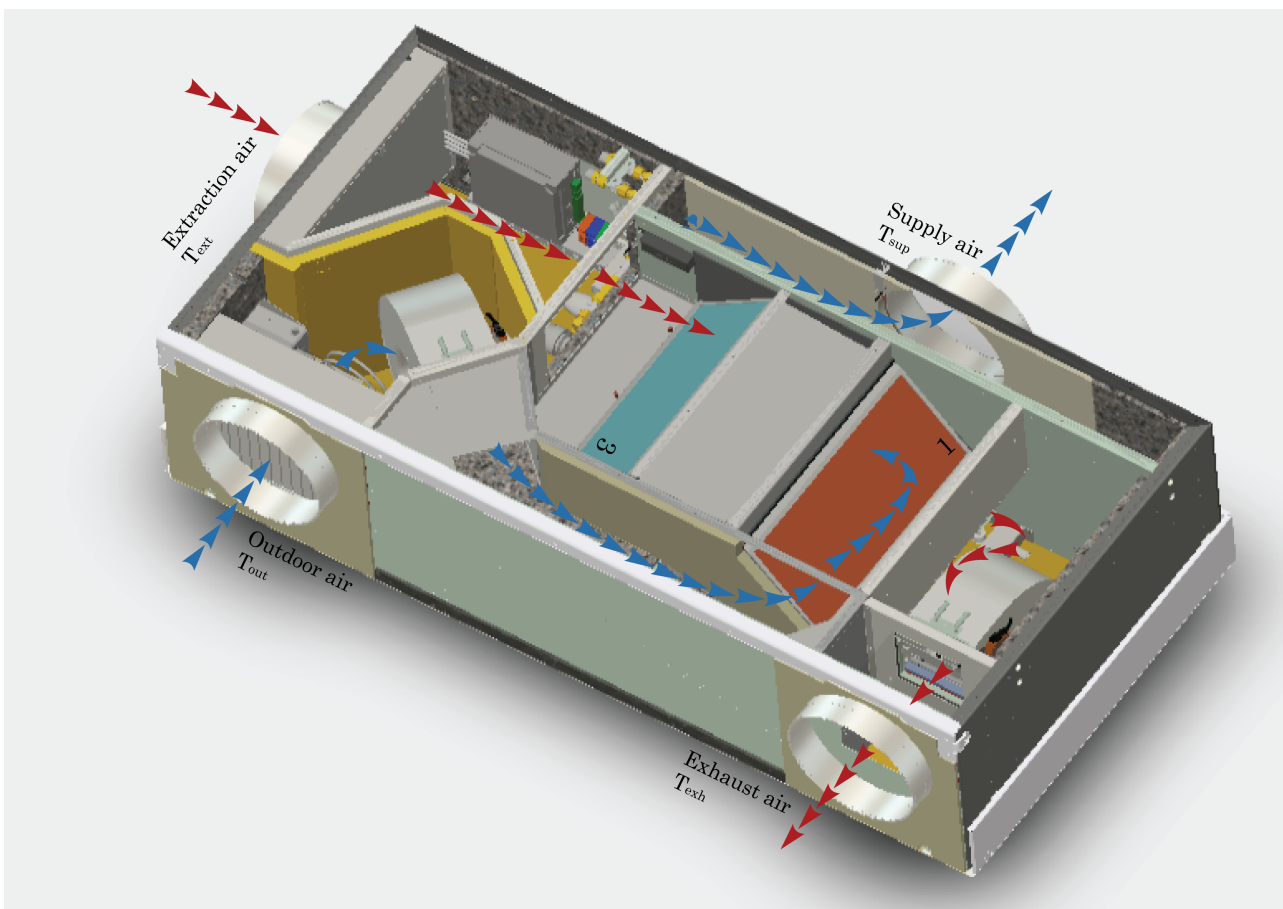


Figure 5.2: 3D drawing for AHU with airflow path

Since the ventilation unit is exposed to the ambient air conditions, insulation around the casing is needed. DS/EN 308:1997 recommends insulation material with a thermal resistance of at least  $1 \text{ m}^2\text{K/W}$  [6], therefore 50mm polystyrene with a thermal conductivity of  $0.037 \text{ W/mK}$ , fulfilling the recommendations and minimizing the heat gains from the room as shown in figure 5.1.

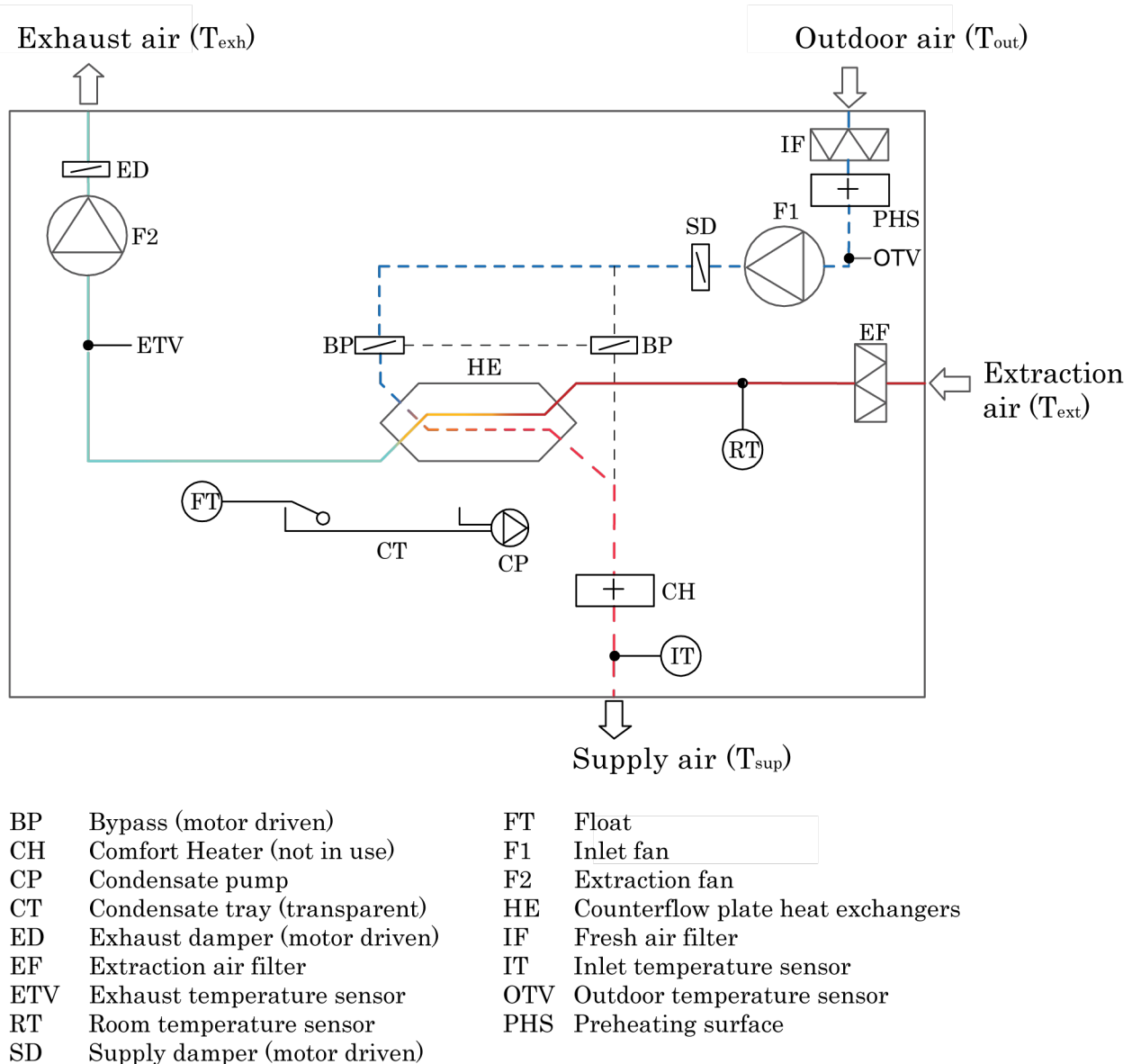


Figure 5.3: AHU working principle

## 5.2 Measurements

The parameters that are measured in order to test the performance of the heat exchangers are air temperature, relative humidity, air flow and differential pressure. For both air streams of the heat exchanger, the parameters are measured at different locations, as shown in figure 5.1.

### Temperature

The air temperature is measured with a type K thermocouple (Chromel /Alumel) that is gold coated, through sputtering technique. In this case, radiative heat exchange that can influence the measurement is decreased by using coating [18]. The temperature is measured with four grids of thermocouples on all ports of the heat exchanger. The grids are developed in accordance with the European Committee of Standardization. The dialogue regarding the position of the sensors on the grid can be seen in appendix C. Since there is a risk of uneven temperature distribution, 16 temperature measuring points are distributed evenly across the grid. The recommended number of temperature sensors for rectangular ducts is 9, according to ASHRAE [3]. In figure C.2 in appendix, the installation of temperature sensors on the grid is shown and figure 5.1 shows the positioning of the grids on the heat exchanger ports. The calibration process is described in appendix C.1.



**Figure 5.4:** Thermocouple grid placed on the heat exchanger

### Relative humidity

The relative humidity is measured with a Sensirion digital humidity sensor type SHT75. This type of sensor can be used for both temperature and relative humidity measurements. In the ventilation unit, as shown in figure 5.1, the relative humidity is measured with the Sensirion sensor, while the temperature measurement is disregarded, since there is the grid of thermocouples. However, to monitor the temperature and relative humidity in the two chambers, 3 sensors are used, in each room. The placement of the sensors can be seen in figure 5.1. The height and placement of each sensor is as shown in 5.1.

Table 5.1 show the measuring range and the uncertainty of a Sensirion sensor, provided by the manufacturer, after it is calibrated individually [31]. To check the performance of the sensors, a comparison with a reference thermometer is performed. The details are presented in appendix C.1.

Measured quantity	Measuring Range		Uncertainty	Units
	Min	Max		
Temperature	-40	123.8	$\pm 0.3$	$^{\circ}\text{C}$
Relative humidity	0	100	$\pm 1.8$	%

**Table 5.1:** Sensirion sensor for relative humidity and temperature details [30]

## Airflow

The airflow rate is measured on both airstreams: for the outdoor - supply airstream the measurement is performed on the outdoor side, while for the extraction - exhaust airstream the measurement is performed on the extraction side, see figure 5.1. The device used is an UltraLink FTSU with a diameter of 315 mm and a length of 391 mm. The flow is measured with an angled ultrasonic beam that provides high accuracy. Nonetheless, to reach good measurement accuracy some recommendations should be fulfilled: the UltraLink should be placed on the suction side of the fan and a flow straightener (no. 10) is used before the device, check figure 5.1. [20]



**Figure 5.5:** Lindab Ultralink extraction airflow direction - warm room



**Figure 5.6:** Lindab Ultralink supply airflow direction - cold room

Table 5.2 shows the uncertainty given by the manufacturer [20] for the velocity range of 0.5 - 15 m/s. The uncertainty is  $\pm 5\%$  for a straight duct.

Measured quantity	Measuring Range		Uncertainty	Units
	Min	Max		
Velocity	0.5	15		m/s
Airflow			$\pm 5$ or $\pm 1$	% or l/s

**Table 5.2:** UltraLink details [20]

## Differential pressure

The pressure difference is measured using a pressure transducer FCO44 manufactured by Furness Control Limited that has a range of  $\pm 500$  Pa. The measurement is performed on the extraction - exhaust side (warm side) of the heat exchanger. The aim is to detect pressure drop increase caused by frost growth on the plates of the exhaust side of the heat exchanger. Pressure taps are drilled on the surfaces on which flow passes, therefore measuring static pressure.

A pressure tap is on the extraction side on the plate separating the extraction and supply side as shown in figure 5.8. The second pressure tap is on the side of the exhaust air as shown in figure 5.7.

More details about the pressure transducer and the calibration can be found in appendix C.1.



**Figure 5.7:** Pressure tap on the side



**Figure 5.8:** Pressure tap on the extraction side

### 5.3 Test procedure

In this section, the guidelines regarding the test procedures have been summed up. They have been gathered from several standards since one standard does not contain all of the information. During the experiments, the aim is to follow these instructions. However, it will be noted under each experiment, if there are any which are not followed.

- Mean values for the respective measurement parameters shall be used to define the performance of the heat exchanger and calculate the heat recovery efficiency. [6] [13]
- The maximum allowed deviation in a measuring plane is  $0.05 \cdot (t_{out} - t_{sup})$  [6].  $t_{out}$  - temperature of outdoor air;  $t_{sup}$  - temperature of supply air to the room
- If the maximum deviation in a measuring plane is exceeded, the mean temperature shall be calculated taking into account the local flow velocity of each measurement point on the plane. [13] Comment: Even if the maximum deviation is higher than the allowed values, the arithmetic mean values will be used, since the local flow velocity of each measurement point is not measured.
- Steady-state conditions shall be obtained and maintained for minimum 1 hour before the measurement starts. Steady-state conditions are achieved when the measured variables remain within the tolerances given in table 5.3 without altering the set points. [5]

Measured quantity	Uncertainty of measurement
Dry bulb temperature	$\pm 0.2$ K
Wet bulb temperature	$\pm 0.3$ K
Airflow rate	$\pm 3$ %

**Table 5.3:** Measurement uncertainties [5]

- The duration of the measurement shall be minimum 30 minutes. [6]
- The measurement interval shall be maximum 30 seconds. [5]
- During measurements, the arithmetic mean values and individual measurements can deviate from the set values within the limits given in table 5.4. [5]

Measured quantity	Permissible deviation of	
	arithmetic mean values from set values	individual measured values from set values
Dry bulb temperature	$\pm 0.3$ K	$\pm 1$ K
Wet bulb temperature	$\pm 0.3$ K	$\pm 1$ K
Volume flow rate	$\pm 5$ %	$\pm 10$ %

**Table 5.4:** Allowed deviations for arithmetic mean values and individual measurements [5]

- For defrost testing, the temperature of the extracted air shall be  $20 \pm 3$  K. [4]

# 6 | Performance data verification

The purpose of verifying the performance of the heat exchanger is to verify the created experimental set-up and its reliability. By measuring the temperatures on the four ports of the heat exchanger with certain extraction and outdoor conditions, the measured temperature efficiency is compared with the calculated one from the manufacturers' software, where the same conditions (temperature, relative humidity and mass flow) are input. Moreover, exhaust temperature comparison is also provided.

The performance verification is established for dry and wet conditions by following the test conditions stated in table 4.1, section 4.1. The tests are conducted with infiltration dampers closed and open (opening equivalent to 1 l/s pr. m<sup>2</sup> of floor area at 50 Pa pressure difference in the warm room and entirely open damper in the cold room). The purpose of having both open and closed damper tests is to see how the flow will be affected. The results with the open dampers are presented in appendix D. Furthermore, the maintained conditions in terms of temperature, relative humidity and mass flow for the duration of the experiments can also be found in appendix D.

Tables 6.1 and 6.2 show the deviations of the mean and individual measurements from the set points. The cells marked with red represent values exceeding the deviation limits given in table 5.4, section 5.3.

Parameters	Set points	Unit	Deviation - mean values	Unit	Deviation - individual measurements		Unit
					max	min	
T_outdoor air	5	°C	-0.2	°C	0.8	-1.2	°C
T_extraction air	25	°C	0.0	°C	1.0	-1.4	°C
RH_extraction air	0.22	-	0.01	-			
Mass flow_outdoor air	0.053	kg/s	2.8	%	6.8	-1.2	%
Mass flow_extract air	0.053	kg/s	-0.2	%	2.4	-2.6	%

**Table 6.1:** Mean and individual measurement deviations for the dry test (infiltration dampers closed)

Parameters	Set points	Unit	Deviation - mean values	Unit	Deviation - individual measurements		Unit
					max	min	
T_outdoor air	5	°C	0.0	°C	1.1	-0.7	°C
T_extraction air	25	°C	-0.1	°C	0.9	-1.4	°C
RH_extraction air	0.51	-	0.00	-			
Mass flow_outdoor air	0.053	kg/s	-5.9	%	-2.0	-9.2	%
Mass flow_extract air	0.049	kg/s	-6.2	%	-2.6	-9.1	%

**Table 6.2:** Mean and individual measurement deviations for the wet test (infiltration dampers closed)

Figures 6.1 and 6.2 show the temperature efficiency comparison between measured values and values provided by the manufacturers' software. The close results provide confidence in the reliability of the test set-up. The differences could be because of difference between the current set-up and the one that

the manufacturer has used to define extraction and exhaust temperatures.

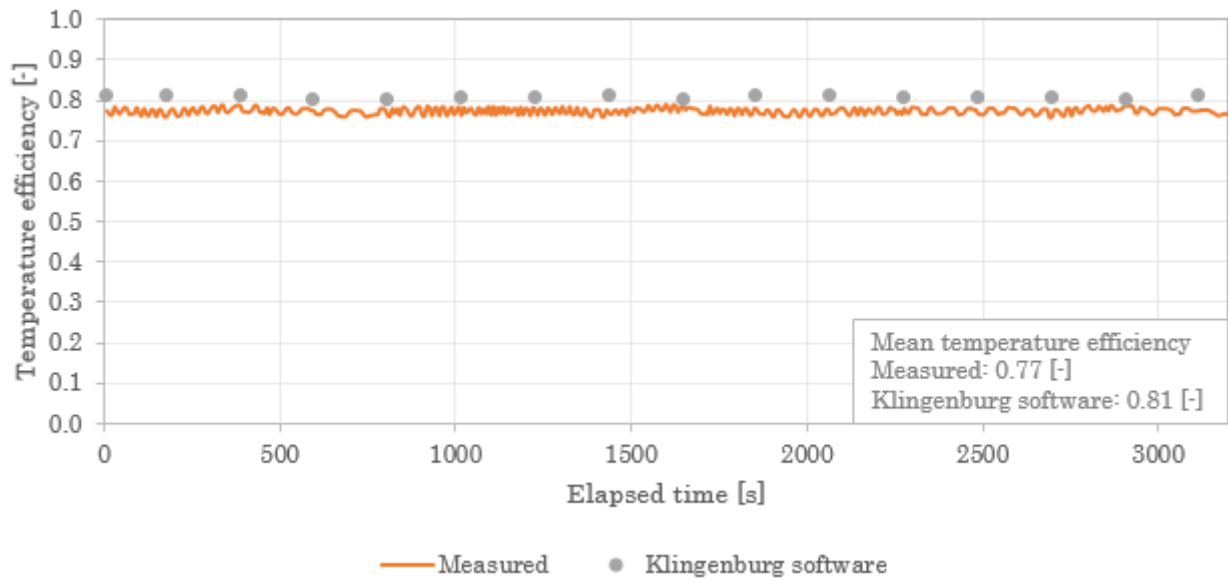


**Figure 6.1:** Temperature efficiency comparison for the dry test (infiltration dampers closed)

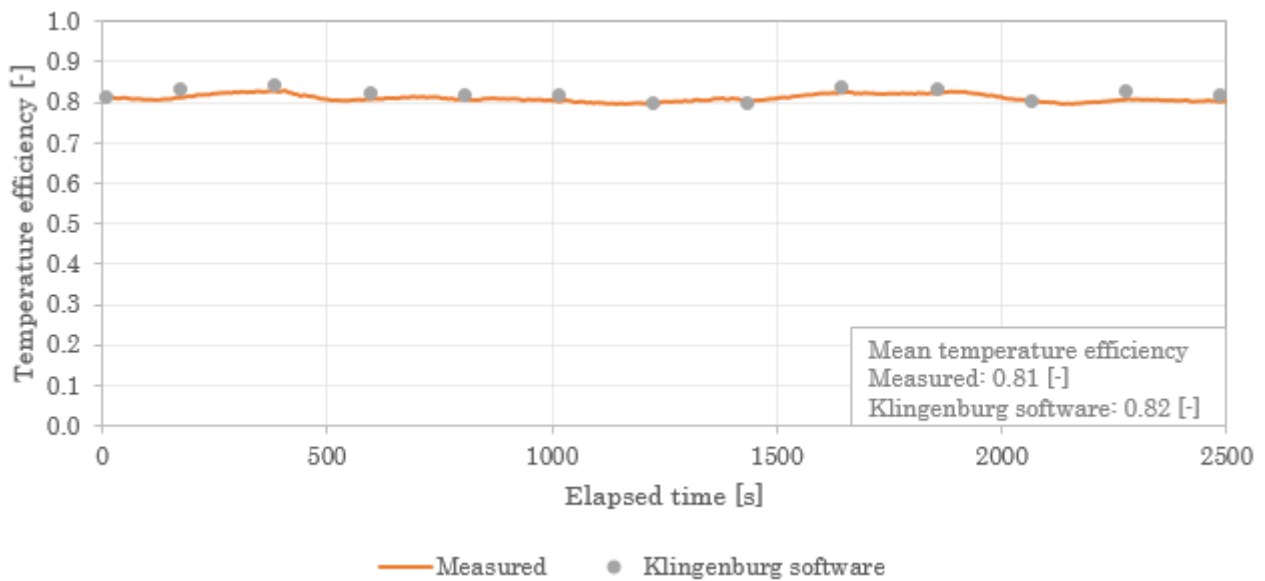


**Figure 6.2:** Temperature efficiency comparison for the wet test (infiltration dampers closed)

Figures 6.3 and 6.4 provide comparison for exhaust temperature. For the dry test, the measured exhaust temperature is close to the one provided by the manufacturer under the same conditions. However, when condensation occurs in the heat exchanger (figure 6.4), the measured exhaust temperature becomes lower than what the manufacturer shows with approximately 2 °C. That is also confirmed by the amount of measured condensation (absolute humidity difference between extraction and exhaust) and the calculated condensation from the software. Due to the lower measured exhaust temperature, the measured condensation amount is greater than the one calculated by the program, as shown in figure 6.4. As a result, with freezing outdoor conditions, the heat exchanger can in reality freeze without it being detected by the manufacturer's software.

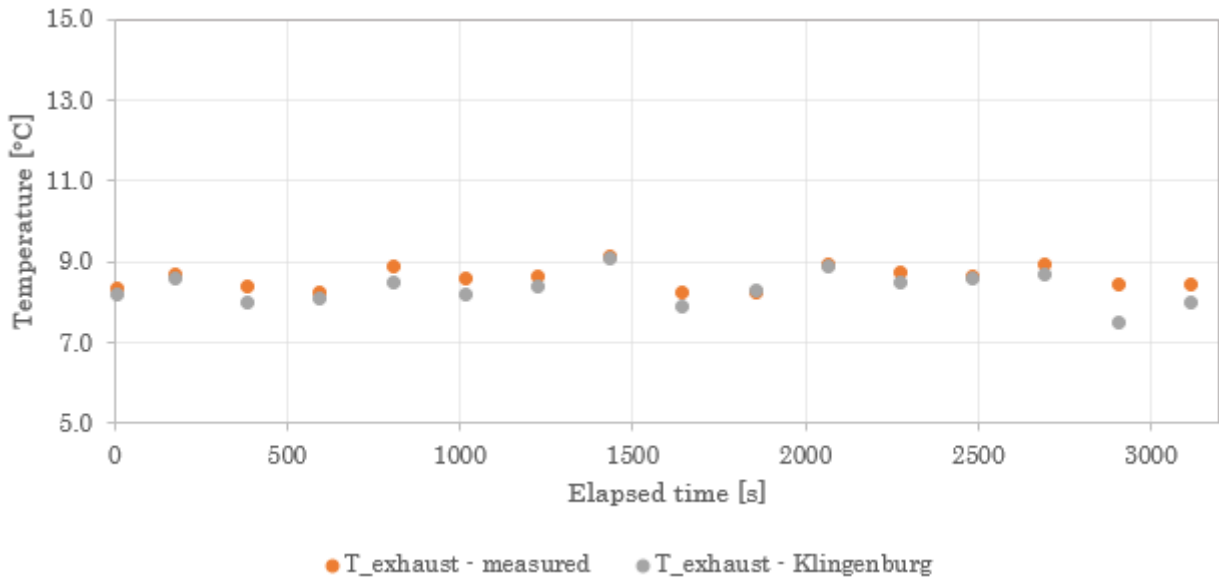


**Figure 6.3:** Exhaust temperature comparison for the dry test (infiltration dampers closed)

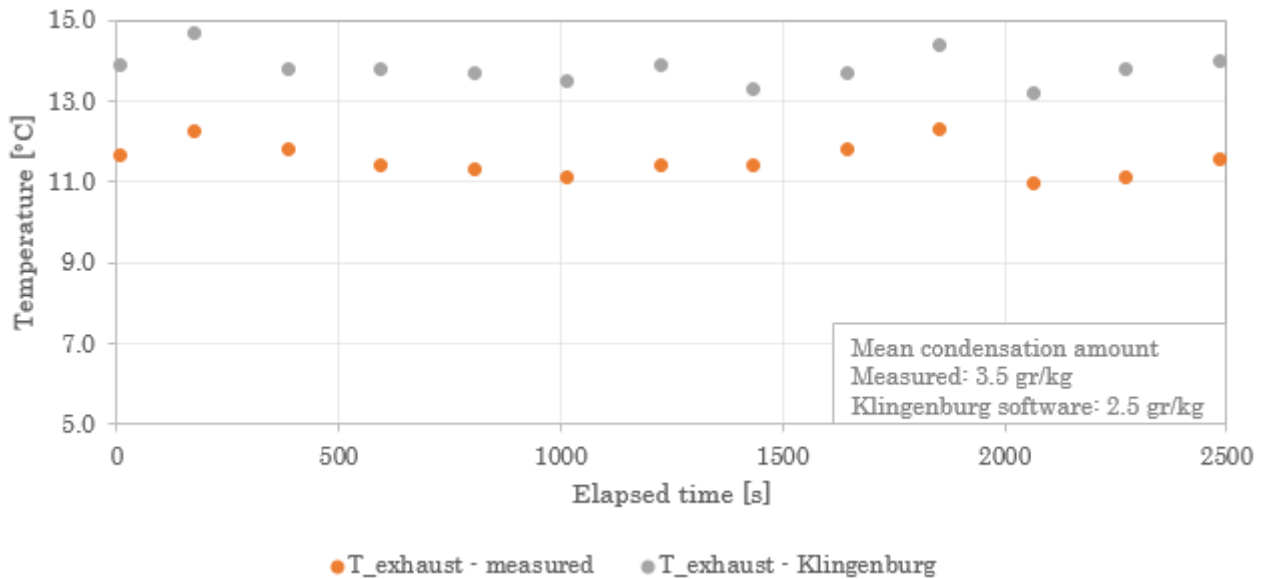


**Figure 6.4:** Exhaust temperature comparison for the wet test (infiltration dampers closed)

The difference in exhaust temperature is looked into further. Table 6.3 shows the input and output conditions for one measurement point during the wet test. Even though the input conditions are the same and supply temperatures are very close, the difference between measured exhaust temperature and the one provided by manufacturer’s software is 1.9 °C. Figure 6.3 illustrates the air treatment process for the warm and cold airstreams.

Input conditions		Output conditions	
Outdoor temperature	5.3 °C	Measured supply temperature	21.5 °C
Extraction temperature	25.0 °C (52.9 kJ/kg)	Supply temperature (Klingenburg)	21.7 °C
Extraction relative humidity	55 %	Measured exhaust temperature	12.3 °C (30.0 kJ/kg)
Mass flow supply	0.050 kg/s	Exhaust temperature (Klingenburg)	14.4 °C (34.7 kJ/kg)
Mass flow extraction	0.045 kg/s		

**Table 6.3:** Input and output conditions for one measurement point with wet conditions

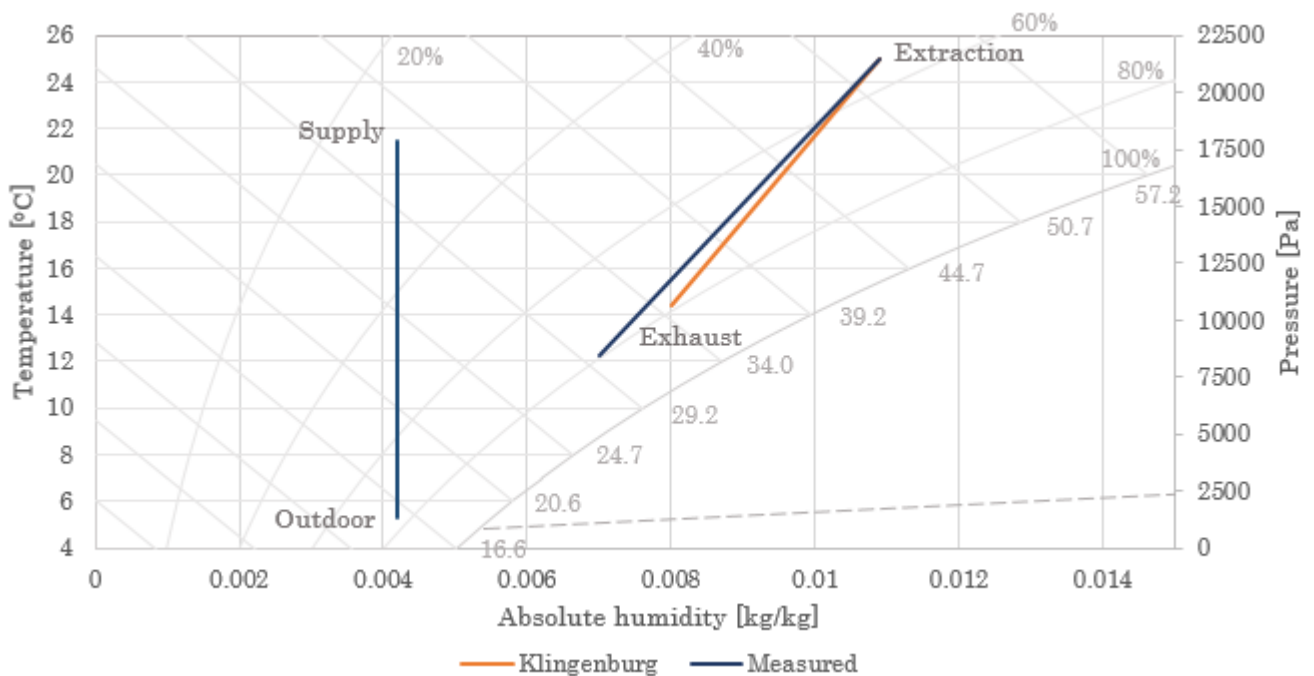


**Figure 6.5:** Air treatment on the warm and cold side measured vs. Klingenburg

The reason for the lower exhaust temperature with wet conditions is not known. The wet test has been repeated with balanced flows as well but the difference in temperature remained. The results with balanced flows can be seen in appendix D.

In conclusion, the reliability of the test set-up has been documented by verifying the performance data of the heat exchangers. However, even though the measured temperature efficiencies are close to the ones provided by the manufacturer, there is a significant difference between the exhaust temperatures with wet conditions.

# 7 | Frost formation limits

This chapter reveals the findings from the experimental tests regarding frost formation limits. In the beginning, a description of the conditions under which the experiments are conducted is provided, followed by analyses with regards to critical indoor relative humidity ranges in terms of frost formations. Lastly, the results from the experiments and Airmaster's current frost prevention practise are analysed.

The purpose of ascertaining the frost formation limit value is to find the circumstances that will create ice in the heat exchanger. By knowing this limit, the energy consumption of defrost can be addressed and a control strategy may follow the limit values.

A key element for frost formation is the amount of humidity in the extracted air. According to Pacak et al. [2], the higher the relative humidity is, the more energy from latent heat there is in the air and consequently, the lower the outdoor air temperature can be before the plate surface temperature falls to freezing conditions. Pacak also states that with higher relative humidity, frost formation starts close to the exit region of the exhaust side, while with lower relative humidity, it starts inside the heat exchanger, where the plate surface temperature gets below 0 °C.

## 7.1 Test procedures

The test conditions and procedures for the experiments were defined previously. They consisted of 22 °C as indoor temperature and 20-65 % as indoor relative humidity, steady-state conditions for min. 30 minutes for the duration of the measurements and one hour before the experiments start, followed by maximum deviation limits for the measured variables (sections 5.3 and 4.2).

The aim of the frost detection experiments was to detect under which outdoor temperature frost would occur in the heat exchanger with different indoor relative humidity conditions. Means of detecting frost were observing the pressure drop over the warm side of heat exchanger and also using the camera installed on the exhaust port for visual evaluation.

Nonetheless, with a cooling system that was undersized and with several other problems (more information in chapter 11), the initial plans and intentions changed. The cold room could not get below -7.5 °C during the measurements. It resulted in -3 °C as mean value on the thermocouple grid measuring outdoor air and that temperature was not low enough to cause frost formation on the warm side. The difference between the measured temperature in the cold room and on the thermocouple grid could be because the conditions in the ventilation box are warmer and the cold air gets heated up until it reaches the thermocouples. The warmer conditions in the box could be because it is located in the warm room and also due to the warm airstream heating the surfaces inside the box. With that in mind, instead of detecting critical outdoor conditions, the focus was shifted to detecting under which exhaust air temperature frost starts forming in the exit region of the exhaust port.

Several changes were made to reduce the exhaust temperature. Firstly, the temperature in the warm room had to be decreased. Moreover, imbalance between the supply and extraction flows was applied, where the extraction was decreased and supply increased.

Additionally, even though frost did form, it was difficult to capture the moment when it started forming.

The tools that were used - pressure drop transducer and camera did not reflect frost formation. The pressure drop did not increase and frost was not clearly visible on the camera. Therefore, the ventilation box had to be opened for visual inspection. The downside of detecting frost only visually is that frost formation inside the heat exchanger cannot be detected and that is where frost would start forming with low (20-30 %) relative humidity. [2]

## 7.2 Risk of frost for the chosen geographical locations

Before running the experiments, analysis on indoor relative humidity - outdoor temperature relation was done. The purpose was to find out which indoor air relative humidity ranges correspond to outdoor negative temperature values during the working hours. The findings from this investigation helped defining the relative humidity ranges that need to be tested for the frost formation experiments.

The results in figures 7.1 and 7.2 are obtained from BSim simulations. They present the relation between the indoor relative humidity (with 22 °C) and outdoor temperature. For classrooms and offices, with relative humidity above 41 % and 37 %, respectively, the outdoor temperature does not fall below 0 °C. This relative humidity limit is the same for the rest of the locations – Groningen, Innsbruck and Leuchars, shown in section E.1.1, in appendix. As for Leuchars, the minimum outdoor temperature for the whole year during the working hours is -1.3 °C for a very short period. Therefore, this location and the area it is representing (Scotland) can be considered as out of risk for frost formation.

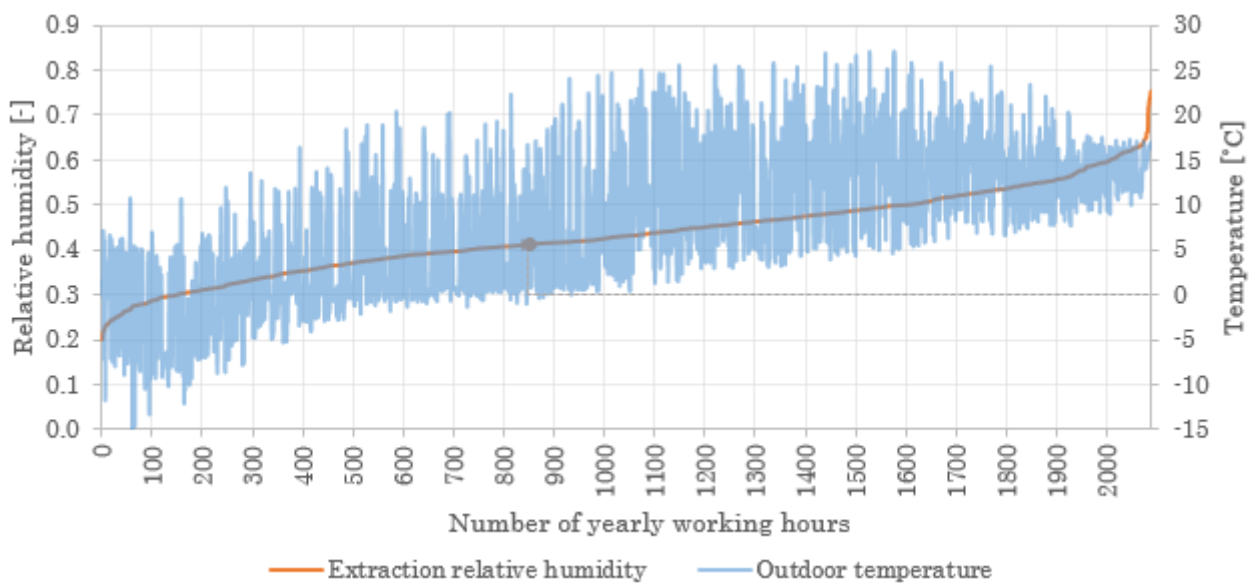


**Figure 7.1:** Indoor relative humidity - outdoor temperature relation for Gothenburg - classroom

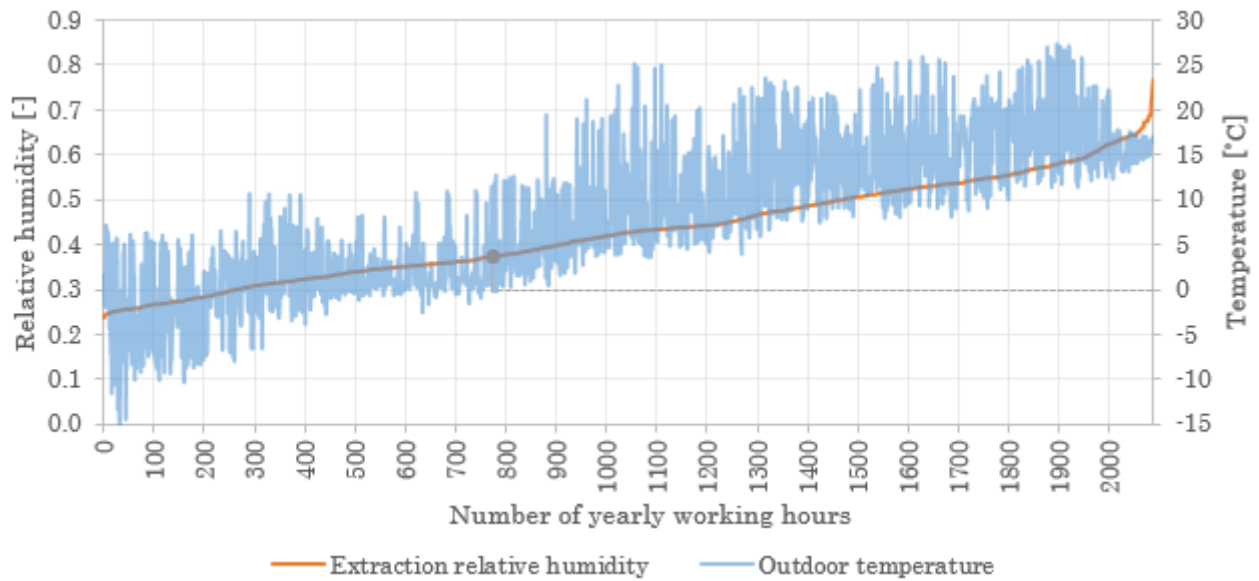


**Figure 7.2:** Indoor relative humidity - outdoor temperature relation for Gothenburg - office

Finally, it can be stated that indoor relative humidity range during frost conditions is up to 41 % for classrooms and 37 % for offices.

Figure 7.3 shows what portion of the total yearly working hours the critical indoor relative humidity ranges, linked to outdoor temperatures below 0 °C, represent for each location. Gothenburg and Innsbruck have the highest percentage of critical indoor humidity ranges.

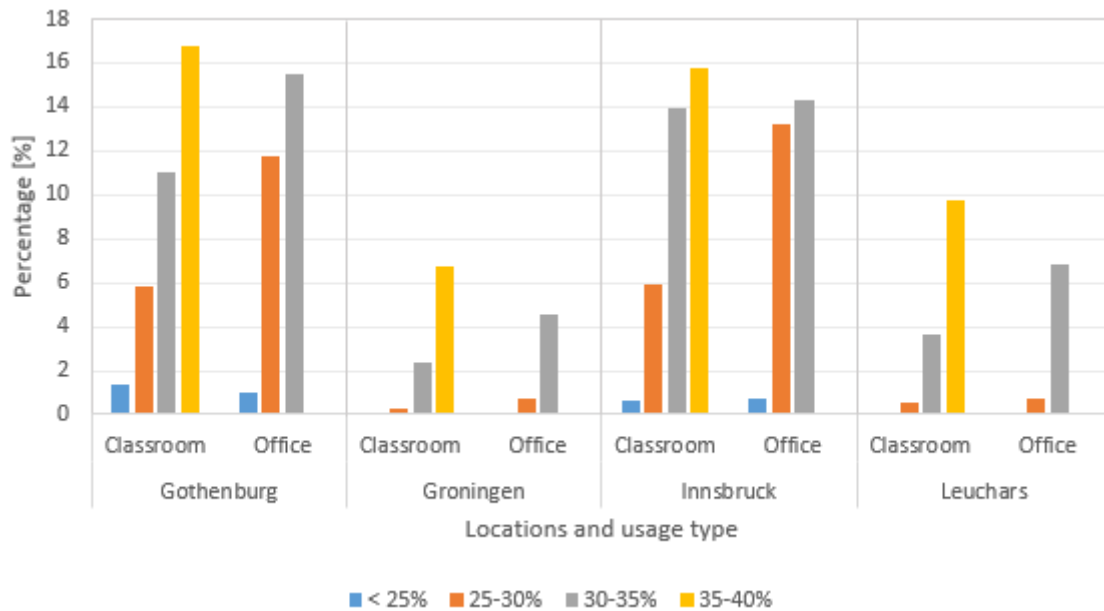


**Figure 7.3:** Percentage of critical indoor relative humidity ranges from the total number of yearly working hours with 22 °C as indoor temperature

## 7.3 Test conditions and results

### 7.3.1 Test conditions

The pre-defined extraction temperature for the tests is 22 °C and the relative humidity range is determined based on the results in the previous section. Due to the need for decreasing the extraction temperature, the indoor parameters had to be adjusted. Table 7.1 presents both actual (measured) indoor parameters with lower extraction temperature and corresponding relative humidity and what these conditions would be equivalent to, if the extraction temperature was 22 °C.

Experiment	Indoor parameters	Equivalent to:
Condition 1	22 °C and 22 % RH	22 °C and 22 % RH
Condition 2	16 °C and 38 % RH	22 °C and 27 % RH
Condition 3	15 °C and 46 % RH	22 °C and 30 % RH
Condition 4	16 °C and 58 % RH	22 °C and 40 % RH

**Table 7.1:** Frost formation test conditions

The recalculation from actual indoor parameters to equivalent is done in the following way. First, the absolute humidity for the actual indoor parameters is calculated using the formula in equation 7.1.

Calculation of absolute humidity: [24]

$$x = 0.622 \cdot \frac{\varphi \cdot P_s}{P - (\varphi \cdot P_s)} \left[ \frac{kg \text{ water}}{kg \text{ dry air}} \right] \quad (7.1)$$

$x$  – absolute humidity  $\left[ \frac{kg \text{ water}}{kg \text{ dry air}} \right]$

$\varphi$  – relative humidity [-]

$P_s$  – saturation pressure [Pa]

$P$  – atmospheric pressure [Pa] (101325 Pa)

Calculation of saturation pressure: [34]

$$P_s = 610.78 \cdot EXP \left( \frac{t}{t + 238.3} \cdot 17.2694 \right) [Pa] \quad (7.2)$$

$t$  – temperature [°C]

Afterwards, the relative humidity is calculated for extraction temperature of 22 °C using the same formula in equation 7.1 and isolating  $\varphi$ .

$$\varphi = \frac{P \cdot x}{P_s \cdot (0.622 + x)} [-] \quad (7.3)$$

### 7.3.2 Results

#### Frost formation limit

Figure 7.4 shows the test conditions on an Ix diagram. The lines for the different conditions indicate the air treatment process and correspond to mean temperature values. During the experiments, it was observed that for all the relative humidity levels, frost on the exit region of the exhaust side appears with 0 °C mean exhaust temperature. However, it is not possible to say when it might have started inside the heat exchanger. Detailed description of each experimental condition can be found in section E.1, in appendix.

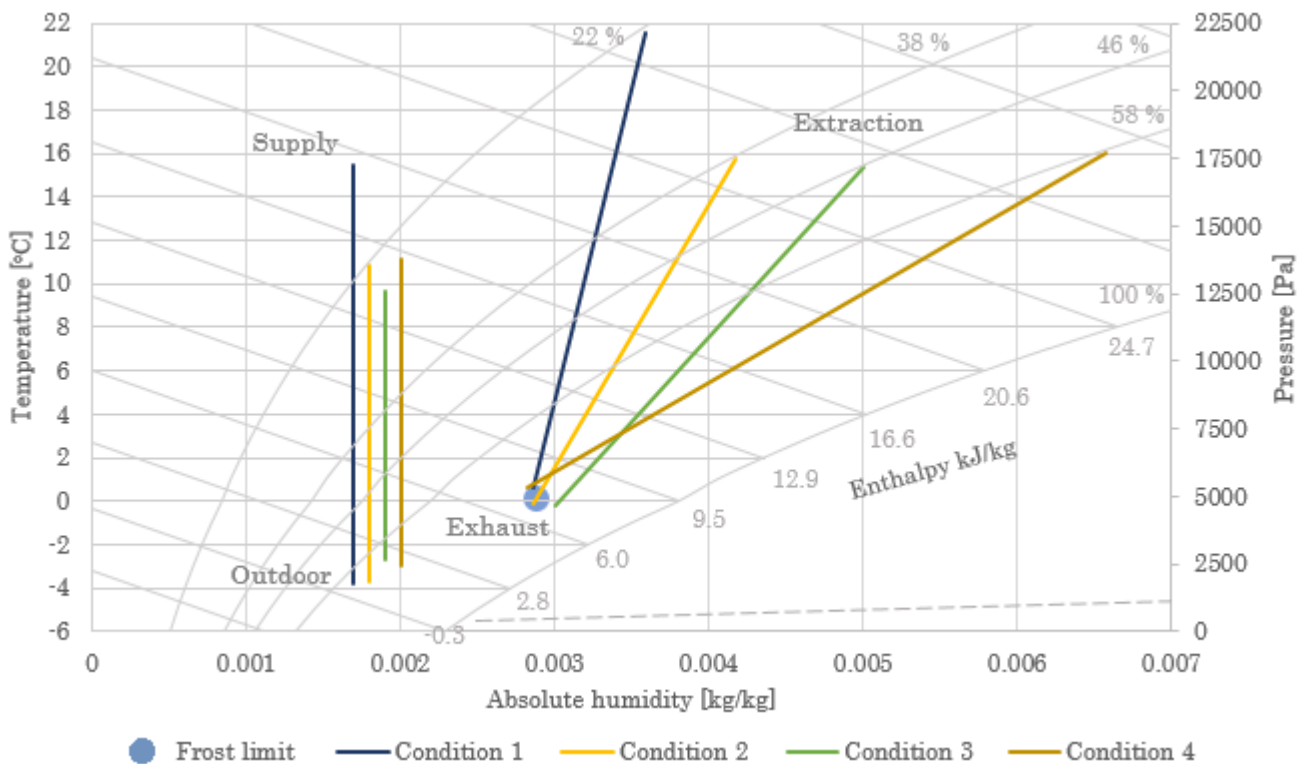
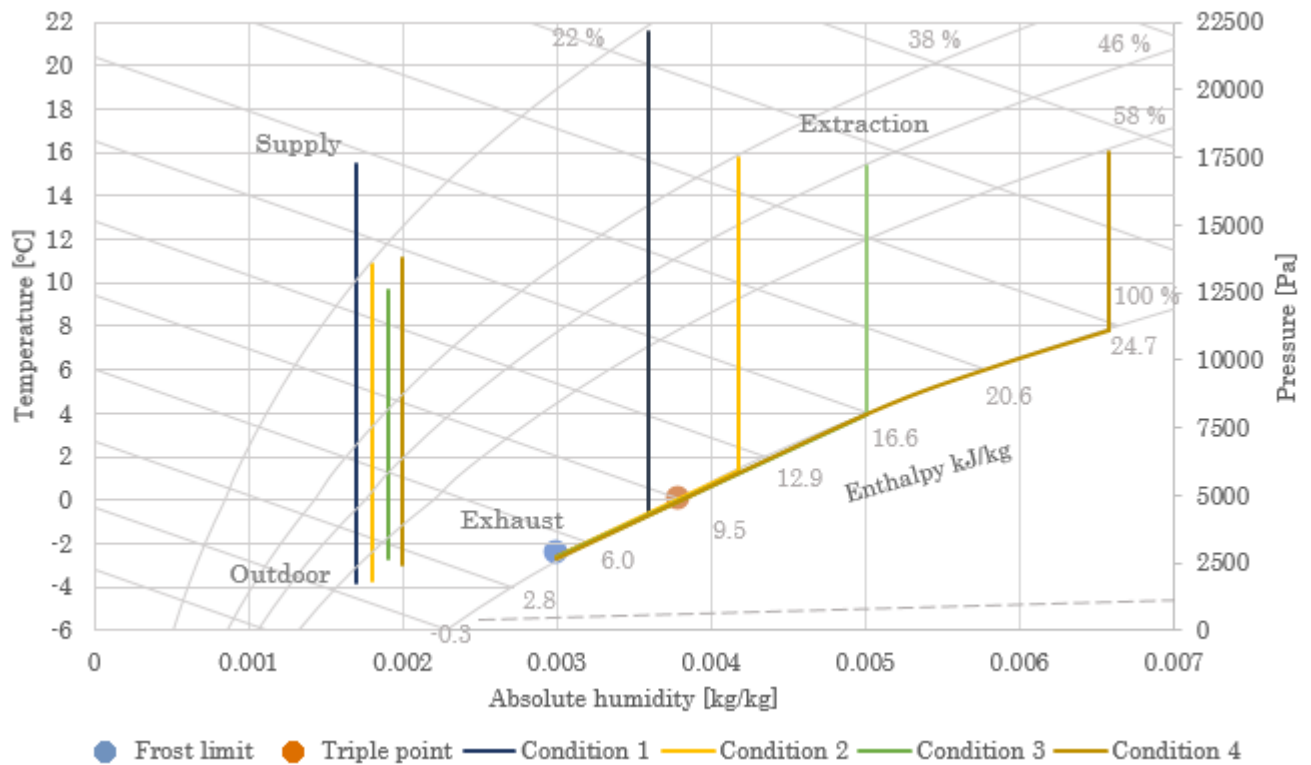


Figure 7.4: Frost formation test conditions presented on an Ix-diagram - mean temperatures

Figure 7.5 also shows how the air is treated during the different test conditions. However, the exhaust temperature that is shown this time is the minimum local temperature on the thermocouple grid. The figure shows that the higher the relative humidity is inside, the more condensation occurs before the temperature drops to the freezing point. The frost limit considering minimum exhaust local temperature is around -2.5 °C, seen in detail in figure 7.6.



**Figure 7.5:** Frost formation test conditions presented on an Ix-diagram - mean temperatures for outdoor, supply and extraction; minimum local temperature for exhaust

What was observed during the experiments was that due to the low level of water vapour in the air with 22 % relative humidity (condition 1), frost formation started without condensation. The water vapour in the air turned directly into a very thin layer of frost on the coldest part of the port. The reason for that is because the dew point for that condition ( $-0.8\text{ }^{\circ}\text{C}$ ) is below the triple point ( $0\text{ }^{\circ}\text{C}$ ). The triple point (gas-liquid-solid point) corresponds to the pressure at  $0\text{ }^{\circ}\text{C}$  below which liquid cannot exist [26]. As a consequence, it would take more time for frost to build up with relative humidity ranges corresponding to dew point value of below  $0\text{ }^{\circ}\text{C}$ .

Figure 7.6 presents the temperature gradient on the exhaust port for all the test conditions. Section E.1 in appendix provides the graphs with the mass flow, temperature and relative humidity for each condition.



**Figure 7.6:** Temperature gradient on exhaust port for all test conditions

With low relative humidity (condition 1 - 22 %), the exhaust temperature could fall low enough to form frost without the need of creating an imbalance between the supply and extraction flow. With the increase of relative humidity, the need of imbalance arose. To be able to maintain the low exhaust temperature, the supply air had to be increased, while exhaust - decreased. With condition 2 (38 % humidity), there was a need of a slight imbalance, while with conditions 3 and 4 (46 % and 58 %), the imbalance was more significant. This indicates that the exhaust temperature is maintained higher with higher relative humidity ranges.

### Frost formation location

Depending on the relative humidity, frost formation started in different places on the port. With low relative humidity (22 %), it started on the coldest part of the port (the top side). With higher relative humidity, it started a bit lower, though still in a spot with a local negative temperature value. As condensation occurs, it drips down along the plates of the heat exchanger. The more condensation there is, the lower on the port the condense droplets reach before they freeze. Figure 7.7 shows where frost started forming with the different relative humidity ranges. The frost formation location is marked with a red circle. A bigger scale of the photos can be seen in section E.1, in appendix.

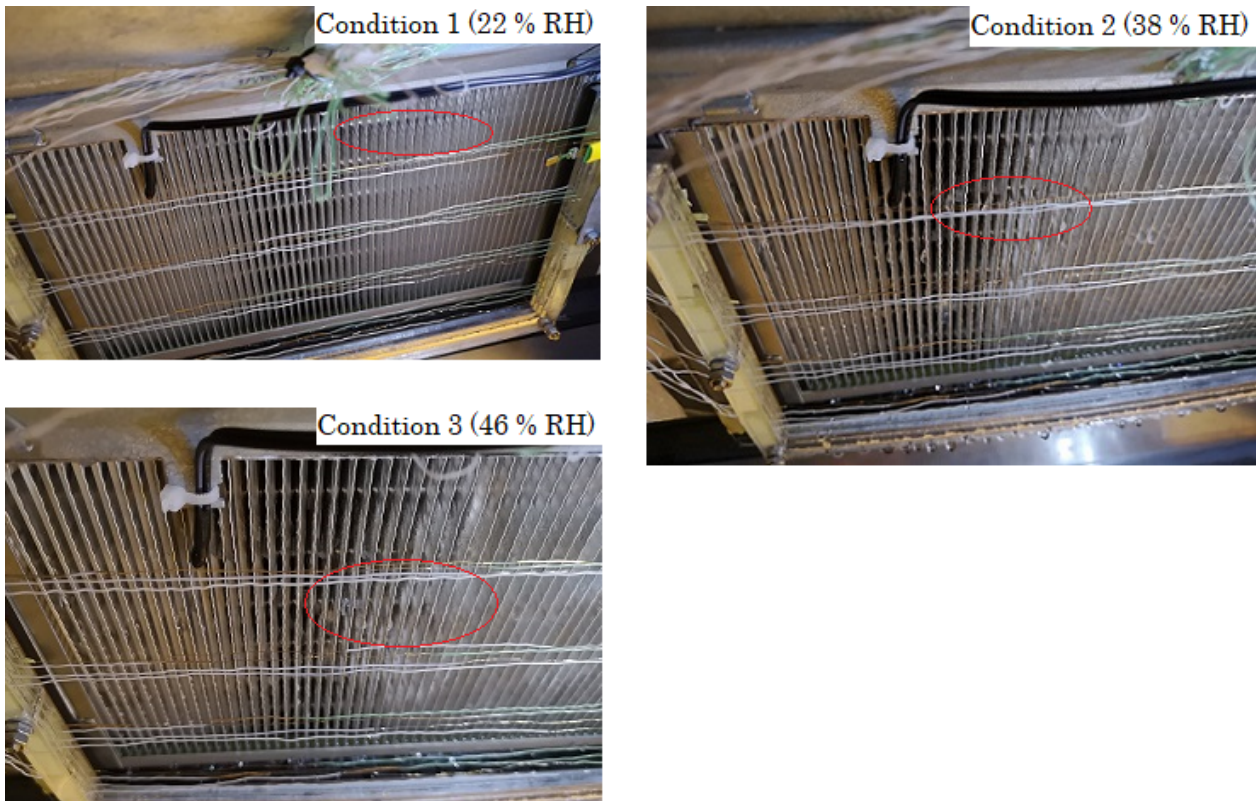


**Figure 7.7:** Frost formation location with different conditions

### Temperature gradient across the exhaust port

As one can see, there is a significant vertical temperature gradient across the port with all the conditions. To understand the reason behind it, the temperature distribution across the other ports is also investigated. Figure 7.8 shows the temperature gradient across all the ports for one of the conditions. While the outdoor and extraction port have more uniform temperature distribution, the exhaust and supply have a greater gradient. That could be because they get influenced by the outdoor and exhaust temperature. The low temperature on the outdoor port decreases the temperature on the top part of the exhaust port. On the other hand, because of the higher extraction temperature, the top part of the supply port has higher values.

Additionally, the temperature gradient increases when there is more condensation, as with condition 4 (56 % relative humidity). Compared to the other cases, the temperature at the bottom of the port is higher. In this case, the greater condensation rate keeps the plate surface temperature higher and maintains higher air temperature values.

**Condition 2**

Temperature gradient across outdoor port

-3.7	-3.7	-3.8	-3.7
-3.5	-3.7	-3.8	-3.8
-3.3	-3.8	-3.8	-3.9
-3.3	-3.8	-3.9	-3.9

Temperature gradient across extraction port

15.8	16.1	16.3	15.7
16.1	16.3	16.2	15.2
15.8	15.8	15.5	15.3
15.4	15.3	15.2	15.5

Temperature gradient across exhaust port

-1.7	-2.2	-2.4	-2.4
-0.3	-0.6	-0.8	-1.0
1.0	0.8	0.3	0.5
2.4	1.6	1.6	1.7

Temperature gradient across supply port

13.2	12.9	12.8	12.6
12.4	12.2	12.1	12.1
10.5	10.0	9.9	9.6
8.2	8.2	8.9	8.8

**Figure 7.8:** Temperature gradient on all ports - Condition 2

The horizontal temperature gradient across the ports could be due to different velocity profiles created by the "air channels" in the ventilation box.

## 7.4 Airmaster's frost prevention control strategy

Airmaster uses a temperature sensor on the exhaust port to control frost prevention, shown in figure 7.9. Its position in relation to the thermocouples and the temperature readings from them is shown in figure 7.10. During all the experiments, the coldest point on the exhaust port remained the same - the point equivalent to  $-2.2\text{ }^{\circ}\text{C}$  in figure 7.10. Therefore, it would be recommended to move the sensor to that point.



**Figure 7.9:** Airmaster's temperature sensor on exhaust port (marked with a red circle)

### Condition 3 - Unbalanced flows

Temperature gradient across exhaust port

-1.6	● -1.8	-2.2	-1.9
-0.4	-0.9	-1.4	-0.7
0.8	0.4	-0.1	0.2
2.0	1.5	1.3	1.6

● Location of Airmaster's sensor

**Figure 7.10:** Airmaster's temperature sensor location in relation to the thermocouple readings

The setpoint that is used for control of frost prevention methods is 1-2 °C. When the temperature falls below 1 °C, defrost starts and when it is above 2 °C, it stops. The minimum measured temperature during frost formation around -2.5 °C for all the tested conditions. Due to the significant difference between Airmaster's setpoint and measured minimum temperature, the defrost control setpoint can be decreased. However, considering that the lowest temperature values were registered when frost appeared on the exit region of the heat exchanger and that frost would start inside the heat exchanger with low humidity levels, Airmaster could decrease their setpoint to -1 °C, instead of -2.5 °C. That would leave some room for uncertainties and also for preventing frost formation from occurring inside the heat exchanger.

In conclusion, several things need to be pointed out:

- Due to the undersized cooling system, the test conditions had to be adjusted in order to provide conditions that would enable frost formation.

- From yearly indoor relative humidity – outdoor temperature relation analysis, humidity levels in the range of 20 – 41 % (with 22 °C extraction air temperature) are found to be critical in terms of frost formation.
- For the relative humidity range of 22 % - 40 % (with 22 °C extraction air temperature), it has been observed that frost appears on the exit region of the exhaust port with 0 °C mean and approximately -2.5 °C minimum exhaust temperature.
- Frost was detected only by visual inspection. Therefore, it is difficult to say under which exhaust conditions, it might have started inside the heat exchanger.
- The relative humidity in the extracted air influences the location where frost starts forming. With low relative humidity (22 %), it starts at the coldest part of the port (the top side) and the more the humidity is increased, the lower the frost formation location gets.
- There is a vertical gradient across the exhaust port which is caused by the outdoor air decreasing the temperature at the top part of the exhaust port. The same effect is observed with extraction and supply ports. Additionally, the higher the amount of humidity is in the air, the higher the temperature at the bottom of the exhaust port is maintained. Thus, leading to a greater temperature gradient.
- There is a horizontal gradient across all of the ports which might be caused due to different velocity profiles on the ports.
- Airmaster's current position of the temperature sensor on the exhaust port is not the coldest point and the defrost control set point is rather higher than what is measured as minimum temperature during frost formation.

## 8 | Calculation validation

Since energy calculations are an essential part of this project, this chapter aims at validating the methods and formulas which are used for that purpose. The imbalance, bypass and preheater methods have been experimentally tested and the measured output has been confirmed by the methods used for calculation. The operation when preheater and bypass were tested is described in appendix A

### Imbalance analysis

With the validation of imbalance it has been tested whether it is possible to control the exhaust temperature by reducing the supply flow. Figure 8.2 shows the temperature of the supply air rises from 17 °C to 18.5 °C, but the heat transfer when there is an imbalance is lower because the supply flow drops. In figure 8.1, the measurements from the imbalance are shown. The heat transfer of 0.73 kW is calculated by taking the temperature difference on the cold side and multiplying it by the air flow and the air heat capacity. When the air flow was balanced, the heat transfer was 0.91 kW.

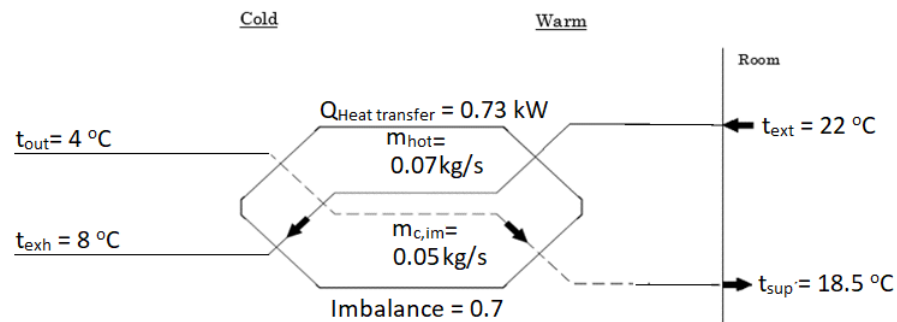
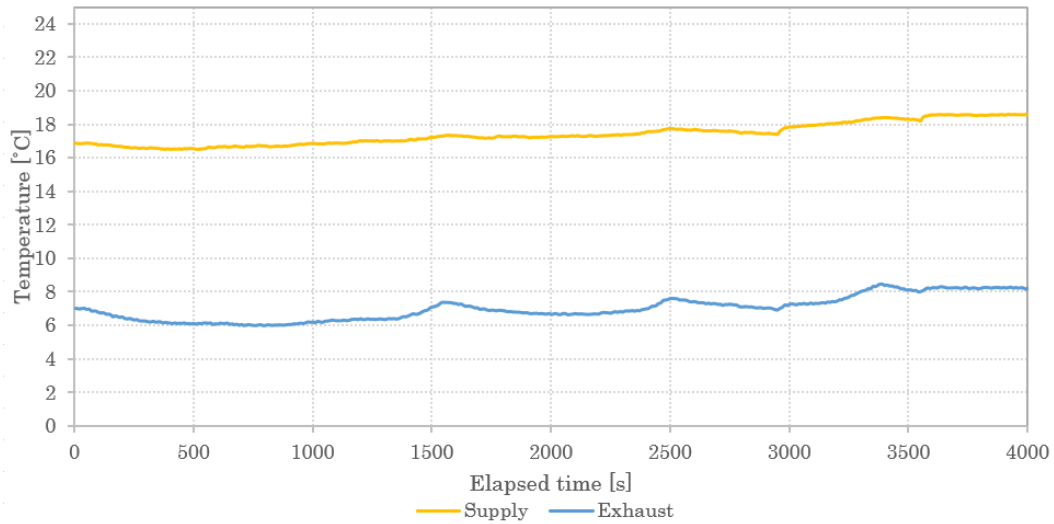


Figure 8.1: Heat exchanger data from imbalance test

The temperature increase from 17 °C to 18.5 °C can also be calculated by using a temperature efficiency for imbalance. This will be necessary to calculate how much the air flow should be reduced on the cold side when the imbalance is controlled during frost prevention.



**Figure 8.2:** Temperature Increase from balance to imbalanced flow

Figure 8.3 shows that the flow on the warm side was constant at approximately 0.07 kg/s throughout the test and on the cold side of the heat exchanger, the flow was reduced to 0.05 kg/s which gives an imbalance of 0.7.

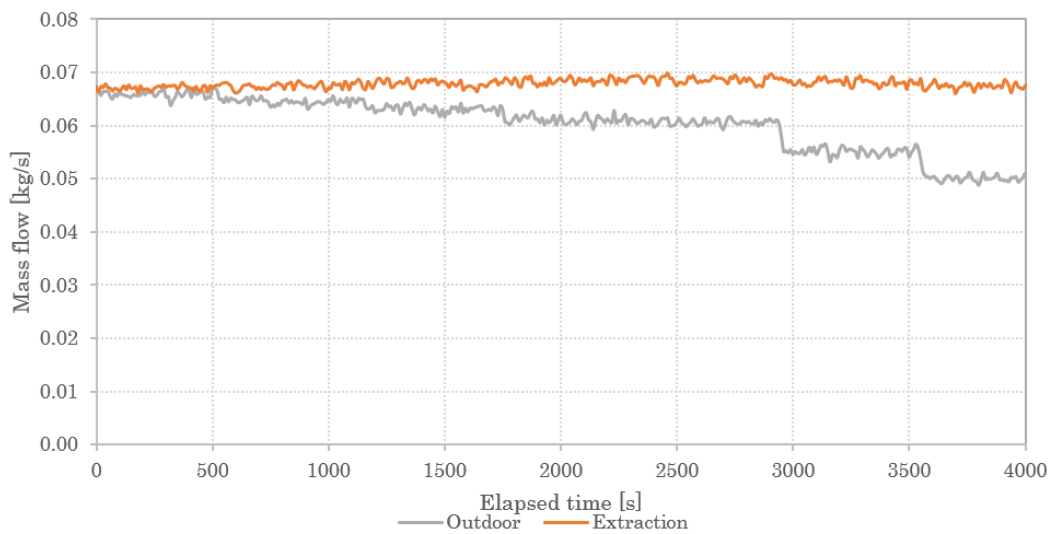


**Figure 8.3:** Flow on cold and hot side from balance imbalanced flow

### Bypass analysis

The bypass method has been validated by analyzing if it is possible to control the mixing temperature of the air that exits the ventilation unit. During the bypass validation, the supply and extraction flow was not balanced even though they were balanced before opening the bypass damper. Figure 8.6 shows that the flow is balanced until the bypass damper is opened (at second 500). After the bypass damper was opened to a certain position, the flow remained stable throughout the test.

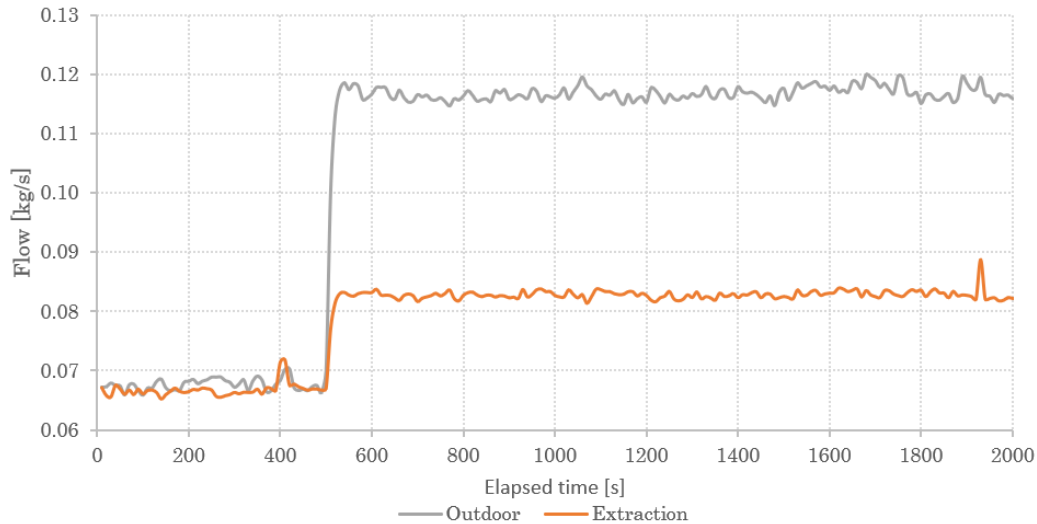


**Figure 8.4:** Supply and extraction flow with closed to open bypass

The temperature of the supply air being heated up in the heat exchanger will increase slightly because the ratio between the flow on the hot side and the cold side changes. Figure 8.5 shows the temperature of the air when it comes out of the supply port on the heat exchanger. It can be seen that even the measured supply temperature on the port remains the same right after the bypass damper is opened, it starts oscillating. This shows that the air from the heat exchanger is not mixed with the bypass air but there is a disturbance due to the bypassed airflow.

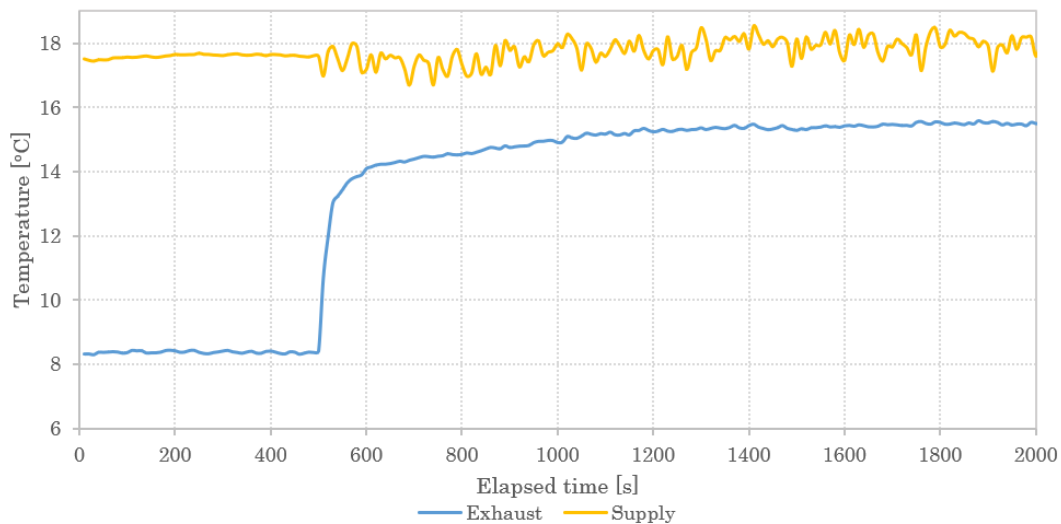


**Figure 8.5:** Supply and extraction temperature with closed and open bypass

The mixing temperature was measured by inserting a Sensirion sensor into the channel, the measurements from this sensor oscillated from 0 °C to 9 °C, which made the measurement from the Sensirion sensor unreliable. The mixing temperature has been checked with calculations instead. The calculated data for the bypass test is shown in figure 8.6

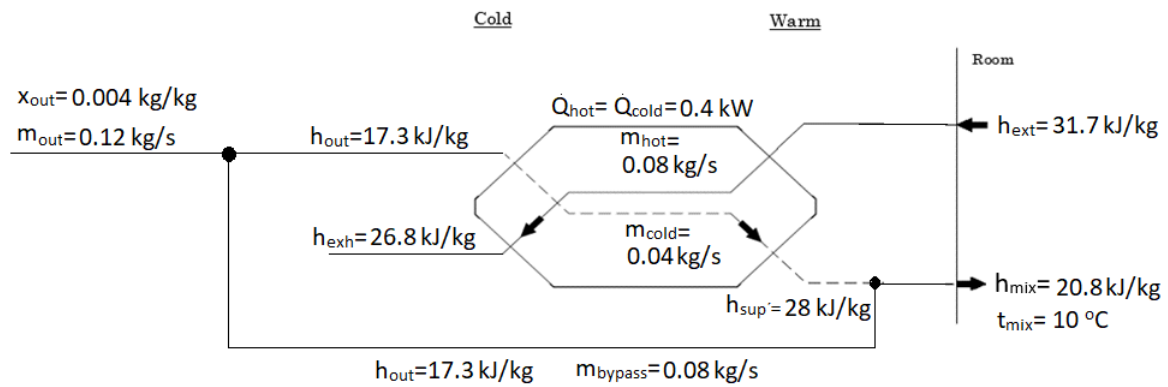


**Figure 8.6:** Bypass measurement

In order to calculate the mixing enthalpy ( $h_{mix}$ ), it is necessary to know the airflow distribution first. The air flow distribution is calculated by assuming that the power on the hot side will be transferred to the cold side. The transferred power is 0.4 kW. That power divided by the enthalpy difference through the cold side, 10.7 kJ/kg ( $28 \text{ kJ/kg} - 17.3 \text{ kJ/kg}$ ), gives a flow of 0.04 kg/s on the cold side. The remaining part of the outdoor airflow will go to bypass.

When the air distribution is calculated, the mixing enthalpy between the outdoor air and the heated air from the heat exchanger can be calculated. This mixing enthalpy is calculated to be 20.8 kJ/kg.

The absolute humidity on the outdoor air and the heated air from the heat exchanger will remain constant therefore the mixing enthalpy can be converted to a mixing temperature which is equal to 10 °C.

### Preheater analysis

The purpose of the preheater validation is to analyze how the heat from the preheater is distributed in the heat exchanger. For this analysis, the power that the exhaust and outdoor air have when the preheating is on is calculated and then compared to the power when the preheater is off. The enthalpy on the outdoor and exhaust air has been multiplied by the mass flow, to get the power of the air. In the test setup, the supply power to the preheater can be adjusted manually with a transformer. The measured data is shown in figure 8.7. In this case, the power output from the preheater has been approximately 117 W (219 minus 102 W) and the transferred power to the exhaust has been approximately 75 W (291 minus 216 W).

It can be seen that the measured supply temperature to the room only increases with 0.6 °C with the preheater on. With a temperature efficiency of 70 %, then 30 % of the added heat will go into the room and 70 % will go to the exhaust port. The heat exchanger will therefore recover less energy when the preheater is on.



It can be concluded that the methods which have been developed to calculate the energy consumption are validated and the results from them can be trusted.

# 9 | Impact of frost prevention methods

## 9.1 Imbalance test

As a preliminary experiment to the imbalance method, the maximum possible imbalance between supply and extraction airflow is tested with two conditions. The first experiment is conducted with infiltration dampers entirely open in cold and warm chambers, while the second experiment is conducted with realistically open dampers (opening equivalent to 1 l/s pr. m<sup>2</sup> of floor area at 50 Pa pressure difference in the warm room and entirely open damper in the cold room).

For each experiment, the airflows are balanced according to the massflow and the supply airflow is gradually decreased by changing the input voltage to the fan and consequently, the fan speed. In the first part of the experiments, the input voltage is decreased by 0.1 volts until second 3000, seen in figure 9.1. Afterwards, the imbalance is created by using increments of 0.4 volts. In appendix, table F.1, an overview of the experiment procedure can be seen.

The minimum input voltage for the supply fan is set to 1.2 volts by Airmaster.

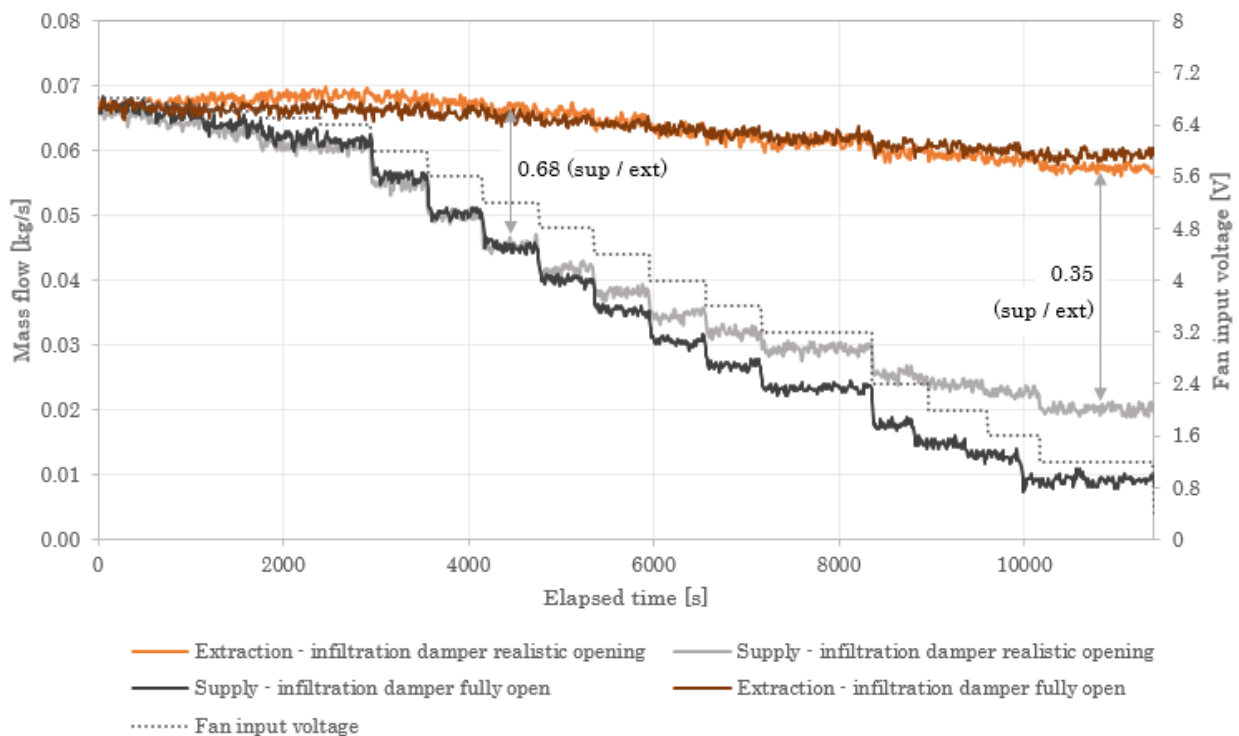


**Figure 9.1:** Imbalance between supply and exaction airflows - infiltration damper realistically open and fully open

As seen in figure 9.1, the ratio between supply / extraction for dampers fully open (that corresponds to a leaky building) is 0.15 correlated to an imbalance of 85%. With realistic damper opening (that corresponds to an airtight building with an air leakage rate of 1 l/s pr. m<sup>2</sup> of floor area at 50 Pa pressure difference), the ratio between supply / extraction is 0.35 correlated to an imbalance of 65 %.

Another observation is that for the realistic opening of the damper, after the fan input voltage is changed from 4.8 to 5.2 volts, the mass flow does not decrease with the same magnitude, seen in figure 9.1 and until the lowest voltage the extraction fan is also extracting less because of the airtight room.

For the full opening of the damper, the supply flow delivered by the fan corresponds to the input voltage even at lower voltage values (shown in figure 9.1). As a result, a higher imbalance is reached.

Figure 9.2 illustrates the relationship between the fan input voltage and the ratio between supply and extraction for the two experiments. The intersection point shows that after 4.8 volts, the rest of the supply air is provided through the infiltration damper (or through construction leaks). With the infiltration dampers fully open, a higher portion of air is supplied due to infiltration, therefore the supply fan provides less fresh air. With the infiltration damper realistically open, there is less infiltration, therefore, the supply fan provides more airflow. [8]

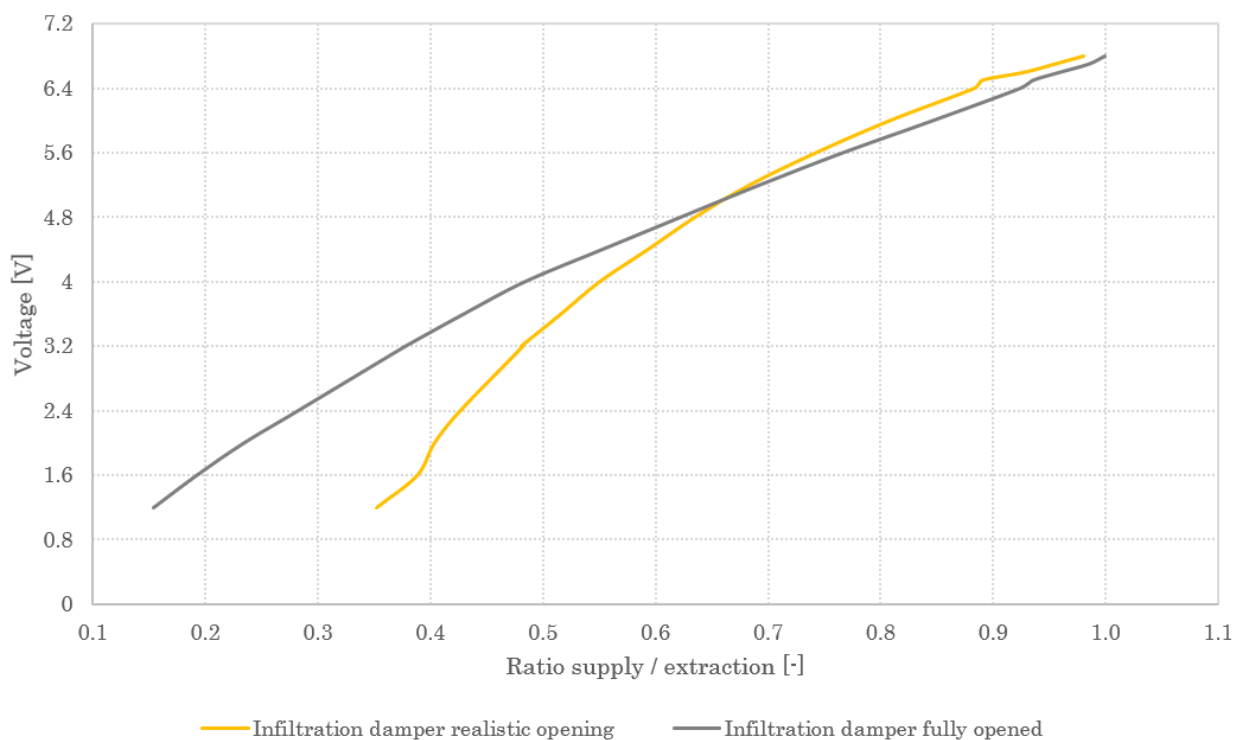


**Figure 9.2:** Relationship between voltage and ratio supply / extraction

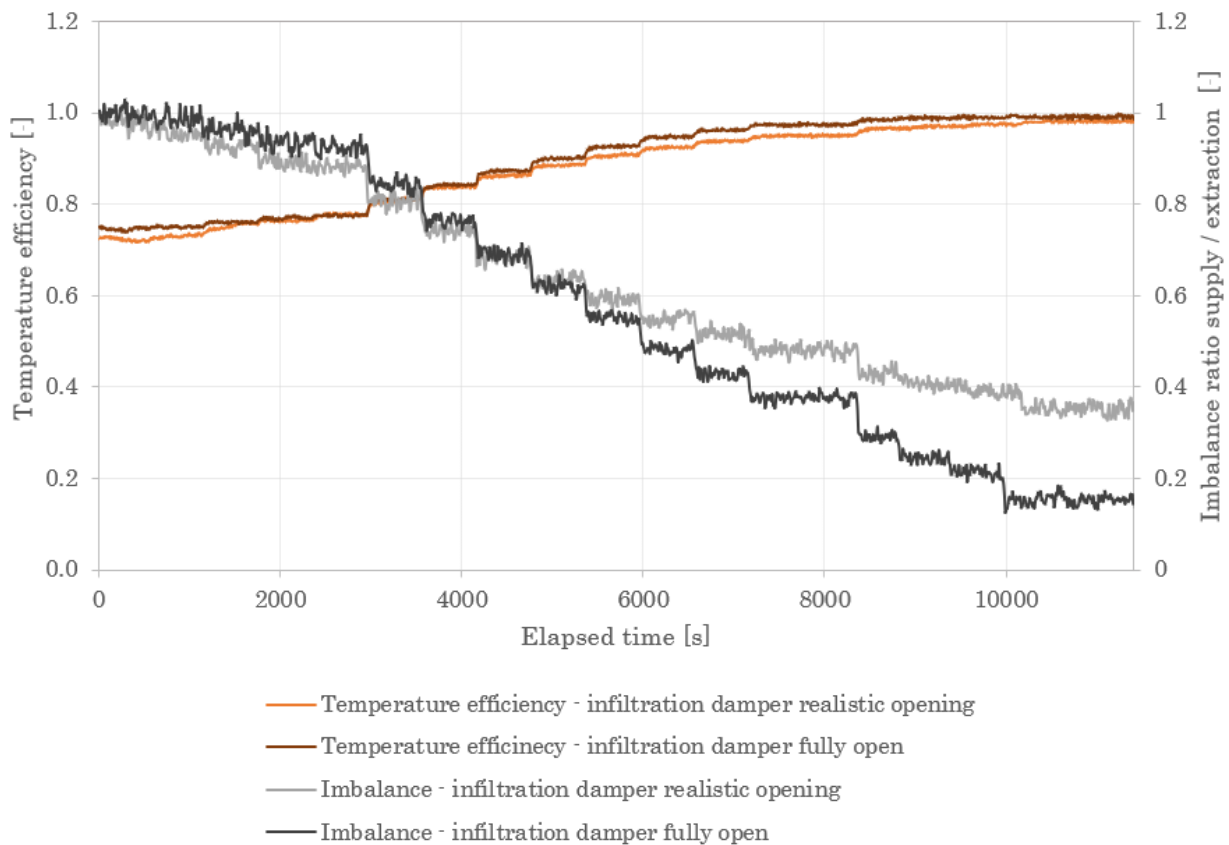


**Figure 9.3:** Temperature efficiency and imbalance ratio - infiltration damper realistically open and fully open

When imbalance is created - the supply airflow is lower than the extraction airflow and the heat exchange is decreased. Though, the temperature efficiency is increased. Figure 9.3 presents the temperature efficiency increase with regards to the ratio between supply and extraction. [8]. The mean temperature graphs can be seen in F.1.

Having an under-balance (the supply airflow rate is lower than the extraction airflow rate) can have consequences on the energy consumption and indoor air quality. These issues are further investigated in sections 9.2 and 9.3. [22] [17]

## 9.2 Impact on energy consumption

Defrost and frost prevention methods can have an impact on the energy consumption, therefore the focus is to define the most energy efficient strategy among the preheating, bypass and imbalance methods by investigating the condition with the lowest outdoor temperature ( $-16\text{ }^{\circ}\text{C}$ ) during the year for Gothenburg. Detailed description of the energy consumption calculation for each method is provided in chapter H, in appendix.

### Imbalance by reducing the outdoor airflow rate

Figure 9.4 illustrates the imbalance ratio between the supply and extraction airstreams plotted with regards to outdoor temperature and indoor relative humidity. It can be noticed that the main factor influencing imbalance is the temperature. However, at  $-12\text{ }^{\circ}\text{C}$  there are two different relative

humidity levels that result in different imbalance ratio. Thus, relative humidity can also be an essential parameter. The calculation method used to estimate the imbalance ratio is explained in chapter H.2, in appendix.

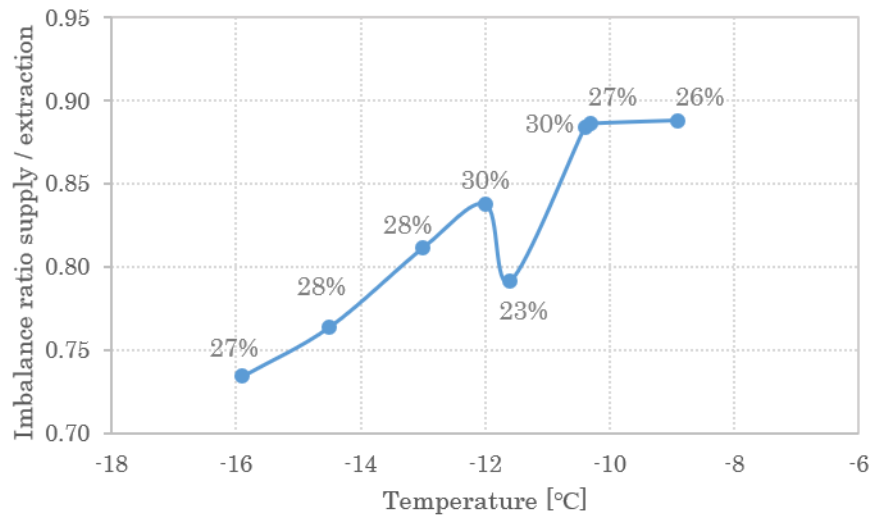


**Figure 9.4:** Imbalance ratio correlation with outdoor temperature / indoor relative humidity - Gothenburg (classroom)

With outdoor temperature which would cause the exhaust air temperature to fall below the freezing limit, the imbalance method can be used as frost prevention strategy for the heat exchanger. As described in one of the following chapters (chapter 10), Gothenburg has the highest percentage of frost conditions, seen in figure 10.4, therefore, the energy consumption for the coldest hour during the year for the classroom is used. The whole calculation method for imbalance can be seen in section H.2, in appendix.

For creating imbalance, the mass flow on the cold side is calculated taking into account the energy that can be extracted from the warm airstream before frost occurs (until the exhaust temperature drops to the frost limit value). That can be seen in equation H.11, in appendix.

Regarding energy consumption during imbalance, the lower supplied power to the room and the higher power need to overcome the increased infiltration are considered as a heat loss, while the decreased supply fan power is considered as a gain. However, the energy "savings" due to reduced fan power are very insignificant and therefore, not noticeable in the final energy consumption value.

Equation H.16 sums up the gains and losses of the imbalance method. As a result, the energy need to avoid frost on the heat exchanger during the lowest outdoor temperature conditions for the working hours for the classroom is 0.37 kW.

### Bypass

With the bypass method, the outdoor air can be bypassed partially or fully with a modulating damper as described in chapter 2. Afterwards, it is mixed with the rest of the air that passes through the heat exchanger in case that it is not fully bypassed.

The calculation for the amount of bypassed air is in the same way as for the imbalance method, seen in equation H.22, in appendix. The portion of bypassed air is controlled by the exhaust temperature.

The whole calculation method can be seen in section H.3, in appendix.

The energy consumption calculation is also similar to the one for the imbalance method, though without the gains from the reduced fan power. For this case, the energy consumption is 0.37 kW, the same as for the imbalance.

### **Air preheating method**

With the air preheating method, frost is avoided by heating the outdoor air before it passes through the heat exchanger with a preheating surface, as shown in figure 5.3. The purpose is to avoid temperatures lower than the frost limit on the exhaust side, as seen in equation H.27.

The energy needed to avoid frost on the heat exchanger with the preheating method is also 0.37 kWh.

From the calculations, it can be concluded that all three methods use the same energy to heat the exhaust temperature to the freezing limit threshold.

## **9.3 Impact on indoor environmental quality**

One of the investigated frost prevention methods is the imbalance by reducing outdoor airflow rate. As described in section 9.1, this affects the infiltration through the envelope due to differences in pressure.

By creating an imbalance ratio of 0.7 to avoid frost formation, seen in figure 9.4, the the desired extraction rate can still be maintained. In figure 9.1, section 9.1, one can see that the desired extraction is maintained until an imbalance ratio of 0.68 for airtight buildings. Consequently, the indoor air quality will not be compromised.

On the other hand, due to the increased infiltration of outdoor air, the thermal comfort would be compromised because of risk of draught.

As a conclusion, based on the analysis above, it is found that the investigated methods for frost prevention have similar impact on energy consumption. In terms of indoor environmental quality, imbalance would lead to a risk of draught due to the increased infiltration of outdoor air through the construction. As a result, bypass or preheating of outdoor air would be recommended.

# 10 | Comparison of dynamic with static efficiency

Due to the varying outdoor conditions during the year, the dynamic temperature efficiency of the heat exchanger is looked into. It is compared with the minimum heat recovery efficiency required by the building regulations [33] and Ecodesign [9] - 73 %. Moreover, the duration of the periods with dry, wet and frost operation conditions for the heat exchanger are also investigated for the chosen geographical locations in this chapter.

Yearly (hourly) data for outdoor, supply, extraction and exhaust air temperature, based on Bsim simulations and Klingenburg's software, is analyzed. Only working hours are investigated. Depending on whether the exhaust temperature is below the dew point for extraction air or below the frost limit temperature of 0 °C, the periods with dry, wet and frost conditions are sorted.

The temperature efficiency for the different conditions is calculated using the formula in equation 10.1. When it comes to calculating the efficiency under freezing conditions, the supply temperature is calculated taking into account the maximum possible heat transfer before frost occurs. The formula which is used can be seen in equation 10.3.

$$\eta_t = \frac{t_{sup} - t_{out}}{t_{ext} - t_{out}} [-] \quad (10.1)$$

$t_{out}$  – outdoor air temperature [°C]

$t_{sup}$  – supply air temperature [°C]

$t_{ext}$  – extraction air temperature [°C]

$$Q_{max\ possible} = m_h \cdot (h_{ext} - h_{exh'}) \quad (10.2)$$

$$t_{sup, frost} = \frac{Q_{max\ possible}}{m_c \cdot Cp_c} + t_{out} [°C] \quad (10.3)$$

$Q_{max\ possible}$  – maximum possible heat flow based on freezing point threshold [W]

$m_h$  – mass flow rate on the warm side  $\left[\frac{kg}{s}\right]$

$m_c$  – mass flow rate on the cold side  $\left[\frac{kg}{s}\right]$

$h_{exh}$  – exhaust air enthalpy  $\left[\frac{kJ}{kg}\right]$

$h_{exh'}$  – freezing limit threshold air enthalpy  $\left[\frac{kJ}{kg}\right]$

$Cp_c$  – heat capacity for the cold side  $\left[\frac{J \cdot kg}{K}\right]$

Figures 10.1 and 10.2 show the periods with dry, wet and frost conditions and the corresponding temperature efficiencies for Gothenburg (classroom and office). The dry period is predominant in the two cases. However, in the office, due to the fewer number of people and the less amount of generated humidity, the period is longer. In terms of wet conditions, the period is longer for classrooms. Due to the greater number of people, the produced humidity is higher, thus it leads to higher dew point temperature for the extracted air, and consequently, more condensation. The duration of the frost period is the same for the two cases, since it is greatly influenced by the outdoor temperature.

The temperature efficiencies which are shown in figures 10.1 and 10.2 are the mean values for the specific conditions. While the dry and wet efficiencies are mostly 82 % for the whole duration of the respective periods, the minimum value for frost efficiency is 67 % with outdoor temperature of -16 °C.

Compared to the required minimum heat recovery efficiency of 73 %, the efficiency of the heat exchanger falls below this value only two times during the year (for two hours) when the outdoor temperature is -15 °C and -16 °C.

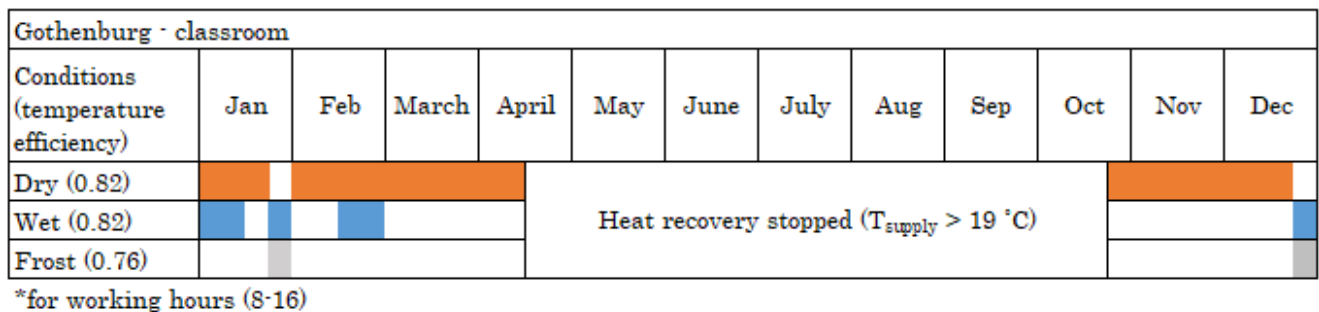


Figure 10.1: Dynamic yearly temperature efficiency for Gothenburg - classroom

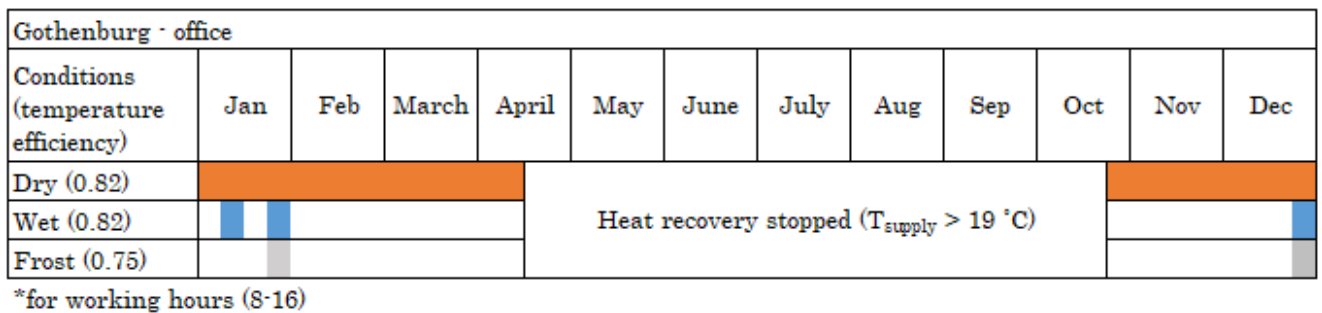
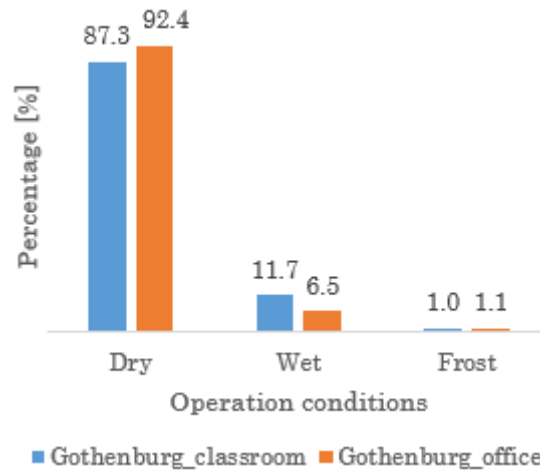


Figure 10.2: Dynamic yearly temperature efficiency for Gothenburg - office

Figure 10.3 shows how big of a portion from the period with heat recovery operation, the different operation conditions represent. It is considered that the heat recovery is in operation with supply temperature below 19 °C. The frost conditions represent only 1.1 % of the time with heat recovery in operation.



**Figure 10.3:** Percentage of operation conditions from the period with heat recovery working (exhaust temperature extracted from Klingenburg)

As described in chapter 6, the exhaust temperature output from Klingenburg for wet/frost conditions is with 2 °C higher compared to measured values. As a result, the other locations - Groningen, Innsbruck and Leuchars do not have periods where the exhaust temperature falls below 0 °C.

When the exhaust temperature for wet/frost conditions is decreased with 2 °C, the percentage of hours with frost increases. Figures 10.4, 10.5 and 10.6 show that Gothenburg has the highest percentage - 5.8 %, followed by Innsbruck - 0.7 % and Groningen - 0.3 %. Appendix G provides information about how the different operation conditions are distributed along the year for all the locations with decreased exhaust temperature.

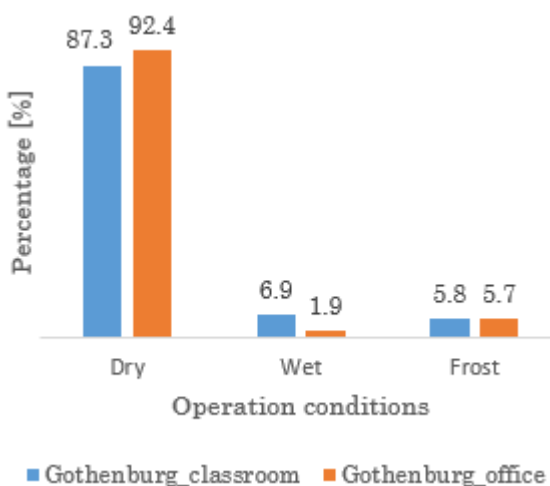


**Figure 10.4:** Percentage of operation conditions from the period with heat recovery working (exhaust temperature decreased with 2 °C) for wet/frost - Gothenburg

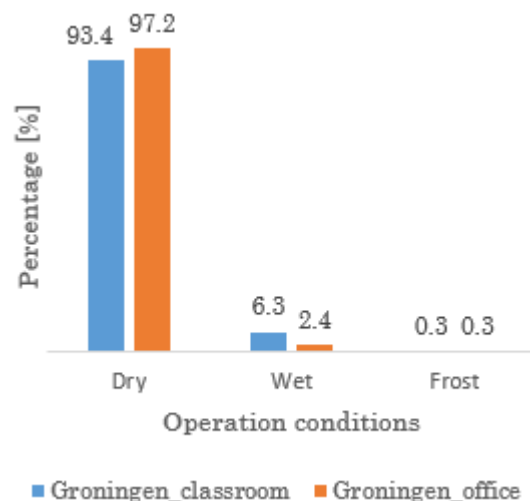


**Figure 10.5:** Percentage of operation conditions from the period with heat recovery working (exhaust temperature decreased with 2 °C) for wet/frost - Groningen

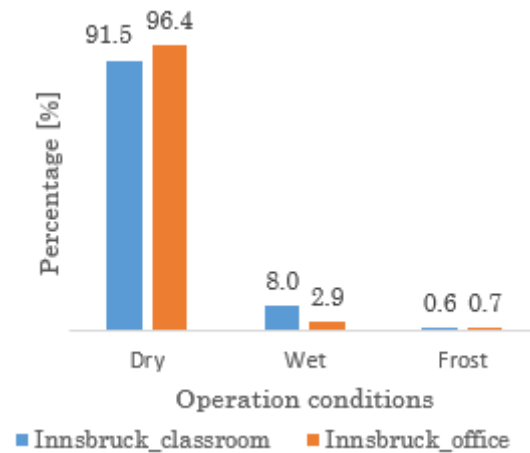


**Figure 10.6:** Percentage of operation conditions from the period with heat recovery working (exhaust temperature decreased with 2 °C) for wet/frost - Innsbruck

To sum up, the dynamic temperature efficiency of the heat exchanger during dry, wet and frost operation conditions is generally kept above the minimum requirement of 73 %. It falls below 73 % when the outdoor temperature drops below -14 °C.

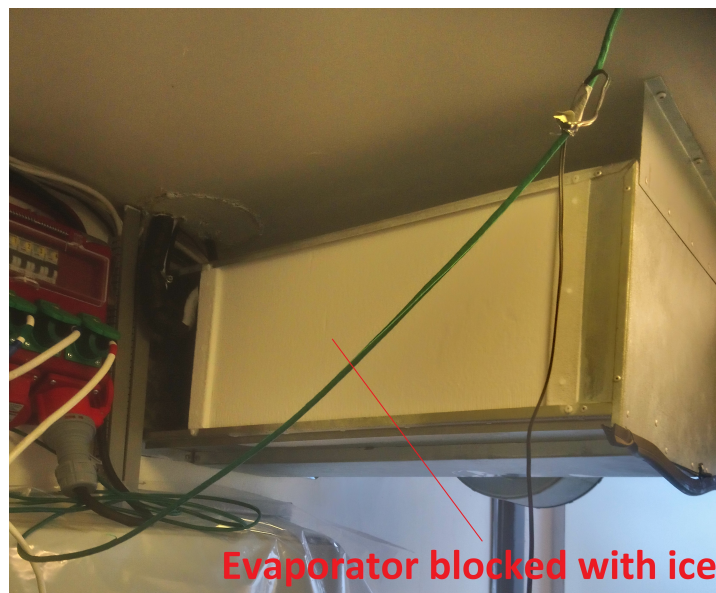
In terms of period with frost conditions, based on exhaust temperature output from Klingenburg's software, only in Gothenburg there is a risk of frost for 1.1 % from the total period with heat recovery is in operation. When the exhaust temperature is decreased 2 °C, the frost period becomes longer - 5.8 % for Gothenburg (Southern Scandinavia), 0.7 % for Innsbruck (Southern Germany and Austria) and 0.3 % for Groningen (Central Europe). Due to the warmer outdoor conditions, there is no risk of frost in Leuchars (Scotland).

# 11 | Challenges and problems during the measurements

## 11.1 Cooling system

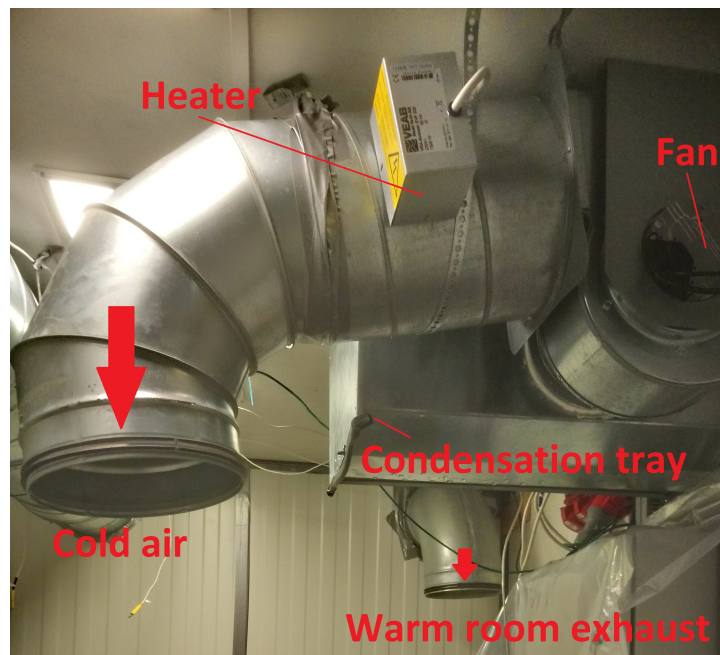
The cooling system from Airmaster arrived with a leakage which caused the system to lose refrigerant and had to be refilled in order to cool. The cooling also had an error on the expansion valve which often got stuck in open position, this meant that the cooling system would not always start. When it was cooling, it required 6 hours to get the cold room cooled down due to a low cooling effect. In the original experimental setup, the evaporator for the cooling system was without a defrost function, which meant that the entire room had to be heated to defrost the evaporator after it has been blocked with ice.

Figure 11.1 shows the evaporator which is completely blocked with ice. When the evaporator is completely frozen, air cannot pass through and the room temperature begins to rise. The cooling effect also decreases before the evaporator freezes completely because the U-value falls due to ice on the surface. To avoid icing, an adsorption dehumidifier was put into the cold room, but it warmed up the room and could not remove enough moisture at low temperatures.



**Figure 11.1:** Airmaster cooling system out of order

The way the cooling system was assembled caused problems due to the high absolute humidity in the cold room. Figure 11.2 shows the evaporator unit from the back. The fan sucks the air through the evaporator, in between there is a tray to collect the condensation, the condensation then drops into a bucket. At freezing temperatures, the condensate tray freezes and becomes filled with ice. In the first experiments, the humid air for the hot room was blown straight into the evaporator, therefore a 90° bend was mounted on the duct from the warm room. It can also be seen that the heater is located after the evaporator.



**Figure 11.2:** Component overview for cooling and heating of the room

### Installing extra cooling system

Due to a lack of cooling power, an extra cooling system has been installed from Aalborg University as a temporary solution for the container. In order to have the new cooling system installed, one of the doors in the container is opened to get the glycol hoses out of the container. The hole for the door have been closed with a thick piece of polystyrene. The cooling system from the University is an external cooling system where the evaporator is connected to a liquid to air heat exchanger inside the cold room, seen in figure 11.3. With this cooling system, the supply temperature to the liquid to air heat exchanger could not become lower than  $-16\text{ }^{\circ}\text{C}$ . With this liquid temperature and only this cooling system, it has been possible to get the room temperature down to  $-9\text{ }^{\circ}\text{C}$  without the ventilation unit being in operation.



**Figure 11.3:** Cooling system from AAU inside the cold room

The original cooling system got extra ducts and two dampers with motors were installed to enable recirculation of the hot air from the preheating surface. The ducts and condensation tray got isolated in the new set-up, seen in figure 11.4. When defrosting, the channels close in and out to the room and the preheating surface is switched on by raising the set point above 0 °C.

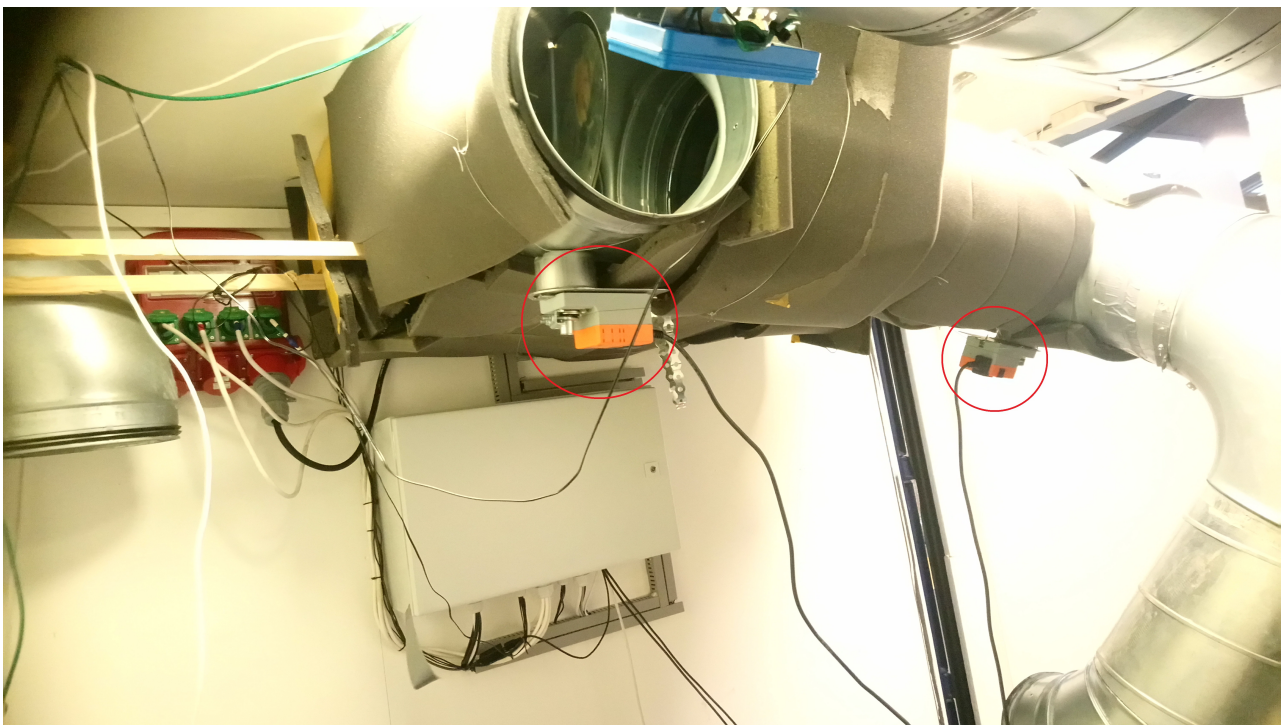


**Figure 11.4:** Updated Airmaster cooling system with defrost function

After the cooling system from AAU was installed, it only worked until the temperature became below 0 °C inside the room. Then it started to start and stop and after a period it stopped completely. The cause of this was that there was an automatic fuse for the circulation pump that shut off the pump. Next morning the cooling system eventually went to a standstill before it had cooled the room to below 0°C and it would not start up again. Hereafter, a cooling technician came to fix it, the reason for the standstill was that there was not enough glycol in the coolant and the coolant was only frost-proof until -5 °C. This caused an ice layer that blocked the evaporator inside the new cooling system, seen in figure 11.5. Fortunately, the ice block did not destroy the cooling system and the cooling system was able to run after more glycol was filled in.

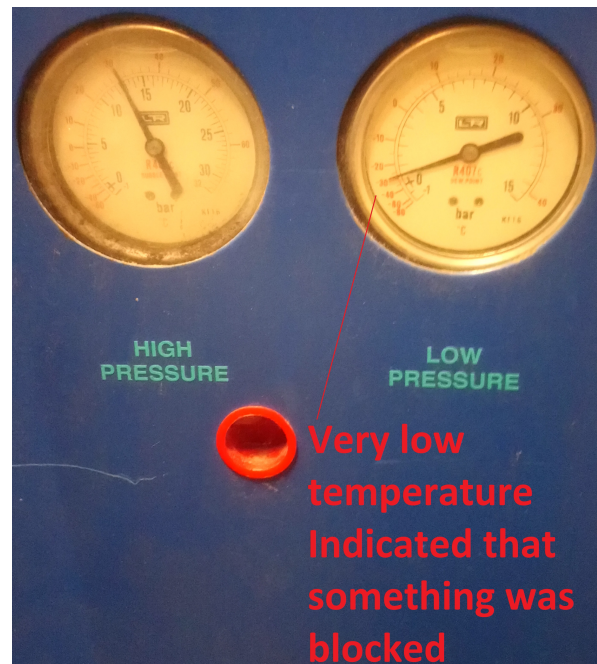


**Figure 11.5:** Cooling system from AAU out of order

## 11.2 Other challenges

- Calibration of the thermocouples got delayed with 3 weeks because they were sent out to be golden tipped and the person that was responsible for the golden tipping went on holiday after the first day with golden tipping.
- During the first tests in the container, it was difficult to maintain a stable room temperature, which meant that the first validation tests of the heat exchanger were discarded. The problem was solved by increasing the thermal mass inside the container by installing steel plates as thermal mass on the inside of the container (only in the cold room).
- There was wireless network in the container so that the equipment could be remotely controlled. But the first days the connection was lost very often. This was solved by mounting external antennas on the container.
- Since the ventilation unit has no feedback control that could give a specific flow, the flow had to be adjusted manually by changing the voltage to the supply and extraction fans. The bypass and

preheater were not prepared in the container so some equipment from AAU was used, so that preheater and bypass could have a variable input signal. The cooling unit was blowing too close to the outdoor air duct which made the flow oscillate. This can be seen in figure 11.6. When the cooling system was turned off, the oscillation on the outdoor air was lower, compared to when the cooling system was running. It was solved by adding extra ducts.

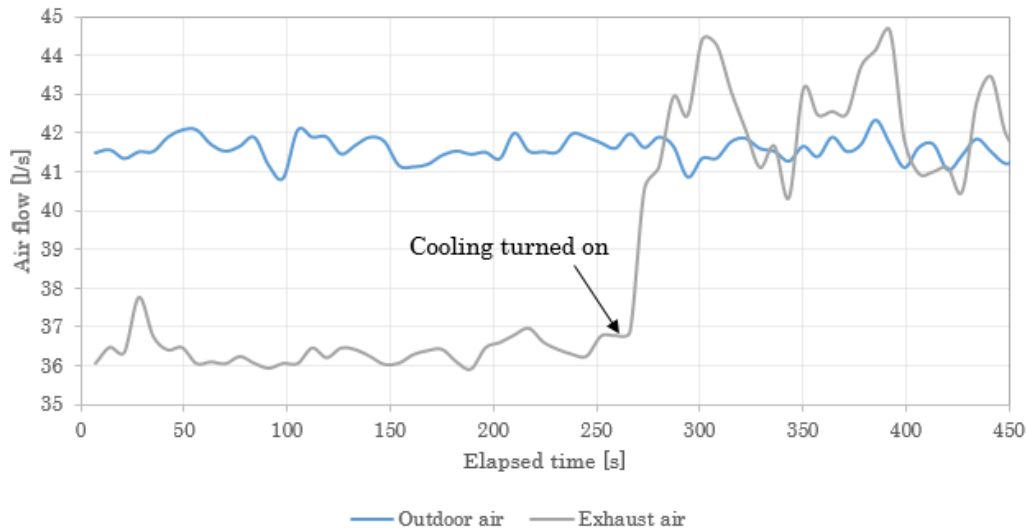


**Figure 11.6:** Flow oscillating because off close ducts

- The Sensirion sensors stopped working once in a while. This most often happened when they were moved around since the cables to the sensors were solid core cables that broke easily. Figure 11.7 shows the warm room after the ventilation duct from the steam humidifier has fallen off. This filled the warm room with steam. After that, all of the Sensirion sensors stopped working and their cables had to be replaced.



**Figure 11.7:** Duct fallen down

- When the measuring equipment was installed in the container, there was a thermocouple sensor which showed the same temperature all the time, the problem turned out to be, that the sensor

did not work in practice with a  $3^{rd}$  order equation. After changing the equation, the problem disappeared.

## 12 | Conclusion

The focus of this report is the frost formation on air to air counterflow heat exchangers. To investigate this topic an experimental setup with a decentralized ventilation unit containing the heat exchanger was built. Moreover, the important parameters that have to be measured have been determined and the extensive calibration process is followed by the installation of the sensors in the experimental setup - the Airmaster mobile laboratory.

The setup consists of a cold room that could maintain freezing temperatures and a warm room where both temperature and relative humidity could be controlled. Weather data from locations where Airmaster sells ventilation units has been used to assess the risk of frost on the heat exchanger. In total, four geographical locations have been distinguished - Southern Scandinavia, Central Europe, Southern Germany and Austria, and Scotland. Regarding indoor conditions, data from BSim has been extracted considering building usage types of classrooms and offices.

Several scientific articles were reviewed to find the most common defrost and frost prevention methods. Based on Airmaster's needs, the following frost prevention strategies are considered: preheating, bypass and imbalance.

To observe when frost occurs in the heat exchanger, a video camera was mounted inside the ventilation unit as well as pressure sensors to measure the pressure increase on the warm side of the heat exchanger. Even though frost formed, it was not possible to detect it with pressure increase or on the camera. Therefore, visual inspection of frost formation was necessary.

In order to measure the temperature distribution on the heat exchanger, 16 temperature sensors have been installed on each port of the heat exchanger. The relative humidity has been measured with 1 sensor on each port. It has been observed that the temperature gradient of the exhaust port can be 6.8 °C. The coldest point is the area close to the outdoor port and the gradient is greater when indoor humidity is also higher.

From the experiments it can be concluded that the mean temperature of the exhaust air is 0 °C when frost occurs on the heat exchanger. Furthermore, it can be stated that even though frost formation depends greatly on the outdoor temperature, the level of indoor humidity also plays a big role.

It is found that the investigated methods for frost prevention have similar impact on energy consumption. In terms of indoor environmental quality, imbalance would lead to a risk of draught due to the increased infiltration of outdoor air through the construction. As a result, bypass or preheating of outdoor air would be recommended.

At last, the risk of frost in the investigated geographical locations has been evaluated. Figure 12.1 shows that the highest percentage of risk is in Southern Scandinavia. In the rest of the locations, the risk of frost formation is insignificant.

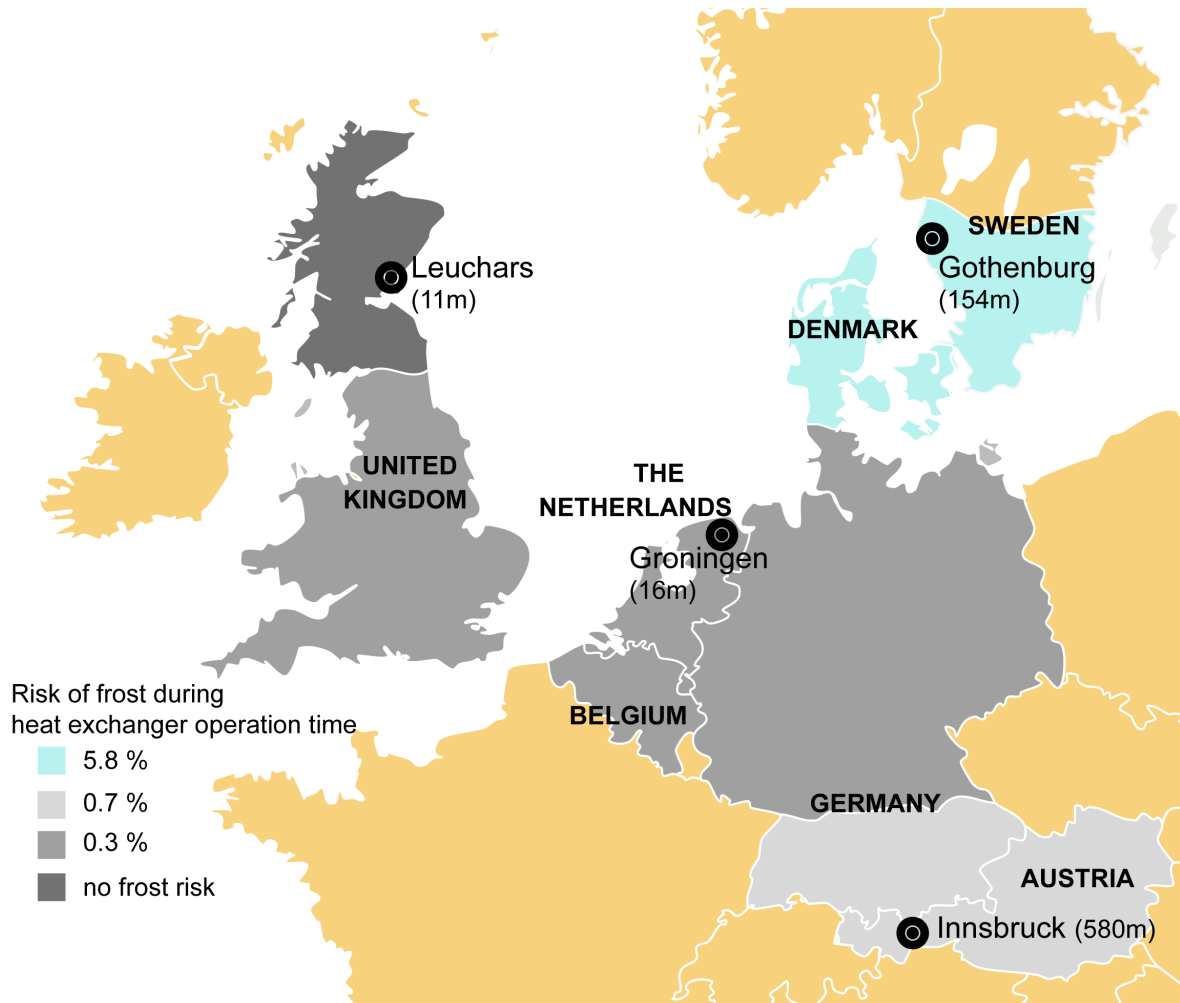


Figure 12.1: Evaluation of frost formation risk in the investigated geographical locations

# 13 | Future work

After being involved not just theoretically but also practically in new tasks such as preparation, welding and thermocouple calibration, one gained insight on how things can be done more efficiently and in an improved manner. During this process, it was concluded that some decisions need more research before putting them in practice. For example, thermocouples were coated with a layer of gold to reduce the exchanging radiative heat with the surrounding elements of the ventilation unit and the plates of the heat exchanger. Further investigation or comparison between a golden coated and a normal thermocouple could have showed if the improvement brought by the coating is significant enough. This is in itself a topic that can be investigated more. Another aspect, related to the measurements, is the the pretest and post-test analysis, recommended by ASHRAE standard 84 - 2013 used to validate the experiment. A lack of time did not permit such an analysis, but this can be considered for similar experiments on heat exchangers.

Another measured parameter is the differential pressure used to detect the moment of frost formation. Unfortunately, the range and / or the pressure transducer was not accurate enough to detect insignificant increase in pressure drop. During the frost limit experiments, it was noticed that there was no increase in pressure drop, therefore careful consideration is needed when deciding what instrument is suitable.

The temperature on each port of the heat exchanger was measured by 16 thermocouples. By doing so, the temperature gradient could be analyzed. For a more in depth analysis, the velocity profile on each port can also be measured. This could help in understanding the reason of having the horizontal temperature gradient.

All the test: the frost limit and the energy consumption for each frost prevention method were performed for certain climatic regions that is described in chapter 4. These regions are with milder conditions compared to arctic climate. To expand more on the topic, arctic climates like Northern Scandinavia can be considered. Furthermore, residential buildings can also be investigated.

The counterflow heat exchanger that was tested is an aluminum heat exchanger. Test can also be performed on other heat exchangers that have different technical specifications. Airmaster showed interest in testing the following heat exchnagers: GS 25/250 (PET) from Klingenburg and LEV-455-230-L-S from Ekocoil. The specifications are shown in table 13.1.

Manufacturer	Klingenburg	Ecokoil
Heat exchanger type	GS 25/250 (PET)	LEV-455-230-L-S
Plate spacing	2.0 mm	2.3 mm
Plate thickness	0.14 mm	0.1 mm
Thermal conductivity	0.24 W/mK	200 W/mK
Number of plates	116	116

**Table 13.1:** Heat exchanger specifications for fututre work

From such an analysis Airmaster might reconsider on using one of the above mentioned heat exchangers, if they have a better performance during periods with frost risk.

# Bibliography

- [1] Andrzej Jedlikowski, S. Anisimov, J. Danielewicz, M. Karpuk, and D. Pandelidis. Frost formation and freeze protection with bypass for counter-flow recuperators. *International Journal of Heat and Mass Transfer*, 108:585–613, May 2017.
- [2] Anna Pacak, A. Jedlikowski, D. Pandelidis, and S. Anisimov. Analysis of freeze protection methods for recuperators used in energy recovery from exhaust air. *International Conference on Advances in Energy Systems and Environmental Engineering (ASEE17)*, 22, November 2017.
- [3] ASHRAE. *ASHRAE Standard - Standard Method for Temperature Measurement*. American Society of Heating, Refrigerating and Air-conditioning Engineers, Inc., 2001.
- [4] Danish Standard. *DS/EN 13053 + A1:2011 Ventilation for buildings - Air handling units - Rating and performance for units, components and sections*. Danish Standard, 2011.
- [5] Danish Standard. *DS/EN 13141-8:2014 Ventilation for buildings - Performance testing of components/products for residential ventilation - Part 8: Performance testing of un-ducted mechanical supply and exhaust ventilation units (including heat recovery) for mechanical ventilation systems intended for a single room*. Danish Standard, 2014.
- [6] Dansk Standard. *DS/EN 308:1997 Heat exchangers - Test procedures for establishing performance of air to air and flue gases heat recovery devices*. Dansk Standard, 1997.
- [7] Dansk Standard. *DS447 Ventilation in buildings - Mechanical, natural and hybrid ventilation systems*. Dansk Standard, 2013.
- [8] Dennis Johansson. Under-balancing mechanical supply and exhaust ventilation systems with heat recovery – effects on energy use . *Reserach and Development, Swegon AB/Building Physics Building Services, Lund University*, 22, June 2008.
- [9] Ecodesign. Regulation (EU) No 1253/2014 with regard to ecodesign requirements for ventilation units. [https://ec.europa.eu/energy/sites/ener/files/documents/implementation\\_guide\\_-\\_ventilation\\_units\\_with\\_cover.pdf](https://ec.europa.eu/energy/sites/ener/files/documents/implementation_guide_-_ventilation_units_with_cover.pdf), 2016.
- [10] E.G. Phillips, L. Bradley, R. Chant, and D. Fisher. Comparison of freezing control strategies for residential air-to-air heat recovery ventilators. *ASHRAE Transactions (American Society of Heating, Refrigerating and Air-Conditioning Engineers)*, 95, Part 2, January 1988.
- [11] EnergyPlus. Weather data sources. <https://energyplus.net/weather/sources#IWEC>.
- [12] European Commission. Cooling and heating degree days by country - monthly data. [https://ec.europa.eu/eurostat/web/products-datasets/product?code=nrg\\_chdd\\_m](https://ec.europa.eu/eurostat/web/products-datasets/product?code=nrg_chdd_m).
- [13] European Standard. *EN 306:1997 Heat exchangers - Methods of measuring the parameters necessary for establishing the performance*. European Committee for Standardization, 1997.
- [14] Eurovent. . <https://eurovent.eu/>, 2019.

- [15] Jerome Le Dreau, P. Heiselberg, and R. L. Jensen. Experimental data from a full-scale facility investigating radiant and convective terminals - uncertainty and sensitivity analysis, description of the experimental data. Technical report, Aalborg University, 2014.
- [16] Jesper Kragh, J. Rose, and S. Svendsen. Mechanical ventilation with heat recovery in cold climates. *Proceedings of the 7th Symposium on Building Physics in the Nordic Countries*, January 2005.
- [17] Larry Palmiter and T. Bond. Impact of Mechanical systems on Ventilation and Infiltration in Homes . June.
- [18] Larsen, Olena Kalyanova, F. Zanghirella, M. J. Heiselberg, Perino, and R. Lund. Measuring Air Temperature in Glazed Ventilated Facades in the Presence of Direct Solar Radiation. *Proceedings of Roomvent 2007 FINVAC*, January 2007.
- [19] Lene Riberholdt. Naesten ingen folkeskoleklasser har over 30 elever, 2017.
- [20] Lindab A/S. Lindab UltraLink Monitor FTMU - Teknisk information. <https://itsolution.lindab.com/LindabWebProductsDoc/PDF/Documentation/ADS/DK/Technical/Technical-FTMU-dk.pdf>, 2018.
- [21] Martin Sternberg. . <http://www.klingenburg.de/>, 2019.
- [22] Martin W Liddament. *A Guide to Energy Efficient Ventilation*. The Air Infiltration and Ventilation Centre, 1996.
- [23] Mohammad Rafati Nasr, M. Fauchoux, R. W. Besant, and C. J. Simonson. A review of frosting in air-to-air energy exchangers. *Renewable and Sustainable Energy Reviews*, 30:538–554, February 2014.
- [24] Mugur Balan. Thermodynamic properties of moist air. [http://www.termo.utcluj.ro/mb/moist\\_airma.html](http://www.termo.utcluj.ro/mb/moist_airma.html).
- [25] Natasa Nord. Building energy efficiency in cold climates. *Reference Module in Earth Systems and Environmental Sciences*, December 2017.
- [26] A. og Aage Bredahl Eriksen. *Termodynamik - teoretisk grundlag, praktisk anvendelse*. Nyt Teknisk Forlag, 2017.
- [27] Ole B. Stampe and F. H. Ludvigsen. *Ventilation Ståbi*. Nyt Teknisk Forslag, 2007.
- [28] Ramesh K. Shah and D. P. Sekulic. *Fundamentals of Heat Exchanger Design*. John Wiley and Sons, Inc., 2003.
- [29] Sensirion AG. Datasheet SHT21 Humidity and Temperature Sensor IC. [http://www.ic-meter.com/dk/wp-content/uploads/2013/06/Sensirion\\_Humidity\\_SHT21\\_Datasheet\\_V3.pdf](http://www.ic-meter.com/dk/wp-content/uploads/2013/06/Sensirion_Humidity_SHT21_Datasheet_V3.pdf), 2011.
- [30] Sensirion AG. Datasheet SHT7x (SHT71, SHT75) Humidity and Temperature Sensor IC. <https://www.sensirion.com/en/download-center/humidity-sensors/pintype-digital-humidity-sensors/>, 2011.

- 
- [31] Sensirion AG. Calibration Certification – Digital Humidity- and Temperature Sensors. <https://www.sensirion.com/en/download-center/humidity-sensors/pintype-digital-humidity-sensors/>, 2018.
- [32] Sergey Anisimov, A. Jedlikowski, and D. Pandelidis. Frost formation in the cross-flow plate heat exchanger for energy recovery. *International Journal of Heat and Mass Transfer*, 90:201–217, November 2015.
- [33] Statens Byggeforsikringsinstitut. *Danish Building Regulations 2018*. Statens Byggeforsikringsinstitut, 2018.
- [34] Tim Padfield. Equations describing the physical properties of moist air. <http://www.conservaionphysics.org/atmcalc/atmoclc2.pdf>.
- [35] Vapac Humidification Ltd. Minivap Humidifier Model DV4. <https://www.vapacparts.com/manuals/vapac-dv4-owners-manual.pdf>, 2006.
- [36] VEAB Heat Tech AB. CV Circular electric duct heaters. [https://veab.com/documents/cv/broschyr/CV\\_VEAB\\_Heat\\_Tech\\_GB.pdf](https://veab.com/documents/cv/broschyr/CV_VEAB_Heat_Tech_GB.pdf), 2018.

# A | Defrost methods

## Preheater test

When ice formation was detected, the ice was removed by turning on the 230V preheater on maximum, seen in figure A.1, until the temperature on the sensor that was measuring the coldest temperature reached 1 °C. This took about 1 minute. Then the power on the preheater was turned down so that the temperature could stay stable and above 0 °C in the given situation. It required about 60 W to keep the heat exchanger free of ice. It gave no measurable increase in pressure drop across the heat exchanger. After the preheater has been running for some time to keep the temperature above 0 °C, the ventilation box was opened to make sure the ice on the heat exchanger was gone. Hereafter, the ventilation unit was closed, and everything stabilized again for a period. Finally, the preheater was completely switched off, until the temperature decreased again. The temperature dropped rapidly to about 0.5 °C where it stabilized for a moment, after which it rapidly dropped below 0 °C. By opening the ventilation unit, it could be confirmed that there was again ice on the heat exchanger.



**Figure A.1:** Voltmeter and watt meter to measure power consumption

## Bypass test

The bypass damper was tested under conditions where there will be no frost formation. The damper is opened by holding in a switch. It takes 75 seconds to open the damper completely. During the test, the damper was opened in several positions to see if the temperature would remain stable. The purpose was to see if it is possible to control the temperature with the damper or whether the temperature will rise/fall drastically. When opening the damper, the temperature of the exhaust port increased to 14 °C and remained fairly stable at this temperature. It turned out that the fans did not maintain the same flow when the damper was opened.

# B | Test conditions

## B.1 Experimental test conditions

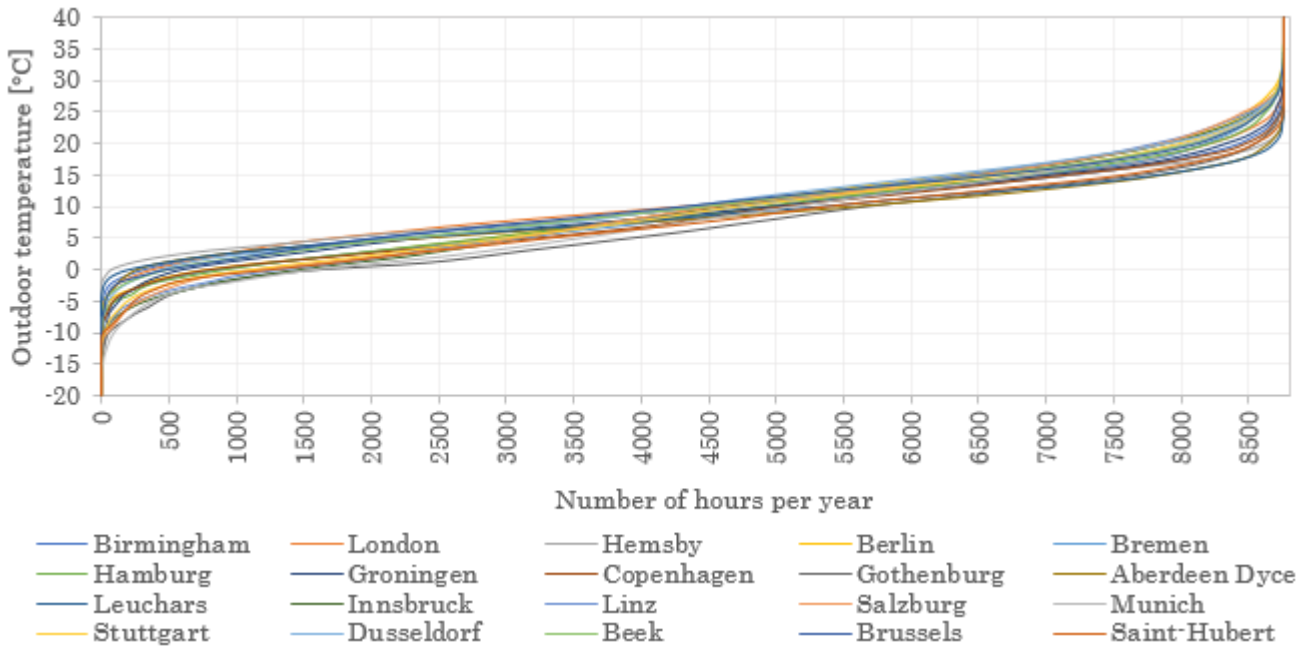


Figure B.1: Cumulative number of hours based on outdoor ambient temperature for all the initially selected locations

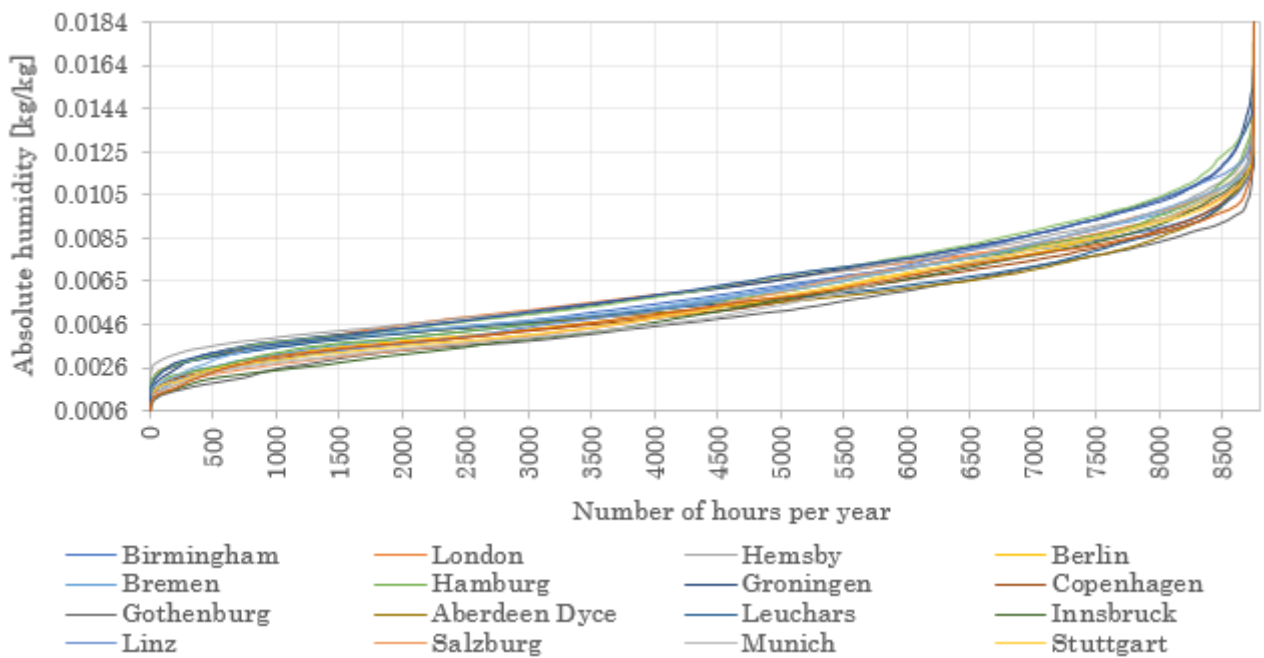


Figure B.2: Cumulative number of hours based on outdoor ambient absolute humidity for all the initially selected locations

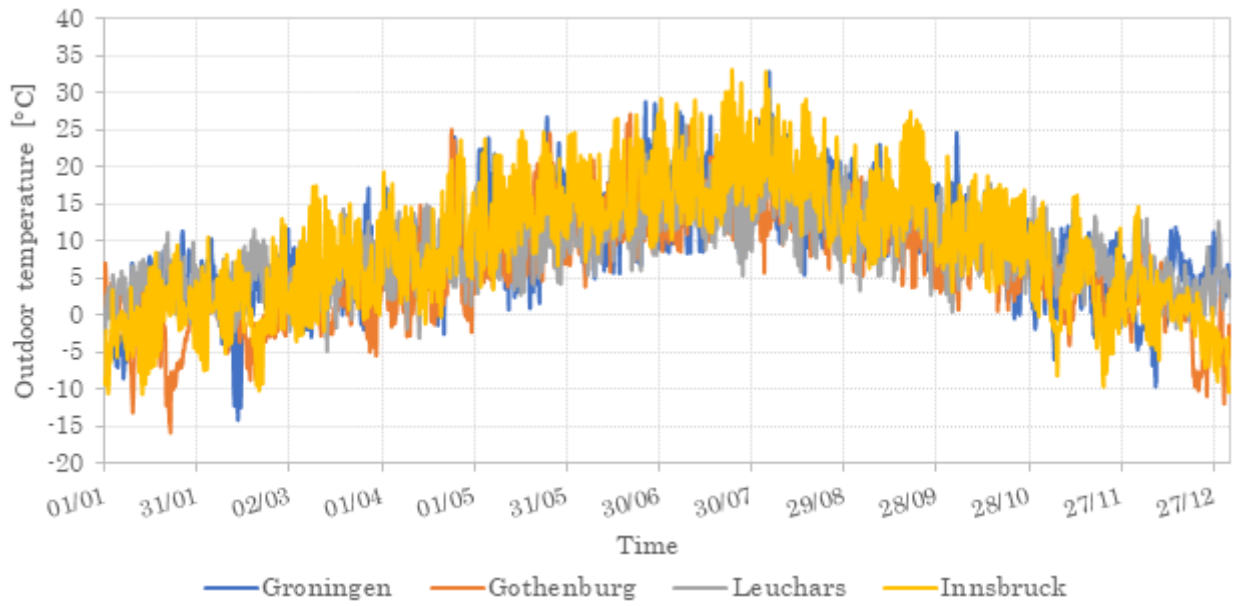


Figure B.3: Full year outdoor ambient temperature variations for the representative locations

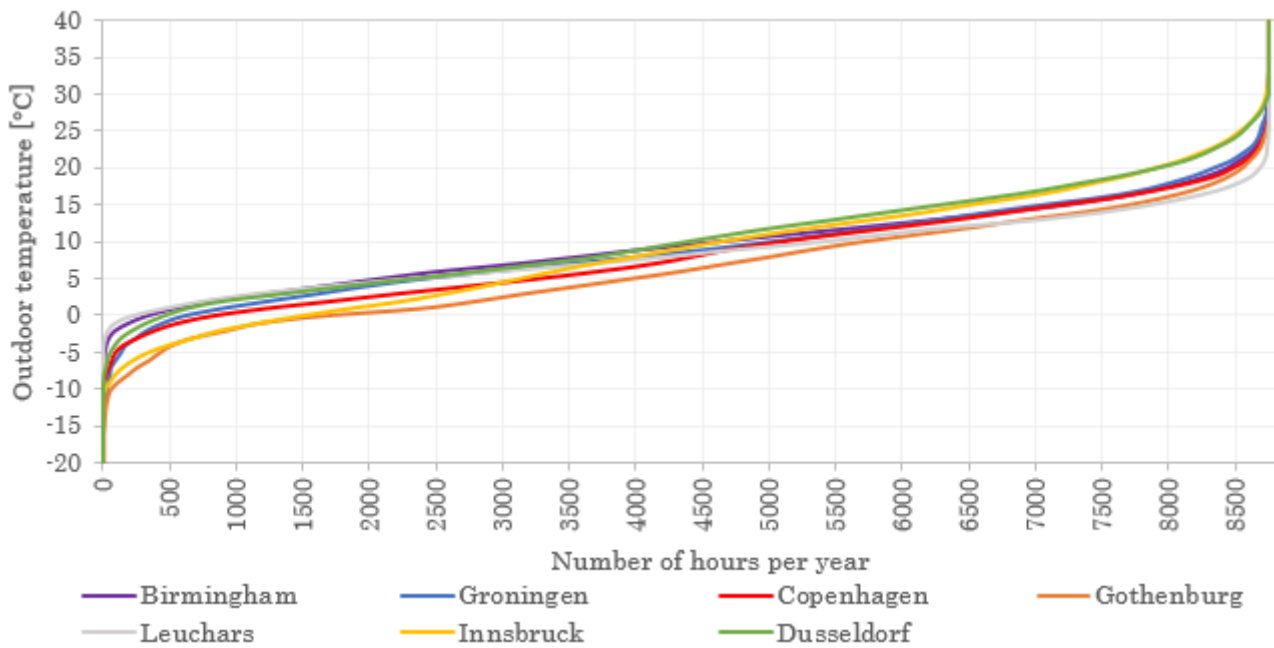
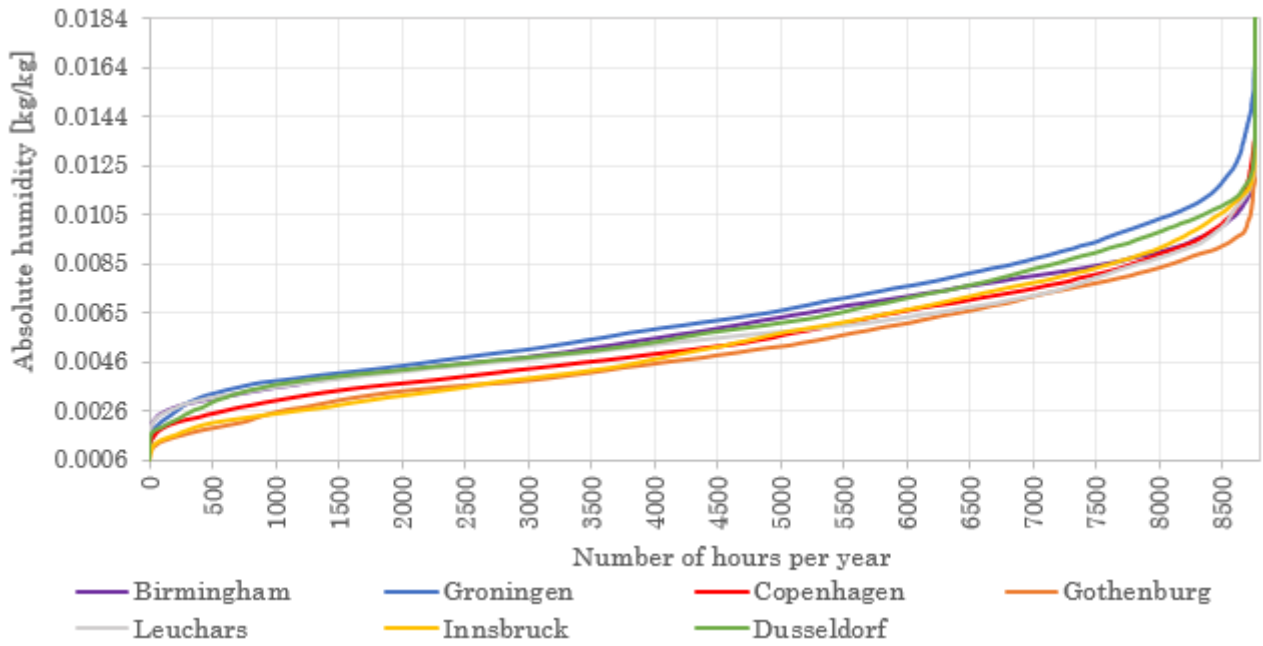
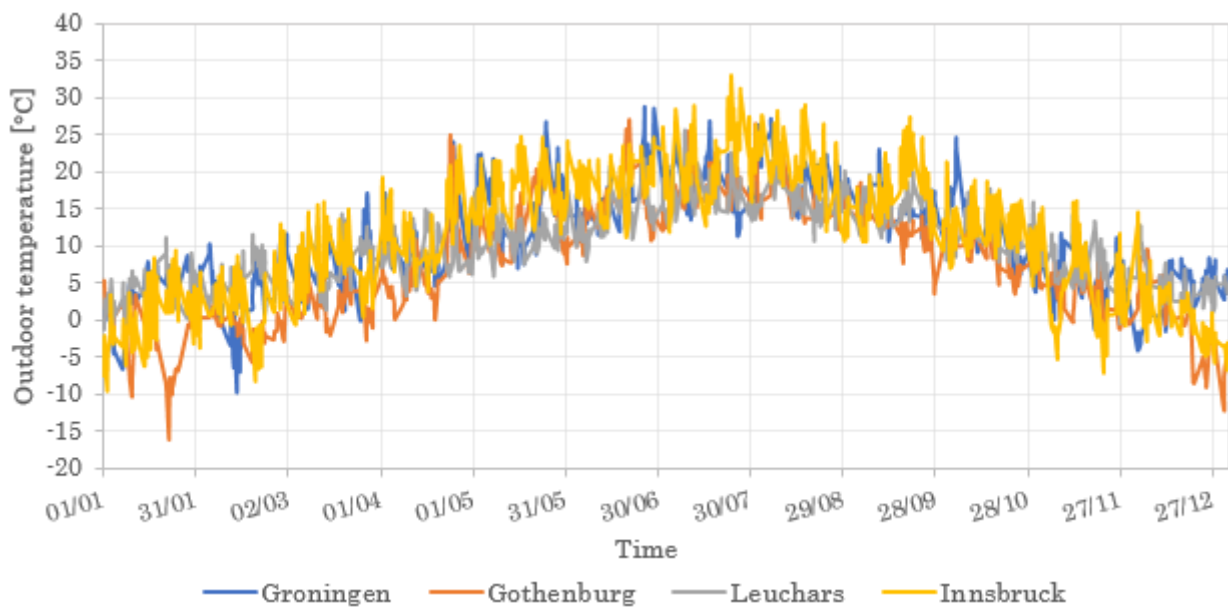


Figure B.4: Cumulative number of hours based on outdoor ambient temperature for all the final locations



**Figure B.5:** Cumulative number of hours based on outdoor ambient absolute humidity for all the final locations



**Figure B.6:** Outdoor temperature variations for the working hours during the whole year for all the final locations

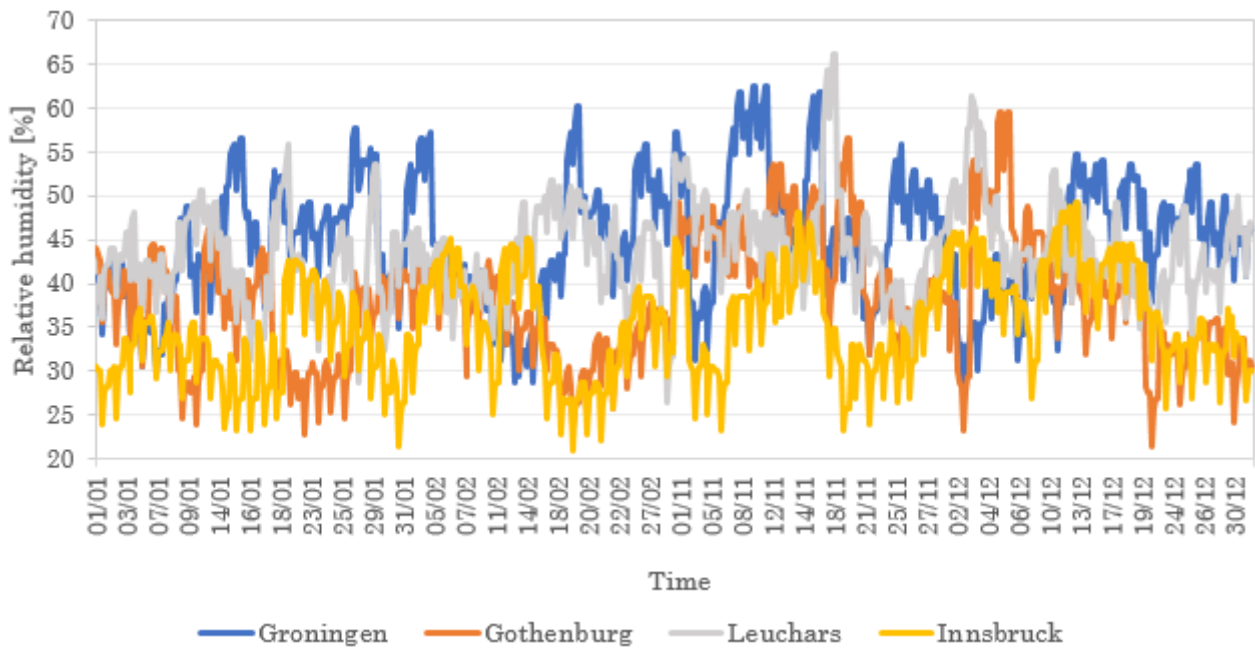


**Figure B.7:** Relative humidity in a classroom during January, February, November, December for the chosen representative locations for working hours

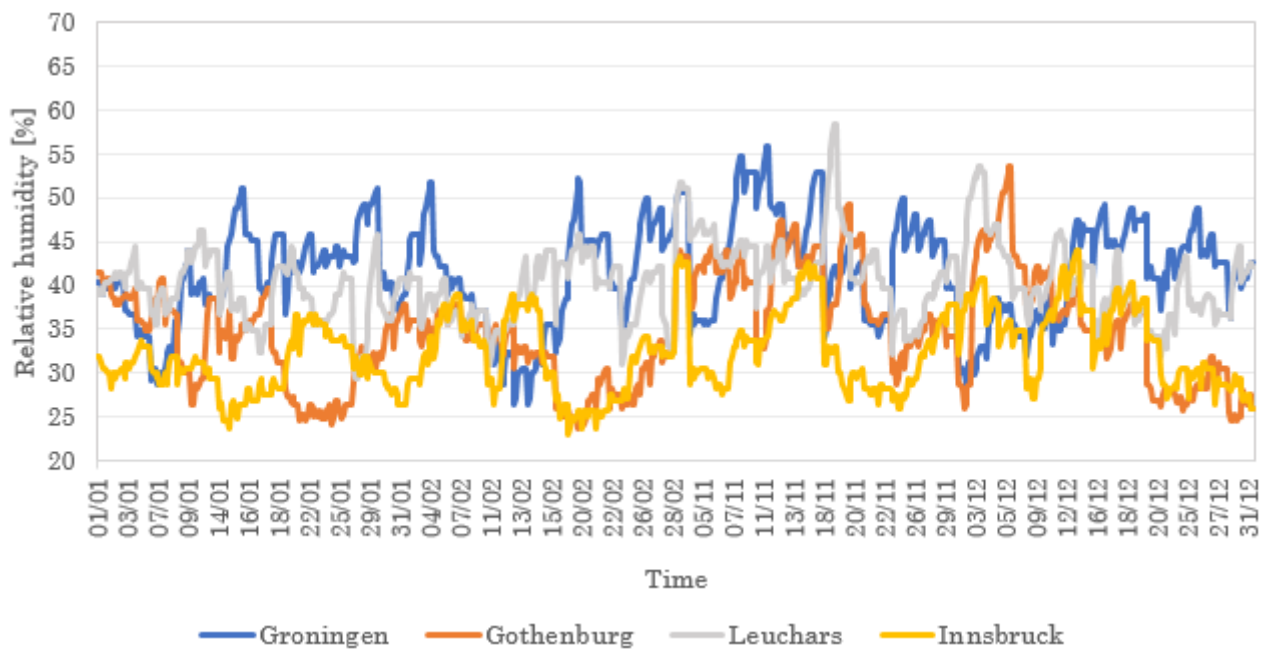


**Figure B.8:** Relative humidity in an office during January, February, November, December for the chosen representative locations for working hours

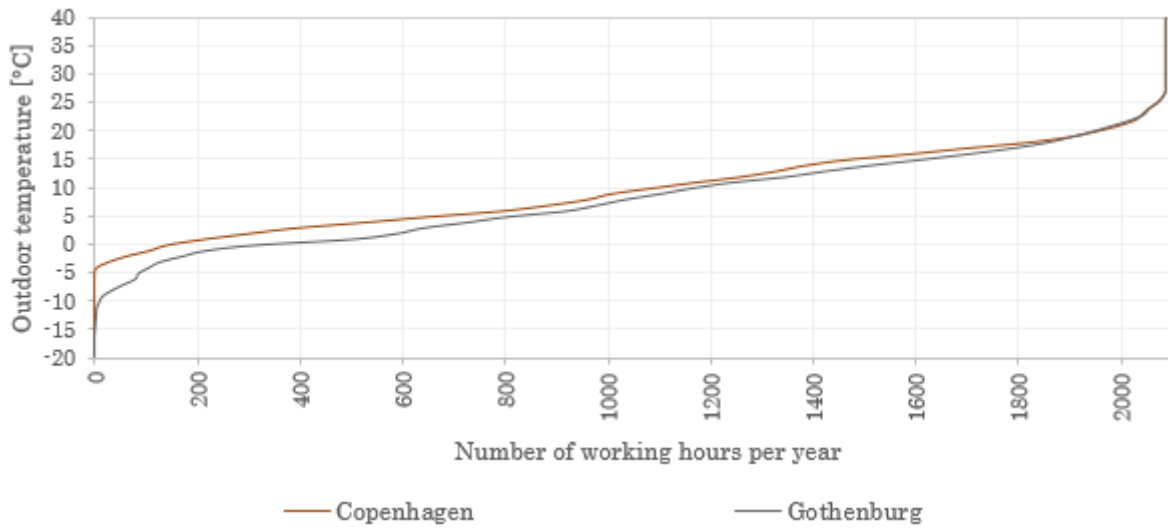


**Figure B.9:** Cumulative number of working hours based on outdoor ambient temperature for Southern Scandinavia (representative location Gothenburg)

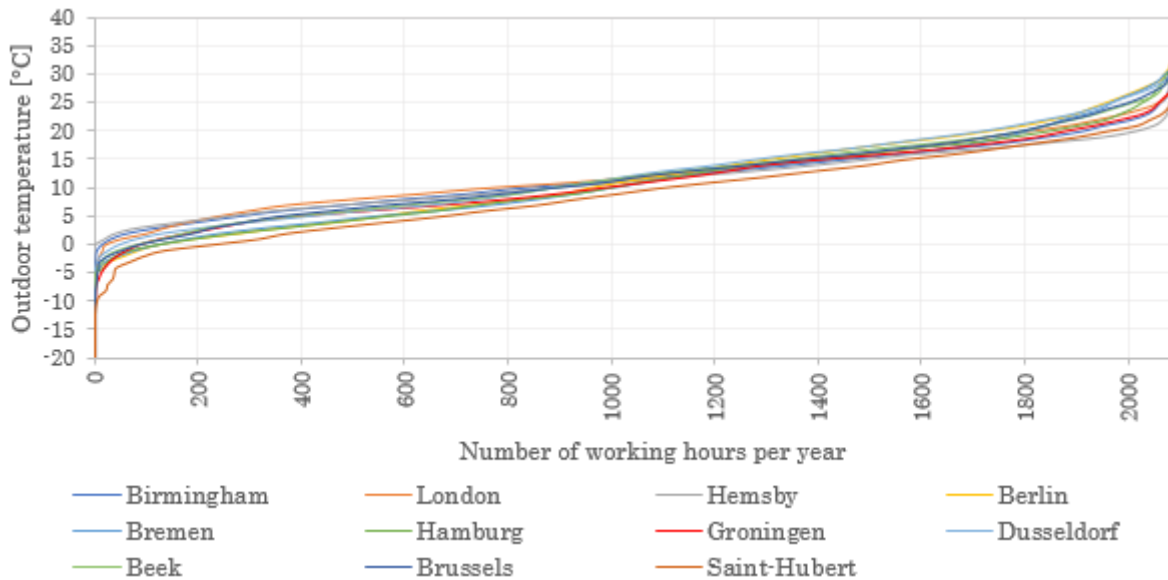


**Figure B.10:** Cumulative number of working hours based on outdoor ambient temperature for England and Central Europe (representative location Groningen)

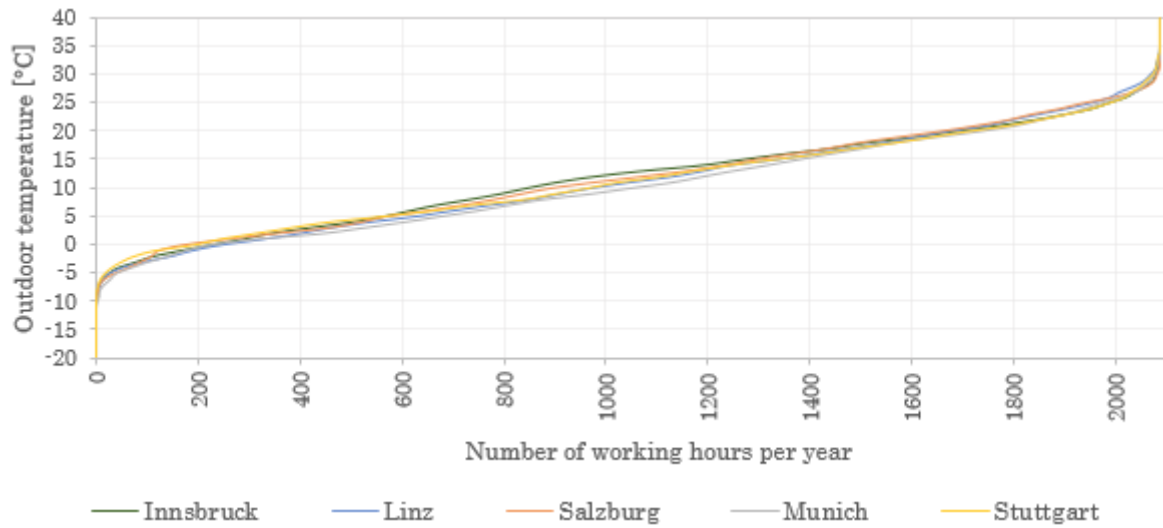


**Figure B.11:** Cumulative number of working hours based on outdoor ambient temperature for Southern Germany and Austria (representative location Innsbruck)

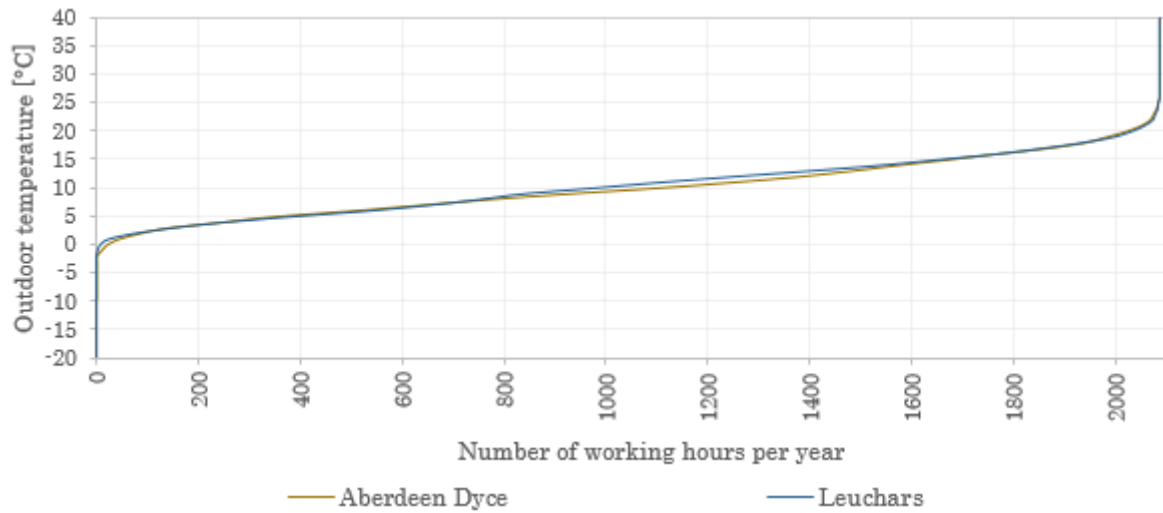


**Figure B.12:** Cumulative number of working hours based on outdoor ambient temperature for Scotland (representative location Leuchars)

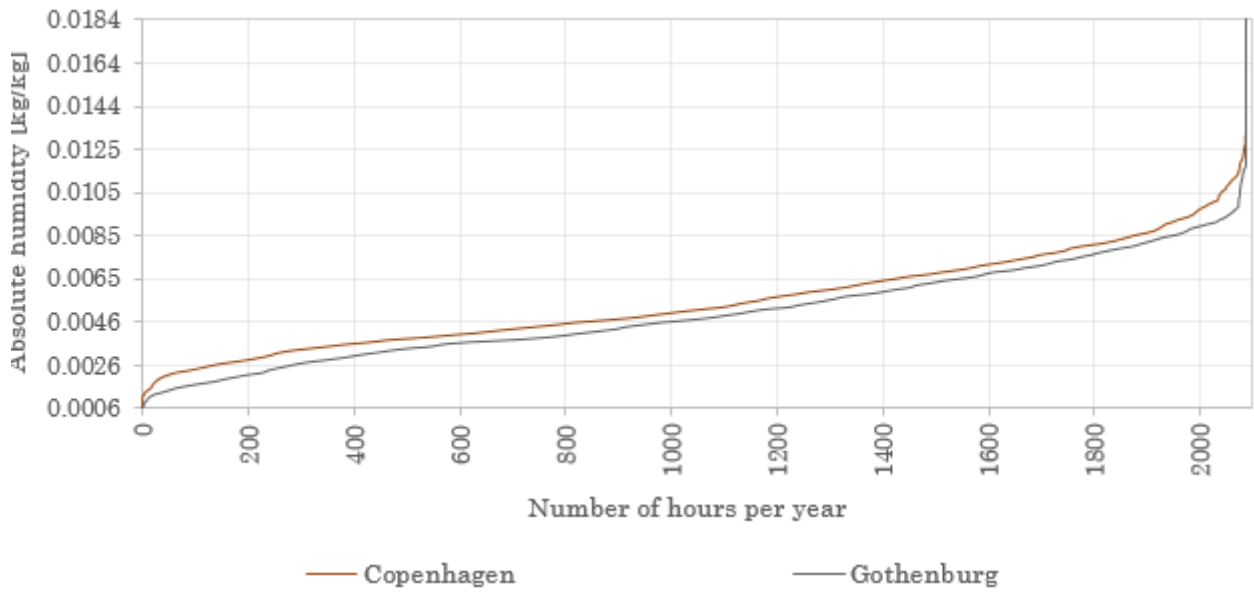


**Figure B.13:** Cumulative number of working hours based on outdoor ambient absolute humidity for Southern Scandinavia (representative location Gothenburg)

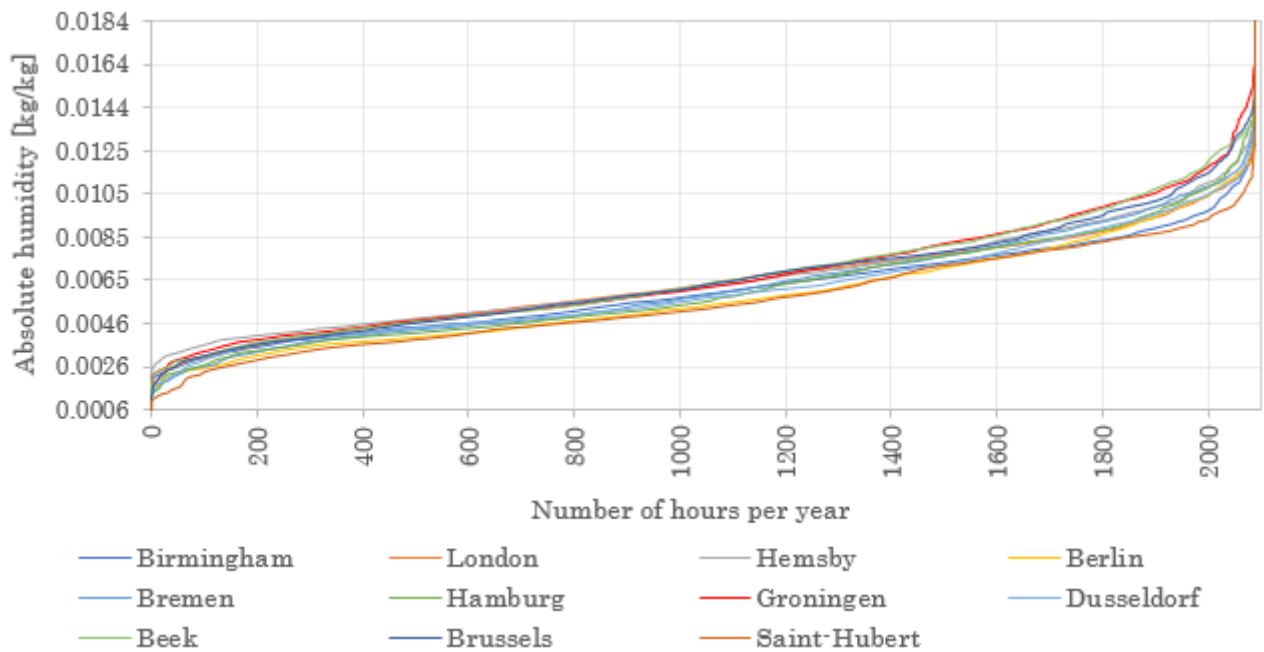


**Figure B.14:** Cumulative number of working hours based on outdoor ambient absolute humidity for England and Central Europe (representative location Groningen)

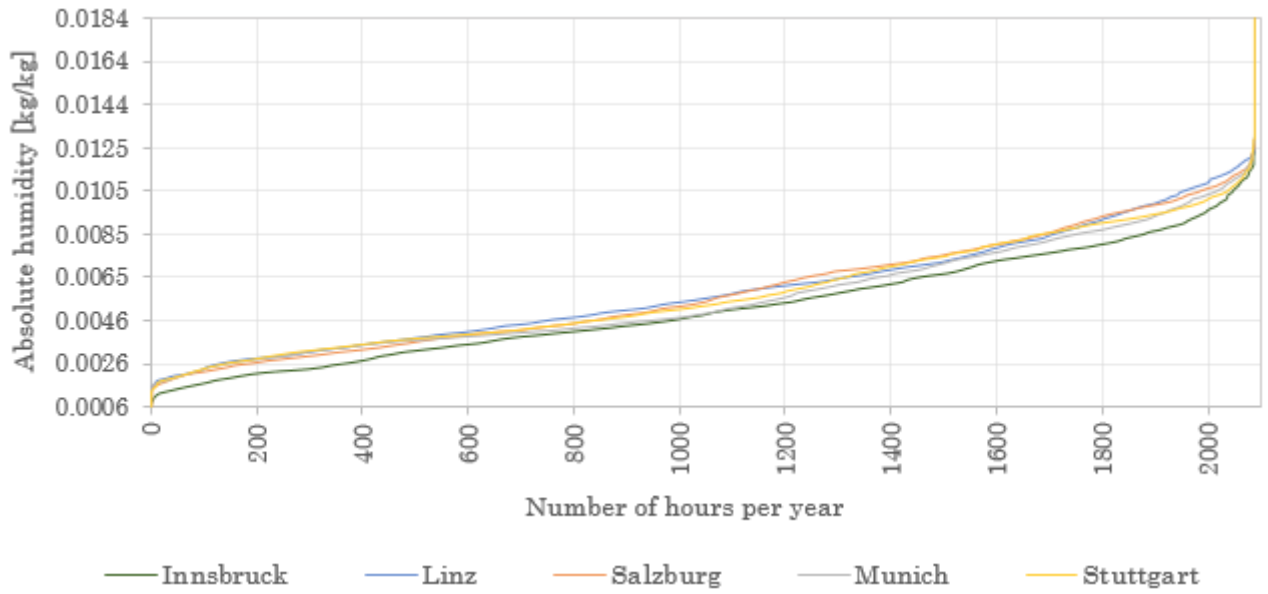


**Figure B.15:** Cumulative number of working hours based on outdoor ambient absolute humidity for Southern Germany and Austria (representative location Innsbruck)

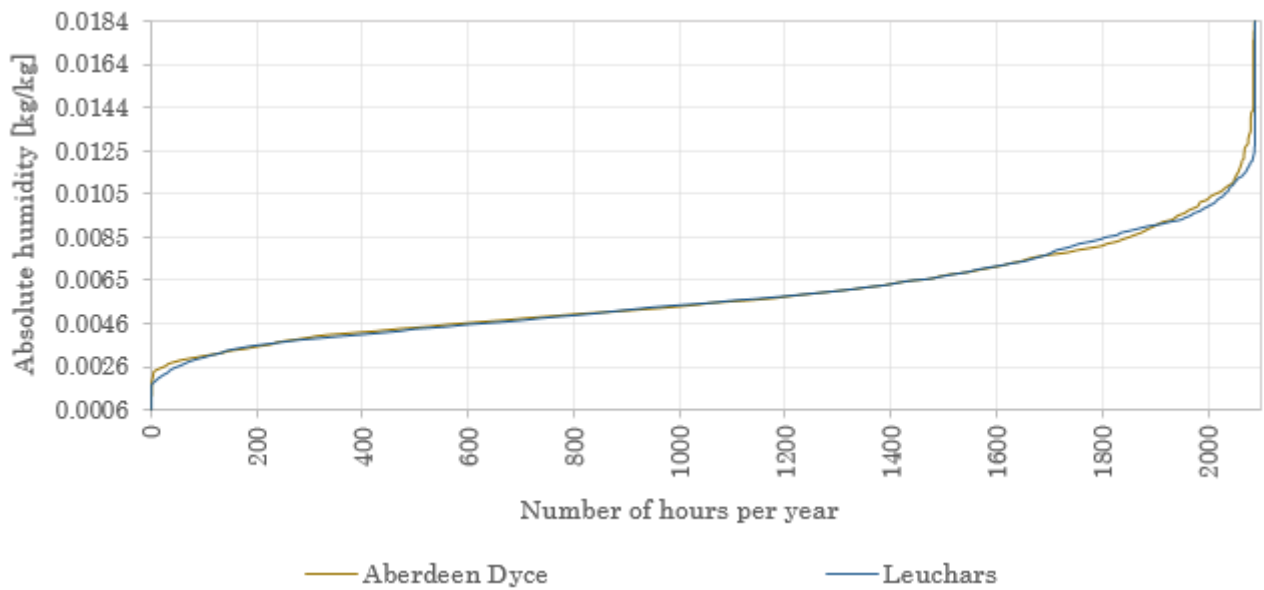


**Figure B.16:** Cumulative number of working hours based on outdoor ambient absolute humidity for Scotland (representative location Leuchars)

**Bsim input**Room sizes:

- BR18 9. Bygningens indretning / Indretning af normalklasserum: min 6 m<sup>3</sup> pr. person in normal classrooms in schools; 8 m<sup>3</sup> pr. person in a work place with mechanical ventilation
- DS1752:2001 p. 26, table A.7 - Personbelastning (pers. per m<sup>2</sup>) - Storrumskontor 0.07 pers / m<sup>2</sup> -> 1 pers / 14.29 m<sup>2</sup>

Room height: 2.5 m / "Normalt skal et arbejdsrum have en arbejds højde på 2.5m" - Arbejdstilsynet/

Classroom: 24 pupils + 1 teacher = 24\*6 m<sup>3</sup> + 8 m<sup>3</sup> = 152 m<sup>3</sup> -> 61 m<sup>2</sup> (24 pupils per class is the number of pupils in most of the classes in public schools in Denmark. Source: Danmarks Statistik <https://backend.folkeskolen.dk/~8/5/naesten-ingen-folkeskoleklasser-har-over-30-elever.pdf>)

Office: 4 people -> 4\*14.29 m<sup>2</sup> = 57 m<sup>2</sup>

Ventilation rate:

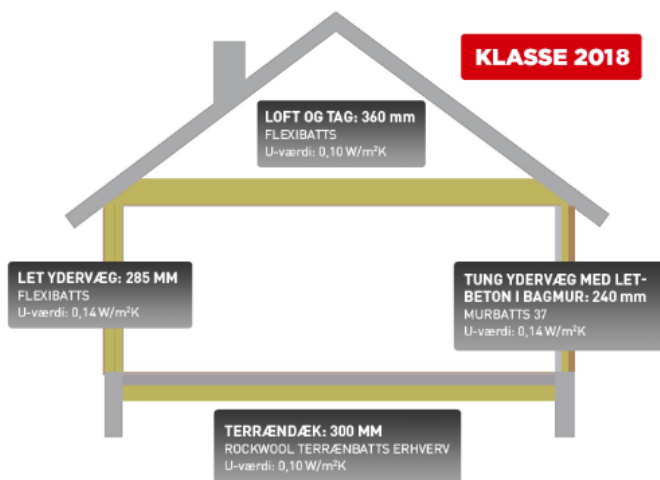
- Min. BR18 ventilation rate 0.35 l/s m<sup>2</sup> floor area -> 76.7 m<sup>3</sup>/h for the classroom; 71.8 m<sup>3</sup>/h for the office
- Calculated ventilation rate based on CO<sub>2</sub> using the dilution equation (classroom): 3.9 l/s m<sup>2</sup> floor area -> 850 m<sup>3</sup>/h
- Calculated ventilation rate based on CO<sub>2</sub> using the dilution equation (office): 0.7 l/s m<sup>2</sup> floor area -> 136.8 m<sup>3</sup>/h

	Classroom:	Office:	
Airflow [Q]	0,236	0,038	m <sup>3</sup> /s
Air change rate [n]	5,58	0,95	h <sup>-1</sup>
Number of people [N]	25	4	person
Room volume [V <sub>R</sub> ]	152,3	142,5	m <sup>3</sup>
Pollutant produced/person [q <sub>0</sub> ]	20,4	20,4	L/h·person
Indoor CO <sub>2</sub> [c]	1000	1000	ppm
outdoor CO <sub>2</sub> [c <sub>i</sub> ]	400	400	ppm
Room height [h]	2,5	2,5	m
Floor area [A]	61	57	m <sup>2</sup>
Min airflow (BR18)	0,021	0,020	m <sup>3</sup> /s

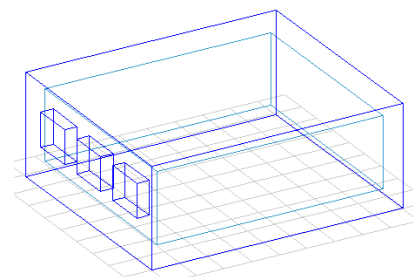
$$n = \frac{q_0 \cdot N}{(c - c_i) \cdot V_R}$$

In BSim, the VAV control is in the following way: the ventilation system supplies minimum ventilation rate until the CO<sub>2</sub> reaches 1000 ppm, after that the system increases the ventilation rate to the one calculated with the dilution equation.

# Minimumstykkelser for isolering i nybyggeri:



The U-values of the components will be based on Rockwool's recommendations for BR18. The U-values have been calculated with the construction types we have.



## People activity level:

- Heat and moisture generation from Ventilation ståbi p. 109 and BSim guide: Medium sedentary activity level, 1.2 met with 1.0 clo clothing level. Heat generation: 120 W per person; Moisture generation: 123 g/h per person
- CO<sub>2</sub> generation from BSim guide: 17\*activity level -> 17\*1.2 -> 20.4 l/h per person

People schedule: Classroom - 8-15 Mon-Friday; (35 hours per week <https://uvm.dk/folkeskolen/fag-timetal-og-overgange/undervisningens-samlede-laengde>). Office - 8-16 from Monday to Thursday and 8-13 Friday (37 hours per week); 1 hour break at 12:00 every weekday; at 12:00 there is 50% presence in the classroom and 75% presence in the office. There is a limitation in BSim, where the period for breaks cannot be less than 1 hour, therefore all the breaks for the classroom have been summed up for 1 hour. As for the office, usually the lunch break would be 30min, to compensate for the 1 hour break in BSim, the occupancy has been decreased only with 25% during the 1-hour break.

Ventilation and heating: ON during occupancy time

## Infiltration:

### CLASSROOM

Infiltration: BR18 §263 - max. 1 l/s m<sup>2</sup> floor area for heated spaces up to 15°C and more at 50Pa pressure difference.

In usage time: 0.04 + 0.06 • q<sub>50</sub> litres/sec. per m<sup>2</sup> heated floorage (SBI 213, p. 59)

$$0.04 + 0.06 \cdot 1 \text{ l/s m}^2 = 0.1 \text{ l/s m}^2$$

$$0.1 \text{ l/s m}^2 \cdot 49 \text{ m}^2 = 4.9 \text{ l/s}$$

$$4.9 \text{ l/s} \cdot 3.6 = 17.64 \text{ m}^3/\text{h}$$

$$17.64 \text{ m}^3/\text{h} \rightarrow 0.14 \text{ h}^{-1}$$

Outside usage time: 0.06 • q<sub>50</sub> litres/sec. per m<sup>2</sup> heated floorage (SBI 213, p. 59)

$$0.06 \cdot 1 \text{ l/s m}^2 = 0.06 \text{ l/s m}^2$$

$$0.06 \text{ l/s m}^2 \cdot 49 \text{ m}^2 = 2.94 \text{ l/s}$$

$$2.94 \text{ l/s} \cdot 3.6 = 10.58 \text{ m}^3/\text{h}$$

$$10.58 \text{ m}^3/\text{h} \rightarrow 0.086 \text{ h}^{-1}$$

**OFFICE**

Infiltration: BR18 §263 - max. 1 l/s m<sup>2</sup> floor area for heated spaces up to 15°C and more at 50Pa pressure difference.

In usage time:  $0.04 + 0.06 \cdot q50$  litres/sec. per m<sup>2</sup> heated floorage (SBI 213, p. 59)

$$0.04 + 0.06 \cdot 1 \text{ l/s m}^2 = 0.1 \text{ l/s m}^2$$

$$0.1 \text{ l/s m}^2 \cdot 57 \text{ m}^2 = 5.7 \text{ l/s}$$

$$5.7 \text{ l/s} \cdot 3.6 = 20.52 \text{ m}^3/\text{h}$$

$$20.52 \text{ m}^3/\text{h} \rightarrow 0.14 \text{ h}^{-1}$$

Outside usage time:  $0.06 \cdot q50$  litres/sec. per m<sup>2</sup> heated floorage (SBI 213, p. 59)

$$0.06 \cdot 1 \text{ l/s m}^2 = 0.06 \text{ l/s m}^2$$

$$0.06 \text{ l/s m}^2 \cdot 57 \text{ m}^2 = 3.42 \text{ l/s}$$

$$3.42 \text{ l/s} \cdot 3.6 = 12.31 \text{ m}^3/\text{h}$$

$$12.31 \text{ m}^3/\text{h} \rightarrow 0.086 \text{ h}^{-1}$$

Construction:**Outer wall**

Material	d (m)	$\lambda$ (W/mK)	R (m <sup>2</sup> K/W)	U (W/m <sup>2</sup> K)
Inner surface resistance			0.13	
Concrete (light)	0.1	0.3	0.33	
Insulation	0.24	0.037	6.49	
Bricks	0.108	0.727	0.15	
Outer surface resistance			0.04	
Total R			7.14	0.14

**Roof**

Material	d (m)	$\lambda$ (W/mK)	R (m <sup>2</sup> K/W)	U (W/m <sup>2</sup> K)
Inner surface resistance			0.10	
Plasterboard	0.026	0.25	0.10	
Insulation	0.36	0.037	9.73	
Concrete (dense)	0.1	1.5	0.07	
Outer surface resistance			0.04	
Total R			10.04	0.10

**Floor**

Material	d (m)	$\lambda$ (W/mK)	R (m <sup>2</sup> K/W)	U (W/m <sup>2</sup> K)
Inner surface resistance			0.17	
Concrete	0.1	2	0.05	
Insulation	0.3	0.038	7.89	
Sand	0.2	0.25	0.80	
Resistance for soil			1.50	
Total R			10.41	0.10

**Windows**

U glass	0.1	W/m <sup>2</sup> K
U wood frame	0.13	W/m <sup>2</sup> K

**Table 6.2.1 – Surface resistance m<sup>2</sup>K/W**

	The heat flow's direction		
	Upwards	Horizontal	Downwards
R <sub>si</sub>	0,10	0,13	0,17
R <sub>se</sub>	0,04	0,04	0,04

DS418

[https://www.engineeringtoolbox.com/thermal-conductivity-d\\_429.html](https://www.engineeringtoolbox.com/thermal-conductivity-d_429.html)

<https://www.rockwool.dk/vaerd-at-vide/bygningsreglement/minimumstykkelser-for-isolering/>

# C | Test set-up

Email correspondence with Kim Ihlow from the Technical Secretariat for CEN/TC 110 on Heat exchangers with regard to positioning of temperature sensors on the grid:

Question:

"Dear Mr. Ihlow

We are a group of master students from Aalborg University, Denmark, doing a master thesis on performance of heat exchangers. We have a question regarding a figure in EN308:1997 (Heat exchangers). The figure in question is the top figure on page 12.

Our master thesis involves measurement of airflow temperature in a rectangular duct. We have 16 temperature sensors on the duct.

In the figure on p. 12, the grid is made of 5x3 sensors. In our case, we will have a grid of 4x4 sensors. Our main questions are:

- 1) Why is the distance from the border to the first sensor different on the L2 and L1? 2) Why is the distance between the 2 sensors, inside the grid, 0.21 L2 and not half of 0.43 L2? 3) What should the distance from the border to the first sensor and between the sensors be in our case (with a 4x4 grid)?"

The figure in question can be seen below.

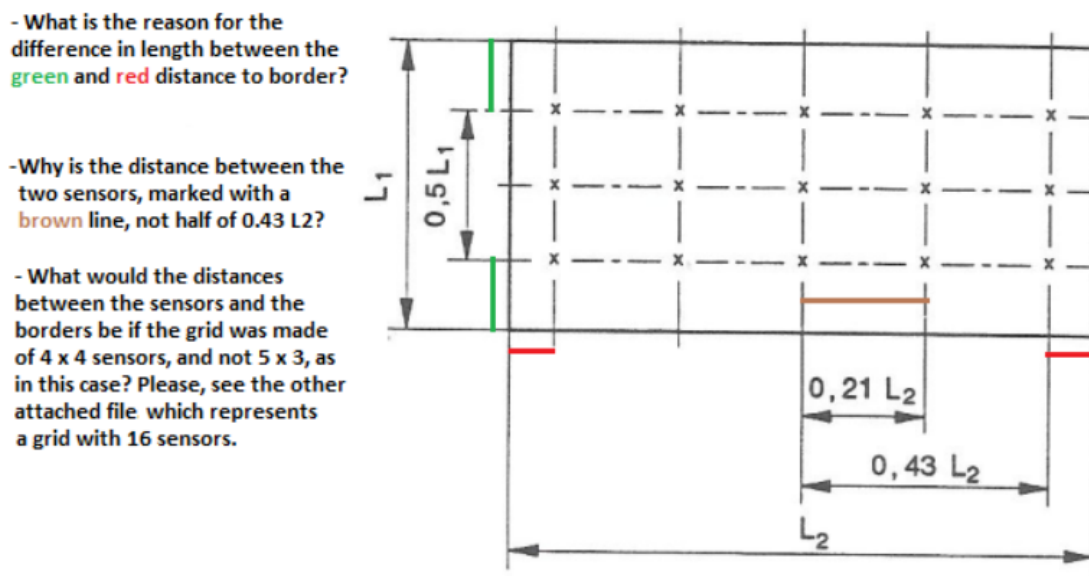


Figure C.1: "Figure 4 Temperature measuring plane" from DS308:1997 - page 12

Answer:

"Hi Dzhanan,

I received an answer from the head of the responsible working group. He said he doesn't know how

and why the sensor positions found their way into the standard. He is of the opinion that the distance between the sensors and between sensors and edges do not reflect what was intended by the standard.

He said that if you have 5 sensors for example, the cross-sectional area will be divided into 5 equally sized parts. The sensors are usually placed in the center of gravity of each of those parts, but this is unfortunately not the case in the figures in EN 308:1997. So I guess in your case you create a grid of 4x4 equally sized parts and place the sensors in the center of each part."

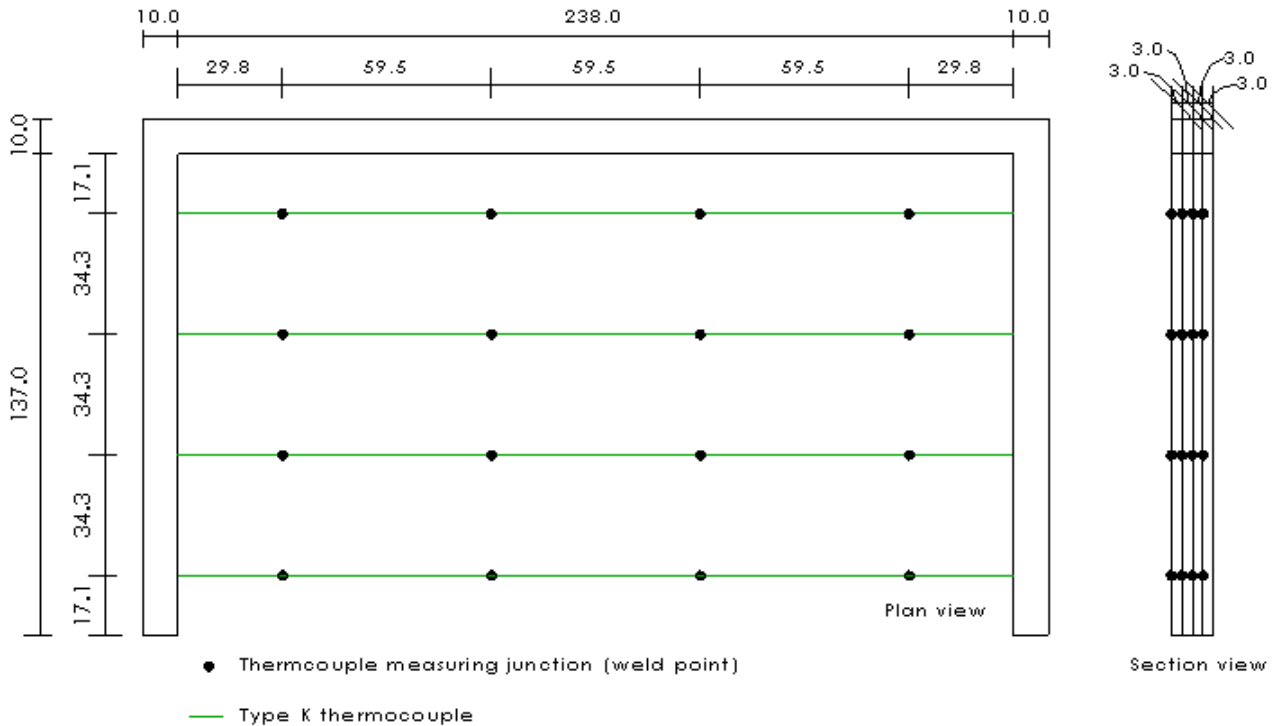


Figure C.2: Installation of thermocouples on the grid

## C.1 Sensor calibration and measurement uncertainty

The sensors have been calibrated prior to conducting the measurements.

### Thermocouples

To measure the airflow temperature, type K thin thermocouples are used. The two different metals, which a thermocouple consists of, are welded together to form the junction end (measuring junction). The temperature difference between the measuring junction and the other end of the thermocouple (ice-point reference/end tail) creates potential, which changes with change of temperature difference between the two ends. A schematic of the thermocouple is shown in figure C.3.

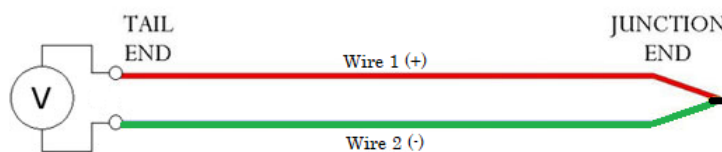
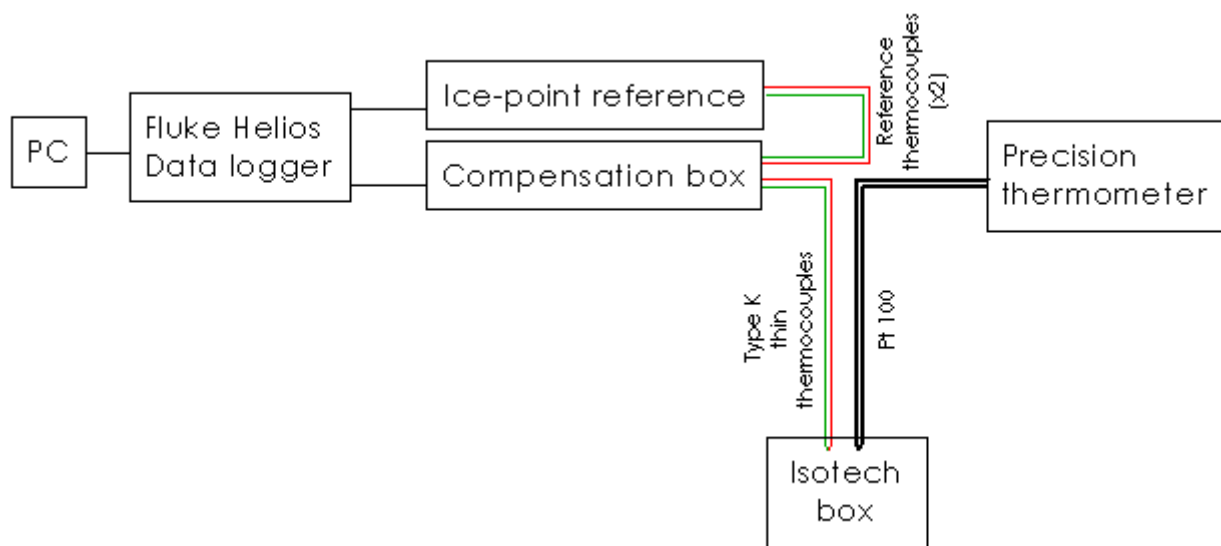


Figure C.3: Thermocouple schematic

The thermocouples have been golden coated in order to reflect as much radiation as possible. However, during the calibration process it has been noticed that the coating is fragile and comes off easily as the thin wires are very flexible. The thermocouples whose measuring points were uncoated during the calibration process have been set aside and not used in the experiment. However, to determine whether uncoating of the thermocouples can lead to some uncertainty in the measurements, one should measure the flow temperature with two calibrated thermocouples, where one of them is coated, while the other one is not. If there is a difference in the readings between the two thermocouples, it would mean that the uncoating increases the uncertainty. Such a test has not been done during this project.

All of the thermocouples are calibrated individually and are connected to a compensation box, where the temperature is measured by 2 reference thermocouples. The calibration set-up can be seen in figure C.4.



**Figure C.4:** Calibration set-up

Equipment:

- Fluke Helios 2287A data logger
- Kaye K170 Ice Point reference
- Compensation box
- Type K thin thermocouples
- Type K thick thermocouples (reference thermocouples)
- Isotech Hyperion 2140 B
- Precision Digital Thermometer ASL F200
- RTD Pt 100 Sensor Probe (reference probe)

The thermocouples and the reference probe are placed in the Isotech dry block. The temperature is logged via the Precision thermometer and the voltage is logged via the Helios data logger, each for every 4 seconds. The temperature in the Isotech box is set to constant values in ranges corresponding to the temperatures that will be measured on each port of the heat exchanger and in the compensation box during the experiments. The increments between the temperature points are 5 °C.

Calibration: First, the reference sensors in the compensation box have been calibrated in order to provide accurate readings for the calibration of the rest of the sensors. To calibrate, the voltage and

temperature readings for each temperature point have been taken for an average of 3 minutes after the temperature has reached stabilization. The temperature-voltage relationship has been plotted for each thermocouple with a linear equation for only positive temperature ranges and 3<sup>rd</sup> order polynomial where negative temperature points are also included [15]. After starting the measurements, only one channel has been modified to have a 2<sup>nd</sup> order polynomial fitting curve, since the 3<sup>rd</sup> order polynomial resulted in inaccurate readings.

Figure C.5 shows the calibration curve for a few of the thermocouples. The calibration of all the thermocouples has been conducted taking into account the temperature in the compensation box, as shown on the Y-axis of the graph.

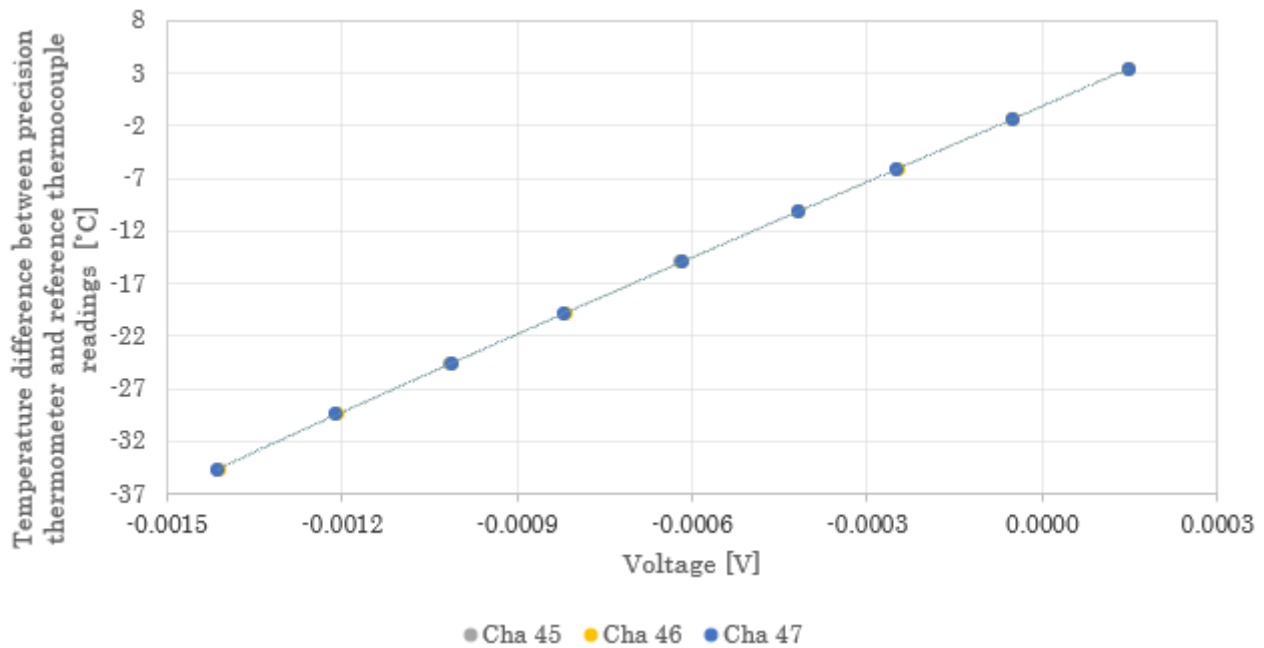
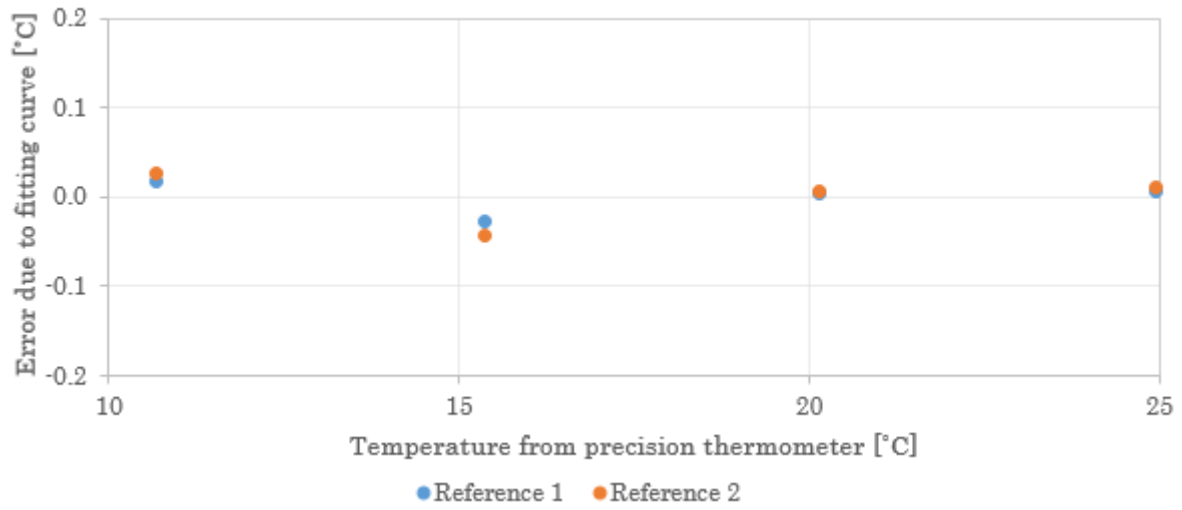


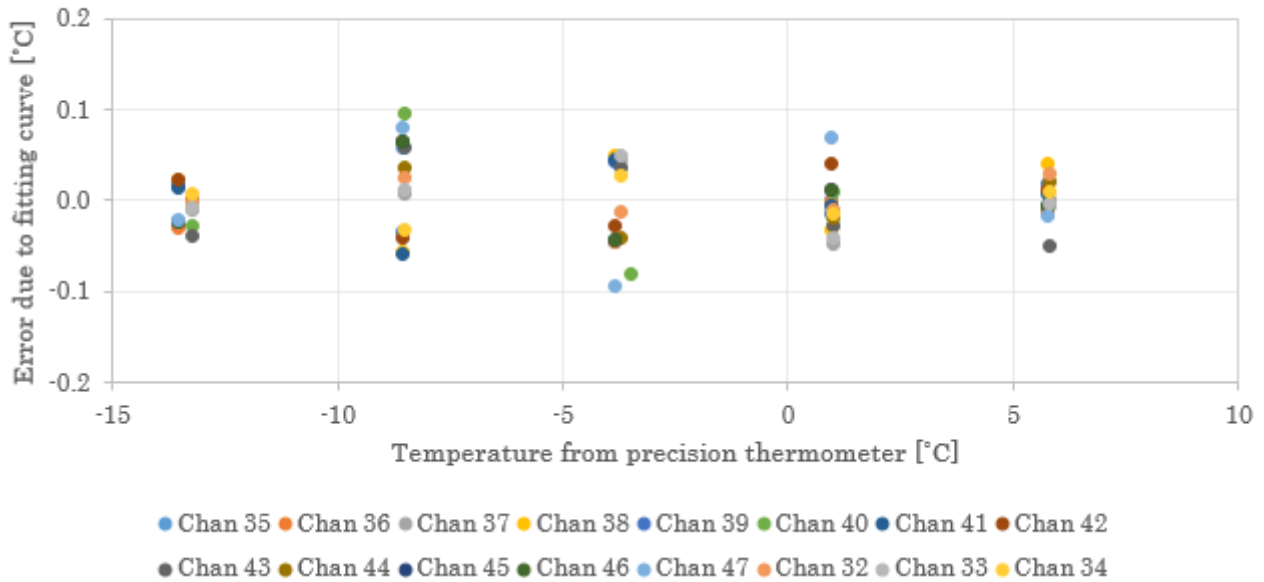
**Figure C.5:** Thermocouple calibration curve

The graphs from figure C.6 show the difference in temperature between the precision thermometer and the calibrated thermocouples created by the fitting of the calibration curve. According to DS/EN 308 [6], the maximum uncertainty for air temperature measurement shall be 0.2 K (dry bulb temperature) and 0.3 K (wet bulb temperature).

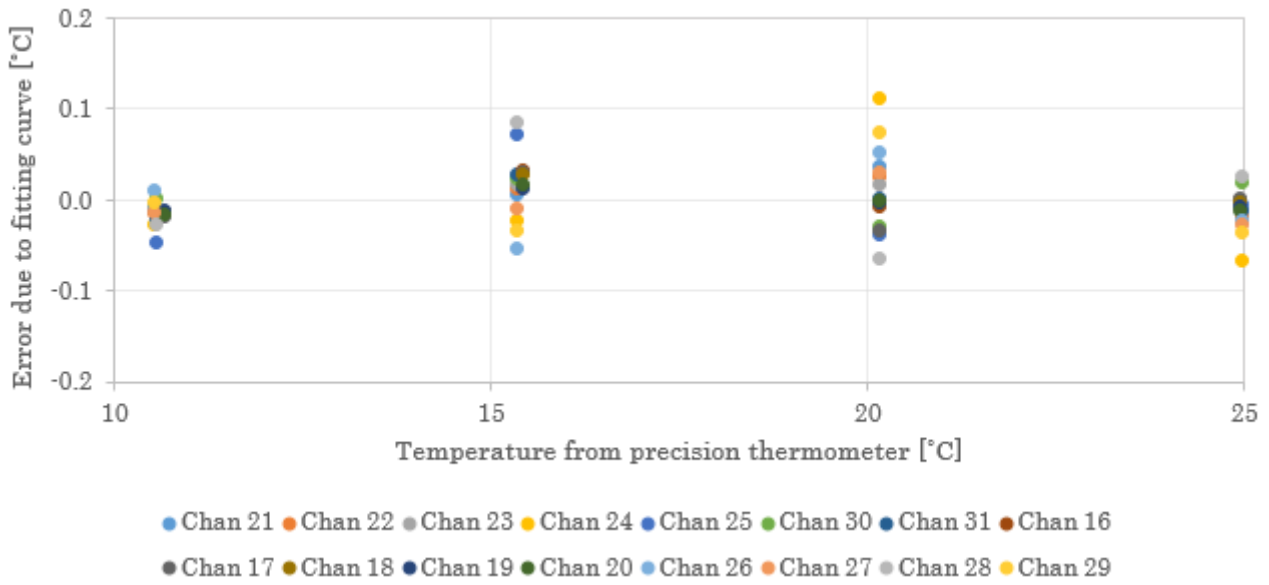
### Reference thermocouples



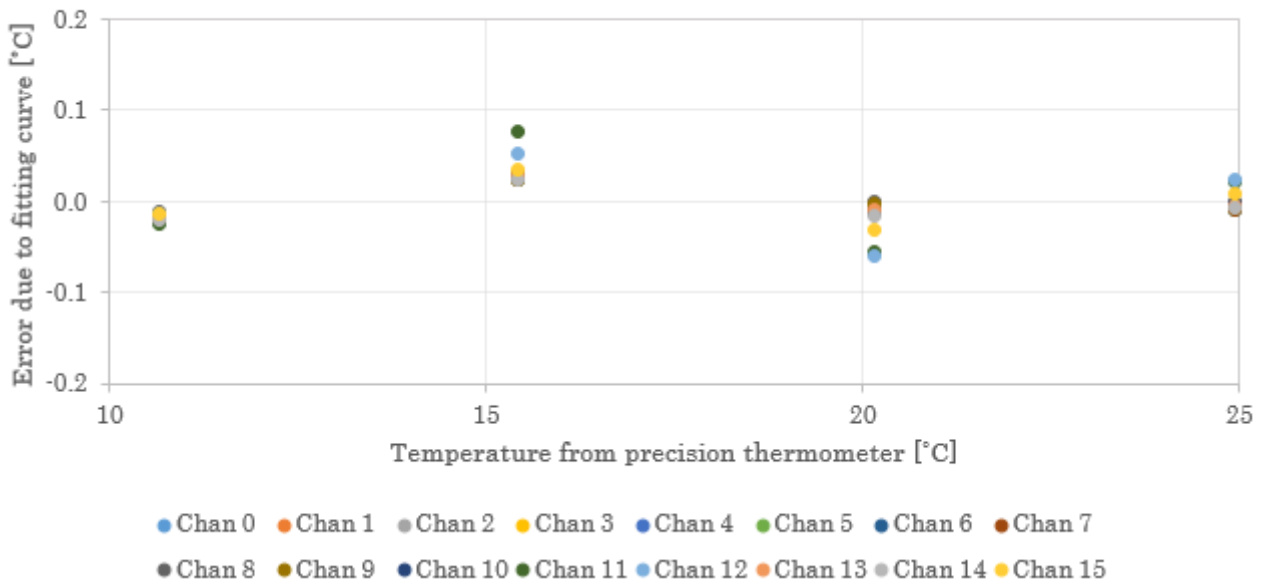
### T1 - outdoor



### T2 - supply



### T3 - extraction



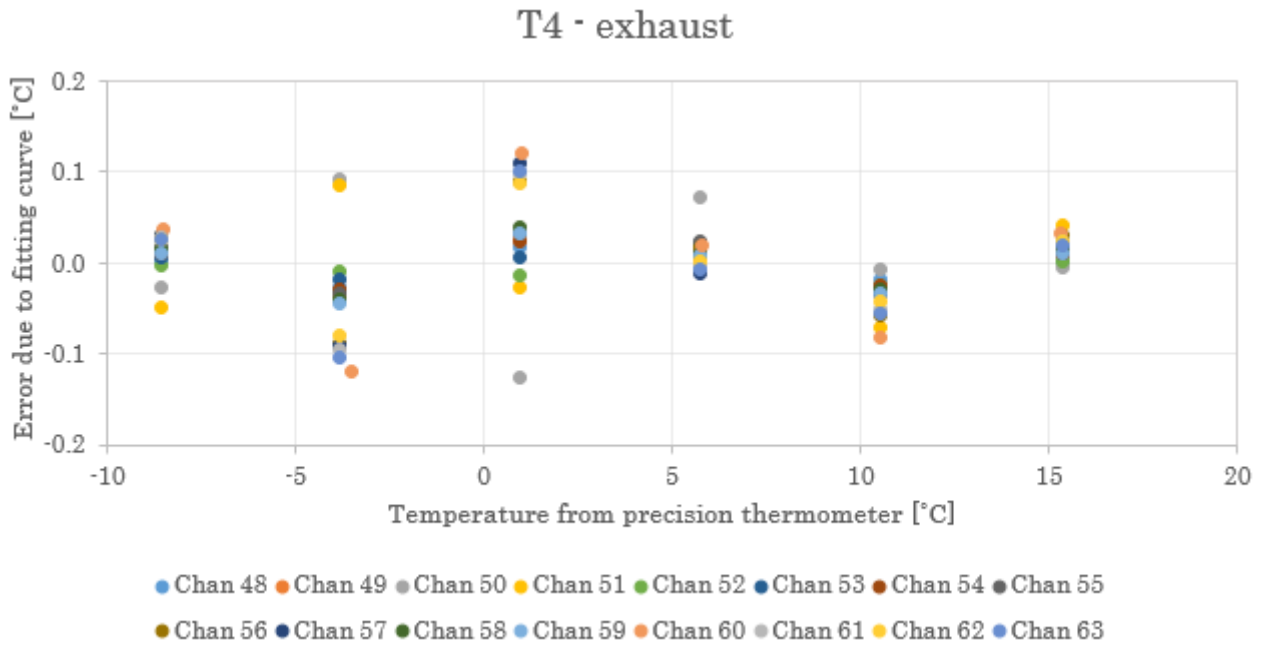


Figure C.6: Error due to calibration curve for all thermocouples

The calibration polynomials are shown in table C.1.

Channel	Calibration polynomial
75 (Ref 1)	$24109 * x + 0.6830$
75 (Ref 2)	$24193 * x + 0.6334$
0	$23612.96 * x - 0.06$
1	$23630.22 * x - 0.05$
2	$23584.64 * x - 0.05$
3	$23720.86 * x - 0.05$
4	$23659.40 * x - 0.04$
5	$23731.84 * x - 0.06$
6	$23670.57 * x - 0.06$
7	$23656.38 * x - 0.06$
8	$23561.75 * x - 0.08$
9	$23576.50 * x - 0.09$
10	$23522.98 * x - 0.09$
11	$23573.70 * x - 0.08$
12	$23481.67 * x - 0.07$
13	$23687.75 * x - 0.07$
14	$23645.93 * x - 0.08$
15	$23607.92 * x - 0.08$

Channel	Calibration polynomial
16	$23570.61 * x - 0.07$
17	$23638.94 * x - 0.06$
18	$23577.94 * x - 0.08$
19	$23702.98 * x - 0.08$
20	$23676.78 * x - 0.08$
21	$24007.32 * x - 0.14$
22	$24034.65 * x - 0.04$
23	$24037.98 * x - 0.08$
24	$23918.57 * x + 0.04$
25	$23763.29 * x - 0.23$
26	$23892.06 * x - 0.08$
27	$23856.98 * x - 0.10$
28	$23588.26 * x - 0.23$
29	$23941.40 * x + 0.02$
30	$24295.75 * x + 0.02$
31	$24295.03 * x + 0.07$
32	$2947170.09 * x^3 - 274512.19 * x^2 + 23864.08 * x - 0.09$
33	$100716949.53 * x^3 - 82455.90 * x^2 + 24067.20 * x - 0.08$
34	$183631865.99 * x^3 + 9212.22 * x^2 + 23980.19 * x + 0.03$
35	$367981298.65 * x^3 + 230084.83 * x^2 + 23896.42 * x - 0.10$
36	$362146622.33 * x^3 + 185721.77 * x^2 + 24009.99 * x - 0.12$
37	$103190122.73 * x^3 - 83093.60 * x^2 + 23881.14 * x - 0.07$
38	$56654280.94 * x^3 - 502777.41 * x^2 + 23450.11 * x - 0.33$
39 (port 64)	$157843073.10 * x^3 - 197307.77 * x^2 + 23723.75 * x - 0.15$
40	$-202636925.12 * x^3 - 611011.30 * x^2 + 23907.39 * x - 0.08$
41	$281143487.47 * x^3 + 57195.18 * x^2 + 23893.53 * x - 0.13$
42	$295375979.55 * x^3 + 177168.69 * x^2 + 24136.75 * x - 0.01$
43	$-87717751.79 * x^3 - 397332.90 * x^2 + 23997.57 * x - 0.02$
44	$-120743617.16 * x^3 - 578379.36 * x^2 + 23953.22 * x + 0.00$
45	$386498696.00 * x^3 + 248603.17 * x^2 + 23983.62 * x - 0.12$
46	$382119359.31 * x^3 + 260273.26 * x^2 + 24070.50 * x - 0.13$
47	$305265123.91 * x^3 + 126942.94 * x^2 + 23956.19 * x - 0.14$
48	$-36149716.57 * x^3 - 474517.18 * x^2 + 23597.32 * x - 0.16$
49	$118584436.19 * x^3 - 107066.82 * x^2 + 23887.97 * x - 0.11$
50	$3053805146.86 * x^3 + 5738389.54 * x^2 + 27459.35 * x + 0.49$
51	$-620461.63 * x^2 + 23688.88 * x - 0.19$
52	$951946388.11 * x^3 + 1659285.99 * x^2 + 25224.57 * x + 0.12$
53	$690024061.41 * x^3 + 1042471.15 * x^2 + 24647.37 * x + 0.09$
54	$238502687.26 * x^3 + 102874.05 * x^2 + 24159.29 * x - 0.08$
55	$601226911.04 * x^3 + 862974.88 * x^2 + 24643.85 * x - 0.03$
56	$221204154.36 * x^3 + 348908.41 * x^2 + 24465.67 * x + 0.06$
57	$-1232844555.51 * x^3 - 2907847.35 * x^2 + 22120.94 * x - 0.43$
58	$-136095345.98 * x^3 - 664642.06 * x^2 + 23513.73 * x - 0.21$
59	$-76052022.86 * x^3 - 575366.81 * x^2 + 23605.15 * x - 0.18$
60	$-3119298216.35 * x^3 - 6820822.02 * x^2 + 20071.83 * x - 0.65$
61	$-627089941.52 * x^3 - 1591404.89 * x^2 + 23003.98 * x - 0.30$
62	$-700960453.43 * x^3 - 1708513.92 * x^2 + 23102.91 * x - 0.29$
63	$-800637227.91 * x^3 - 1899040.76 * x^2 + 22892.90 * x - 0.27$

**Table C.1:** Calibration polynomials for the thermocouples

Figure C.7 presents photos from the calibration process.



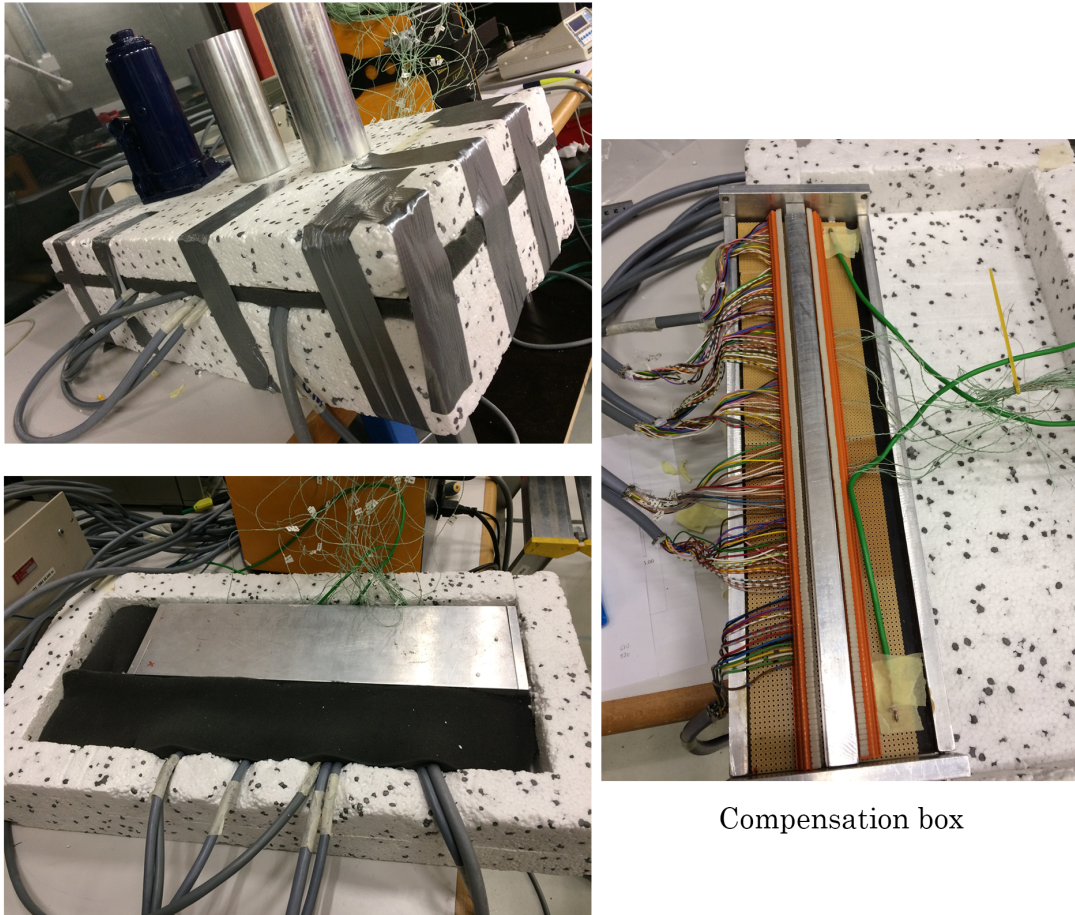
Thermocouples folded and taped form one side on the paper to avoid short circuit. The tip (measuring point) is not taped.



Thermocouples inside the Isotech box during calibration process.



The golden coating has come off on one of the thermocouples.



Compensation box

**Figure C.7:** Photos from the calibration process

### Differential pressure transducer

In the defrost set-up, differential pressure transducer FCO44 is used to measure the differential pressure across the heat exchanger exhaust side. To get accurate readings, the transducer is calibrated.

The equipment used for that purpose is:

- Precision Micromanometer FCO510 - Reference manometer
- Differential pressure transducers FCO44 (range 0-500 Pa)
- Power supply for the transducer
- Jet wind tunnel
- Orifice plate (23 mm)
- Digital multimeter DM 100
- Fluke Helios 2287 PAI data logger

The wind tunnel is connected both to the reference manometer and differential pressure transducer via T connection tubes. They are connected both to + / - side to detect pressure drop. The differential pressure is set in the range of 20-220 Pa.

Data from the differential pressure transducer is logged via the Helios data logger, logging data for each 1 second.

Calibration: To calibrate the differential pressure transducers, the wind tunnel (in horizontal position) is set first to a low differential pressure value of 20 Pa and data is logged for a period of 5-7 min to ensure a stable measurement. This is repeated for 40, 60, 80, 100..., 220 Pa. While the differential pressure reading is done from the reference Precision Micromanometer FCO510, the voltage signal is logged via the data logger. For each reading from the Precision Micromanometer FCO510, an average of one minute of stable voltage signal is taken to form the calibration curve, seen in figure C.8.

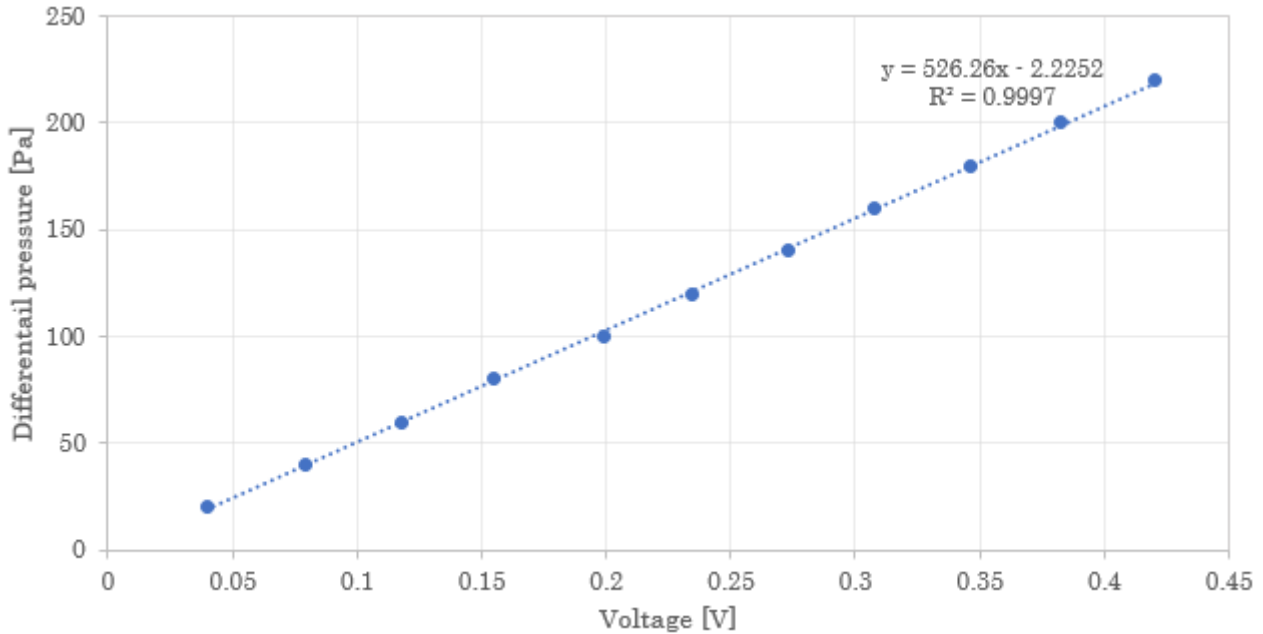


Figure C.8: Differential pressure transducer calibration curve

Finally, figure C.9 shows the error created by the fitting curve between the Precision Micromanometer and the calibrated differential pressure transducer.

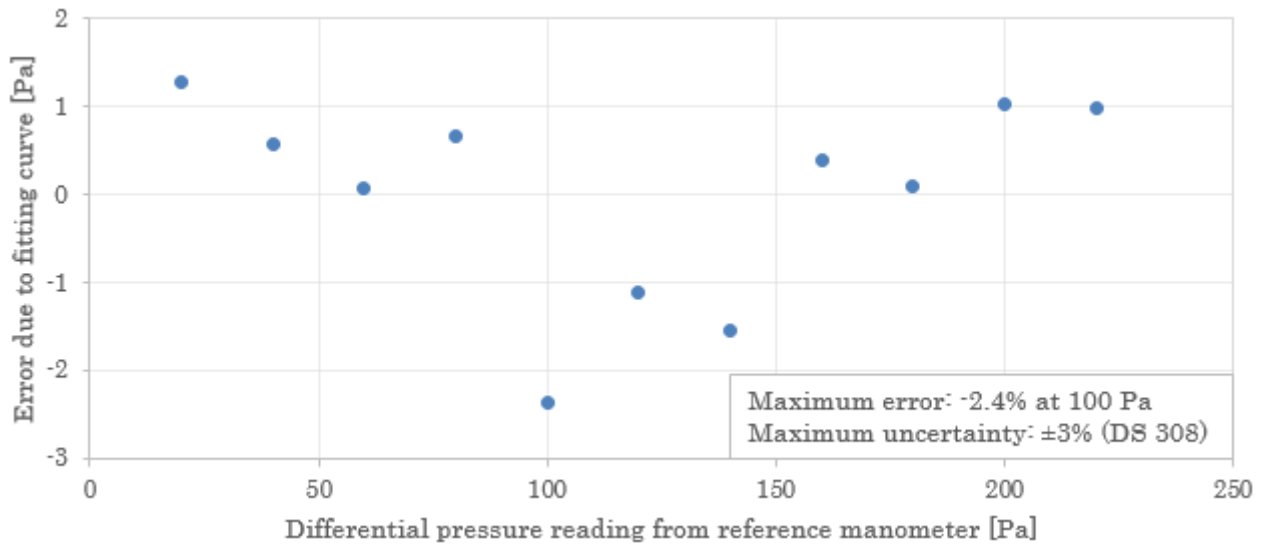


Figure C.9: Error due to calibration curve

Sensirion sensor validation

The Sensirion sensors are measuring both relative humidity and temperature on the heat exchanger ports and in the cold and warm room. The type used for the measurements, namely SHT75 is individually calibrated from the factory [30][31]. However a comparison with a reference thermometer is performed to check if the sensors have an offset in the temperature reading. Since a reference hygrometer is not available the offset in humidity can not be analyzed. Ten Sensirion sensor are available for the measurement, but only seven of them are checked.

The equipment used to check the offset is:

- Precision Digital Thermometer ASL F200 with RTD Pt 100 Sensor Probe (reference probe)
- Isotech Hyperion 2140 B
  
- IC-meter with Sensirion SHT21 sensor

The Sensirion sensors are compared against a Pt 100 Sensor Probe at different temperatures by having all the sensors in a Isotech Hyperion 2140 B. First of all, the Sensirions are checked to see if they operate in the temperature range that the measurements will be performed (-15 to 25 °C). Secondly, the temperature offset will also be analyzed.

In table C.2 and figure C.10 to figure C.13 the difference between each temperature sensor and the Pt 100 Sensor Probe (reference probe) is shown. It can be concluded that there is an offset from the reference thermometer. For the range of 25 - 0 °C, the maximum temperature difference is 0.77 °C, while for -15°C the difference increases, reaching 1.00 °C.

Temperature steps [°C]	Temperature [°C] for sensors 1 → 7						
	T1	T2	T3	T4	T5	T6	T7
25.02	0.44	0.37	0.29	0.22	0.21	0.55	0.50
15.25	0.58	0.51	0.50	0.43	0.27	0.59	0.22
0.72	0.77	0.69	0.77	0.75	0.31	0.60	-0.24
-13.73	0.86	0.76	0.92	1.00	0.22	0.47	-0.75

**Table C.2:** Difference between reference thermometer and each Sensirion sensor

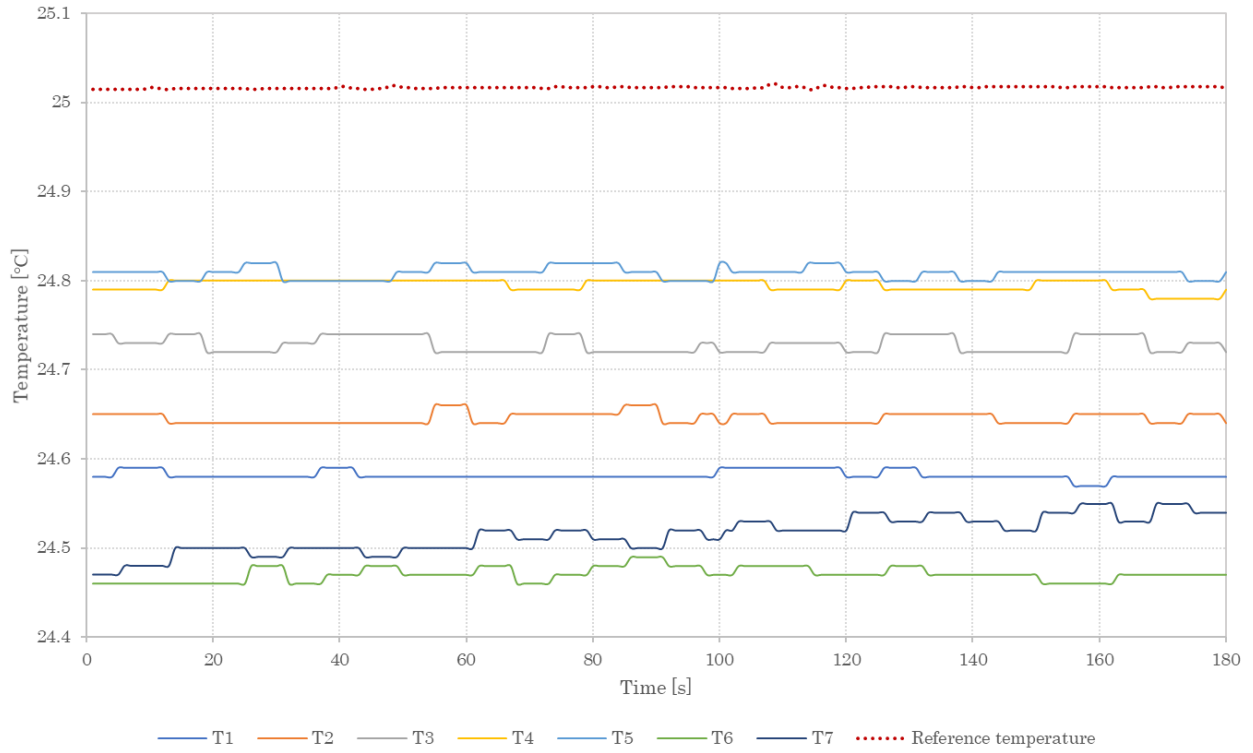


**Figure C.10:** Sensirion temperature comparison with reference thermometer at 25 °C



**Figure C.11:** Sensirion temperature comparison with reference thermometer at 15 °C

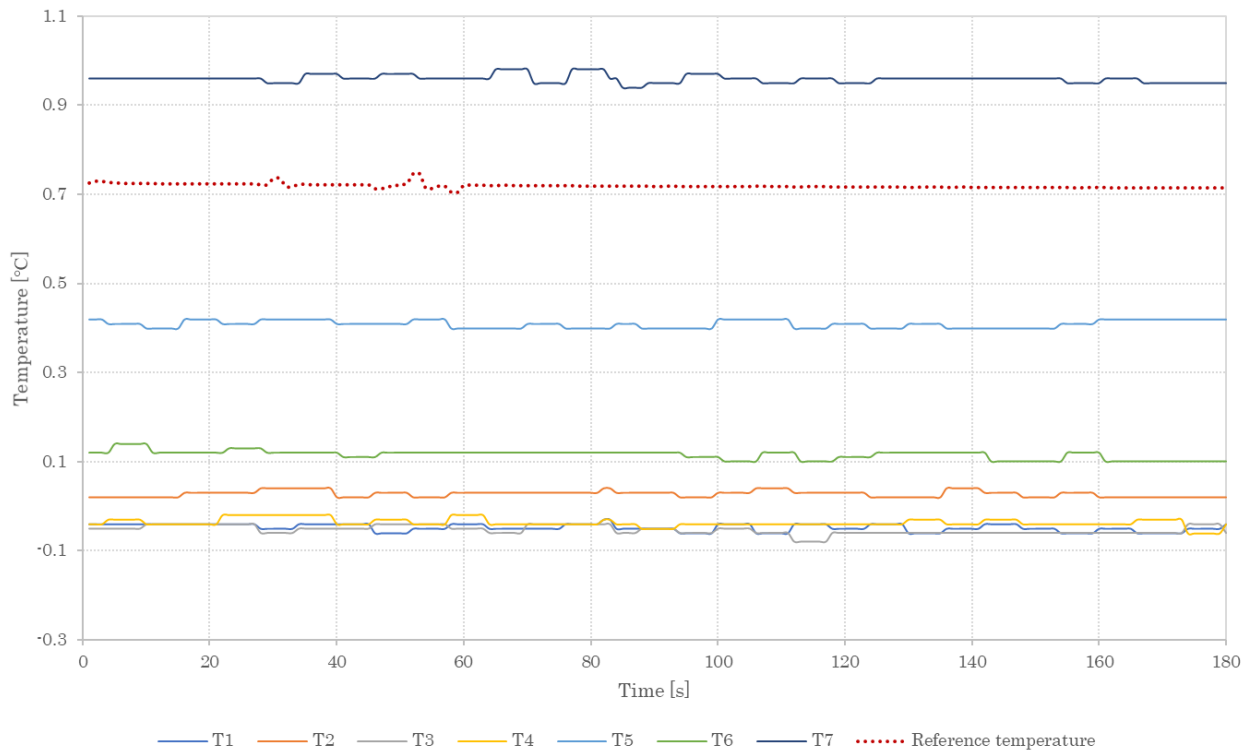


**Figure C.12:** Sensirion temperature comparison with reference thermometer at 0 °C

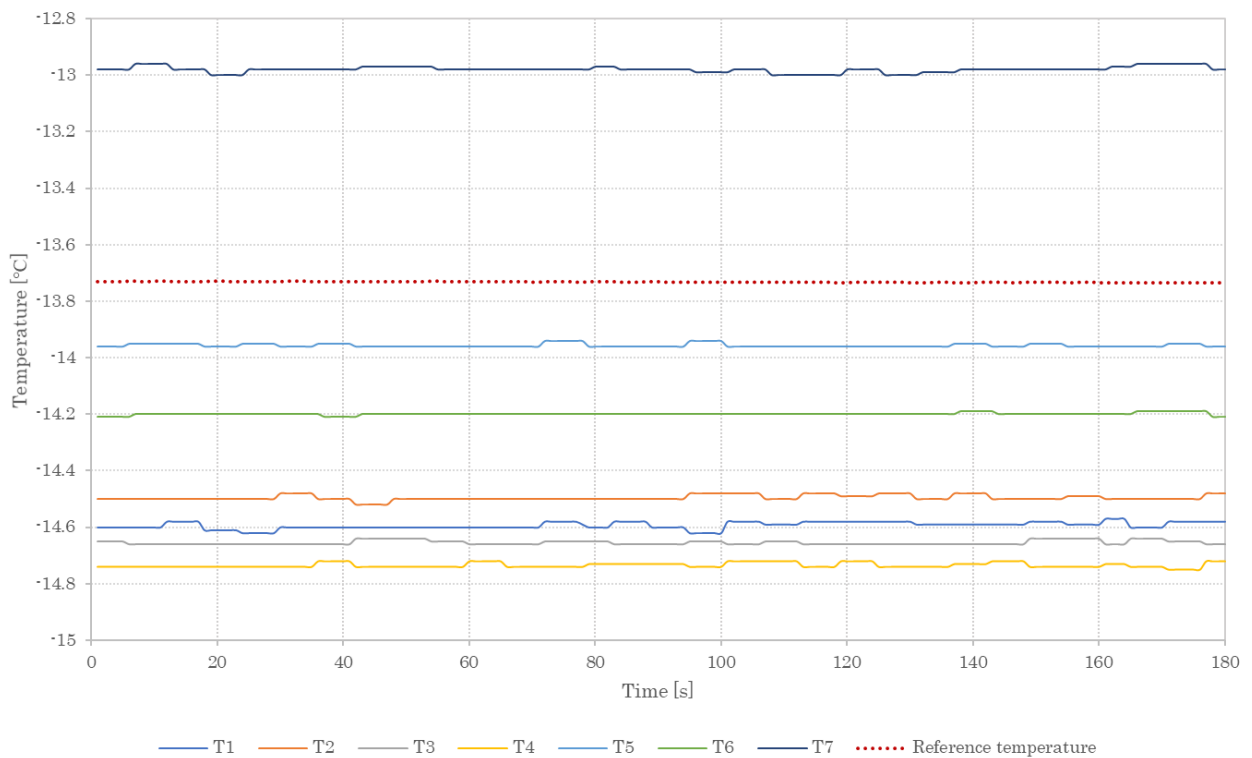


**Figure C.13:** Sensirion temperature comparison with reference thermometer at -15 °C

To have an overview of the relative humidity offset, the available sensor that can be used for comparison is the IC-meter, which has a SHT21 humidity and temperature sensor. This type of sensor is a new

generation of sensors with improved performance as stated by the manufacturer [29]. In figure C.14 the placement of the reference thermometer, the Sensirion sensors and the IC-meter is shown. The data is logged at a stable temperature at AAU University in the Indoor Climate laboratory.

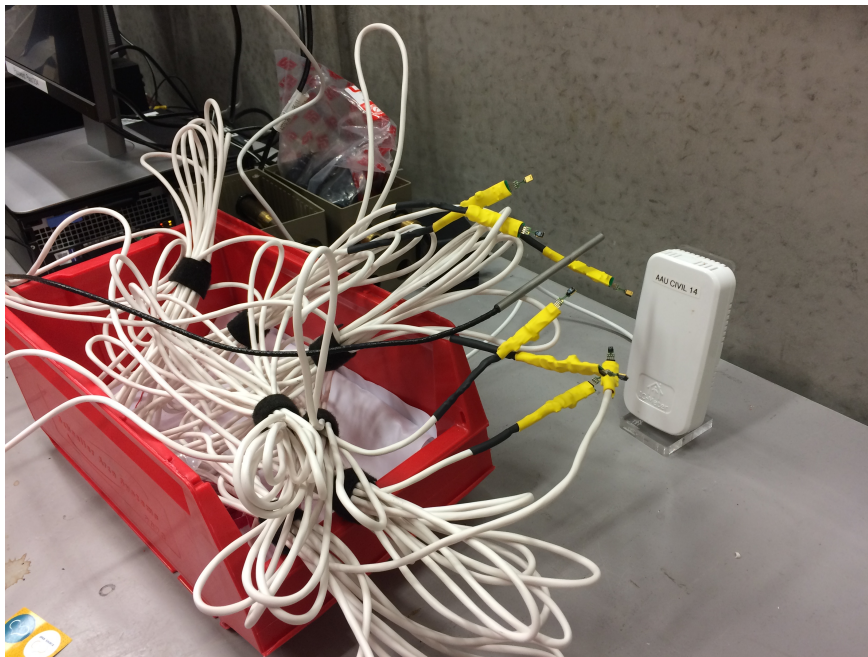


**Figure C.14:** Placement of Sensirion, reference thermometer and IC-meter

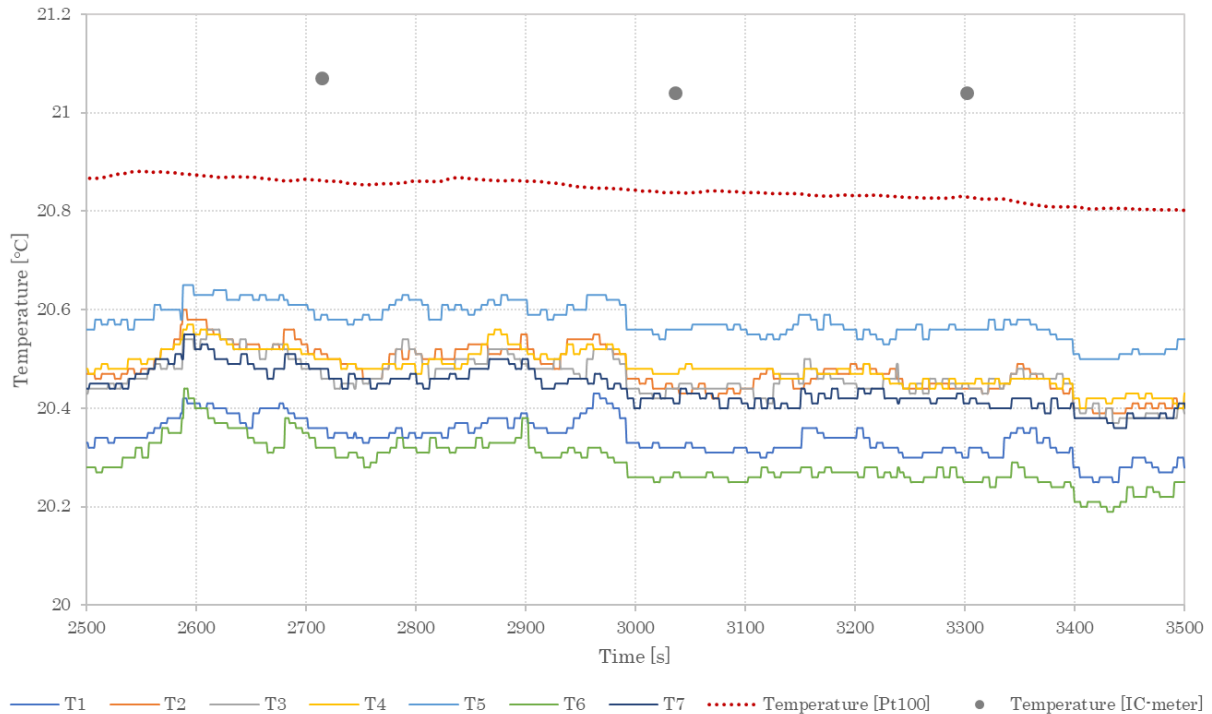


**Figure C.15:** Sensirion temperature comparison with reference thermometer and IC-meter

Figure C.15 shows that the temperature reading of the IC-meter is higher than the Pt 100 and the other sensors. Compared to the other Sensirion sensors, its offset from the reference probe (Pt 100) is

even larger. Hence, the reading in relative humidity for the IC-meter should be lower.

For the relative humidity, in figure C.16 and table C.16 the offset can be seen. The highest difference in relative humidity is seen on sensor 3 - 4.6%, while the others oscillate between 2.2% and 4%.

Since it is shown that there is an offset in temperature and considering that the relative humidity changes in relation to temperature, the absolute humidity is calculated for each sensor. Table C.4 shows that the absolute humidity from the IC-meter is slightly different from the absolute humidity of each sensor. Nevertheless, the IC-meter is not a reference hygrometer, therefore it is difficult to indicate if the uncertainty does not lie within the range specified by the manufacturer ( $\pm 0.3$  °C for temperature and  $\pm 1.8\%$  for relative humidity [30]).

In conclusion, the Sensirion sensors have an offset regarding temperature and humidity (relative and absolute) readings. However, due to the lack of a reference hygrometer, the humidity offset cannot be established with certainty, therefore the sensors will not be calibrated.

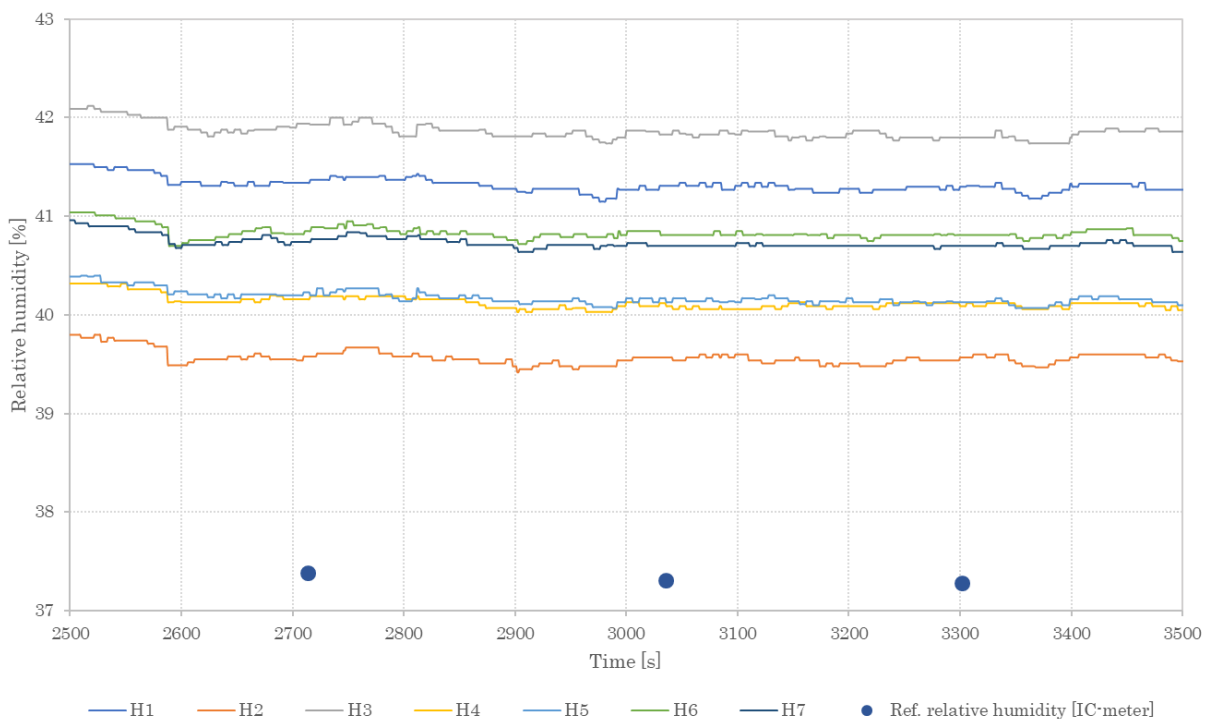


**Figure C.16:** Sensirion relative humidity comparison with IC-meter

Relative humidity [%] for sensors 1 $\rightarrow$ 7						
H1	H2	H3	H4	H5	H6	H7
4.0	2.2	4.6	2.8	2.8	3.5	3.4
4.0	2.3	4.5	2.8	2.8	3.5	3.4
4.0	2.3	4.5	2.8	2.9	3.5	3.4

**Table C.3:** Difference between IC-meter and each Sensirion sensor for relative humidity

IC-meter							
Absolute humidity [kg water / kg dry air]	Absolute humidity [kg water / kg dry air] for sensors 1 → 7						
x	x1	x2	x3	x4	x5	x6	x7
0.00575	0.00609	0.00589	0.00622	0.00597	0.00601	0.00601	0.00605
0.00573	0.00607	0.00586	0.00620	0.00595	0.00599	0.00598	0.00602
0.00573	0.00607	0.00586	0.00620	0.00594	0.00599	0.00597	0.00602

**Table C.4:** Absolute humidity calculation for IC-meter and each sensor

### Airflow measurement uncertainty

The airflow is measured with a 315mm Lindab UltraLink device. According to the manufacturer, the maximum uncertainty is the highest value among  $\pm 5\%$  and  $\pm 1$  l/s with a velocity range of 0.5-15 m/s [20].

During the measurements, the flow is at  $200 \text{ m}^3/\text{h}$ , resulting in a velocity of 0.7 m/s. In this case, the maximum uncertainty is  $\pm 5\%$ .

According to DS/EN 308 [6], the maximum uncertainty for airflow measurement shall be  $\pm 3\%$ . Therefore, to decrease the uncertainty level as much as possible, flow straighteners have been installed.

## C.2 Infiltration rate of the experimental facility

Using the available and adjustable openings to the outside (a valve and a damper), the airtightness level of the experimental facility has been adjusted to represent newly-built buildings with maximum leakage of 1 l/s pr.  $\text{m}^2$  of floor area at 50 Pa pressure difference [33]. The adjustment has been done by making several blower-door tests. The final combined result from a pressurization and depressurization test is 1.041 l/s pr.  $\text{m}^2$  of floor area at 50 Pa.

## C.3 Leakage test for the heat exchangers and heat recovery unit

A leakage test can be done for the heat exchanger and for the heat recovery device. The heat recovery device is specified as "the heat exchanger itself installed in a casing having the necessary air duct connecting elements and in some cases the fans and pumps, but without any additional components of the HVAC system" [6].

With this set-up and measurement locations, leakage inside the heat exchanger will influence the measured temperature on the four ports and leakage of the heat recovery device will influence the measured airflow for supply and extraction.

DS/EN 308 [6] requires internal and external leakage tests of the heat recovery device. For systems with maximum static pressure of 250 Pa, as in this case, the internal leakage should be measured at 100 Pa pressure difference and the external leakage at 250 Pa. Internal leakage means leakage between the primary and secondary airstream in a heat recovery device. External leakage is the leakage between the heat recovery device and the environment.

Airmaster A/S has conducted a leakage test for the heat recovery device with one of the heat exchanger types that will be tested during the experiments, namely Ekocoil LEV-455-230-L-S. The test was done prior to installing the sensors in the unit and mounting the unit in the experimental test facility. Data for leakage of the heat exchangers has been received from the manufacturers.

Table C.5 shows the leakage test results. The internal leakage test was initially performed at 250 Pa pressure difference and then recalculated for 100 Pa differential pressure [7]. The calculated percentage for external and internal leakage in the last column of the table shows the actual leakage as a percentage from the nominal flow. The nominal flow is the airflow at 100 Pa pressure difference, as stated by the manufacturers. According to DS/EN 308 [6], the maximum leakage should be 3 %.

Manufacturer and heat exchanger model			Leakage [m <sup>3</sup> /h]	Leakage [%]	
Ecokoil: LEV-455-230-L-S; length 250 mm	Heat recovery device (performed by Airmaster A/S)	Nominal flow 205 m <sup>3</sup> /h	Pressure difference at 100 Pa	Internal 5.5 m <sup>3</sup> /h	Internal 2.7 %
	Heat exchanger (performed by manufacturer)		Pressure difference at 250 Pa	External 7.8 m <sup>3</sup> /h	External 3.8 %
Internal & external <1.03 m <sup>3</sup> /h				Internal & external <0.5 %	
Klingenburg: GS-25 Aluminium & GS-25 PET; width 250 mm	Heat exchanger (performed by manufacturer)		Pressure difference at 200 Pa	Internal & external <1.03 m <sup>3</sup> /h	Internal & external <0.5 %

**Table C.5:** Leakage test results for the heat exchangers and heat recovery unit

In conclusion, the external leakage for the heat recovery device with Ekocoil's heat exchanger is higher than the limits defined in the standards [6].

# D | Performance data verification

## Volume to mass flow conversion

In the Klingenburg tool the flow is entered as standard volume, which means that if the same volume flow is entered as supply and extraction, the mass flow will then automatically be balanced. The density for a standard volume is  $1.2\text{kg}/\text{m}^3$  which has the values in figure D.1.

Temperatur [°C]	Absolute pressure [Pa]	Relative humidity [%]
20	101325	50

**Table D.1:** The properties of a standard volume

Ultralink measures a volume flow which has to be converted into mass flow. In the room there is no sensor that measures absolute pressure and the humidity of the air has only a small influence on the density of the air. Therefore, when converting to mass flow, it is assumed that the air is dry, and the atmospheric air pressure is constant. For conversion from volume flow, the ideal gas equation is used.

$$P \cdot V = \frac{m \cdot 10^{-3}}{M} \cdot R \cdot T \rightarrow m = \frac{M \cdot P \cdot V}{R \cdot T} \cdot 10^3 \left[ \frac{\text{kg}}{\text{s}} \right] \quad (\text{D.1})$$

$P$  – Atmospheric air pressure 101325 [Pa]

$V$  – Volume flow  $\left[ \frac{\text{m}^3}{\text{s}} \right]$

$m$  – Mass flow  $\left[ \frac{\text{kg}}{\text{s}} \right]$

$M$  – Molar mass atmospheric air 29  $\left[ \frac{\text{g}}{\text{mol}} \right]$

$R$  – Universal gas constant 8.314  $\left[ \frac{\text{J}}{\text{mol} \cdot \text{K}} \right]$

$T$  – Air temperature [K]

## Klingenburg GS 25/250 (Aluminium)

With closed infiltration dampers, the dry test had balanced mass flows (figure D.6), while the wet test did not (figure D.8). After opening the dampers, for the dry test, the flows got unbalanced, while the unbalance between the outdoor and extraction flows for the wet test increased. This relation between the two flows with open dampers is caused by the different infiltration opening areas in the two chambers. The bigger opening area in the cold chamber results in higher outdoor air mass flow. The mass flows for outdoor and extraction air with open dampers can be seen in figures D.10 and D.12

Parameters	Set points	Unit	Deviation - mean values	Unit	Deviation - individual measurements		Unit
					max	min	
T_outdoor air	5	°C	-0.3	°C	0.7	-1.3	°C
T_extraction air	25	°C	0.0	°C	0.8	-1.2	°C
RH_extraction air	0.22	-	0.01	-			
Mass flow_outdoor air	0.053	kg/s	8.0	%	11.6	4.2	%
Mass flow_extract air	0.053	kg/s	-5.9	%	-2.9	-8.5	%

**Table D.2:** Mean and individual measurement deviations for the dry test (infiltration dampers open)

Parameters	Set points	Unit	Deviation - mean values	Unit	Deviation - individual measurements		Unit
					max	min	
T_outdoor air	5	°C	-0.3	°C	0.8	-0.9	°C
T_extraction air	25	°C	-0.2	°C	0.9	-1.6	°C
RH_extraction air	0.51	-	-0.01	-			
Mass flow_outdoor air	0.053	kg/s	3.6	%	7.7	-0.7	%
Mass flow_extract air	0.049	kg/s	-17.2	%	-14.4	-20.9	%

**Table D.3:** Mean and individual measurement deviations for the wet test (infiltration dampers open)

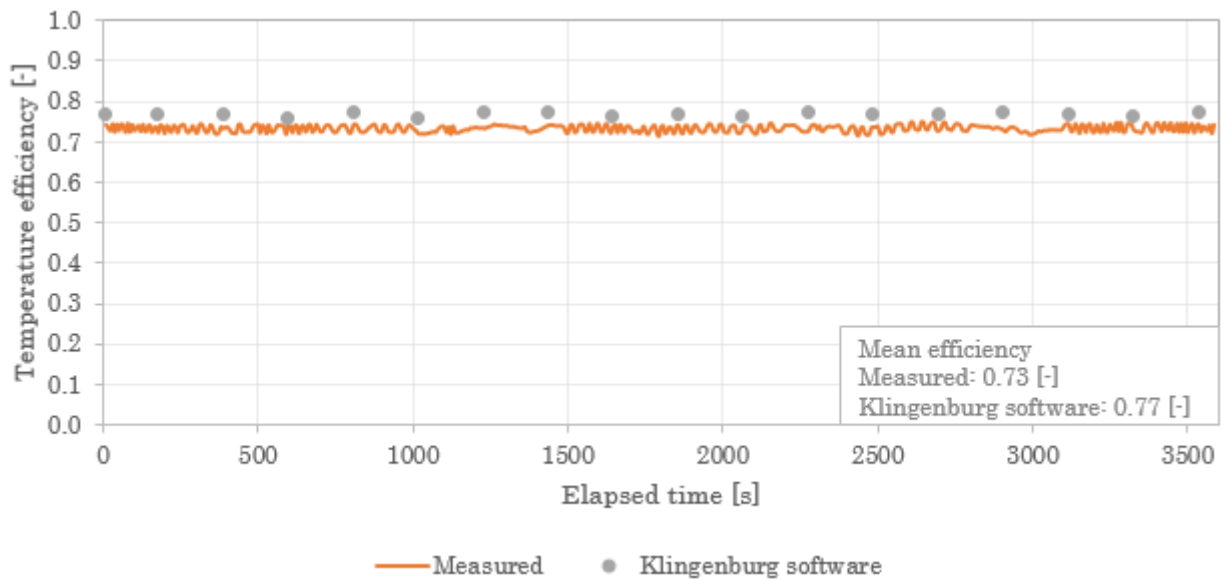


**Figure D.1:** Temperature efficiency comparison for the dry test (infiltration dampers open)

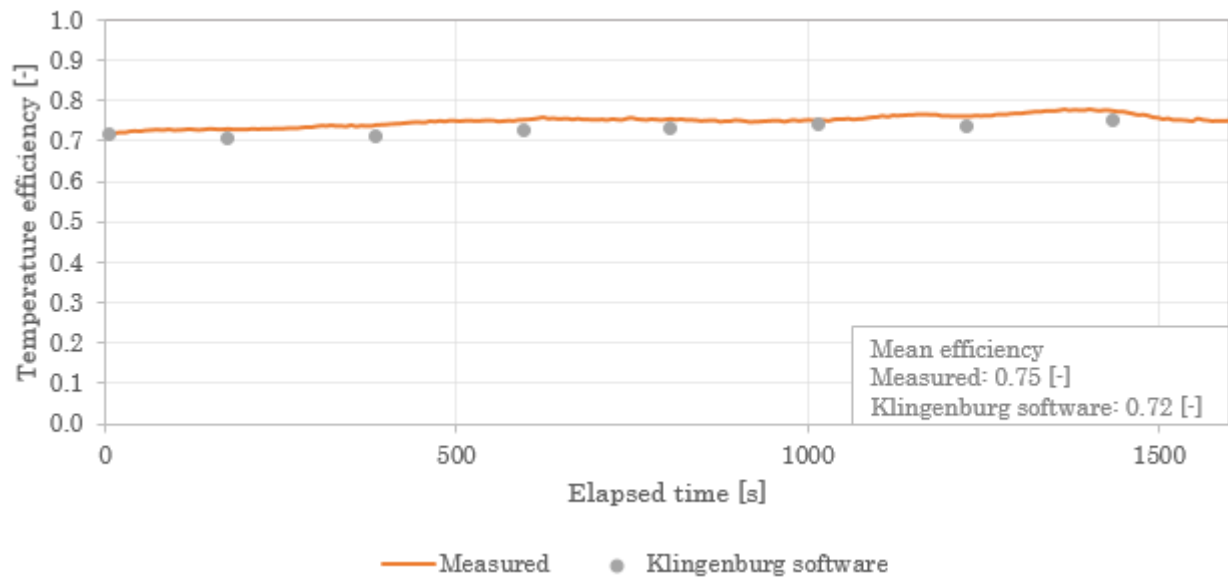


**Figure D.2:** Temperature efficiency comparison for the wet test (infiltration dampers open)

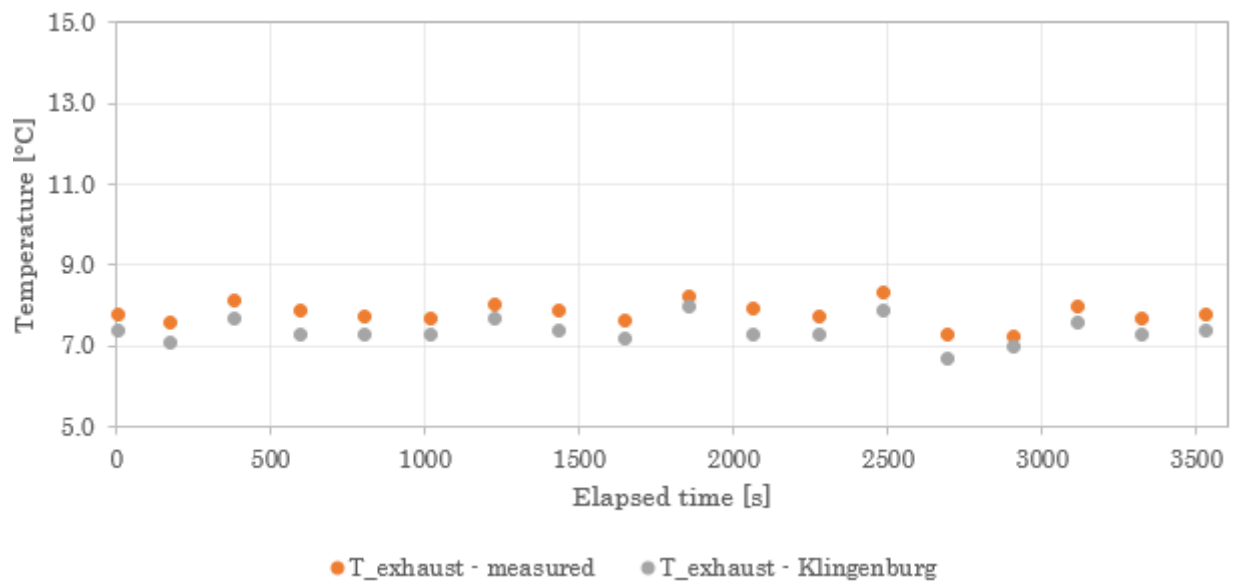


**Figure D.3:** Exhaust temperature comparison for the dry test (infiltration dampers open)

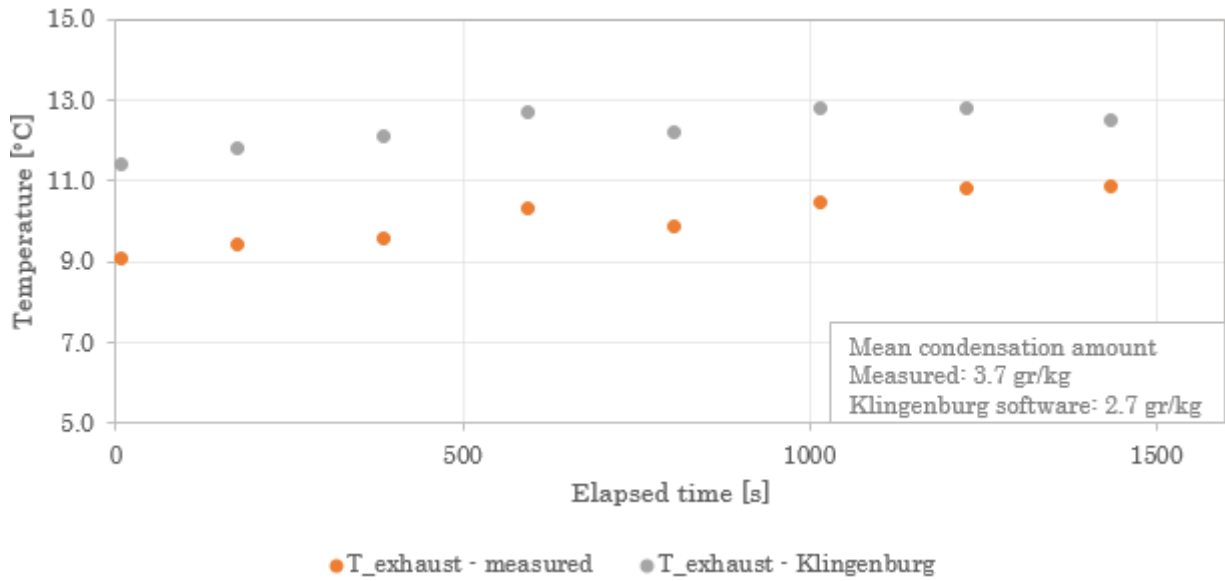


Figure D.4: Exhaust temperature comparison for the wet test (infiltration dampers open)

Maintained conditions during the experiments

Dry test - infiltration dampers closed

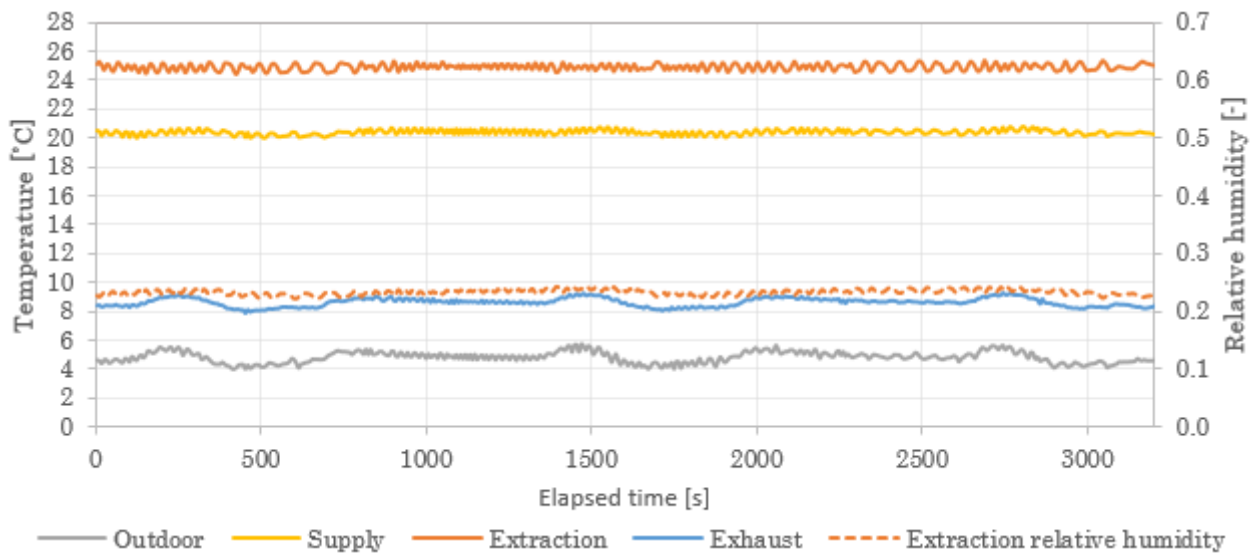


Figure D.5: Mean air temperatures and extraction relative humidity during the dry test (infiltration dampers closed)

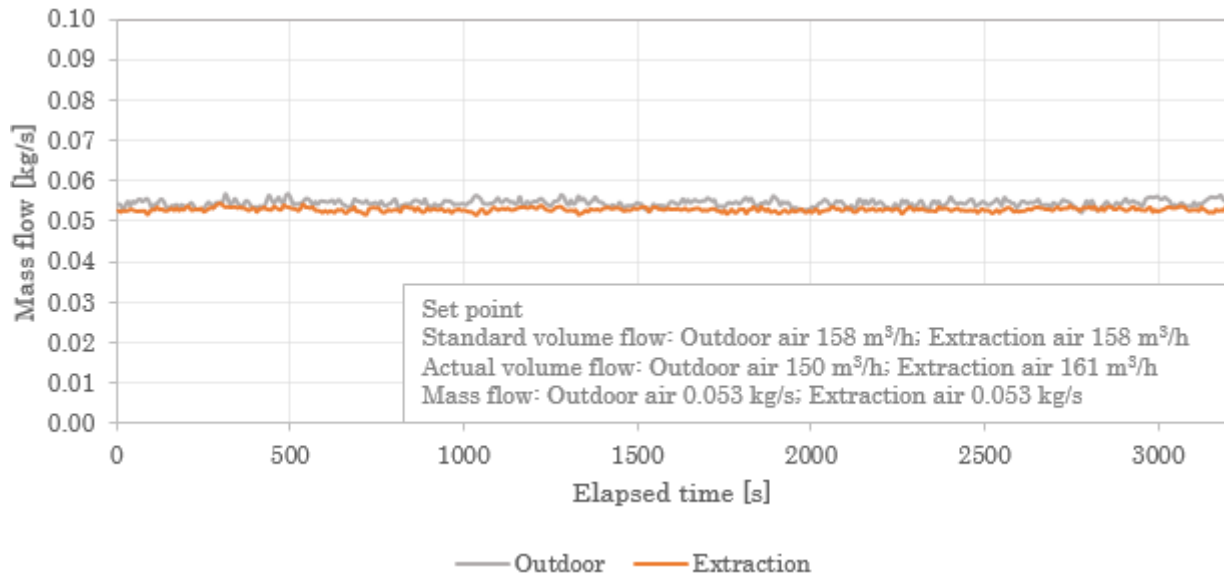


Figure D.6: Mass flow during the dry test (infiltration dampers closed)

#### Wet test - infiltration dampers closed

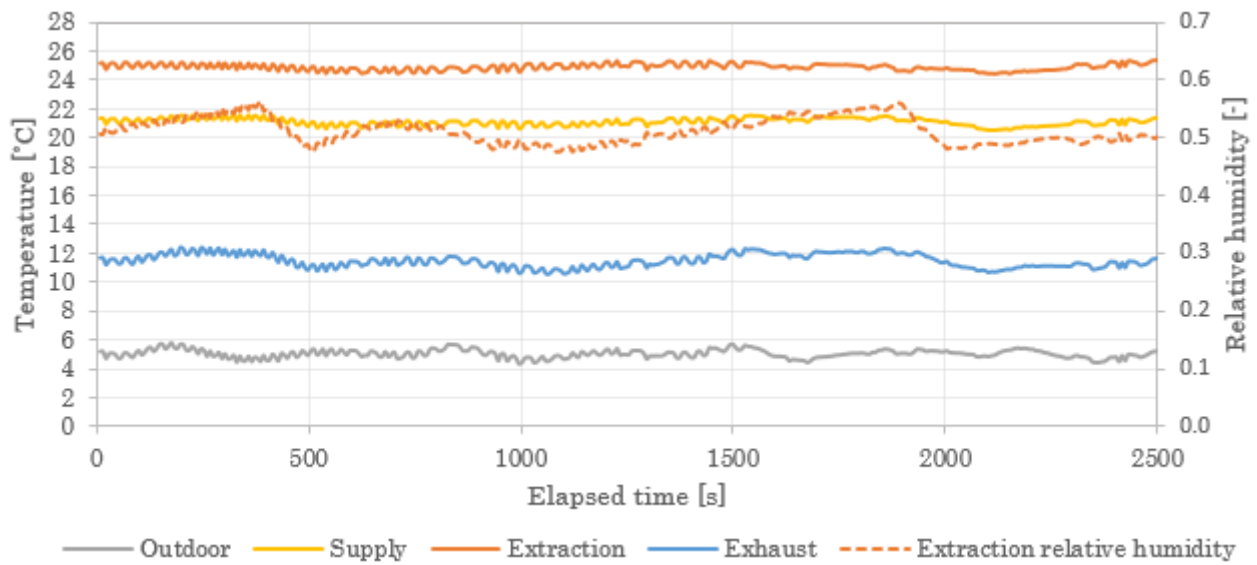


Figure D.7: Mean air temperatures and extraction relative humidity during the wet test (infiltration dampers closed)

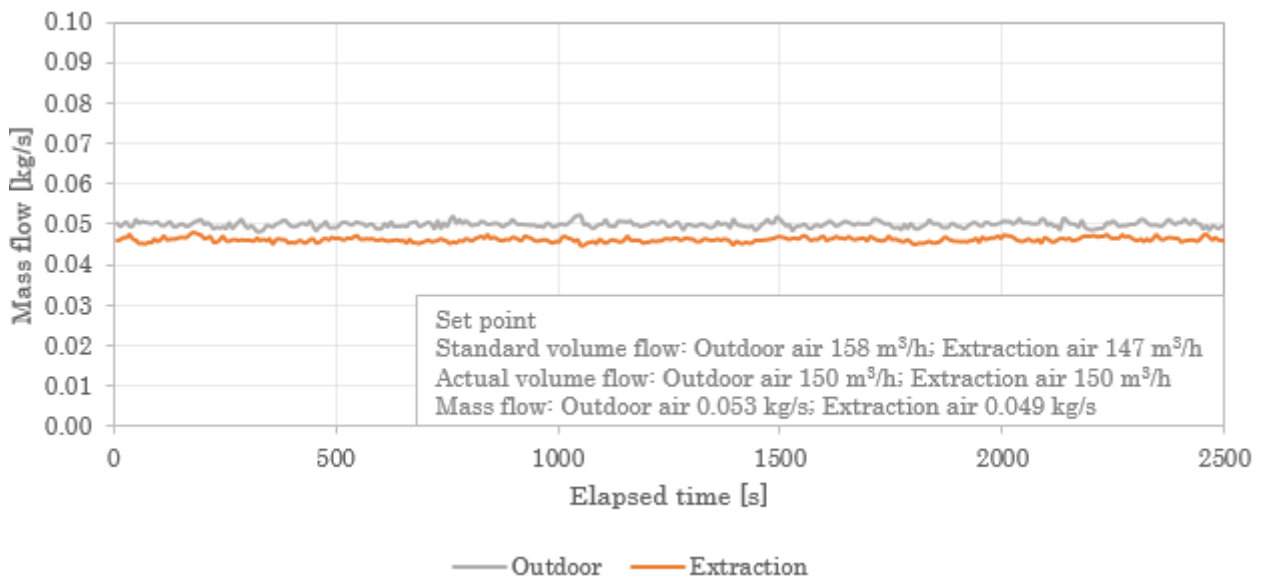


Figure D.8: Mass flow during the wet test (infiltration dampers closed)

#### Dry test - infiltration dampers open

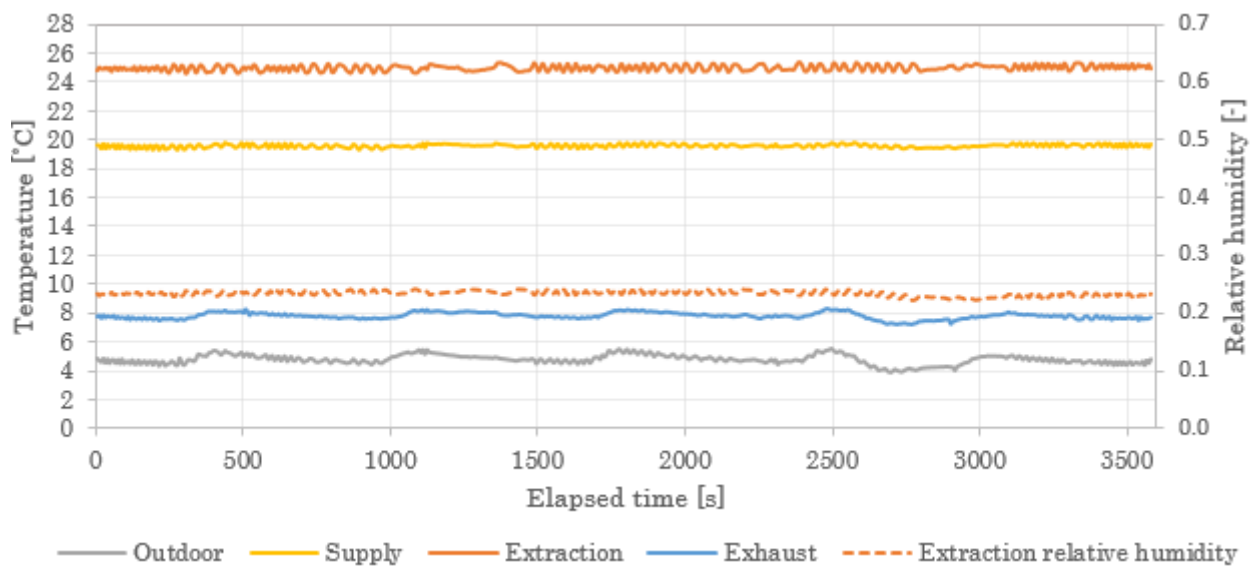
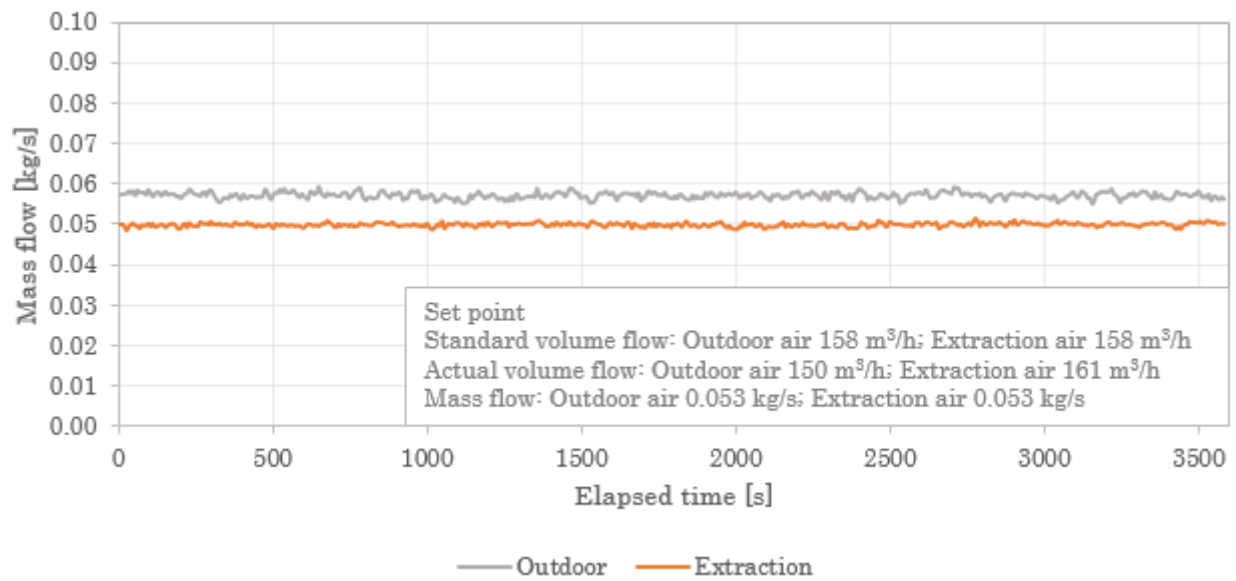
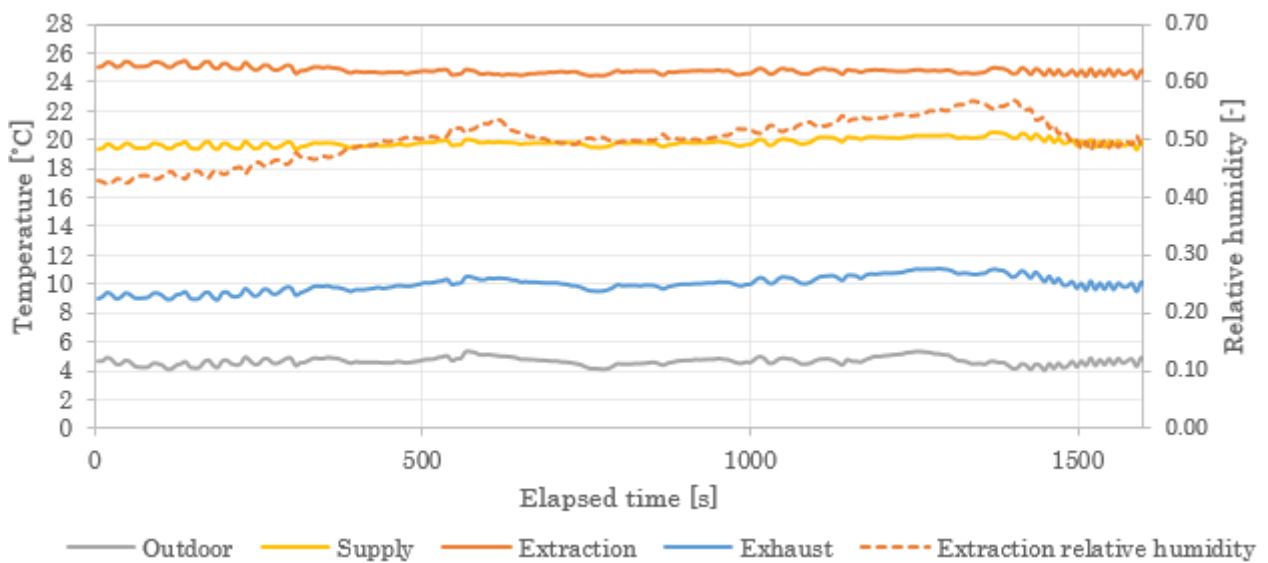


Figure D.9: Mean air temperatures and extraction relative humidity during the dry test (infiltration dampers open)



**Figure D.10:** Mass flow during the dry test (infiltration dampers open)

#### Wet test - infiltration dampers open



**Figure D.11:** Mean air temperatures and extraction relative humidity during the wet test (infiltration dampers open)

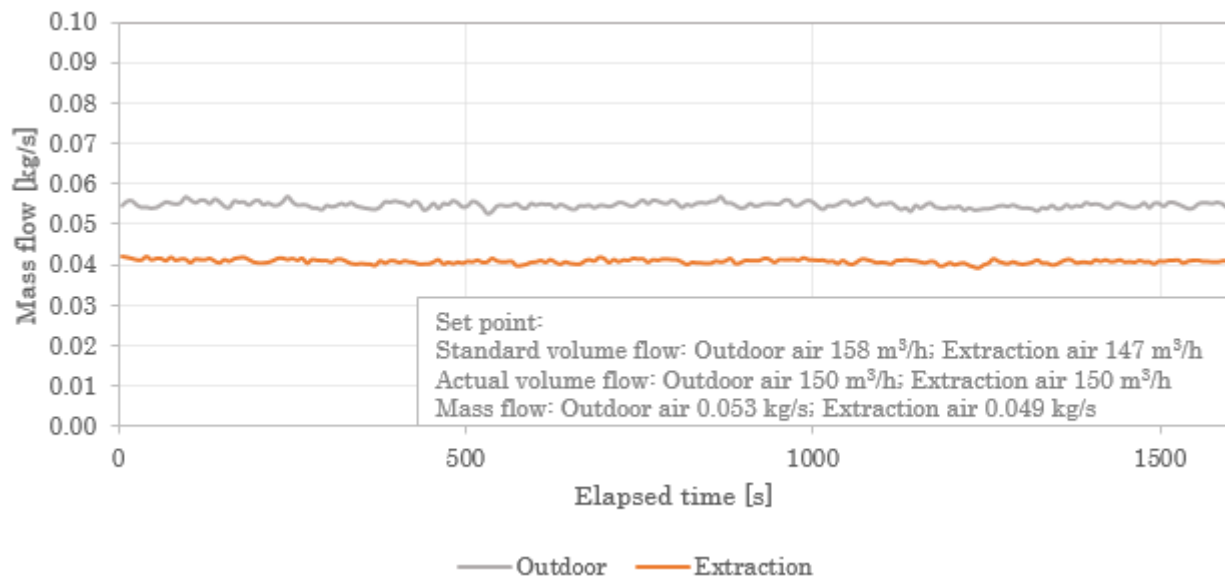


**Figure D.12:** Mass flow during the wet test (infiltration dampers open)

#### Wet test - infiltration dampers closed (balanced flow)

Since the wet test did not have balanced mass flows, the test is repeated for a shorter time period to check if the difference between measured exhaust and the extracted data from Klingenburg software is due to measurement uncertainty.

If comparing the measurement deviation from the wet test (infiltration damper closed) from table 6.2 with the measurement deviation of the wet test (table D.4) in case of balanced flows, it can be seen that the limits are not exceeded. Though, there is deviation in the temperature measurement.

Parameters	Set points	Unit	Deviation - mean values	Unit	Deviation - individual measurements		Unit
					max	min	
T_outdoor air	5	°C	-0.4	°C	-0.5	-0.8	°C
T_extraction air	25	°C	-0.5	°C	0.1	-1.5	°C
RH_extraction air	0.51	-	-0.09	-			
Mass flow_outdoor air	0.067	kg/s	-2.4	%	3.3	-7.6	%
Mass flow_extract air	0.067	kg/s	-0.9	%	1.9	-2.9	%

**Table D.4:** Mean and individual measurement deviations for the wet test (balanced airflows)

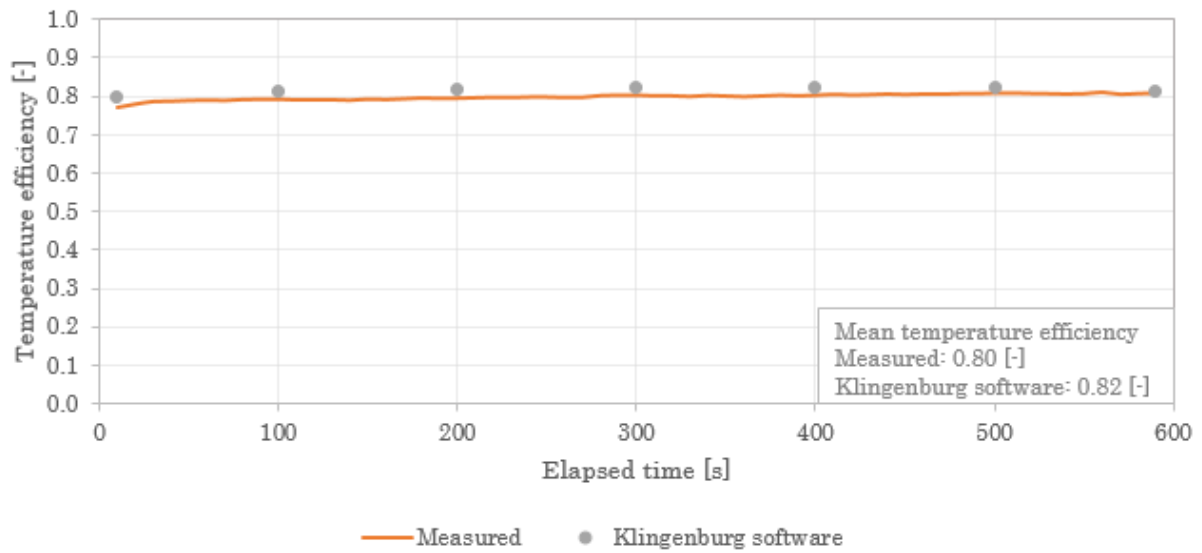


Figure D.13: Temperature efficiency comparison for the wet test (balanced mass flow)

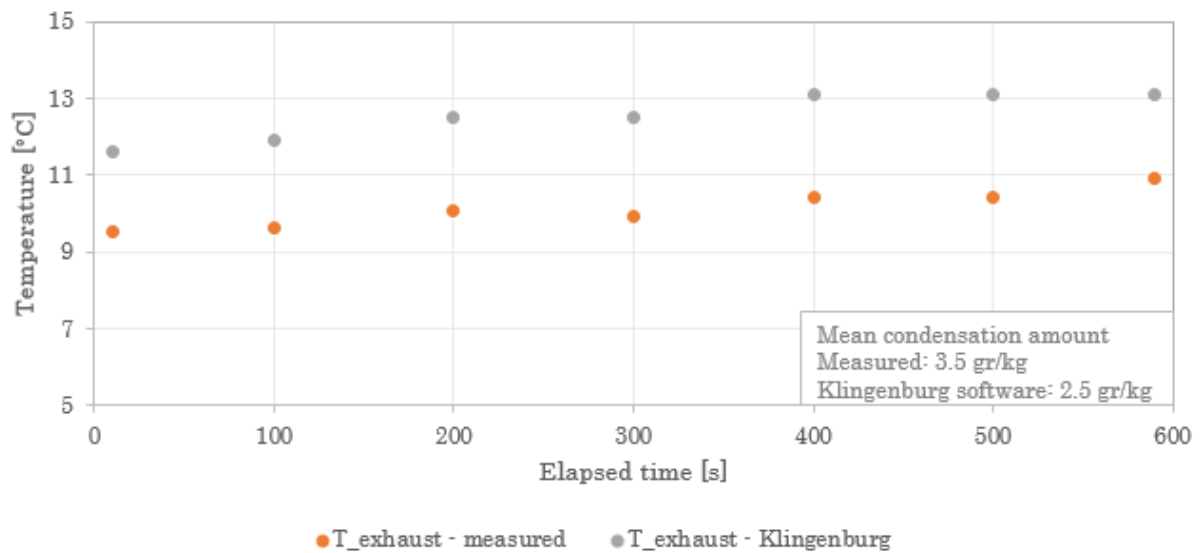
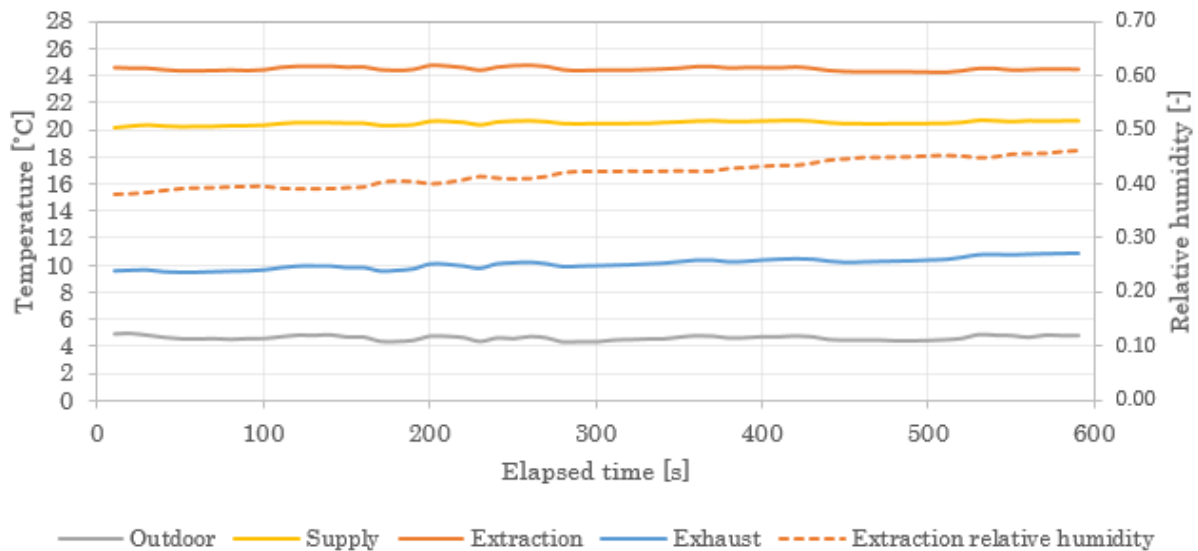
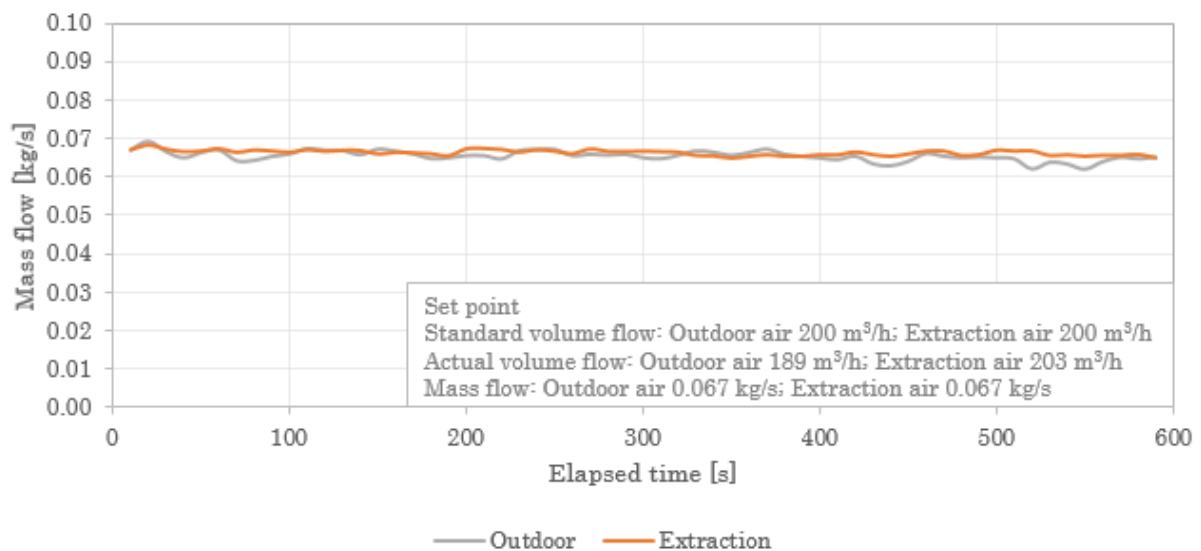


Figure D.14: Exhaust temperature comparison for the wet test (balanced mass flow)



**Figure D.15:** Mean air temperatures and extraction relative humidity during the wet test (balanced mass flow)



**Figure D.16:** Mass flow during the wet test (balanced mass flow)

Even with balanced flows (figure D.16), the exhaust measured temperature is different from the one extracted from the software even though inputting the same parameters (figure D.14). To check further if the measurement uncertainty can greatly influence the measurement, it was considered that temperature uncertainty is  $\pm 0.3$  °C and for the flow  $\pm 5\%$ .

In figure D.17, it can be noticed that with the thermocouple uncertainty of 0.3 °C, the difference is still great. Since the airflow can influence more (uncertainty of  $\pm 5\%$ ) the same input data obtained with the Texhaust in terms of temperatures is used but the airflows are changed with  $\pm 5\%$ . It was noticed that this case does not change the exhaust temperature. Therefore a check is performed having the outdoor airflow of 5% and for the extraction -5%.

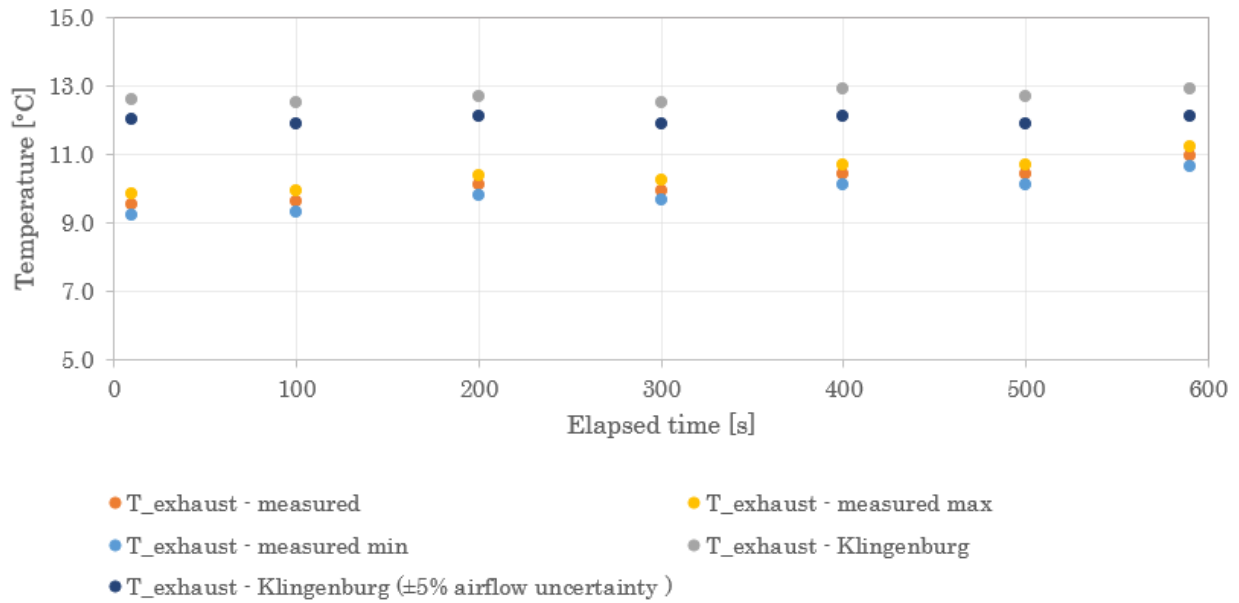


**Figure D.17:** Exhaust temperature comparison for the balanced wet test with uncertainties

Finally, with the assumption of an increase of 5% in outdoor airflow and with a decrease of 5% in extraction, the exhaust temperatures reach a lower difference

# E | Frost formation limits

## E.1 Experimental analysis

### Condition 1

The first attempts in running the frost limit experiment with the new cooling unit consisted of understanding the limitations of the improved setup. Firstly, the predefined conditions for the warm chamber (temperature of 22 °C and relative humidity of approximately 22% described in 4.2) and a balanced mass flow are applied, as seen in E.3 until second 2200. By having this input, the average exhaust temperature is still above 0 °C.

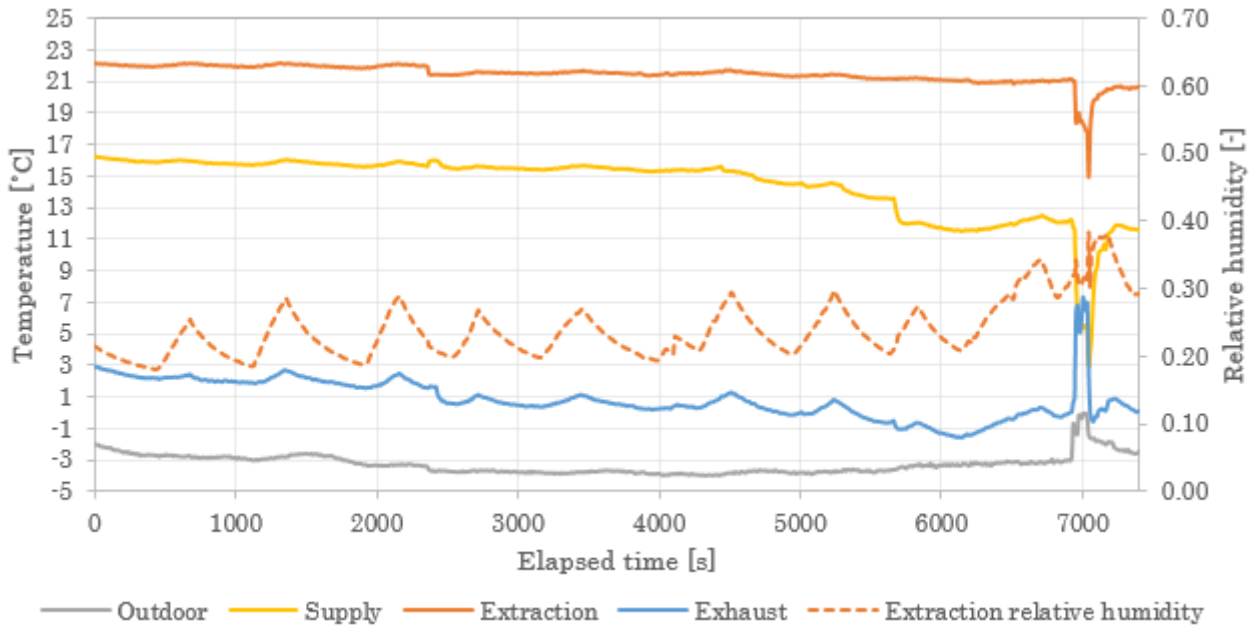
Secondly, both supply and extraction mass flows are decreased. Having less mass flow, the temperature in the cold chamber does not decrease much more than in the previous case. However, having considerably lower mass flow the temperature efficiency is increased, resulting in a lower exhaust temperature. This change decreases the average temperatures on outdoor air port and on the exhaust port (figure E.3 between second 2200 - 4300). Since there is a temperature gradient on the exhaust port, as shown in figure E.4, the mean exhaust temperature should be considered. For this case the mean exhaust temperature is 0.6 °C.

To further lower the temperature on the exhaust, an imbalance is created by increasing the massflow on the supply side and lowering the massflow on the extraction side. By doing so the mean temperatures on the exhaust port decreased from 0.6 °C to -0.7 °C. At this point, second 7000, as seen in figure E.2, the ventilation box is opened and frost might have formed as little particles of frost, as shown in figure E.1.

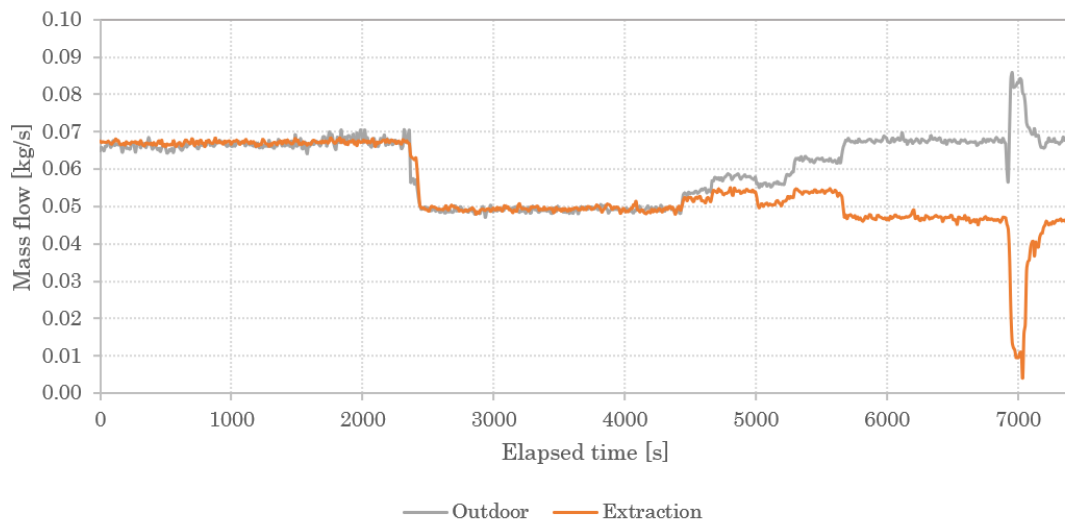


Figure E.1: Frost formation - condition 1

Figure E.2 shows the mean air temperature on each port and the relative humidity of the extracted air. Since the frost formation starts at 0 °C, frost can have started forming when having balanced flows (after second 2200).



**Figure E.2:** Mean air temperature and extraction relative humidity - condition 1



**Figure E.3:** Mass flow - condition 1

Temperature gradient across outdoor port

-3.8	-3.9	-3.9	-3.8
-3.6	-3.8	-4.0	-3.9
-3.4	-3.9	-4.0	-4.1
-3.4	-3.9	-4.0	-4.0

Temperature gradient across outdoor port

-3.3	-3.3	-3.4	-3.3
-3.1	-3.2	-3.4	-3.4
-2.9	-3.4	-3.4	-3.5
-3.0	-3.3	-3.4	-3.4

Temperature gradient across exhaust port

-1.2	-2.3	-2.5	-2.3
0.1	-0.3	-0.5	-0.5
1.8	1.5	1.2	1.2
3.8	3.1	3.1	3.3

Temperature gradient across exhaust port

-1.8	-2.5	-2.6	-2.6
-0.9	-1.1	-1.3	-1.3
0.0	-0.1	-0.3	-0.4
1.1	0.6	0.7	0.9

**Figure E.4:** Temperature gradient across outdoor and exhaust port (balanced massflows) - condition 1

**Figure E.5:** Temperature gradient across outdoor and exhaust port (imbalanced massflows) - condition 1

Figure E.4 and E.5 shows the temperature gradient across the outdoor and exhaust port for the two cases: with balanced flows and imbalanced flows. For both, the temperatures at the critical zone is similar, while for the balanced flows the gradient is higher. Considering that for both cases an average temperature of the whole port is at approximately 0 °C, frost is formed with low relative humidity.

## Condition 2

After realizing that there is a risk of not reaching low enough temperatures for frost formation on the exhaust port, a different approach was taken. The temperature in the warm room was decreased and the focus became finding out at which exhaust temperature frost will occur with different relative humidity levels in the warm room. In this regard, finding critical outdoor temperature which would cause frost was no longer relevant.

The second test is performed with higher indoor relative humidity, 38 % and 16 °C – equivalent to 22 °C and 27 % relative humidity.

Figure E.6 shows the readings from all the sensors on the exhaust port. The peaks indicate opening the ventilation box for taking photos. Around second 1000, there was only condensation in form of small droplets on the walls of the heat exchanger, seen in figure E.7. Around second 3000, the small droplets turned into slightly bigger ones and around second 6000, there was more condensation, as

seen in figures E.8 and E.9. After observing that frost did not occur with minimum temperature of  $-2.7\text{ }^{\circ}\text{C}$  on the exhaust port (around sec 6000), after second 9000, the outdoor airflow was increased, while the extraction was decreased to ensure that the exhaust temperature falls even more and causes frost (figure E.12). Finally, frost on the heat exchanger was captured around second 12000, shown in figure E.10.

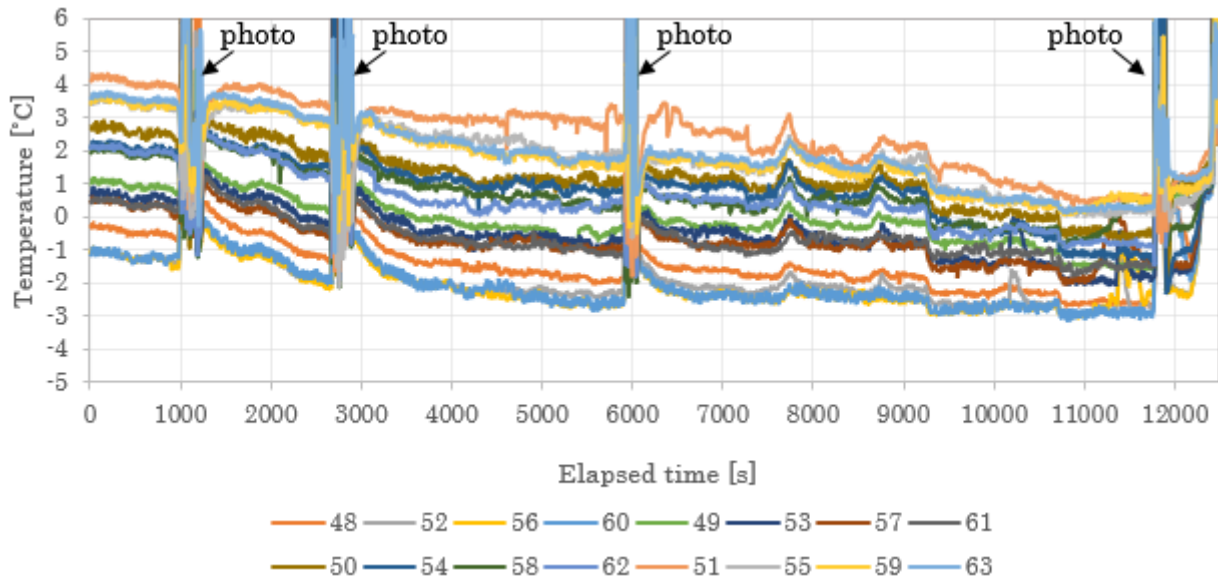


**Figure E.6:** Temperature readings from all sensors on exhaust port - condition 2



**Figure E.7:** Small droplets of condensation at second 1000 - condition 2



**Figure E.8:** Bigger droplets of condensation at second 3000 - condition 2



**Figure E.9:** Condensation at second 6000 - condition 2



Figure E.10: Frost formation at second 12000 - condition 2

Figure E.11 shows the mean air temperature on each port and the relative humidity of the extracted air. Since the heat exchanger had frozen on the last photo (sec 12000), it is believed that ice formation started earlier, probably after second 6000 and while the mean exhaust temperature was 0 °C. Therefore, the period between seconds 6600 – 7600 will be taken to define the conditions at which frost starts forming and for looking into the temperature distribution across the exhaust port.

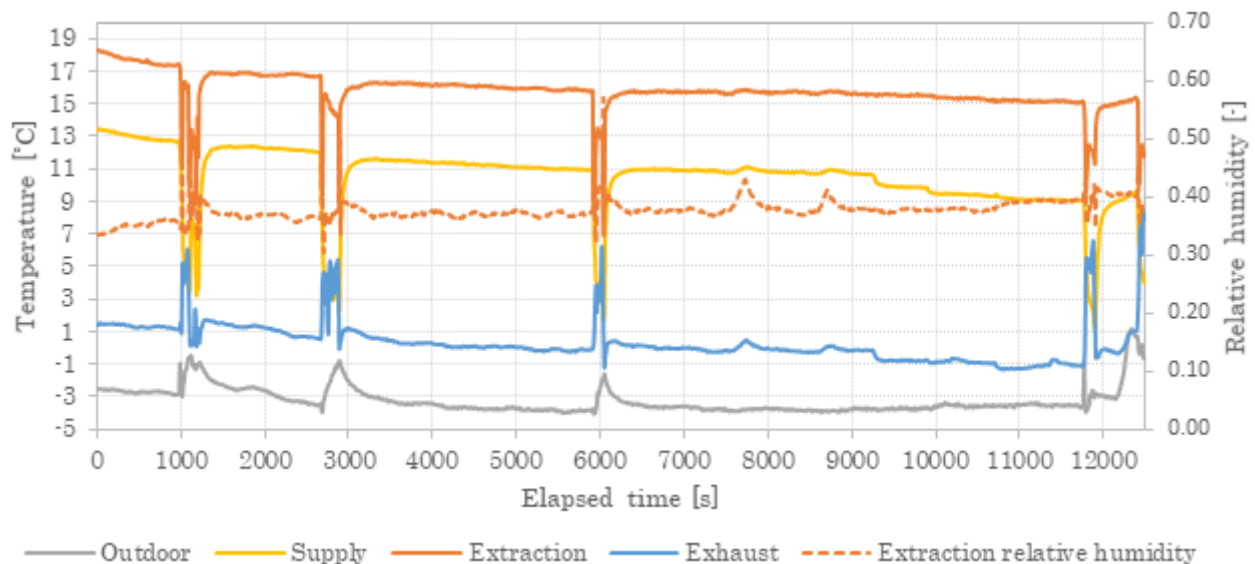


Figure E.11: Mean air temperature and extraction relative humidity - condition 2

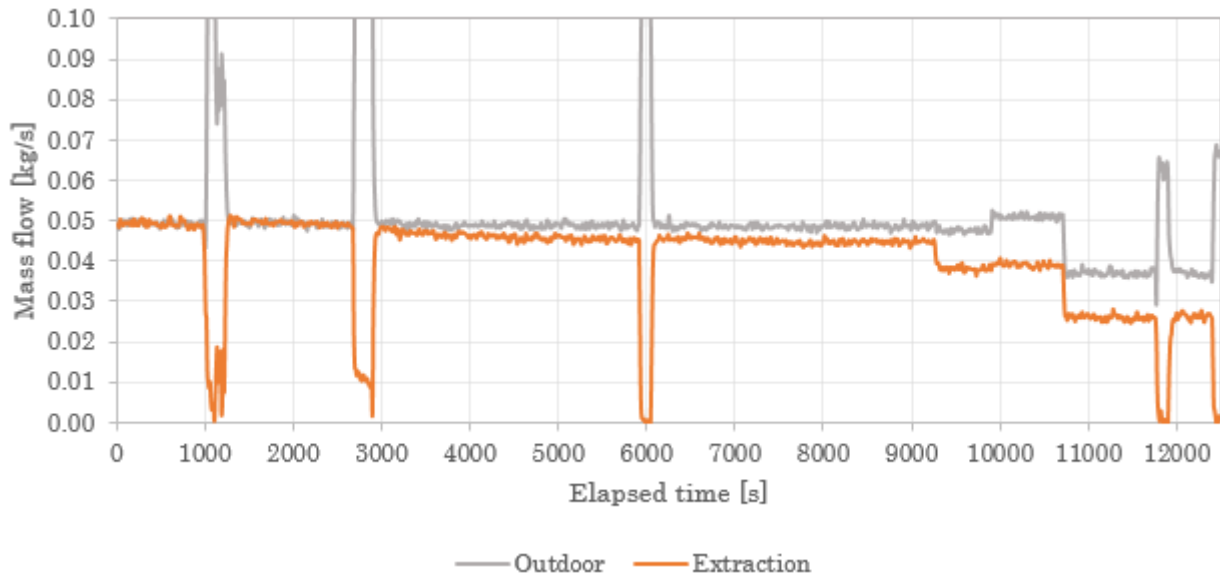


Figure E.12: Mass flow - condition 2

Figure E.13 shows the temperature gradient across the outdoor and exhaust port for the period between 6600-7600 seconds on figure E.11.

Temperature gradient across outdoor port

-3.7	-3.7	-3.8	-3.7
-3.5	-3.7	-3.8	-3.8
-3.3	-3.8	-3.8	-3.9
-3.3	-3.8	-3.9	-3.9

Temperature gradient across exhaust port

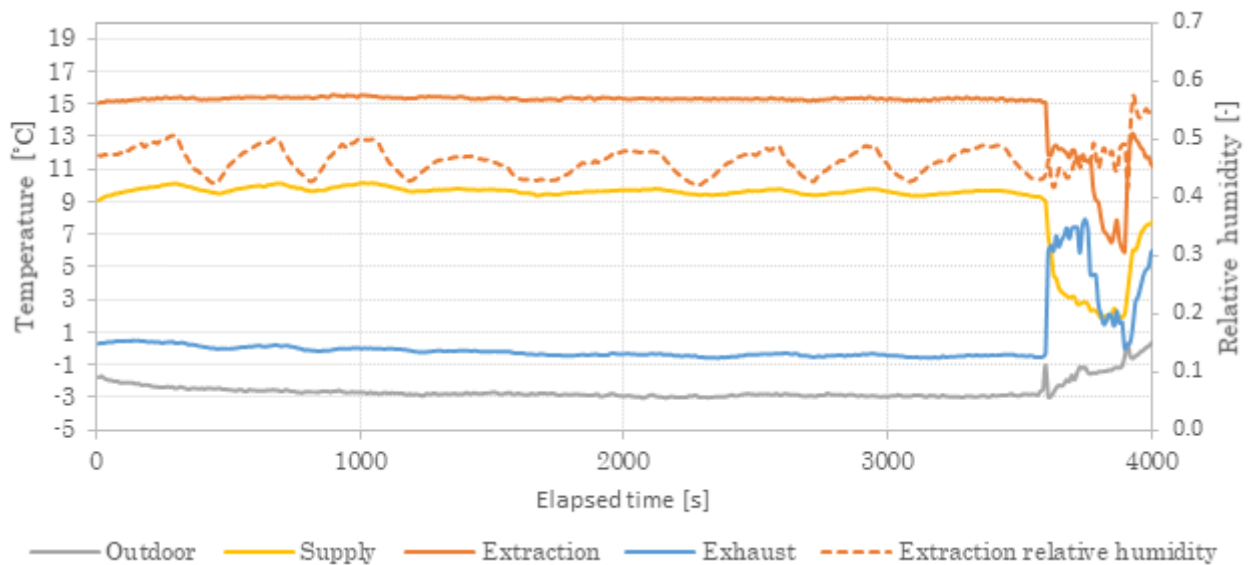
-1.7	-2.2	-2.4	-2.4
-0.3	-0.6	-0.8	-1.0
1.0	0.8	0.3	0.5
2.4	1.6	1.6	1.7

Figure E.13: Temperature gradient across outdoor and exhaust port - condition 2

Condition 3

The third test was run with unbalanced flows – higher supply than extraction, mean temperature of 15.3 °C and 46 % relative humidity. The absolute humidity in the extracted air was equivalent to indoor conditions of 22 °C and 30 % relative humidity.

Figure E.14 shows the mean air temperature on all ports and the mean relative humidity for the extracted air. The temperature disturbance between sec 3000 and 4000 is caused by opening the ventilation box for photos. Frost formation was detected at mean exhaust temperature of 0 °C, as shown in figure E.16.



**Figure E.14:** Mean air temperature and extraction relative humidity - condition 3

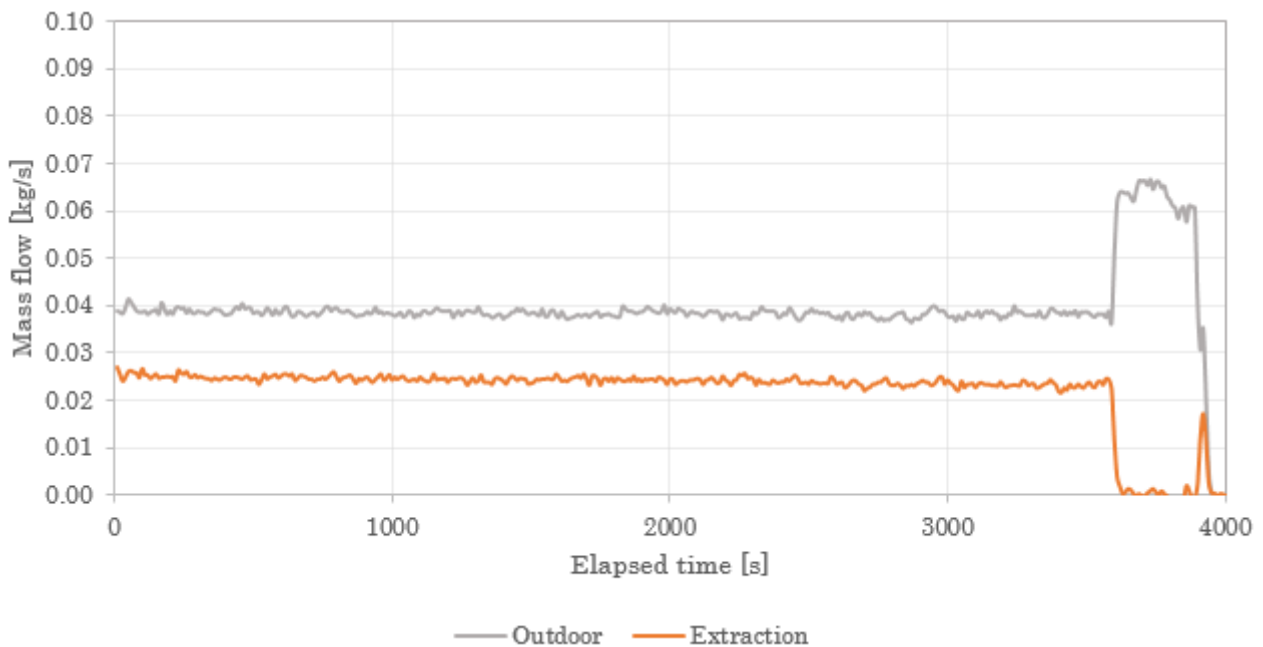


**Figure E.15:** Mass flow - condition 3



**Figure E.16:** Frost formation - condition 3

Figure E.17 shows the temperature gradient across the outdoor and exhaust port for the analysed period in figure E.14.

## Temperature gradient across outdoor port

-2.7	-2.8	-2.9	-2.7
-2.6	-2.8	-2.9	-2.7
-2.4	-2.9	-2.9	-2.9
-2.4	-2.8	-2.9	-2.9

## Temperature gradient across exhaust port

-1.6	-1.8	-2.2	-1.9
-0.4	-0.9	-1.4	-0.7
0.8	0.4	-0.1	0.2
2.0	1.5	1.3	1.6

**Figure E.17:** Temperature gradient across outdoor and exhaust port - condition 3

#### Condition 4

The fourth test was run with unbalanced flows – higher supply than extraction, mean temperature of 16.1 °C and 58 % relative humidity. The absolute humidity in the extracted air was equivalent to indoor conditions of 22 °C and 40 % relative humidity.

Figure E.18 shows the mean air temperature on all ports and the mean relative humidity for the extracted air. At sec 2500, by opening the ventilation box for photos there is a disturbance in temperature and relative humidity. Frost formation was detected at mean exhaust temperature of 0 °C, as shown in figure E.20.

Figure E.19 shows that the test was run with unbalanced flows. After sec 2000, the flow becomes linear. This is because of an issue with the data logging software. Even though the data is not logged properly, the flows is not adjusted or change therefore the same mass flow is available until opening the ventilation box.

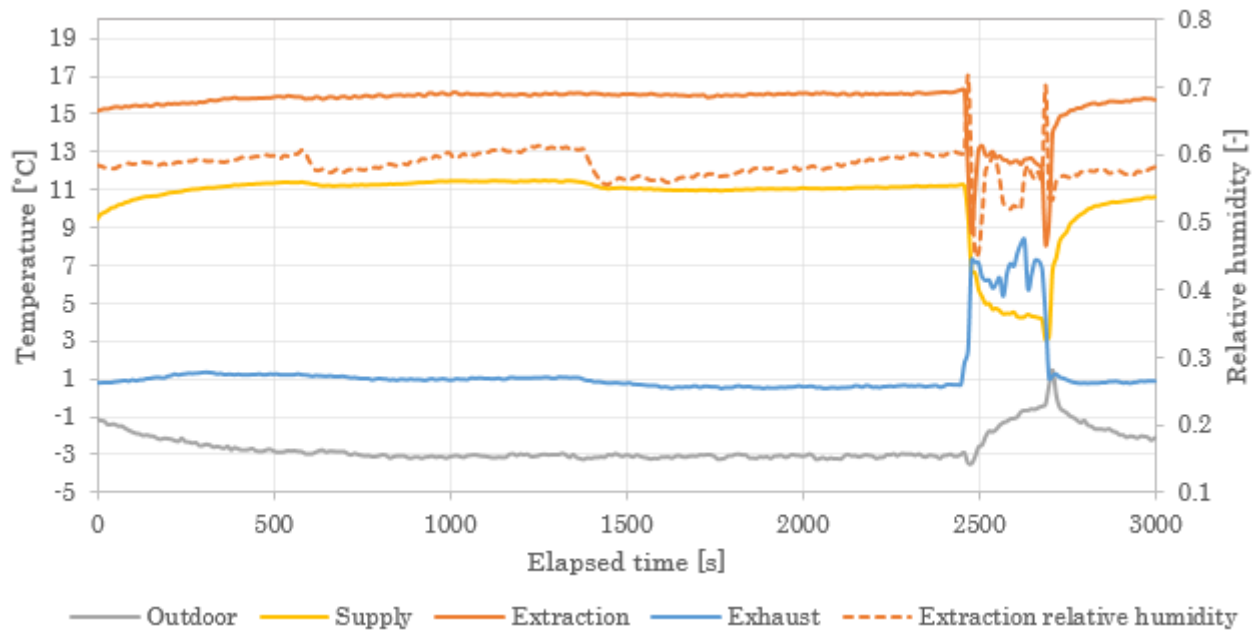


Figure E.18: Mean air temperature and extraction relative humidity - condition 4

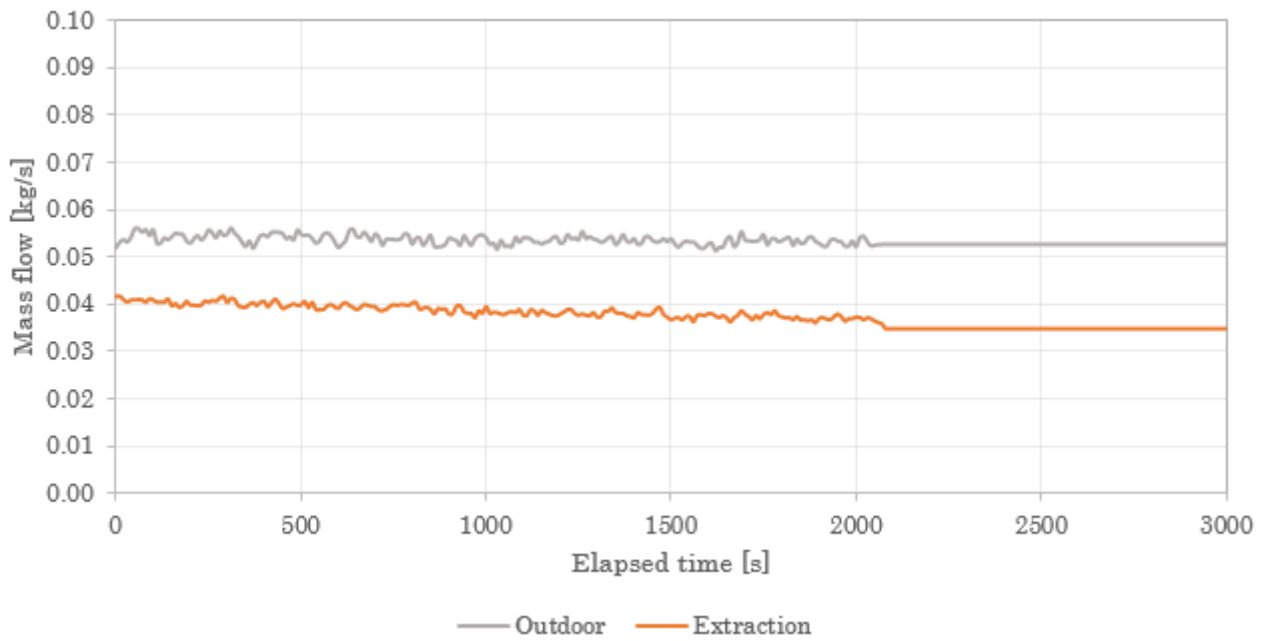


Figure E.19: Mass flow - condition 4



**Figure E.20:** Frost formation - condition 4

Temperature gradient across outdoor port

-3.0	-3.1	-3.2	-3.0
-2.9	-3.0	-3.2	-3.1
-2.7	-3.1	-3.2	-3.2
-2.5	-3.1	-3.2	-3.2

Temperature gradient across exhaust port

-1.6	-2.3	-2.7	-2.3
0.5	-1.8	-2.0	0.1
3.3	-0.3	-0.6	2.0
5.2	4.0	3.7	4.1

**Figure E.21:** Temperature gradient across outdoor and exhaust port - condition 4

In the last frost limit test, the highest temperature difference between the coldest and the warmest part of the heat exchanger can be observed. In test 2 and 3 the difference is approximately 4 °C, while for test 4 the difference is around 6 °C. Since with higher relative humidity there is more condensation, the heat exchanger's plate temperature is not decreased as much for the lower part of the port compared to the cold part.[2]

## E.1.1 Risk of frost for the chosen geographical locations

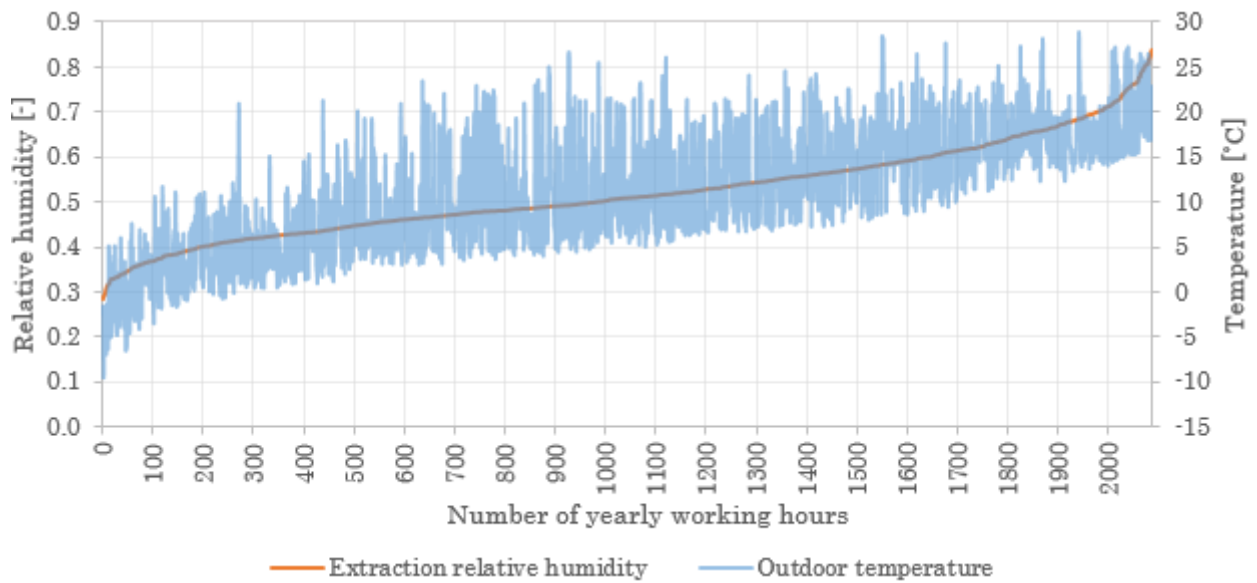


Figure E.22: Indoor relative humidity - outdoor temperature relation for Groningen - classroom

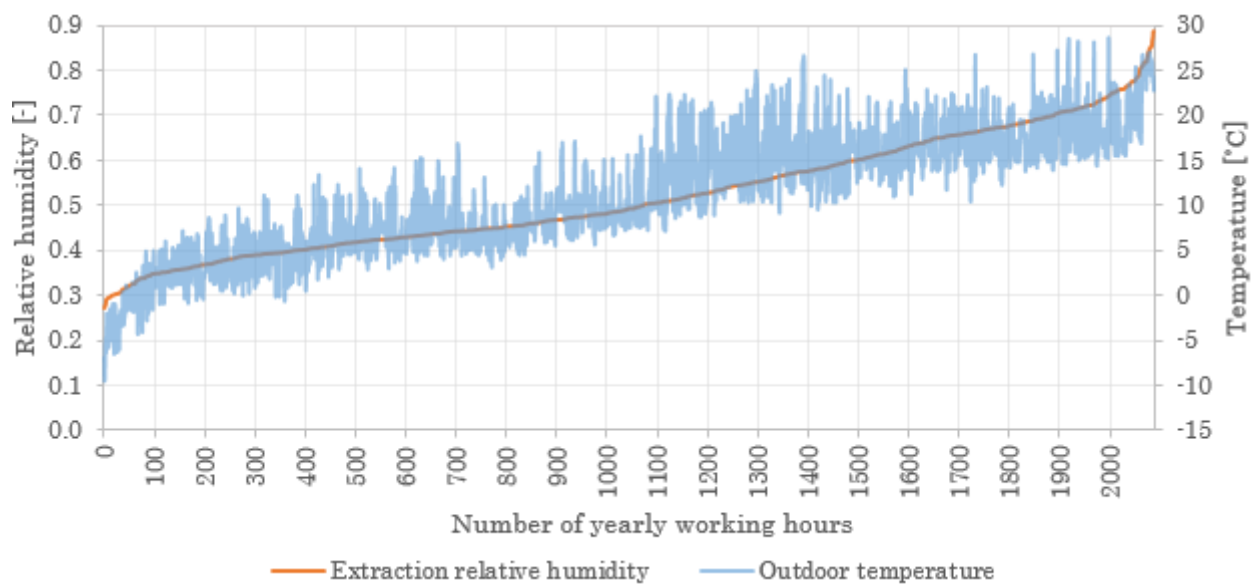


Figure E.23: Indoor relative humidity - outdoor temperature relation for Groningen - office

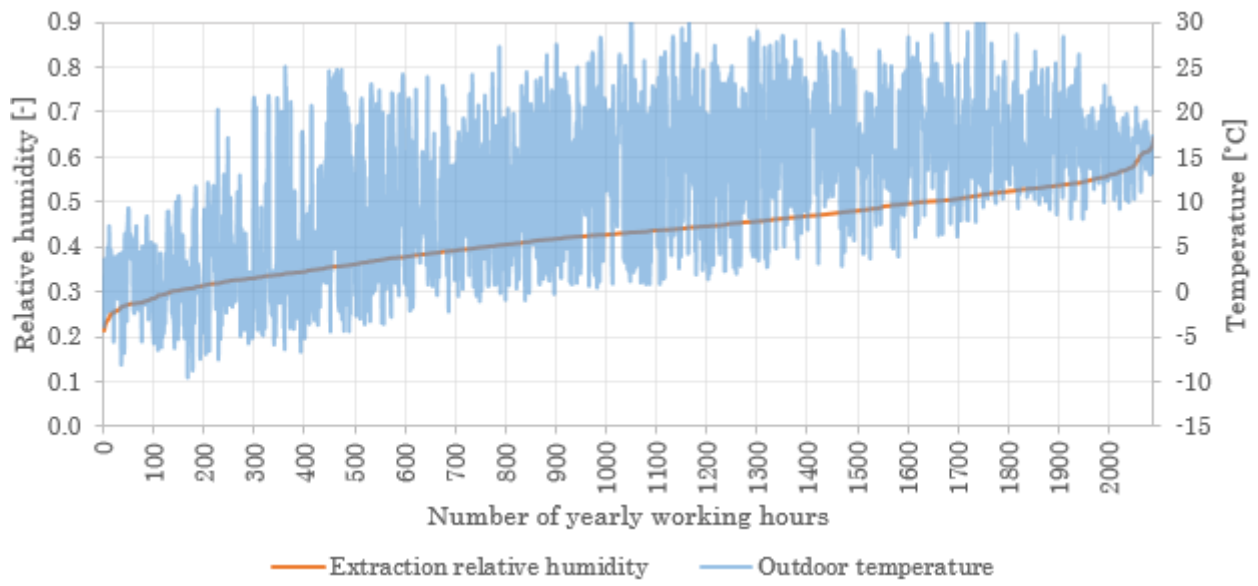


Figure E.24: Indoor relative humidity - outdoor temperature relation for Innsbruck - classroom

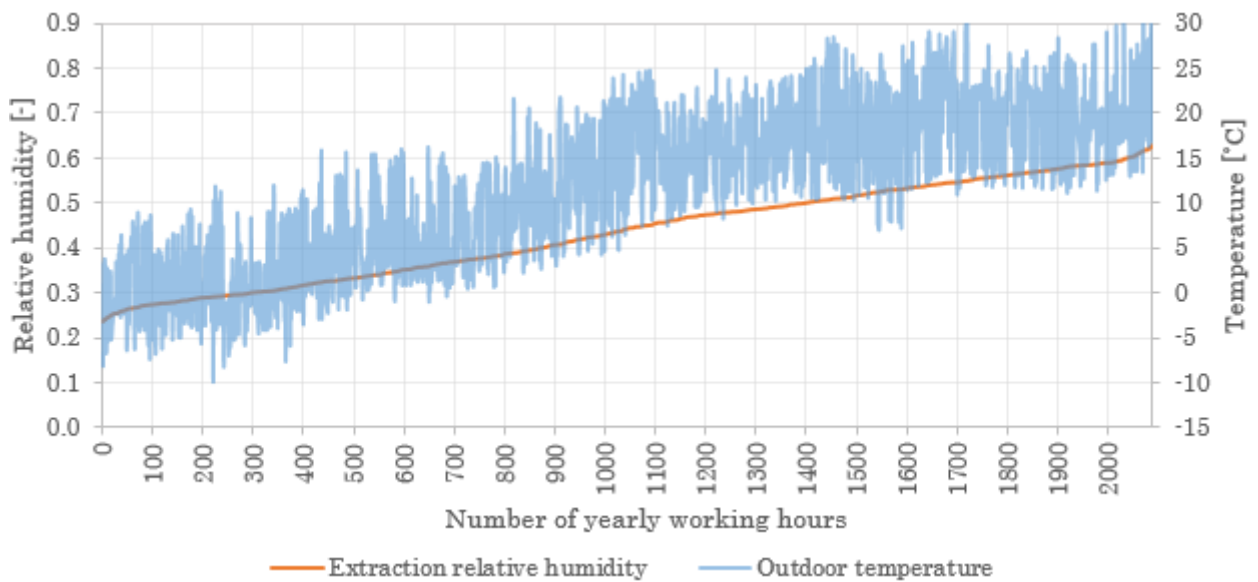


Figure E.25: Indoor relative humidity - outdoor temperature relation for Innsbruck - office

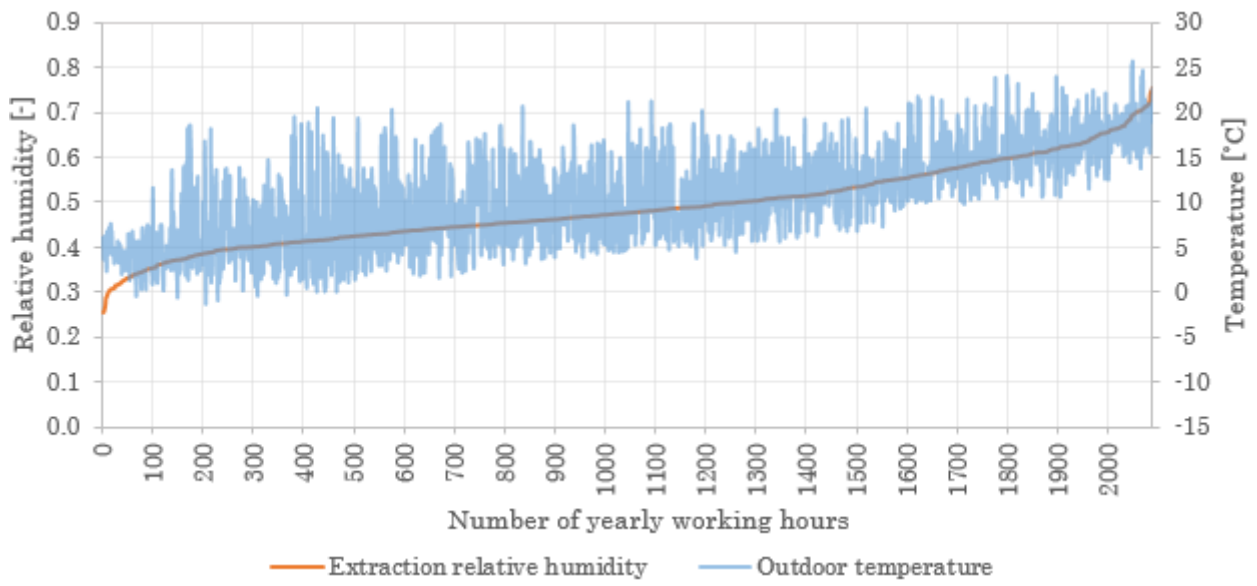


Figure E.26: Indoor relative humidity - outdoor temperature relation for Leuchars - classroom

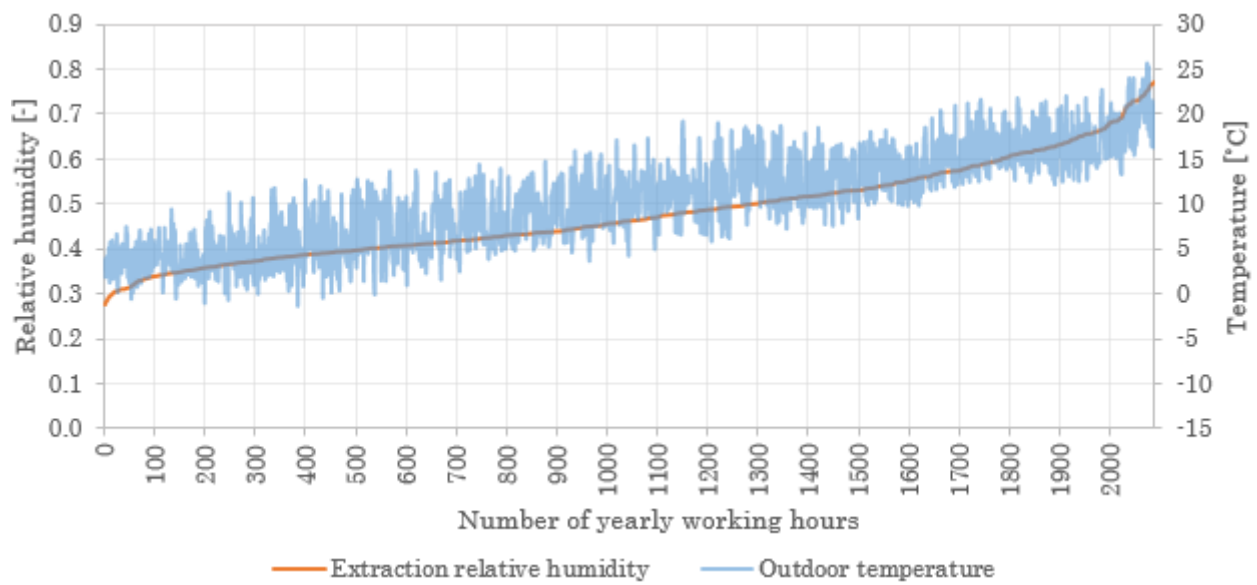


Figure E.27: Indoor relative humidity - outdoor temperature relation for Leuchars - office

# F | Impact of defrost methods

## F.1 Defrost methods

### Imbalance

The imbalance ratio of the airflows is expressed as mass flow of supply air / mass flow of extraction air. In table F.1 the ratio is shown with regards to each fan input voltage step.

Time [sec]	Fan input (outdoor) Voltage steps	Mean ratio outdoor / extraction	
		Infiltration damper realistically open [-]	Infiltration damper fully open [-]
0	6.8	0.98	1.00
600	6.7	0.95	0.98
1200	6.6	0.93	0.96
1800	6.5	0.89	0.93
2400	6.4	0.88	0.92
3000	6	0.81	0.85
3600	5.6	0.74	0.77
4200	5.2	0.68	0.69
4800	4.8	0.64	0.62
5400	4.4	0.59	0.55
6000	4.0	0.55	0.48
6600	3.6	0.52	0.43
7200	3.2	0.48	0.38
8400	2.4	0.43	0.28
9000	2.0	0.40	0.23
9600	1.6	0.39	0.19
10200	1.2	0.35	0.15

**Table F.1:** Fan voltage input steps and imbalance ratio for each step

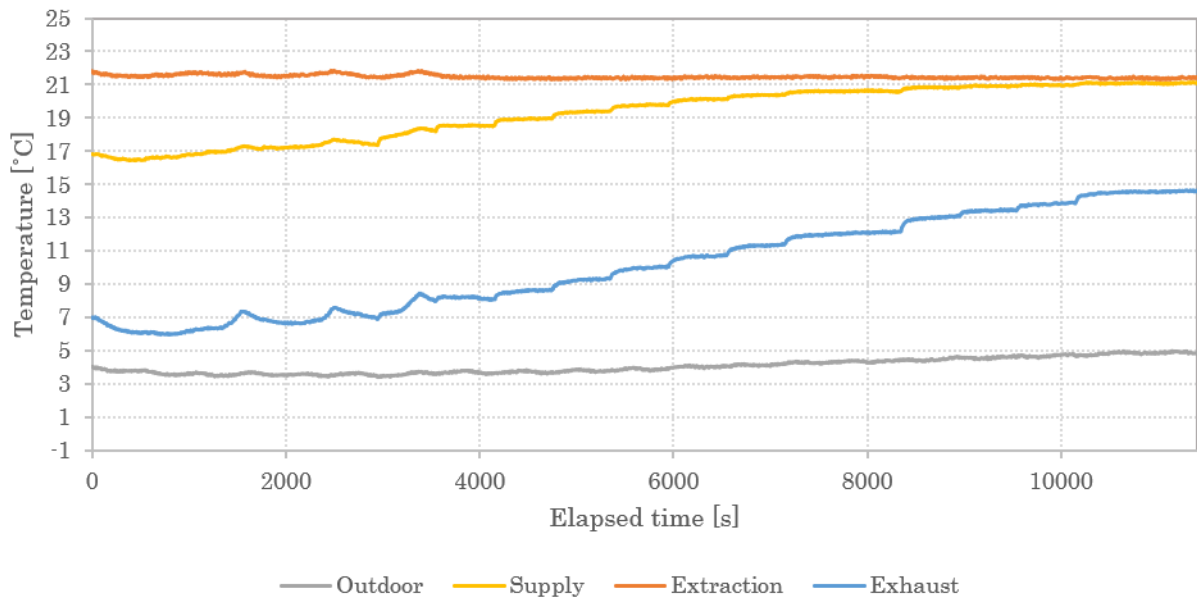


Figure F.1: Mean air temperature - infiltration damper realistically opening

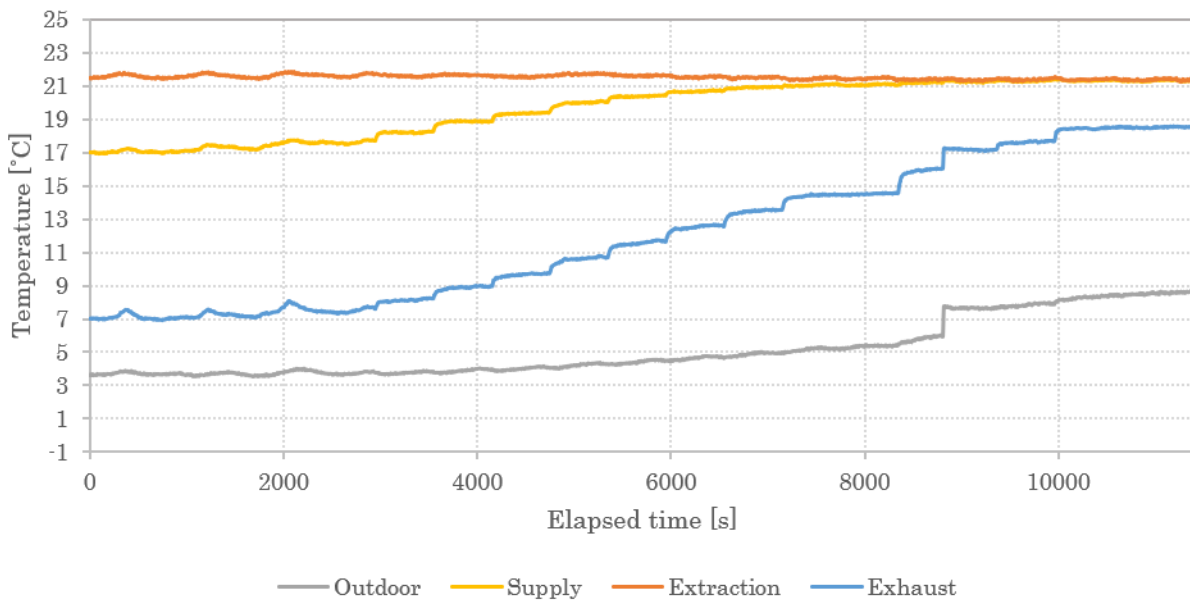


Figure F.2: Mean air temperature -infiltration damper fully open

# G | Comparison of dynamic with static efficiency

The heat exchanger operation condition distribution in the following figures is taking into account decreased exhaust temperature with 2 °C for wet/frost conditions.

Gothenburg - classroom												
Conditions	Jan	Feb	March	April	May	June	July	Aug	Sep	Oct	Nov	Dec
Dry	■			Heat recovery stopped ( $T_{\text{supply}} > 19 \text{ }^\circ\text{C}$ )						■		
Wet	■		■	Heat recovery stopped ( $T_{\text{supply}} > 19 \text{ }^\circ\text{C}$ )						■		
Frost	■											

\*for working hours (8-16)

Figure G.1: Distribution of heat exchanger operation conditions during the year for Gothenburg - classroom

Gothenburg - office												
Conditions	Jan	Feb	March	April	May	June	July	Aug	Sep	Oct	Nov	Dec
Dry	■			Heat recovery stopped ( $T_{\text{supply}} > 19 \text{ }^\circ\text{C}$ )						■		
Wet	■											
Frost	■											

\*for working hours (8-16)

Figure G.2: Distribution of heat exchanger operation conditions during the year for Gothenburg - office

Groningen - classroom												
Conditions	Jan	Feb	March	April	May	June	July	Aug	Sep	Oct	Nov	Dec
Dry	■		■	Heat recovery stopped ( $T_{\text{supply}} > 19 \text{ }^\circ\text{C}$ )						■		
Wet	■											
Frost	■											

\*for working hours (8-16)

Figure G.3: Distribution of heat exchanger operation conditions during the year for Groningen - classroom

Groningen - office												
Conditions	Jan	Feb	March	April	May	June	July	Aug	Sep	Oct	Nov	Dec
Dry	■			Heat recovery stopped ( $T_{\text{supply}} > 19 \text{ }^\circ\text{C}$ )						■		
Wet	■											
Frost	■											

\*for working hours (8-16)

Figure G.4: Distribution of heat exchanger operation conditions during the year for Groningen - office

Innsbruck - classroom												
Conditions	Jan	Feb	March	April	May	June	July	Aug	Sep	Oct	Nov	Dec
Dry				Heat recovery stopped ( $T_{\text{supply}} > 19 \text{ }^\circ\text{C}$ )								
Wet												
Frost												

\*for working hours (8-16)

Figure G.5: Distribution of heat exchanger operation conditions during the year for Innsbruck - classroom

Innsbruck - office												
Conditions	Jan	Feb	March	April	May	June	July	Aug	Sep	Oct	Nov	Dec
Dry				Heat recovery stopped ( $T_{\text{supply}} > 19 \text{ }^\circ\text{C}$ )								
Wet												
Frost												

\*for working hours (8-16)

Figure G.6: Distribution of heat exchanger operation conditions during the year for Innsbruck - office

Leuchars - classroom												
Conditions	Jan	Feb	March	April	May	June	July	Aug	Sep	Oct	Nov	Dec
Dry				Heat recovery stopped ( $T_{\text{supply}} > 19 \text{ }^\circ\text{C}$ )								
Wet												
Frost												

\*for working hours (8-16)

Figure G.7: Distribution of heat exchanger operation conditions during the year for Leuchars - classroom and office

# H | Calculations

## H.1 Input data

### Measured values

$t_{out}$  – outdoor air temperature [ $^{\circ}C$ ]

$t_{sup}$  – supply air temperature [ $^{\circ}C$ ]

$t_{ext}$  – extraction air temperature [ $^{\circ}C$ ]

$t_{exh}$  – exhaust air temperature [ $^{\circ}C$ ]

$t_{exh'}$  – freezing limit temperature [ $^{\circ}C$ ]

$RH_{out}$  – outdoor air relative humidity [–]

$RH_{sup}$  – supply air relative humidity [–]

$RH_{ext}$  – extraction air relative humidity [–]

$RH_{exh}$  – exhaust air relative humidity [–]

$m_h$  – mass flow rate on the warm side ; nominal flow rate [ $\frac{kg}{s}$ ]

$m_{nominal}$  – mass flow rate of the nominal flow (equal to warm side) [ $\frac{kg}{s}$ ]

Freezing limit temperature - temperature of the exhausted air below which frost will occur on the warm side

### Calculated values

$t_{sup'}$  – supply air temperature imbalanced flow [ $^{\circ}C$ ]

$x_{out}$  – outdoor air absolute humidity [ $\frac{kg}{kg}$ ]

$x_{sup}$  – supply air absolute humidity [ $\frac{kg}{kg}$ ]

$x_{sup'}$  – supply air absolute humidity imbalanced flow [ $^{\circ}C$ ]

$x_{ext}$  – extraction air absolute humidity [ $\frac{kg}{kg}$ ]

$x_{exh}$  – exhaust air absolute humidity [ $\frac{kg}{kg}$ ]

$x_{exh'}$  – freezing limit absolute humidity [ $\frac{kg}{kg}$ ]

$h_{out}$  – outdoor air enthalpy [ $\frac{kJ}{kg}$ ]

$h_{sup}$  – supply air enthalpy [ $\frac{kJ}{kg}$ ]

$h_{sup}$  – supply air enthalpy imbalanced flow [ $^{\circ}C$ ]

$h_{ext}$  – extraction air enthalpy [ $\frac{kJ}{kg}$ ]

$h_{exh}$  – exhaust air enthalpy [ $\frac{kJ}{kg}$ ]

$h_{exh'}$  – freezing limit air enthalpy [ $\frac{kJ}{kg}$ ]

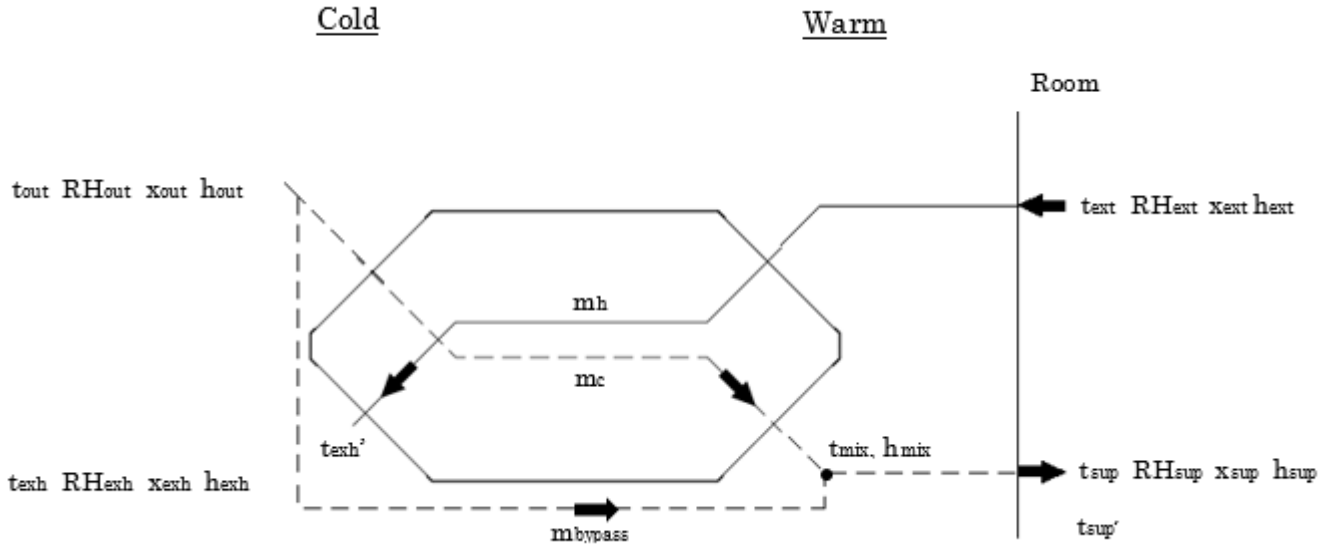


**Figure H.1:** Calculation parameters illustrated

Calculation of absolute and relative humidity: [24]

$$x = 0.622 \cdot \frac{\varphi \cdot P_s}{P - (\varphi \cdot P_s)} \left[ \frac{kg \text{ water}}{kg \text{ dry air}} \right] \quad (\text{H.1})$$

$$\Rightarrow \varphi = \frac{P \cdot x}{P_s \cdot (0.622 + x)} \quad (\text{H.2})$$

$x$  – absolute humidity [ $\frac{kg \text{ water}}{kg \text{ dry air}}$ ]

$\varphi$  – relative humidity [–]

$P_s$  – saturation pressure [Pa]

$P$  – atmospheric pressure [Pa] (101325 Pa)

Calculation of saturation pressure: [34]

$$P_s = 610.78 \cdot EXP \left( \frac{t}{t + 238.3} \cdot 17.2694 \right) [Pa] \quad (\text{H.3})$$

$$P_s \text{ ice} = EXP \left( -\frac{6140.4}{273 + t} + 28.916 \right) [Pa] \quad (\text{H.4})$$

$t$  – temperature [ $^{\circ}C$ ]

Calculation of enthalpy: [24]

$$h = 1.006 \cdot t + x \cdot (2500 + 1.863 \cdot t) \left[ \frac{kJ}{kg \text{ dry air}} \right] \quad (H.5)$$

$t$  – temperature [ $^{\circ}C$ ]

$x$  – absolute humidity  $\left[ \frac{kg \text{ water}}{kg \text{ dry air}} \right]$

## H.2 Imbalance method

With this defrost method, the outdoor airflow rate is controlled by the temperature of the exhaust air. The purpose is to maintain the temperature of the exhaust air above the freezing limit to avoid frost on the warm side of the heat exchanger.

Main heat balance formula: [28]

$$Q = C_h \cdot (t_{ext} - t_{exh}) = C_c \cdot (t_{sup} - t_{out}) [W] \quad (H.6)$$

$$C_h = m_h \cdot Cp_h \left[ \frac{W}{K} \right] \quad (H.7)$$

$$C_c = m_c \cdot Cp_c \left[ \frac{W}{K} \right] \quad (H.8)$$

$Q$  – heat flow [W]

$C_h$  – heat capacity rate on the warm side  $\left[ \frac{W}{K} \right]$

$C_c$  – heat capacity rate on the cold side  $\left[ \frac{W}{K} \right]$

$m_h$  – mass flow rate on the warm side  $\left[ \frac{kg}{s} \right]$

$m_c$  – mass flow rate on the cold side  $\left[ \frac{kg}{s} \right]$

$Cp_h$  – specific heat capacity for the warm side  $\left[ \frac{J \cdot kg}{K} \right]$

$Cp_c$  – specific heat capacity for the cold side  $\left[ \frac{J \cdot kg}{K} \right]$

The amount of imbalance is calculated in the following way. First, the maximum possible heat that can be extracted from the warm airstream is calculated by multiplying the enthalpy difference from the extraction to the frost limit  $h_{ext} - h_{exh'}$  with the mass flow on the warm side, seen in equation H.10. This would be the maximum energy that can be extracted before the exhaust temperature falls below the frost limit. Second, the calculated maximum possible heat transfer is set to be equal to what

is "received" as heat on the cold side during imbalance and the mass flow for imbalance is calculated (equation H.11).

The calculation for "received" heat on the cold side during imbalance includes higher supply temperature compared to what the supply temperature would be with balanced flows. To calculate the "new" supply temperature ( $t_{sup'}$  - calculation seen in equation H.12), a temperature efficiency equivalent to an imbalance ratio  $\frac{m_c}{m_h}$  of 0.7 is taken. It is recommended by Klingenburg [21] to not have lower imbalance ratio than 0.7. By contacting Klingenburg, it became clear that there are two reasons behind it: 1) When Eurovent [14] tests the heat exchangers, it uses a range of 0.66 to 1.5 for an imbalance ratio. This range is set by EN 308 [6]. 2) With an imbalance ratio lower than 0.7, there is a risk that the pressure drop through the heat exchanger increases so much that the air channels on the warm side would expand, thus causing physical damage to the heat exchanger.

The dialogue with Martin Sternberg from Klingenburg regarding the imbalance ratio can be seen at the end of this section.

The  $Q_{max}$  heat flow is the heat transfer without defrosting, when the flow is not imbalanced.

$$Q_{max} = m_h \cdot (h_{ext} - h_{exh}) = m_c \cdot (t_{sup} - t_{out}) \cdot C_{Pc} \left[ \frac{kg}{s} \right] \quad (H.9)$$

$$Q_{max\ possible} = m_h \cdot (h_{ext} - h_{exh'}) = m_{c,im} \cdot (t_{sup'} - t_{out}) \cdot C_{Pc} \left[ \frac{kg}{s} \right] \quad (H.10)$$

$$\Rightarrow m_{c,im} = m_h \cdot \frac{(h_{ext} - h_{exh'})}{(t_{sup'} - t_{out}) \cdot C_{Pc}} \left[ \frac{kg}{s} \right] \quad (H.11)$$

$Q_{max}$  - maximum heat flow [W]

$Q_{max\ possible}$  - maximum possible heat flow based on freezing point temperature [W]

$m_{c,im}$  - cold side flow at imbalance  $\left[ \frac{kg}{s} \right]$

$t_{sup'}$  isolated: [27]

$$\eta_{t,im} = \frac{t_{sup'} - t_{out}}{t_{ext} - t_{out}} \Rightarrow t_{sup'} = \eta_{t,im} \cdot (t_{ext} - t_{out}) + t_{out} [^{\circ}C] \quad (H.12)$$

$t_{sup'}$  - supply temperature imbalanced flow [ $^{\circ}C$ ]

$\eta_{t,im}$  - temperature efficiency imbalanced flow [-]

Calculation of absolute humidity on the frost limit point ( $x_{sup'}$ ). It is needed to calculate the enthalpy on that point.

Knowing that the line representing the air treatment from extraction to exhaust is linear, the function for it would be a linear one,  $y = ax + b$ .

$y$  – freezing limit temperature [ $^{\circ}C$ ]

$a$  – slope of the line

$b$  – intercept point of the line from extraction to exhaust with the  $y$  (temperature) axis

$x$  – freezing limit absolute humidity  $\left[\frac{kg}{kg}\right]$

The slope of the line is found by:

$$y = \frac{t_{ext} - t_{exh}}{x_{ext} - x_{exh}} \quad (H.13)$$

The intercept point is calculated by:

$$b = t_{exh} - a \cdot x_{exh} \quad (H.14)$$

Finally, the absolute humidity on the frost limit point is calculated by:

$$x_{exh'} = \left(\frac{t_{exh'} - b}{a}\right) \quad (H.15)$$

Energy consumption: [27]

The first part of the formula in equation H.16 gives the power needed to overcome the infiltration and ventilation losses. The second part takes into account the energy saving for running the supply fan on a lower speed.

For calculating the fan power, the pressure drop of the supply fan is extracted from Klingenburg's software.

$$\begin{aligned} Q_{cons} = & ((h_{sup} \cdot m_{nominal}) - ((h_{sup'} \cdot m_{c,im}) + (h_{out} \cdot m_{inf}))) \\ & - (Q_{sup\ fan\ (nominal\ flow)} - Q_{sup\ fan\ (imbalanced\ flow)}) [W] \end{aligned} \quad (H.16)$$

$$Q_{sup\ fan\ (nominal\ flow)} = \frac{\left(\frac{m_{c,im}}{\rho}\right) \cdot \Delta P_{sup\ fan\ (nominal\ flow)}}{\eta_{fan}} [W] \quad (H.17)$$

$$\frac{Q_{sup\ fan\ (imbalanced\ flow)}}{Q_{sup\ fan\ (nominal\ flow)}} = \left(\frac{m_{c,im}}{m_{nominal}}\right)^3 \quad (H.18)$$

$$\Rightarrow Q_{sup\ fan\ (imbalanced\ flow)} = Q_{sup\ fan\ (nominal\ flow)} \cdot \left(\frac{m_{c,im}}{m_{nominal}}\right)^3 [W] \quad (H.19)$$

$m_{inf}$  – mass flow rate of infiltrated air  $\left[\frac{kg}{s}\right]$

$\Delta P_{sup fan (nominal flow)}$  – pressure drop on the supply fan with nominal air flow [Pa]

$Q_{sup fan (nominal flow)}$  – fan power with nominal flow [W]

$Q_{sup fan (imbalanced flow)}$  – fan power with imbalanced flow [W]

$\eta_{fan}$  – fan efficiency [-] (0.4 used)

$\rho$  – density of air  $\left[\frac{kg}{m^3}\right]$

Dialogue with Martin Sternberg from Klingenburg [21] regarding the imbalance ratio.

"Dear Dzhanan,

In general for all products (rotary heat exchanger, counterflow plate heat exchanger and crossflow plate heat exchanger) the test procedure in the independent laboratories is done according EN 308. Here you have to test with air flow ratios between 0,66 and 1,5. Therefore our software shows the results only in that ratio.

Additional to that we have a second limitation which is the pressure loss of the heat exchanger which should depending on the size not exceed 200 Pa ( for sizes GS 16 up to GS 45).

So this 2 limitations in the software should also grant the correct use of the unit, as the software is free for the market and therefore also people with less information to that products might do selections.

Important to know is that the pressure difference for the sizes GS 16 up to GS 62 should not increase 400 Pa. The pressure difference is measured between fresh air and extract air.

So in combination with an unfavorable installation of fans and air ratio it might be possible that we have an higher pressure difference than recommended.

So with the limitations in the software we can grant that in critical cases the customer don't get an result from the calculation and will ask us for more information. We are then able to support the customer and to prevent later on damages due to wrong selection and implementation in the AHU.

Hope to give you as much information as possible.

Do not hesitate to contact me in case of any further question or unclear explanations.

Good luck for your study.

Mit freundlichen Grüßen | With kind regards i.A. | o.b.o. Martin Sternberg

Regional Vertrieb Export | Regional Sales Management Export "

### H.3 Bypass method

The amount of bypassed air is controlled in the same way as the outdoor airflow in the imbalance method.

$$Q_{max} = m_h \cdot (h_{ext} - h_{exh}) = m_c \cdot (t_{sup} - t_{out}) \cdot C_{Pc} \left[ \frac{kg}{s} \right] \quad (H.20)$$

$$Q_{max\ possible} = m_h \cdot (h_{ext} - h_{exh'}) = m_c \cdot (t_{sup'} - t_{out}) \cdot C_{Pc} \left[ \frac{kg}{s} \right] \quad (H.21)$$

$$\Rightarrow m_c = m_h \cdot \frac{(h_{ext} - h_{exh'})}{(t_{sup'} - t_{out}) \cdot C_{Pc}} \left[ \frac{kg}{s} \right] \quad (H.22)$$

The amount that is bypassed can be calculated by subtracting the cold and warm air passing through the heat exchanger.

$$m_{bypass} = m_{nominal} - m_c \left[ \frac{kg}{s} \right] \quad (H.23)$$

When the supply air comes out of the heat exchanger, it is mixed with the bypass air which gives a mixing enthalpy.

$$m_{bypass} \cdot h_{out} + m_c \cdot h_{sup} = (m_c + m_{bypass}) \cdot h_{mix} \Rightarrow h_{mix} = \frac{h_{out} \cdot m_{bypass} + h_{sup} \cdot m_c}{m_{bypass} + m_c} \left[ \frac{kJ}{kg} \right] \quad (H.24)$$

Mixing enthalpy can be converted to a mixing temperature.

$$h_{mix} = 1.006 \cdot t_{mix} + x_{out} \cdot (2500 + 1.863 \cdot t_{mix}) \Rightarrow t_{mix} = \frac{h_{mix} - 2500 \cdot x_{out}}{1.006 + 1.863 \cdot x_{out}} [^{\circ}C] \quad (H.25)$$

$m_{bypass}$  – mass flow of bypassed air  $\left[ \frac{kg}{s} \right]$

$h_{mix}$  – enthalpy of combined bypass and cold airstream  $\left[ \frac{kJ}{kg} \right]$

$t_{mix}$  – temperature of combined bypass and cold airstream  $[^{\circ}C]$

Energy consumption:

$$Q_{cons} = (h_{sup} \cdot m_{nominal}) - \left( (h_{sup'} \cdot m_{c,im}) + (h_{out} \cdot m_{inf}) \right) [W] \quad (H.26)$$

The energy consumption is calculated similar to the imbalance method, though without the "savings" from the reduced speed of the fan.

## H.4 Air preheating method

With this method, the heating output of the preheater is controlled by the freezing limit temperature on the exhaust side ( $t_{exh'}$ ). The heat delivered from the preheater needs to cover the energy that would be needed to increase the exhaust temperature from freezing condition to the freezing limit temperature.

Energy consumption:

$$Q_{cons} = m_h \cdot \frac{(h_{ext} - h_{exh'})}{\eta_t} [W] \quad (H.27)$$

The denominator of the formula takes into account that only a portion, equivalent to the temperature efficiency of the heat exchanger, is supplied to the exhaust side.

## H.5 Step-by-step walk through the excel spreadsheet

For the imbalance method BSim and Klingenburg software is used to extract the input data necessary for the calculation of imbalance. Yearly hourly data is extracted, but only working hours are investigated.

The purpose of this extended calculation is to calculate the needed imbalance ratio based on the combination of indoor and outdoor conditions provided by the two software. Afterwards, the total energy consumption is estimated. Input (corresponding columns in Excel):

A -  $T_{out}$  (simulated outdoor temperature with BSim)

B -  $T_{sup}$  (calculated supply temperature with Klingenburg software)

C -  $T_{supf}$  (calculated by equation (H.12))

D -  $T_{ext}$  (simulated extraction temperature with BSim)

E -  $T_{exh}$  (calculated exhaust temperature with Klingenburg Software)

F -  $T_{exh'}$  (based on chapter 7, frost formation appears on the exhaust port, when the mean exhaust temperature reaches 0 °C, therefore this temperature is considered)

As described previously in section H.2, when imbalance is created, temperature efficiency increases, therefore  $T_{supf}$  has a higher temperature than  $T_{sup}$ .  $T_{supf}$  is calculated with an imbalance ratio of 0.7. By having this imbalance, the wet temperature efficiency is calculated with Klingenburg, as 0.924. Further, the wet temperature efficiency and the outdoor and extraction temperatures, applied in equation H.12 result in  $T_{supf}$ .

H -  $RH_{out}$  (the outdoor air relative humidity is assumed to be 80 % - since it is not influencing the temperature efficiency or the heat transfer)

I -  $RH_{sup}$  (the supply air relative humidity is calculated by equation H.2)

J -  $RH_{ext}$  (simulated extraction air relative humidity with BSim)

K -  $RH_{exh}$  (calculated exhaust air relative humidity with Klingenburg software)

The yearly data from BSim - the outdoor / extracted air temperature and extracted relative humidity with the outdoor relative humidity assumption, allow the calculation of supply / exhaust air temperature and exhaust relative humidity By Klingenburg's software.

N -  $x_{out}$  (the absolute humidity is calculated by equation H.1)

O -  $x_{sup}$  (since the air treatment on the cold side is a dry process,  $x_{out} = x_{sup}$ )

P -  $x_{ext}$  (the absolute humidity is calculated by equation H.1)

Q -  $x_{exh}$  (the absolute humidity is calculated by equation H.1)

If the temperature and relative humidity of the air are known, based on equation H.1, the absolute humidity can be calculated. When having temperature and absolute humidity, the relative humidity is given by H.2. At this step, the air temperature, relative humidity and absolute humidity is known for all the four ports of the heat exchanger.

T -  $x_{exh}$  (the absolute humidity is calculated by equation H.15).

All the enthalpies are calculated by equation H.5.

V -  $h_{out}$

W -  $h_{sup}$

X -  $h_{sup'}$

Y -  $h_{ext}$

Z -  $h_{exh}$

AA -  $h_{exh'}$

AD -  $m_c$  (the  $m_c$  is the supply air flow rate which is decreased. It is calculated by equation H.11.)

AE -  $m_h$  (the  $m_c$  - constant air flow rate, nominal flow)

AF -  $m_{inf}$  (blower door test value or  $m_{inf}$  value + the difference between the air streams - that is the compensation for having unbalanced flows )

AG -  $m_c/m_h$  ratio

AH -  $Q_{max}$  (calculated by equation H.9)

AI -  $Q_{max\ possible}$  (calculated by equation H.10)

Once the imbalance ratio is known, the energy consumption can be estimated by taking into account:

Infiltration

Ventilation losses

## Fan power

More infiltration is caused due to the imbalance of the aiflows. Therefore, the power needed to heat the supplied air by infiltration is considered as a loss. Moreover, the air supplied to the room has lower power than what is required in the room, therefore there are also ventilation losses. On the other hand, by running the supply fan on low power, there is potential in savings energy. Though, the savings are very insignificant and therefore, not noticable.

AK -  $\eta_{fan}$  (fan efficiency is assumed to be 0.4)

AL -  $P_{hx}$  (the pressure drop of the supply fan is taken form the Klingenburg's software)

AM - *nominal total fan power* (calculated by equation H.17)

AN - *total fan power with imbalance* (calculated by equation H.19)

With the parameters mentioned above, the energy consumption is calculated by equation H.16 for imbalance, equation H.26 for bypass and equation H.27 for preheater.